SANDIA REPORT

SAND90—2726 • UC—814
Unlimited Release
Printed June 1991

Yucca Mountain Site Characterization Project

Technical Summary of the Performance Assessment Calculational Exercises for 1990 (PACE-90)

Volume 1: "Nominal Configuration" Hydrogeologic Parameters and Calculational Results

R. W. Barnard, H. A. Dockery, Editors

Prepared by
Sandia Natic
Albuquerque
for the Unite
under Contra

RETURN

SF2900Q(8-81)

2/91 - 700

"Prepared by Yucca Mountain Site Characterization Project (YMSCP) participants as part of the Civilian Radioactive Waste Management Program (CRWM). The YMSCP is managed by the Yucca Mountain Project Office of the U.S. Department of Energy, Nevada Operations Office (DOE/NV). YMSCP work is sponsored by the Office of Geologic Repositories (OGR) of the DOE Office of Civilian Radioactive Waste Management (OCRWM)."

Issued by Sandia National Laboratories, operated for the United States Department of Energy by Sandia Corporation.

Available to DOE and DOE contractors from
Office of Scientific and Technical Information
PO Box 62
Oak Ridge, TN 37831

Prices available from (615) 576-8401, FTS 626-8401

Available to the public from
National Technical Information Service
US Department of Commerce
5285 Port Royal Rd
Springfield, VA 22161

NTIS price codes
Printed copy: A09
Microfiche copy: A01

Distribution Category
UC-814

SAND90-2726
Unlimited Release
Printed June, 1991

Technical Summary of the Performance Assessment Calculational Exercises for 1990 (PACE-90) Volume 1: "Nominal Configuration" Hydrogeologic Parameters and Calculational Results

R. W. Barnard and H. A. Dockery, Editors

Nuclear Waste Repository Technology Department
Sandia National Laboratories
Albuquerque, NM 87185

ABSTRACT

A Performance Assessment Calculational Exercise for 1990 (PACE-90) was coordinated by the Yucca Mountain Site Characterization Project Office for a total-system performance-assessment problem. The primary objectives of the exercise were to develop performance-assessment computational capabilities of the Yucca Mountain Project participants and to aid in identifying critical elements and processes associated with the calculation. The organizations involved in the calculational effort were LANL, PNL, and SNL. Organizations involved in developing the source term were LBL, LLNL, PNL, and UCB.

The problem defined for PACE-90 was simulation of a "nominal case" groundwater flow and transport of a selected group of radionuclides through a portion of Yucca Mountain. Both 1-D and 2-D calculations were run for a modeling period of 100,000 years. The nuclides used, ^{99}Tc, ^{135}Cs, ^{129}I, and ^{237}Np, were representative of "classes" (i.e., variable sorption and release characteristics) of long-lived nuclides expected to be present in the waste inventory. The water infiltration rate at the repository was specified at 0.01 mm/yr, consistent with the measured unsaturated conditions at Yucca Mountain. Movement of the radionuclides was simulated through a detailed hydrostratigraphy developed from Yucca Mountain data specifically for this exercise. The results showed that, for the specified conditions with the conceptual models used in the problem, no radioactive contamination reached the water table, 230 m below the repository. However, due to the unavailability of sufficient site-specific data, there exists large uncertainty associated with the selected range of parameter values and with the validity of conceptual models used in the problem formulation. Therefore, the results of this exercise cannot be considered a comprehensive total-system-performance assessment of the Yucca Mountain site as a high-level-waste repository.

Table of Contents

List of Figures

List of Tables

PREFACE

This report combines the work of many contributors. The following persons provided input for the indicated sections of this report:
Sections 3.1 and 3.2, H. A. Dockery (SNL) and M. L. Wheeler (LATA/ICF Kaiser).
Section 3.3, M. J. Apted (PNL/Intera Technologies), D. Langford (PNL), W. W.-L. Lee (LBL), and T. H. Pigford (UCB).
Section 3.4, K. G. Eggert (LANL).
Section 4.1, P. W. Eslinger, M. A. McGraw, and T. Miley (PNL).
Section 4.2, G. A. Valentine (LANL).
Section 4.3, J. H. Gauthier (Spectra Research Institute).
Section 4.4, D. P. Gallegos (SNL), C. E. Lee (Applied Physics, Inc), and C. D. Updegraff (GRAM, Inc.).
Section 4.5, R. C. Dykhuizen, R. R. Eaton, P. L. Hopkins, and M. J. Martinez (SNL).

In addition, P. G. Kaplan (SNL) was consulted on the development of the hydrogeologic data, and A. E. Van Luik (PNL) was consulted on the writing of the source-term section.

This report benefitted from extensive technical and editorial review by F. W. Bingham and F. C. Lauffer (SNL), and J. M. Boak (DOE/YMP).

1.0 INTRODUCTION

The Performance Assessment Calculational Exercises (PACE-90) were coordinated by the Department of Energy (DOE) Yucca Mountain Site Characterization Project Office (YMPO) to demonstrate and improve performance assessment (PA) expertise within the Yucca Mountain Site Characterization Project (YMP). Three working groups (WG) participated in the PACE analyses: Total Systems PA (WG 1), Engineered Barriers PA (WG 2), and Natural Barriers PA (WG 3). The WGs were composed of representatives from the Project Participants. The WGs were directed by the DOE in December, 1989, to conduct specific PA exercises during the remainder of fiscal year 1990. The first PACE-90 problem was specified to be calculations of "expected performance" of Yucca Mountain with respect to the release of radionuclides from a potential nuclear waste repository. The second exercise was measures of the "disturbed performance" of Yucca Mountain. A third exercise was requested to be "sensitivity studies." This report describes the calculations performed by WG 1 participants to satisfy the first PACE problem.

There were several objectives for this PA exercise: to demonstrate the development of computational capabilities by Yucca Mountain Project participants, to identify critical elements and processes within the numerical problems, and to demonstrate the ability of participants to work interactively. The latter objective was of particular importance; PACE-90 not only encouraged an interactive effort within the project community of computational modelers, but also created an environment where experts in data collection and interpretation could contribute to the analysis. The immediate result was a better-posed PACE problem. The long-term gain is that the modelers better understand the breadth of resources available within the Project, and have become accustomed to using them for solving practical problems. The exercises demonstrated progress toward a preliminary assessment of the postclosure repository-system performance.

The participants elected to perform groundwater flow and radionuclide transport problems similar in nature to those done

previously by several of the participants (Prindle and Hopkins, 1990; Carrigan et al.*; Birdsell and Travis, 1991; Eslinger et al., 1989). This was done to facilitate intercomparison of results with prior studies and to gain better understanding of the sensitivities inherent in different numerical and geological models. Thus, the expected-case problems were defined to be the transport of specific radionuclides by groundwater and by gaseous releases. The disturbed cases were defined to be groundwater-transport problems in which the geologic/hydrologic parameters were modified by volcanic intrusion, human intrusion and climate change. Sensitivity studies compared the effects of increased water-infiltration rates and different interpretations of the stratigraphy.

Previous hydrologic problems of this type used the limited geologic and hydrologic data available from the Yucca Mountain site. For this problem, the participants used these data and, as later sections explain in detail, also incorporated qualitative ("soft") data from Yucca Mountain and data from analogous sites. The computer codes available to the participants were not under quality assurance control. Not all the conceptual-model assumptions or alternatives that have been suggested by YMP researchers were considered in the development of the problems. Consequently, the PACE-90 problems were "scoping" in nature. Several constraints, such as lack of time and data, prevented the formulation of problems that would comprehensively model the conditions at Yucca Mountain (thus, only a limited subset of the radionuclide inventory was included in the transport calculations). Therefore, the PACE-90 analyses were not suffiently comprehensive to describe all the conditions that may be considered "expected" at Yucca Mountain. The analyses reflected a few realizations of a "nominal configuration" of a variably saturated sequence of bedded tuffs through which a limited number of radionuclides were transported by groundwater. These nominal-configuration analyses were only one component of the expected case.

* Carrigan, C. R., N. E. Bixler, P. L. Hopkins, and R. R. Eaton, in preparation. "COVE 2A Benchmarking Calculations using NORIA," SAND88-0942, Sandia National Laboratories, Albuquerque, NM.

Benchmarking of codes, answering questions on conceptual models, or providing a calculational representation of "reality" at Yucca Mountain were not the objectives of PACE-90. Benchmarking requires solution of a rigidly structured problem to test the numerical attributes of a code. This exercise set basic guidelines, but also allowed the flexibility of participants to incorporate modeling interpretations. The participants did not all calculate exactly the same problem. They all used the same input data and boundary conditions, but detailed problem specifications and interpretations of input data were left open. This was done partially so participants could take advantage of the strengths of individual codes. Consequently, the results were more a sensitivity study on the effects of variable interpretation of the input data by investigators than a code intercomparison. In a broad sense, these analyses could be considered verification efforts because similarity of results based on the same physical model calculated using different codes indicated that the codes were performing comparably. It also allowed use of various conceptual models. Conceptual-model validation and "realistic" calculations were not attempted, primarily because PACE-90 was intended to exhibit the development of computational tools. Without additional site-specific data, the assumptions on parameter values and conceptual models must be considered speculative. Thus, these results cannot be used for predictions regarding the suitability of Yucca Mountain as a potential nuclear waste repository.

This report presents the results of five participants' analyses of the nominal-configuration transport problem. The perturbed-configuration analyses and sensitivity studies are reported in Volume 2 of this document (in preparation).

2.0 PARTICIPANTS

The organizations from WG 1 that participated directly in the modeling efforts for groundwater transport of radionuclides were Los Alamos National Laboratory (LANL), Pacific Northwest Laboratory (PNL) and Sandia National Laboratory (SNL). Table 2-1 lists the participant organizations, the codes used, and the dimensionality of their analyses.

TABLE 2-1
LIST OF PACE-90 PARTICIPANTS

Participant	Hydrology Code	Transport Code	Dimensionality
Pacific Northwest Laboratory	SUMO	SUMO	2-D
Los Alamos National Laboratory	TRACRN	TRACRN	1-D
Sandia National Laboratories (Performance Assessment Development Division)	TOSPAC	TOSPAC	1-D
Sandia National Laboratories (Waste Management Systems Division)	DCM-3D	NEFTRAN	1-D
Sandia National Laboratories (Fluid Mechanics and Heat Transfer Division)	LLUVIA NORIA	LLUVA-S FEMTRAN	1-D 2-D

Lawrence Berkeley Laboratory participated in the WG 1 problems for gaseous transport of radionuclides. This work is reported elsewhere and will not be discussed here.

Contributions from WG 2 provided the radionuclide source term used in the transport calculations. Lawrence Livermore National Laboratory, Pacific Northwest Laboratory, University of California, Berkeley, Lawrence Berkeley Laboratory, and SAIC participated in this aspect of the problem.

3.0 STATEMENT OF THE PROBLEM

For the PACE-90 nominal-configuration analyses, a groundwater radionuclide-transport problem and a gas-transport problem were chosen. The groundwater-transport problem covered flow in the unsaturated (and locally saturated) zone to the water table. The gas-transport problem is reported separately from this document*.

The parameters of the groundwater radionuclide transport problem were (1) the physical extent of the rock volume through which the groundwater traveled, (2) the hydrogeologic properties of the rock strata, (3) the groundwater net infiltration rate, (4) the inventory and release rates of the radionuclides, and (5) the retardation and other geochemical interactions between the radioactive solutes and the surrounding rock. The groundwater-transport problem was roughly site-scale in physical extent.

The choice of dimensionality for the analyses was left to the modelers; some were done in one dimension, some were done in two dimensions, and some in a combination of one and two dimensions. The radionuclides to be transported were selected to be representative of various "classes" of nuclides in the waste inventory, (i.e., long half-life, highly sorbing, nonsorbing, solubility-limited, etc). The requested outputs were the radionuclide releases at the water table (or at the "accessible environment," for those who took the analysis that far). A steady-state water flux for 100,000 years was specified, although some analyses were taken to one million years. This detailed set of parameters was formulated to make the problem as specific as possible. As explained in Chapter 4, however, all participants did not elect to use exactly the same parameters in their analyses.

* Light, W. B., E. D. Zwahlen, T. M. Pigford, P. L. Chambre, and W. W.-L Lee, in preparation. "C-14 Release and Transport from a Nuclear Waste Repository in an Unsaturated Medium," LBL-28923, Lawrence Berkeley Laboratory, Berkeley, CA.

3.1 Hydrology and Stratigraphy

3.1.1 Modeled Region

The region selected for simulation modeling encompassed only a portion of Yucca Mountain. The results of this exercise were not intended to provide a complete total-system performance assessment of the potential repository; therefore, analysis of the entire repository was not specified. However, the region did contain a representative range of conditions that will eventually be included in performance-assessment models. The modeled region was located in the northeastern quadrant of the potential repository and was bounded by four drill holes (Figures 3-1 and 3-2). It extended from the top of the Topopah Spring Member down to the water table. This region did not encompass the accessible environment. However, some of the participants made an independent decision to extend the problem to include the accessible environment. The extent and location of the modeled region were selected because (1) this region was bounded by four drill holes (G-1, G-4, H-1, and UE-25a #1), from which site-specific lithologic and hydrogeologic data were available; (2) it extended beyond the boundaries of the potential repository, permitting simulation of lateral flow into and out of the repository, as well as vertical flow through the repository; and (3) it included a segment of the Ghost Dance Fault, which intersected the region (Figure 3-2) that was used in 2-D analyses to define one of the problem boundaries. For this simplified calculation, the fault region was modeled as having no physical properties different from those of the surrounding rock. However, the fault was included because some models have indicated that faults have a significant effect on groundwater flow. In future PA problems, we expect to model the same region, and include more realistic fault properties in order to determine the effect of a fault on groundwater flow.

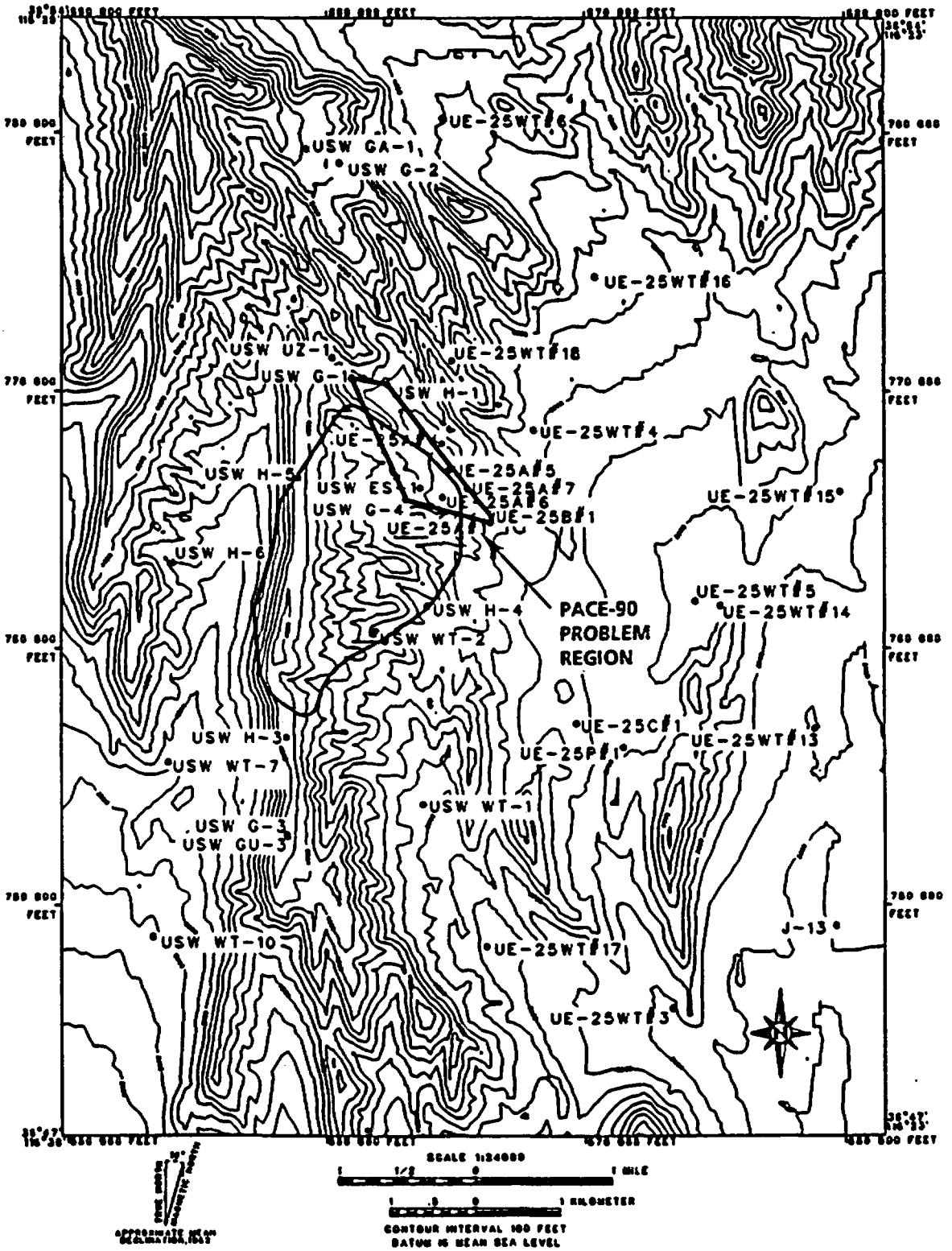

Figure 3-1
Site of Potential Repository at Yucca Mountain,
Showing Repository Boundary and Modeled Region

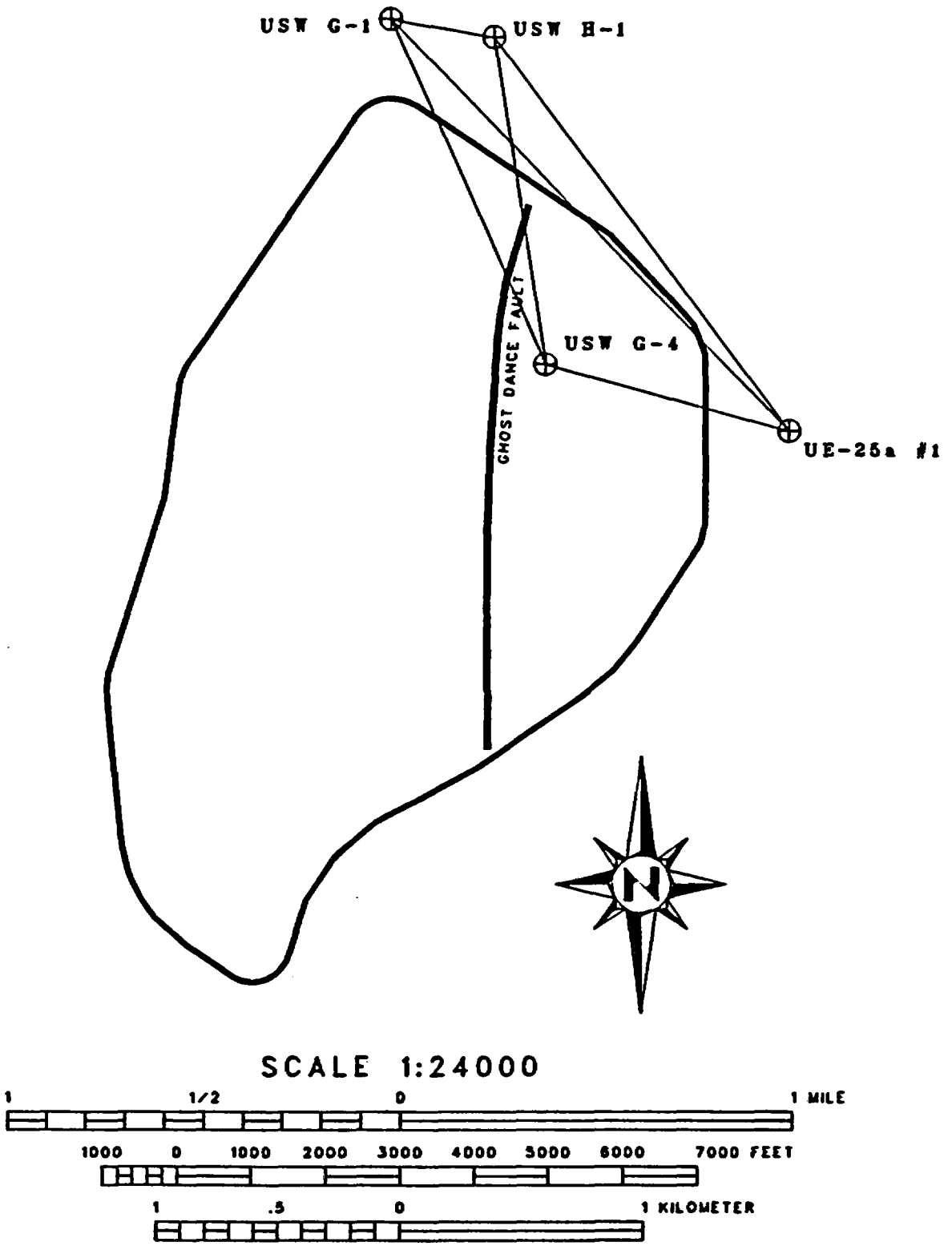

Figure 3-2
Location of Boundaries of PACE-90 Problems
Superimposed on Boundaries of Potential Repository

3.1.2 Geology

3.1.2.1 Stratigraphy

The units within the modeled region were Miocene (~12 - 14 my BP) silicic ash-flow tuffs and related tuffaceous rocks (Byers et al., 1976). The major stratigraphic units in the modeled region were the Paintbrush Tuff, the tuffaceous beds of the Calico Hills, and the Prow Pass Member of the Crater Flat Tuff. The Paintbrush Tuff is subdivided into four members: the Tiva Canyon, the Yucca Mountain, the Pah Canyon, and the Topopah Spring. The potential repository occurs in the lower portion of the Topopah Spring Member. The location of these geologic units within the two cross-sections used for simulation modeling is illustrated in Figures 3-3 and 3-4. The Topopah Spring Member comprised three distinct cooling units. Although each cooling unit was composed of multiple depositional layers, those individual layers cooled together to form a single unit. A large range in the degree of welding is observed within the Topopah Spring Member, from vitrophyric to nonwelded. Most of the underlying Calico Hills Formation was deposited at much lower temperatures, and some of the rocks in the section are reworked, older tuffs. As a result, the Calico Hills tuffs exhibited a much-decreased degree of welding in comparison to the Topopah Spring Member. The Prow Pass Member, in the lowermost part of the modeled region, consisted of nonwelded to partially welded tuffs similar to portions of the Topopah Spring Member. Alternation of welded and non-welded layers within the modeled region provided the vertical control on the distribution of physical and mechanical properties. Thus, a stratigraphy based on the geohydrologic properties of the rock was used for this modeling exercise, rather than one based on the genesis of an eruptive sequence. Use of geohydrologic properties for defining a hydrostratigraphy is discussed in the next section.

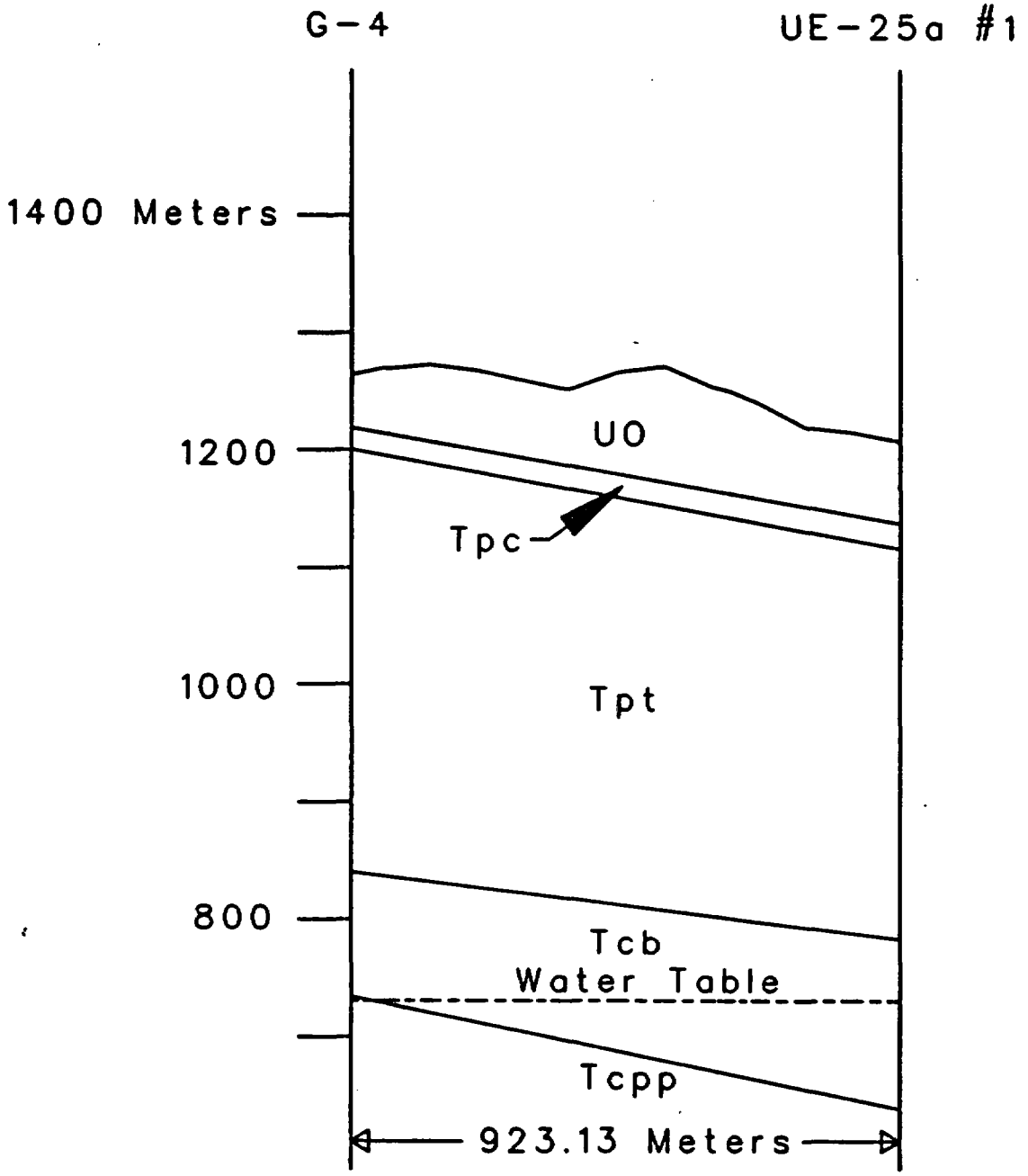

UO = Undifferentiated Overburden
Tpc = Paintbrush Tuff, Pah Canyon Member
Tpt = Topopah Spring Member
Tcb = Tuffaceous Beds of Calico Hills
Tcpp = Crater Flat Tuff, Prow Pass Member

Figure 3-3
Cross-Section of G-4 to UE-25a #1

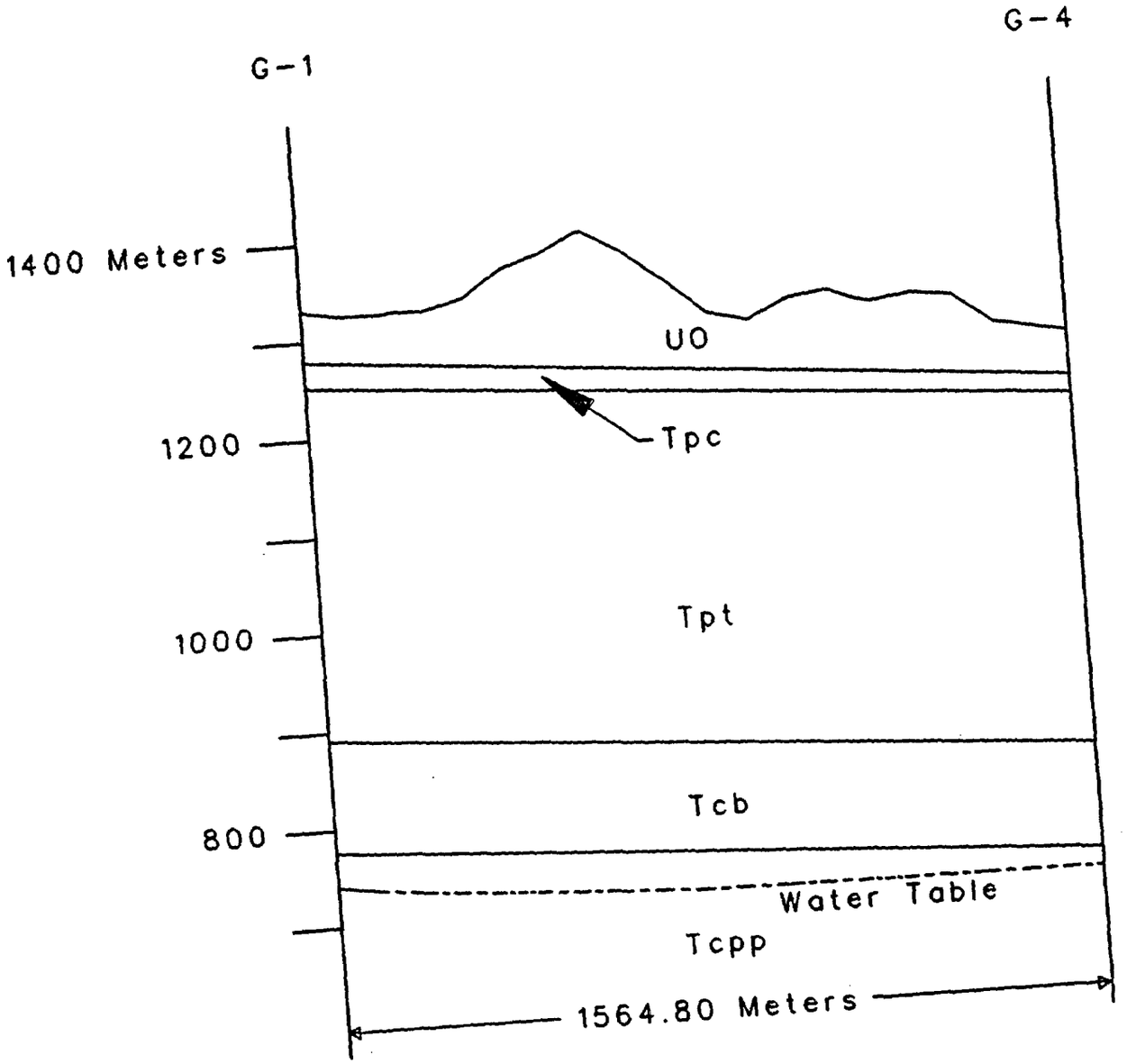

UO = Undifferentiated Overburden
Tpc = Paintbrush Tuff, Pah Canyon Member
Tpt = Topopah Spring Member
Tcb = Tuffaceous Beds of Calico Hills
Tcpp = Crater Flat Tuff, Prow Pass Member

Figure 3-4
Cross-Section of G-4 to G-1

All the units dipped approximately ten degrees southeast. Thus, the apparent dip in the north-south section (Figure 3-3) was to the south, and the apparent dip in the east-west section (Figure 3-4) was to the east. The elevation of the water table was variable in the region; it ranged from 730 m at G-4 to 746 m at G-1. Because of the dip of the units, the water table within the modeled region intersected both the Prow Pass and Calico Hills units.

3.1.2.2 Fracturing

The block containing the potential repository includes fractures, faults, and fault zones with varying degrees of offset (e.g., Carr, 1984; SNL, 1987). The sense of offset along these faults is both horizontal and vertical. The faults may alter the hydrogeologic properties of the adjacent rocks by fracturing and brecciation. The fault planes themselves may serve as barriers to lateral groundwater flow and/or pathways for vertical flow. Also, flow paths might be altered by the offset of originally continuous units by fault motion. There is evidence from 3-D modeling that the simple change in conductivity across a fault may be sufficient to cause major diversion of groundwater flow*.

The presence (or absence) of faults was extrapolated from observations at the surface; few data exist regarding the subsurface extent or hydrogeologic characteristics of the faults. Accordingly, no attempt was made to describe the nature and extent of faulting within the modeled region. However, the Ghost Dance Fault, one of the larger faults intersecting the potential repository area, occured within the modeled region. As discussed previously, no specific hydrogeologic characteristics were assigned to the Ghost Dance Fault. It was modeled as a lateral boundary on the 2-D cross-sections.

* Birdsell, K., K. Campbell, K. Eggert, and B. Travis, "Interim Report: Sensitivity Analysis of Integrated Radionuclide Transport Based on a Three-Dimensional Geochemical/Geophysical Model", Los Alamos National Laboratories report, in preparation.

3.1.3 PACE-90 Hydrostratigraphy

3.1.3.1 Definition of the Hydrostratigraphic Zones

Geologic, lithologic, and hydrogeologic data were used to delineate hydrostratigraphic zones. They were defined so that the hydrogeologic properties could be considered uniform within a single zone, for the purposes of the PACE-90 modeling. A summary of the geologic and hydrologic characteristics of these zones is presented in Table 3-1. The hydrologic characteristics in the table were based on very limited data, and at best only represent the general nature of each zone. The location of these zones, and the corresponding properties, are presented in Tables 3-2 and 3-3. Table 3-4 lists the locations of the drill holes and the repository boundaries pertinent to the PACE problem.

The definition of the stratigraphy of Yucca Mountain tuffs is typically based on either lithologic or depositional characteristics (e.g., Byers et al., 1976; Scott and Bonk, 1984), as discussed above. A prior study defined a "stratigraphy" that was used primarily to understand the thermal/mechanical properties of the tuffs (Ortiz et al., 1985), although it has also been used as a basis to perform hydrologic calculations. The thermal/mechanical hydrostratigraphy was defined using the lithology, grain density, and porosity of the rock section. The resulting stratigraphy contained 16 units within a 1250-m-thick section.

TABLE 3-1

HYDROSTRATIGRAPHIC ZONES WITHIN YUCCA MOUNTAIN

Symbol	Hydrostratigrahic Zone Description	Significant Geologic Characteristics	Relationship of Vertical to Horizontal Conductivity
UO	Includes alluvium, and Tiva Canyon and Yucca Mtn. Member of Paint-brush Tuff		
Tpc-TN	Ash-flow, non-welded	few fractures, high pumice content, zeolitic	$K_V < K_h$
Tpc-BT	Bedded tuff (reworked ash fall)	few fractures, high pumice, bedded, well-sorted sandstone, zeolitic	$K_V << K_h$
Tpt-TM	Ash-flow, moderately welded, non-lithophysal	highly jointed and fractured, non-zeolitic	$K_V >> K_h$ in fractures $K_V = K_h$ in matrix
Tpt-TD	Ash-flow, densely welded, non-lithophysal	moderately jointed, highly brec-ciated and fractured, vapor-phase mineralization, non-zeolitic	$K_V >> K_h$
Tpt-TDL	Ash-flow, densely welded, lithophysal	limited to no jointing or fracturing, abundant lithophysae, zeolitic	$K_V = K_h$
Tpt-TML	Ash-flow, moderately welded, lithophysal	highly jointed and fractured, zeolitic	$K_V > K_h$ in fractures $K_V = K_h$ in matrix
Tpt-TM	Ash-flow, moderately welded, non-lithophysal	jointed and fractured, non-zeolitic	$K_V >> K_h$ in fractures $K_V = K_h$ in matrix
Tpt-TV	Ash-flow, densely welded, vitrophyre	non-zeolitic, highly jointed and fractured	$K_V > K_h$
Tpt-TNV	Ash-flow, non-welded, vitric	few fractures, non- to partially-welded, non-zeolitic	$K_V = K_h$
Tpt-TN	Ash-flow, non-welded	few fractures, zeolitic	$K_V = K_h$
Tcb-TN	Ash-flow, non-welded	few fractures, zeolitic	$K_V = K_h$
Tcb-BT	Bedded tuff (reworked ash-fall)	few fractures, high pumice content, bedded, well-sorted sandstone, zeolitic	$K_V << K_h$
Tcpp-TN	Ash-flow, non-welded	few fractures, zeolitic	$K_V = K_h$
Tcpp-TP	Ash-flow, partially to moderately welded	slightly fractured, non-zeolitic	$K_V = K_h$

K_V = vertical component of hydraulic conductivity
K_h = horizontal component of hydraulic conductivity

TABLE 3-2

HYDROGEOLOGIC PROPERTIES AT DRILL HOLES G-1 AND H-1

Unit	Porosity (Total)	Bulk Density (g/cm^3)	K_s (Total) (m/s)	Van Genuchten Coefficients — Alpha (m^{-1})	Beta	S_r	Grain Density (g/cm^3)	Elevation at Base of unit — G-1 (m)	H-1 (m)
UO(a)	***	***	***	***	***	***	***	1280.2	1241.8
Tpc-TN	0.50	1.14	$2.0x10^{-11}$	0.004	1.50	0.15	***	1264.5	1225.1
Tpc-BT	0.22	1.95	$2.4x10^{-06}$	0.016	10.00	0.10	2.45	1253.8	1217.8
Tpt-TM	0.10	2.30	$2.0x10^{-11}$	0.005	1.90	0.10	2.57	1243.2	1207.1
Tpt-TD	0.06	2.45	$5.0x10^{-12}$	0.004	2.00	0.15	***	1191.9	1167.2
Tpt-TDL	0.18	2.06	$2.0x10^{-12}$	0.005	1.52	0.00	***	1084.7	1048.6
Tpt-TML	0.12	2.23	$2.0x10^{-11}$	0.005	1.52	0.00	2.50	959.7	923.7
Tpt-TM	0.08	2.30	$2.0x10^{-11}$	0.005	1.49	0.00	2.53	933.2	895.9
Tpt-TV	0.04	2.32	$4.0x10^{-11}$	0.005	1.46	0.00	2.38	916.4	883.7
Tpt-TNV	0.33	1.59	$3.0x10^{-10}$	0.020	4.00	0.20	***	900.6	852.6
Tpt-TN	0.36	1.57	$3.0x10^{-12}$	0.020	1.20	0.00	2.35	897.8	850.5
Tpt-BT	0.24	2.00	$7.0x10^{-12}$	0.003	1.65	0.06	***	891.1	843.8
Tcb-TN	0.36	1.57	$2.0x10^{-11}$	0.005	1.37	0.00	2.28	856.4	809.1
Tcb-BT	0.24	2.00	$7.0x10^{-12}$	0.003	1.65	0.06	2.32	855.8	808.5
Tcb-TN	0.36	1.57	$2.0x10^{-11}$	0.005	1.37	0.00	2.28	850.9	803.6
Tcb-BT	0.24	2.00	$7.0x10^{-12}$	0.003	1.65	0.06	2.32	850.2	802.9
Tcb-TN	0.36	1.57	$2.0x10^{-11}$	0.005	1.37	0.00	2.28	846.9	799.6
Tcb-BT	0.24	2.00	$7.0x10^{-12}$	0.003	1.65	0.06	2.32	846.6	799.3
Tcb-TN	0.36	1.57	$2.0x10^{-11}$	0.005	1.37	0.00	2.28	796.3	749.0
Tcb-BT	0.24	2.00	$7.0x10^{-12}$	0.003	1.65	0.06	2.32	776.2	736.8
Tcpp-TN	0.28	1.60	$4.0x10^{-11}$	0.006	1.48	0.00	2.33	767.7	729.8
Tcpp-TN	0.28	1.60	$2.0x10^{-11}$	0.020	1.40	0.00	2.33	746.3	693.2
Tcpp-TP	0.25	1.90	$2.0x10^{-09}$	0.010	2.70	0.05	2.59	715.9	601.2

(a) Data for this interval are generally sparse and are not tabulated
*** = no data available

TABLE 3-3

HYDROGEOLOGIC PROPERTIES AT DRILL HOLES G-4 AND UE-25A #1

Unit	Porosity (Total)	Bulk Density (g/cm^3)	K_S (Total) (m/s)	Van Genuchten — Coefficients — Alpha (m^{-1})	Beta	S_r	Grain Density (g/cm^3)	Elevation at — Base of unit — G-4 (m)	UE-25 a#1 (m)
UO(a)	***	***	***	***	***	***	***	1219.2	1137.7
Tpc-TN	0.50	1.14	$2.0x10^{-11}$	0.004	1.5	0.15	***	1212.2	1127.1
Tpc-BT	0.22	1.95	$2.4x10^{-06}$	0.016	10.0	0.10	2.45	1200.6	1116.4
Tpt-TM	0.10	2.30	$2.0x10^{-11}$	0.005	1.9	0.10	2.57	1183.2	1093.6
Tpt-TD	0.06	2.45	$5.0x10^{-12}$	0.004	2.0	0.15	***	1148.2	1073.7
Tpt-TDL	0.08	2.40	$2.0x10^{-12}$	0.003	1.8	0.10	***	1082.9	1006.4
Tpt-TML	0.12	2.25	$2.0x10^{-11}$	0.010	1.7	0.05	2.50	930.2	871.1
Tpt-TM	0.10	2.30	$2.0x10^{-11}$	0.005	1.9	0.10	2.53	868.6	810.7
Tpt-TV	0.04	2.25	$3.0x10^{-12}$	0.002	1.7	0.00	2.38	860.1	797.3
Tpt-TNV	0.20	1.90	$2.4x10^{-06}$	0.030	2.2	0.15	***	850.9	787.2
Tpt-TN	0.36	1.54	$3.0x10^{-12}$	0.020	1.2	0.00	2.35	841.2	784.2
Tpt-BT	0.23	1.79	$2.0x10^{-11}$	0.002	1.6	0.10	2.32	840.6	783.3
Tcb-TN	0.36	1.54	$1.0x10^{-11}$	0.004	1.5	0.15	2.28	836.0	776.9
Tcb-BT	0.23	1.79	$2.0x10^{-11}$	0.002	1.6	0.10	2.32	835.4	775.9
Tcb-TN	0.36	1.54	$1.0x10^{-11}$	0.004	1.5	0.15	2.28	829.0	743.9
Tcb-BT	0.23	1.79	$2.0x10^{-11}$	0.002	1.6	0.10	2.32	826.3	739.1
Tcb-TN	0.36	1.54	$1.0x10^{-11}$	0.004	1.5	0.15	2.28	794.6	716.5
Tcb-BT	0.23	1.79	$2.0x10^{-11}$	0.002	1.6	0.10	2.32	793.7	715.6
Tcb-TN	0.36	1.54	$1.0x10^{-11}$	0.004	1.5	0.15	2.28	750.4	653.4
Tcb-BT	0.23	1.79	$2.0x10^{-11}$	0.002	1.6	0.10	2.32	733.3	639.4
Tcpp-TN	0.28	1.60	$5.0x10^{-12}$	0.001	3.0	0.20	2.33	730.6	630.3
Tcpp-TN	0.28	1.60	$1.0x10^{-11}$	0.004	1.6	0.15	2.33	721.4	604.4
Tcpp-TP	0.25	1.90	$5.0x10^{-08}$	0.010	2.7	0.05	2.59	660.5	584.9

(a) Data for this interval are generally sparse and are not tabulated
*** = no data available

TABLE 3-4

LOCATIONS AND ELEVATIONS OF DRILL HOLES

Drill hole	Easting (m)	Northing (m)	Surface Elevation (m)	Elevation of Water Table (m)	Elevation of Repository Horizon (m)
USW G-1	170992.9	234848.5	1325.5	746.3	***
USW H-1	171415.9	234773.5	1302.8	731.4	***
USW G-4	171627.3	233417.9	1270.1	730.6	960-965
UE-25a #1	172623.5	233141.6	1198.7	728.8	***
Repository Boundary Contacts:					
G-1 to G-4	171200.0	234383.0	***	741.2	985-990
G-4 to UE-25	172285.0	233235.0	***	729.4	920-925

*** - not applicable

The PACE-90 modelers believed that the distribution of hydrogeologic properties based on the thermal/mechanical stratigraphy was inadequate. A different method was to capture the hydrologic properties of the rock mass, and thus provide the basis for a more realistic model of groundwater percolation flux on the scale of the site. A more detailed stratigraphy was developed for PACE-90, using data on the geologic and hydrogeologic characteristics of the tuffs within the modeled region. The information used to define the PACE stratigraphy included data on lithology, porosity, grain and bulk density, saturated hydraulic conductivity, fracture conductivity, and moisture-retention characteristics obtained from drill holes in the area. As a result, the PACE stratigraphy delineated 19 units within a 600-m-thick section. Figure 3-5 compares the thermal/mechanical and PACE-90 stratigraphies.

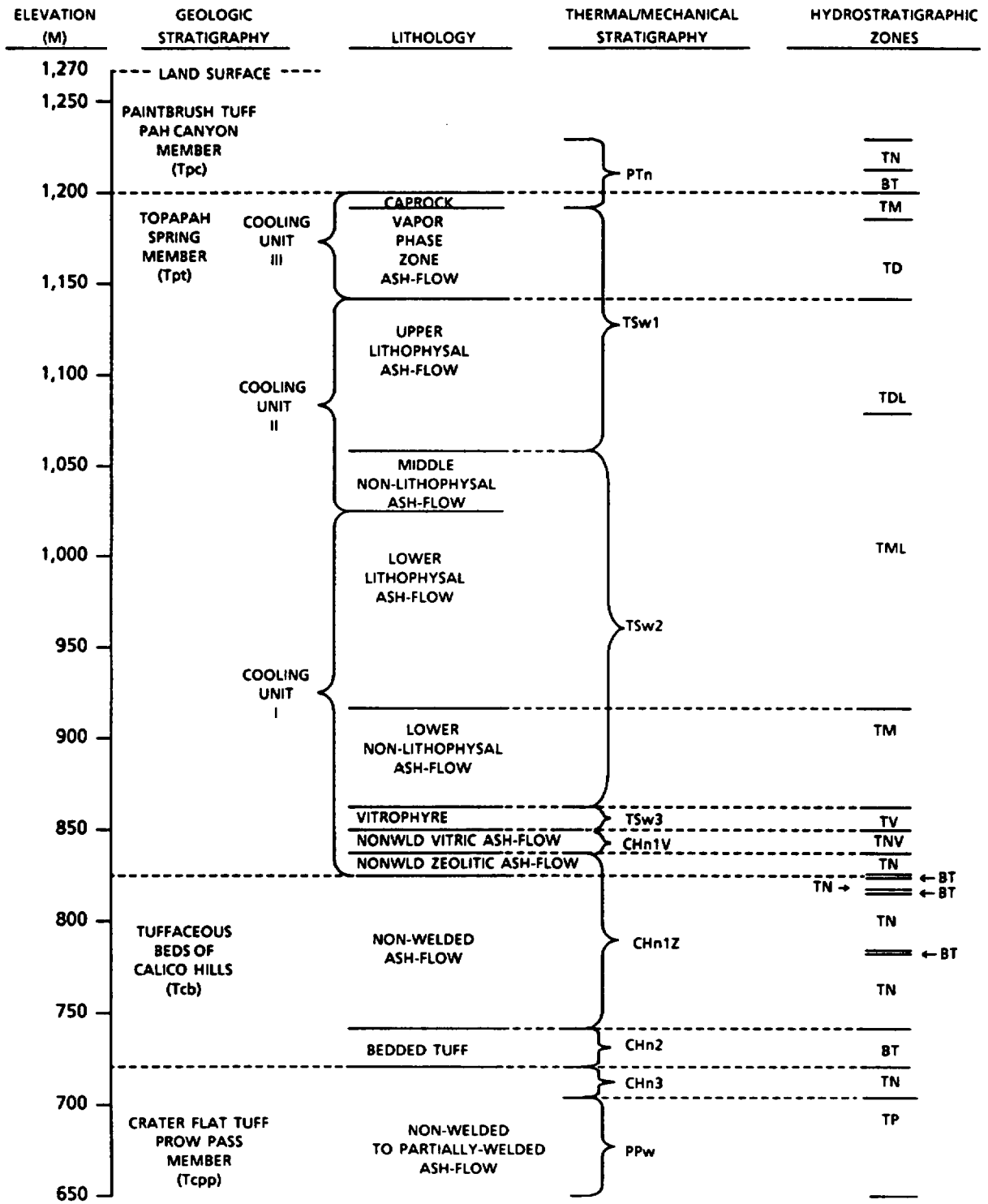

Figure 3-5
Relationship of Stratigraphy, Lithology and Hydrostratigraphic Zones at G-4

Several steps were used to develop the PACE-90 hydrostratigraphy. The initial step was to divide the tuffs into lithologic-stratigraphic units. Then the units were further subdivided into layers having similar geologic characteristics. The characteristics used to distinguish among layers included degree of welding, size and amount of pumice and lithic fragments, composition and amount of phenocrysts, extent of vapor-phase recrystallization, presence of zeolitization, extent of devitrification, lithophysal content, reworking of fragments, and formation of bedding. Individual candidate zones were categorized as being densely, moderately, or non-welded tuffs, or as bedded tuffs. Finally, the exact boundary locations between adjacent zones were determined by the changes in porosity. Although porosity varied within each zone by as much as 30 percent, the mean values between adjacent zones varied by a greater amount.

3.1.3.2 Hydrogeologic Data Sources

Lithologic data were available for core samples collected in drill holes G-1 (Bish et al., 1981), G-4 (Bentley, 1984), H-1 (Rush et al., 1983), and UE-25a #1 (Spengler et al., 1979). Table 3-5 shows from which drill holes the different types of data used to define the PACE-90 hydrostratigraphy were derived. Many geologic characteristics, such as degree of welding, had a direct effect on hydrogeologic characteristics. As the welding increased, the intrinsic porosity typically decreased, reducing the saturated matrix hydraulic conductivity. However, fracturing generally increased with increased welding. Other geologic characteristics, such as recrystallization or devitrification had an indirect effect on hydrogeologic characteristics, perhaps affecting the pore size distribution and related moisture retention. Extensive mineralogical analyses were conducted on these core samples (e.g., Bish and Chipera, 1989). These mineralogic data were not used in delineating these units. However, these data could potentially be used to better define the units and to extrapolate the hydrogeologic characteristics to other similar units.

TABLE 3-5

DATA SOURCES FOR PACE-90 HYDROSTRATIGRAPHY

DATA TYPE	DRILLHOLE G-1	G-4	H-1	UE-25a#1
Geologic contacts	XX	XX	XX	XX
Physical characteristics	XX	XX		XX
Hydraulic conductivity	XX	XX		
Moisture retention		XX		
Fracture density		XX		XX

Table 3-6 summarizes the lithology of drill hole G-4, based on the descriptions of core samples in Bentley, 1984. This lithology was essentially the same as that observed in drill holes G-1, H-1, and UE-25a. The primary differences were associated with the thicknesses and with the degree of welding of the various layers.

A limited data base of hydrogeologic properties was constructed from core samples collected in the drill holes that formed the boundaries of the modeled region. These data consisted of porosity, bulk density, grain density, saturated hydraulic conductivity (measured under confined and unconfined conditions), fracture conductivity, and moisture-retention characteristics (Peters et al., 1984). Although both confined and unconfined values were reported, only the unconfined values were used to develop the hydrogeologic description used here. Van Genuchten coefficients (alpha and beta) (van Genuchten, 1980) and the residual saturation were obtained from regression analyses of the moisture-retention characteristics.

TABLE 3-6

SUMMARY OF LITHOLOGY, DRILL HOLE G-4

Stratigraphy and Lithologic Description	Thickness of Interval (m)	Depth to bottom of Interval (m)
Paintbrush Tuff		
Tiva Canyon Member	20.0	20.0
Yucca Mountain Member	31.3	51.3
Pah Canyon Member		
Non-welded, ash-fall and bedded tuffs, vitric	18.2	69.5
Topopah Spring Member		
Moderately to densely welded tuffs; devitrified; rare lithophysae; 3-20 percent phenocrysts	52.5	122.0
Moderately to densely welded tuffs; devitrified; up to 30 percent lithophysal cavities	217.0	339.0
Moderately welded tuff; devitrified, but partially vitric; rare to no lithophysal cavities; pumice; less than 5 percent phenocrysts	62.0	401.0
Densely welded vitrophere, black, glassy; 1-2 percent phenocrysts; numerous fractures	9.0	410.0
Non- to moderatelywelded ash-flow, vitric	9.9	419.9
Non- to partially welded ash flow, zeolitized; zeolitized bedded tuff at base, primarily pumice	9.7	429.6
Tuffaceous Beds of Calico Hills		
Non-welded ash-flow tuff; primarily zeolitic; contains bedded tuff layers 0.5 to 3 m thick composed primarily of pumice	90.2	519.8
Ash-fall bedded tuff, reworked (tuffaceous sandstone), zeolitic; high pumice content	17.1	536.9
Crater Flat Tuff, Prow Pass Member		
Non- to partially welded ash-flow tuff; zeolitic; 5-10 percent phenocrysts	10.6	547.5
Partially welded ash-flow tuff, devitrified; pumice; up to 7 percent phenocrysts	48.3	595.8

Additional data on saturated conductivity, porosity, and bulk density have been reported in the Site and Engineering Properties Data Base (SEPDB, 1989). Data from the SEPDB were used to augment information from Peters et al. (1984). The extrapolation of the conductivity of an individual fracture to an estimate of the fracture conductivity of the bulk rock required an estimate of fracture aperture and density. For this report, the values used for fracture apertures were those reported by Peters et al. (1984). Fracture densities were estimated from drilling logs (Spengler et al., 1979).

The Reference Information Base (RIB) contains data for some of the parameters listed above; however, input values were not taken from the RIB. RIB values are often averages, or are derived in other ways from the raw data. The intent of this exercise was to try to use parameter values as close to the observed values as possible, despite the likely increase in variability of the data. The values used for the PACE-90 hydrostratigraphy are appropriate for, and will be included in, the RIB.

3.1.3.3 Discussion of Hydrogeologic Values

Only a limited number of hydrogeologic measurements have been performed on the cores from the four drill holes used in this study. Where values were available, they were applied throughout the modeled region to zones with similar geologic characteristics. Characterization of candidate zones with similar lithologic properties relied primarily on the measured moisture retention and saturated hydraulic conductivities. The moisture-retention curves for the various hydrostratigraphic zones are presented in Figures 3-6 to 3-9. Where there were no measured moisture-retention data available, data were extrapolated from similar zones, modified as necessary to account for differences in degree of welding. The hydrogeologic properties of fractures in each of these zones are presented in Table 3-7.

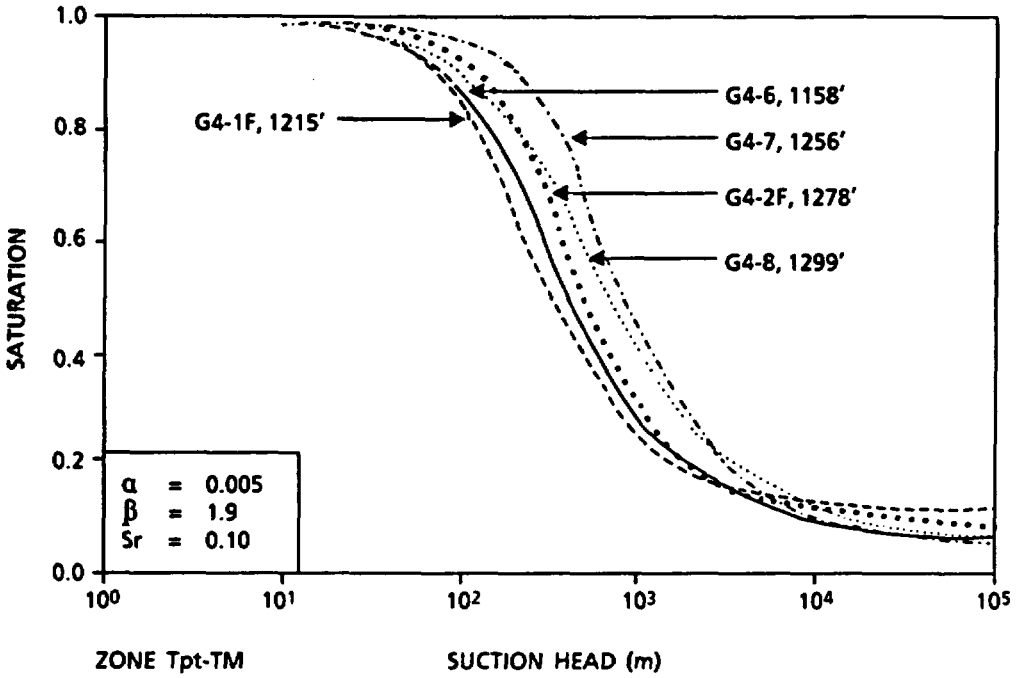

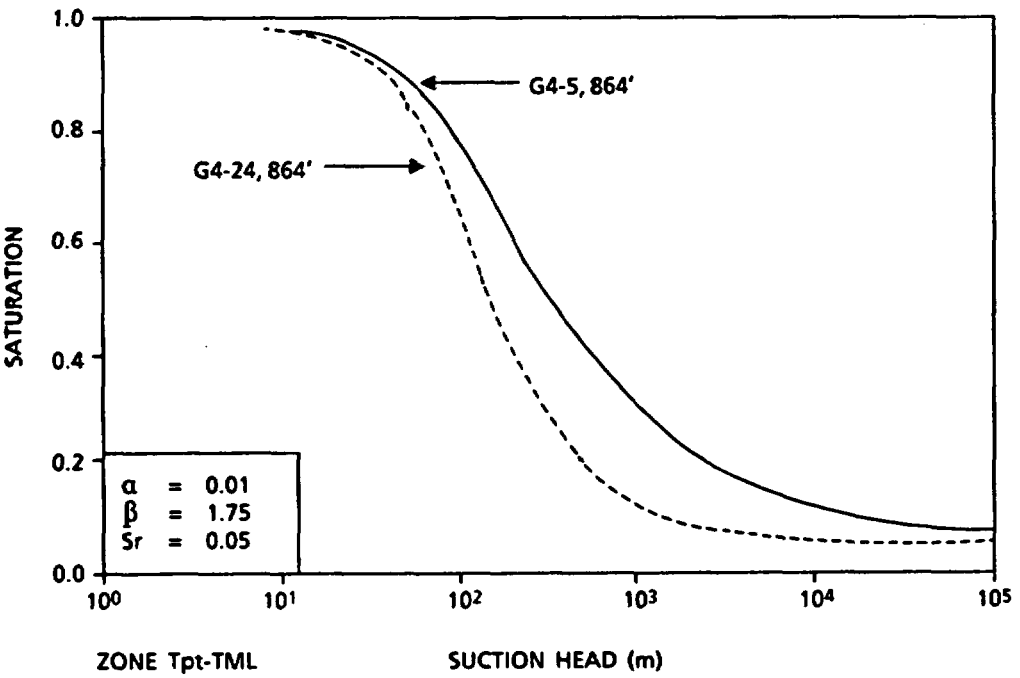

Figure 3-6
Moisture Retention Curves for Zones
Tpt-TM (top) and Tpt-TML (bottom)

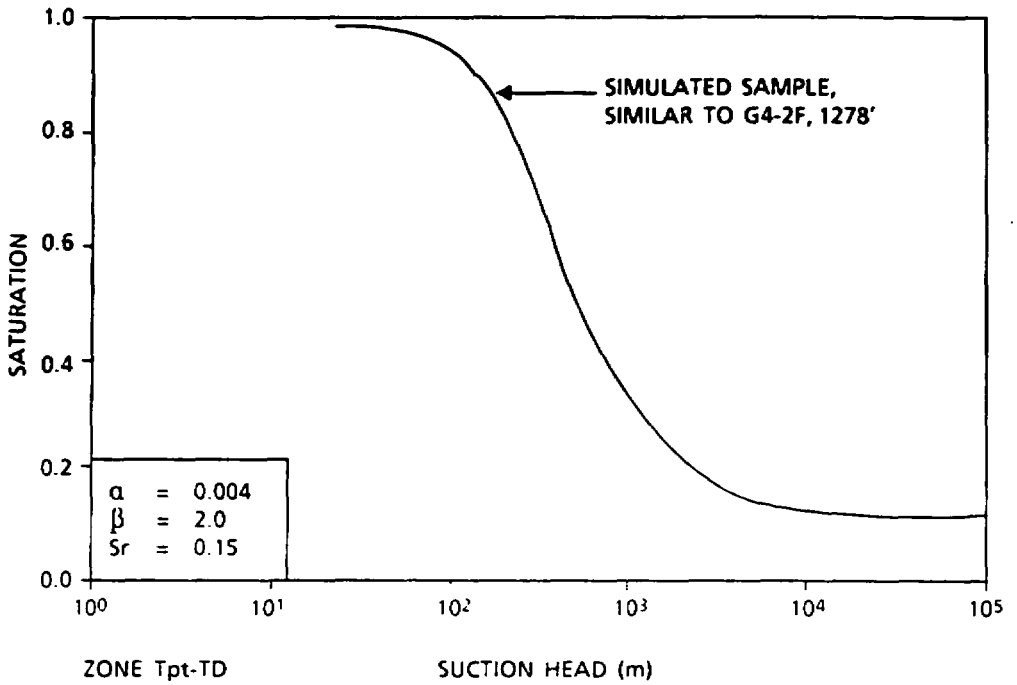

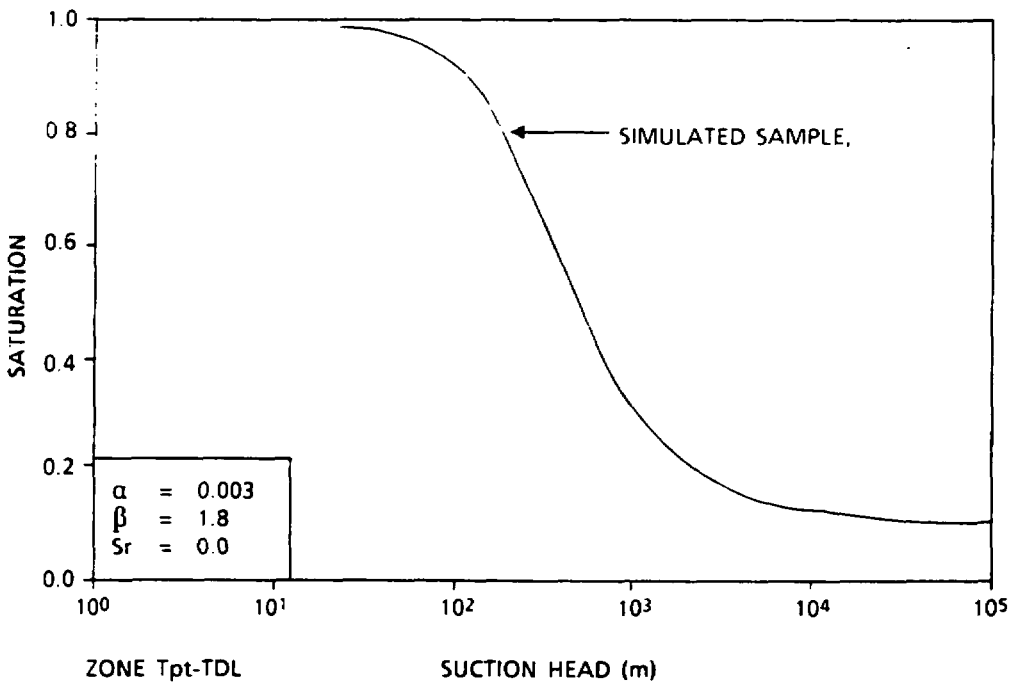

Figure 3-7
Moisture Retention Curves for Zones
Tpt-TD (top) and Tpt-TDL (bottom)

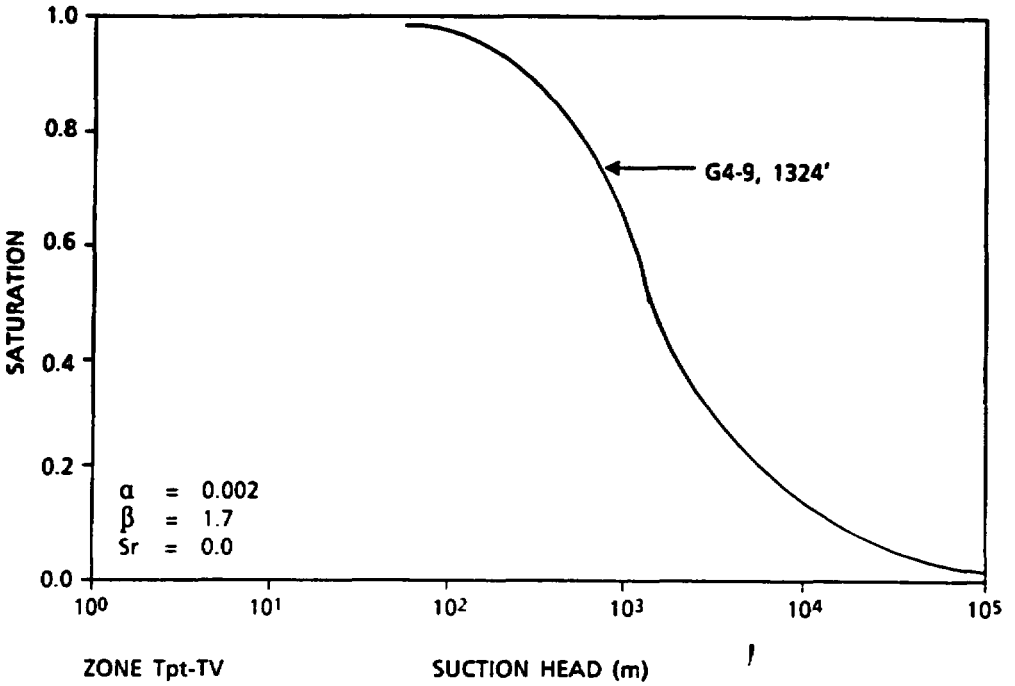

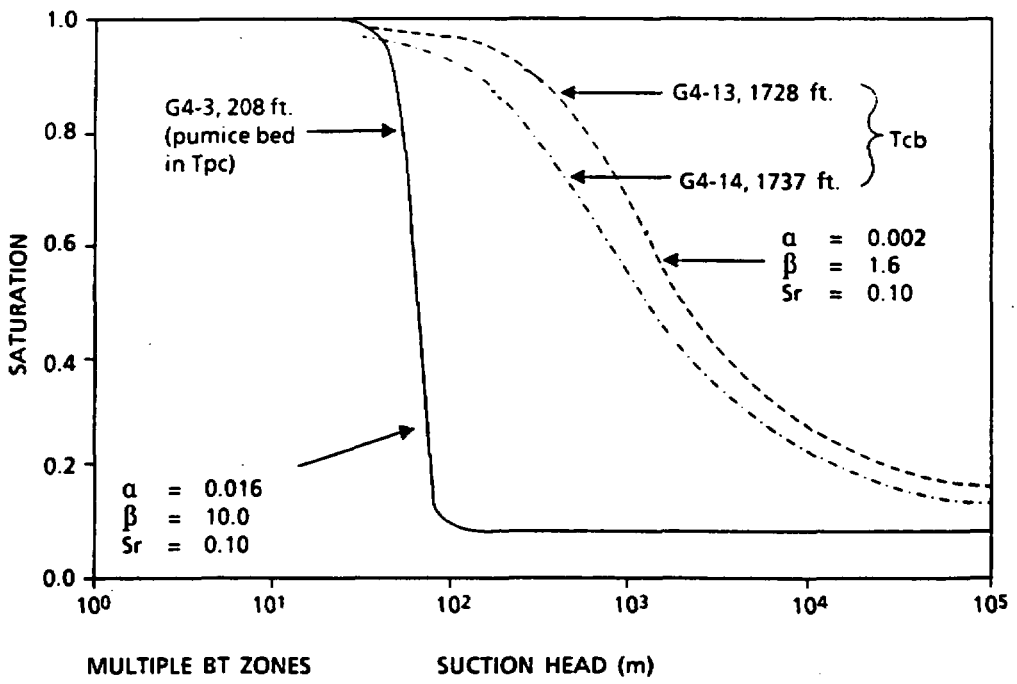

Figure 3-8
Moisture Retention Curves for Zones
Tpt-TV (top) and Multiple BT Zones (bottom)

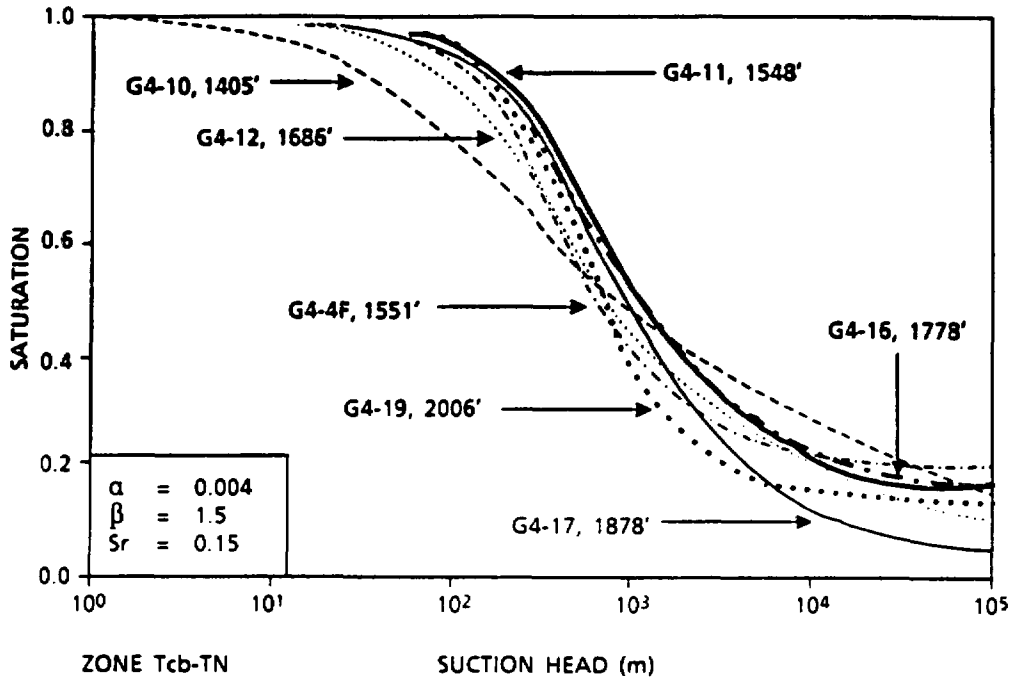

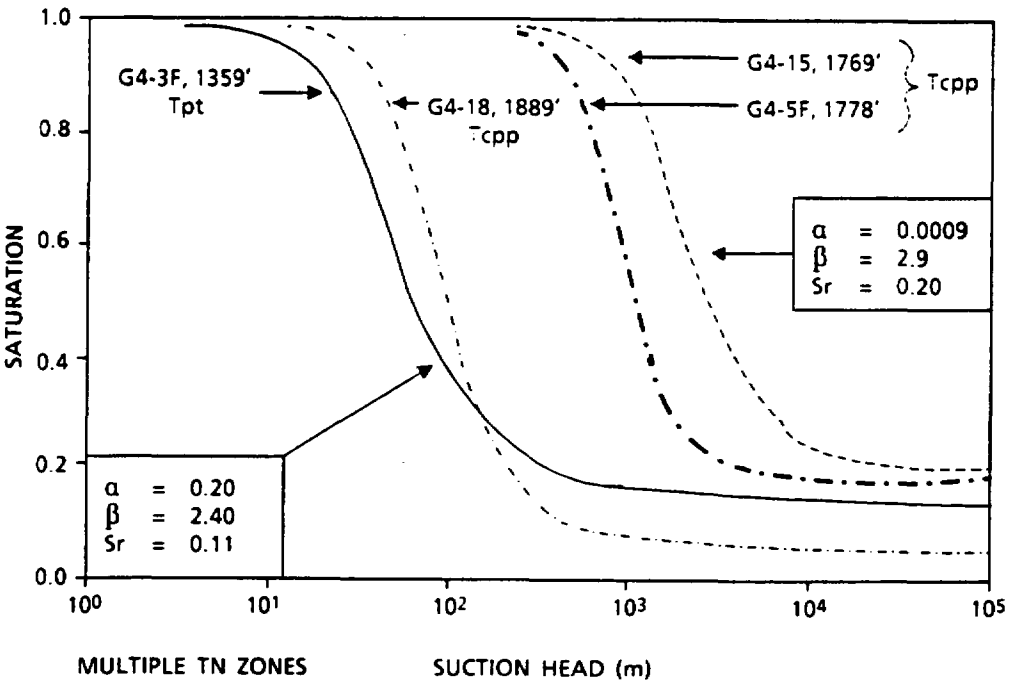

Figure 3-9
Moisture Retention Curves for Zones
Tcb-TN (top) and Multiple TN Zones (bottom)

TABLE 3-7

FRACTURE CHARACTERISTICS FOR PACE-90 HYDROSTRATIGRAPHY

Unit	$K_{f,s}$ (m/s)	Aperture (um)	Frequency (#/m3)	Porosity (volume fraction)	$K_{f,b}$ (m/s)
Tpt-TM	$4x10^{-5}$	6	5	$3.0x10^{-5}$	$1.2x10^{-09}$
Tpt-TD	$4x10^{-5}$	6	5	$3.0x10^{-5}$	$1.2x10^{-09}$
Tpt-TDL	$4x10^{-5}$	6	3	$1.8x10^{-5}$	$7.2x10^{-10}$
Tpt-TML	$4x10^{-5}$	6	5	$3.0x10^{-5}$	$1.2x10^{-09}$
Tpt-TM	$4x10^{-5}$	6	5	$3.0x10^{-5}$	$1.2x10^{-09}$
Tpt-TV	$4x10^{-4}$	20	10	$3.0x10^{-5}$	$8.0x10^{-08}$
Tpt-TNV	$4x10^{-4}$	22	3	$6.6x10^{-5}$	$2.6x10^{-08}$
Tpt-TN	$8x10^{-4}$	30	3	$9.0x10^{-5}$	$7.2x10^{-08}$
Tpt-BT	$3x10^{-5}$	6	3	$1.8x10^{-5}$	$5.4x10^{-10}$
Tcb-TD	$3x10^{-5}$	6	3	$1.8x10^{-5}$	$5.4x10^{-10}$
Tcb-BT	$3x10^{-5}$	6	3	$1.8x10^{-5}$	$5.4x10^{-10}$
Tcb-TN	$3x10^{-5}$	6	3	$1.8x10^{-5}$	$5.4x10^{-10}$
Tcb-BT	$3x10^{-5}$	6	3	$1.8x10^{-5}$	$5.4x10^{-10}$
Tcb-TN	$3x10^{-5}$	6	3	$1.8x10^{-5}$	$5.4x10^{-10}$
Tcb-BT	$3x10^{-5}$	6	3	$1.8x10^{-5}$	$5.4x10^{-10}$
Tcb-TN	$3x10^{-5}$	6	3	$1.8x10^{-5}$	$5.4x10^{-10}$
Tcb-BT	$3x10^{-5}$	6	3	$1.8x10^{-5}$	$5.4x10^{-10}$
Tcpp-TN	$3x10^{-5}$	6	3	$1.8x10^{-5}$	$5.4x10^{-10}$
Tcpp-TN	$3x10^{-5}$	6	3	$1.8x10^{-5}$	$5.4x10^{-10}$
Tcpp-TP	$4x10^{-4}$	20	3	$6.0x10^{-5}$	$2.4x10^{-08}$

$K_{f,s}$ = intrinsic fracture hydraulic conductivity
$K_{f,b}$ = bulk fracture hydraulic conductivity
Van Genuchten Coefficients (all fractures)

alpha = 1.28/m; beta = 4.23; S_r = 0.04

The van Genuchten coefficients shown in the figures represented a mid-range or average value of the coefficients (Peters et al., 1984). The greatest variability in the values of the van Genuchten parameters among the hydrostratigraphic zones was in the value of alpha. This parameter reflected the size of the larger pores in the material, decreasing as pore size decreased. The slope of the curves (beta) reflected the uniformity of pore-size distribution. More uniform materials (i.e., pore sizes restricted to a narrow range) had the steepest slopes. The value of the residual saturation, S_r, decreased roughly proportionally to the increase in size of the smallest pores.

Saturation coefficients of various bedded tuff zones varied considerably (Figure 3-8). Pumiceous beds, such as the Pah Canyon Member of the Paintbrush Tuff (Tpc), exhibited high values for alpha and beta. Considerable variability was also seen in the saturation coefficients of non-welded tuff zones (TN), (Figure 3-9).

An apparently anomalous value of 2.4×10^{-6} m/s is presented in Table 3-3 for the saturated conductivity of the Topopah Spring nonwelded zeolitic zone (Tpt-TNV) in drill hole G-4. A single value for the permeability of that zone was given by Peters et al. (1984); the value there (4.0×10^{-11}) was significantly lower than that presented in Table 3-3. Additional data contained in the SEPDB indicated that a value of 3.0×10^{-10} might be more appropriate for that layer. However, Peters et al. (1984) reported the measured value for that same zone in drill hole GU-3 as significantly higher (2.7×10^{-7}) and very similar to the measured value for Pah Canyon Member bedded tuff zone (Tpc-BT) (3.7×10^{-7}). Preliminary modeling reported by Dudley et al. (1988) proposed the use of the value measured in drill hole GU-3 for the layer identified as Tpt-TNV in this work. There was considerable variability in the permeability of this layer at various locations. To demonstrate the significance of this possible variability, it was decided that for drill hole G-4, a high value equal to that of the Tpc-BT layer would be used for Tpt-TNV; in drill hole G-1, a lower value of 3.0×10^{-10} would be used, consistent with the SEPDB data.

For some zones, such as the densely welded nonlithophysal (TD) and lithophysal (TDL) zones (Figure 3-7), no sample data were available to provide the van Genuchten coefficients. For the PACE-90 modeling, values for these coefficients were extrapolated from similar zones where data were available. Slight adjustments were made in the values of the parameters to account for expected differences in pore-size distributions. Thus, the values of parameters given in Figure 3-7, for Tpt-TD and Tpt-TDL, are similar to those for moderately welded Tpt-TM, but with lower values for alpha and higher values for S_r, reflecting assumed smaller pore sizes. These assumed values may not represent the correct values for these zones.

The assumption that correlations existed between model coefficients was not well supported by the sparse data from Yucca Mountain. Scoping studies by WG 3 indicated that stochastic models of flow might be sensitive to the correlation structure. Natural-analog data are being reviewed to determine possible correlation structures and other limits to the parameter space that could be used to constrain a stochastic model.

3.1.3.4 Variability and Uncertainty

The geologic data from the four drill holes were of comparable quality. However, some differences in qualitative interpretation for each drill hole might result in differences in lithologic data. Qualitative distinctions among the various units penetrated by the drill holes served as a major basis for distinction between hydrostratigraphic zones. Although this information was "soft data," it was meaningful and repeatable. The primary uncertainties resulted from the inherent variability of these properties within hydrostratigraphic zones, and from the scarcity of data. Often, a hydro- stratigraphic zone was represented by only one sample, so no estimate of variability was possible using statistical techniques. Where multiple values existed for a zone, a mean value was used. Where multiple data sets for moisture-retention characteristics existed, a mid-range curve was considered representative of that zone.

No estimate was made of the statistical variability among multiple data sets for a given zone, or between zones. The data were sufficiently sparse that no meaningful statistical distinctions could be expected among the various zones. An analysis of the statistical variability of moisture-retention data between the major thermal/mechanical units concluded that for most of the Topopah Spring and Calico Hills tuffs, there were no significant differences among the layers. Until sufficient data have been collected during the site-characterization process, there is no reason to believe that we can better estimate statistical variability. Figure 3-5 shows the greater number of subdivisions used in the PACE hydrostratigraphy compared with the number of

thermal/mechanical units. The use of so many zones reduced the data density for individual zones below that used elsewhere*, rendering the statistical comparison of individual zones even more difficult.

It is recognized that for all natural systems there are ranges of values associated with any parameter. The hydrologic flow and transport problem done for PACE-90 had many parameters, ranging from site physical and hydrological data to behavior of the source term. For each parameter the inherent uncertainty was reflected by a range of values, resulting in an n-dimensional parameter space. The nominal-case problem used one realization of values drawn from that parameter space using expert judgement. The Project participants recognized that comprehensive PA analyses must reflect the uncertainties in the conceptual models and in parameter data. A single analysis using specified data is unlikely to do this.

The tuffs above the water table at Yucca Mountain all originated in volcanic centers to the north and west of Yucca Mountain (Byers et al., 1976) at a distance of approximately 25 to 50 km from the repository area. Many of the properties of interest in the tuff units were directly related to the original thickness of the unit. Moving away from the source, the thickness of a unit could generally be expected to decrease gradually. Thus, the geologic (and related hydrogeologic) properties varied gradually with distance from the source. Properties were relatively similar over short distances, and could be interpolated between control points with some confidence. Eventual enhancement of qualitative information with quantitative data on mineralogical characteristics would reduce the uncertainties regarding the location of boundaries between zones and the correlation of zones between sampling locations.

* Rutherford, B. M., I. J. Hall, R. G. Easterling, R. R. Peters, and E. A. Klavetter, in preparation. "Statistical Analysis of Yucca Mountain Hydrological Data," SAND87-2380, Sandia National Laboratories, Albuquerque, NM.

3.2 Hydrogeological Modeling Data

A net water-infiltration rate of 0.01 mm/yr at the repository horizon was used for the nominal case. Three net infiltration rates were originally specified for the nominal-configuration problem: 0.01 mm/yr, 0.1 mm/yr, and 0.5 mm/yr. Review of preliminary solutions to the groundwater flow problem, using the hydrostratigraphy developed for PACE-90, showed that the two higher infiltration rates generated high matrix saturations that were inconsistent with the measured saturations in drill hole H-1. Therefore, to ensure internal consistency of the problem, the nominal-configuration problem was limited to the lowest infiltration rate. The two higher rates have been considered later as part of the perturbed-configuration problems. Other nominal configurations, with higher infiltration rates and different hydrogeologic properties, were investigated as part of the sensitivity studies.

3.3 Radionuclide Source Term

Several radionuclide source terms were provided by WG 2, and will be described in a summary document*. The WG 2 participants also individually reported on their source-term work (Apted et al., 1989; O'Connell, 1990; Pigford and Lee, 1989; Sadeghi et al., 1990a,b). This section summarizes the release scenarios and mechanisms that are described in detail in the WG 2 document.

The information provided was preliminary data for the time-dependent release rates of selected radionuclides from spent nuclear fuel in the engineered-barrier system (EBS) of a high-level-waste repository in unsaturated tuff. The radionuclides selected were ^{99}Tc, ^{129}I, ^{135}Cs, and ^{237}Np for groundwater transport. The source for gaseous transport, ^{14}C, has been modeled elsewhere and will not be discussed here.

* Apted, M. J., W. J. O'Connell, K. H. Lee, A. T. MacIntyre, T.-S. Ueng, T. H. Pigford, and W.W.-L Lee, in preparation. "Preliminary Calculations of Release Rates of Tc-99, I-129, Cs-135, and Np-237 from Spent Fuel in a Tuff Repository," Lawrence Berkeley Laboratory, Berkeley, CA.

The selection of these radionuclides was based on several considerations. Because one thousand years of complete containment was assumed, no short-lived nuclides (e.g., ^{90}Sr, ^{137}Cs) were considered. The half-lives for the selected radionuclides ranged from 215,000 years to 16,000,000 years. Fission products (^{99}Tc, ^{129}I, ^{135}Cs) and actinides (^{237}Np) were represented. Nuclides whose dissolution mechanisms were either solubility-limited (^{237}Np) or reaction-rate-limited were included. Furthermore, ^{129}I and ^{135}Cs had rapid-release fractions, as well as fractions controlled by alteration rate. Finally, these radionuclides represented a range of sorption properties, ranging from nonsorbing ^{129}I, to weakly sorbing ^{99}Tc and ^{237}Np, up to strongly sorbing ^{135}Cs.

Two primary processes (water-contact modes) were postulated for the mobilization of the waste by contact with groundwater: the "wet-drip" scenarios and the "moist-continuous" scenarios. For these modes, parametric variations, such as diffusion rate, alteration rate, and effective fuel surface area, provided different numeric values for source terms. The source terms used in these exercises were based on the release rates from individual containers which were convolved, with a distribution of failure times of all the containers in the repository.

3.3.1 Release by the Wet-Drip Scenarios

If the normal flow field of water percolating through the tuff surrounding a waste container has been disturbed, water might be diverted into fractures which intersect the emplacement hole. The design of the EBS assumed a 3-cm air gap between the container and the borehole wall, so water had to drip from the rock to reach the container. This water might drip onto a waste container, eventually causing perforations, through which water could enter the container. Water entering the container could either fill the container and flow out through the holes in the top (the "bathtub model"), or flow out through holes in the bottom of the container (the "flow-through" model). Reaction of the groundwater with the fuel elements in the waste container would mobilize the radionuclides. The rate that water drips onto the container was assumed

to be the product of the net infiltration rate (0.5 mm/yr) in the rock matrix and a "catchment area" of twice the cross-section of the borehole.

Although the groundwater net infiltration rate for the nominal-case problem was specified as 0.01 mm/yr, using a source-term drip rate 50 times larger was not necessarily inconsistent. WG 2 assumed that 90 percent of the containers would not be subjected to water dripping, because of the low infiltration rate, but that the other 10 percent might be subject to dripping because of enhanced flow (SNL, 1987). This interpretation was based on an estimate of the variation of hydrological conditions in the rock.

In the wet-drip bathtub model, the first release from a container occured when the container filled with groundwater and overflowed. During the filling time, the nuclides dissolved into the groundwater according to their respective dissolution mechanisms. Three elements, ^{129}I, ^{135}Cs, and ^{99}Tc, had readily soluble fractions that were rapidly dissolved by the groundwater; also, as the UO_2 fuel matrix was chemically altered by the groundwater, additional radionuclides were released. The concentrations of the three elements dissolved inside the container increased as the container filled with water. When the container overflowed, new groundwater replaced some of the contaminant-saturated water, but alteration caused the contaminants to continue to be released. After all the fuel was altered, the concentration decreased as new groundwater diluted the solution in the container. Release from the container to the surrounding rock started with an abrupt release when the container overflowed. The release increased more slowly as the fuel alteration continued, and then decayed as the concentrations in the contaminated water decreased when the inventory was exhausted. Because ^{237}Np has a low solubility, its release rate was lower than that congruent with the alteration of the fuel; there was no large initial release of ^{237}Np, nor did the release rate decrease (within the time considered).

Release from the flow-through model occured after the top and bottom of the container were breached. Thus, there might not be a

large collection of water to accept dissolved nuclides. There were spikes in the releases of the rapidly dissolved elements, followed by slower releases controlled by the constant alteration rate of the fuel matrix. The release of ^{237}Np was the same as for the bathtub model, except for the absence of a bathtub fill-time delay.

For releases from the whole repository, the releases described above for individual packages were convoluted with the distribution of failures of the packages. Compared with the release from a single package, this resulted in a less-steeply increasing release profile, followed by a longer decay (except for Np, which did not decrease significantly for either mode in this time period). Furthermore, since the single-package release was based on an intermediate failure start time, releases started sooner and persisted longer. Figures 4.2.1 through 4.2.16 of the WG 2 report* show the release profiles.

For water-infiltration rates less than the assumed 0.5 mm/yr, the initial release from a package would be delayed by the longer time necessary to fill the container (in the bathtub model). However, the rate of release would not necessarily be reduced, because of the assumed constant alteration rate. For both models, the release would persist longer because the lower flux would take longer to release all the inventory.

3.3.2 Release by the Moist-Continuous Scenario

If the air-filled annulus surrounding the spent-fuel container became filled with rubble, or if the container was displaced in the borehole, then release could occur by liquid-diffusion pathways. This process would require at least partial saturation of the rock matrix surrounding the container and would proceed by molecular diffusion in fluids in the rock matrix. This process does not re-

* Apted, M. J., W. J. O'Connell, K. H. Lee, A. T. MacIntyre, T.-S. Ueng, T. H. Pigford, and W.W.-L Lee, in preparation. "Preliminary Calculations of Release Rates of Tc-99, I-129, Cs-135, and Np-237 from Spent Fuel in a Tuff Repository," Lawrence Berkeley Laboratory, Berkeley, CA.

quire a nonzero groundwater flow rate. It is insensitive to any but very large changes in water velocity. An effective diffusion coefficient several orders of magnitude lower than the coefficient in intact rock was used to account for the transfer through rubble surrounding the container. To calculate the time-dependent release rate for solubility-limited ^{237}Np, a constant-saturation concentration of Np was assumed. The release rates of the readily soluble species were calculated by assuming instantaneous release into any water which reaches the waste.

3.3.3 Source-Term Data

Time-dependent releases of the four radionuclides were provided in tabular form by WG 2 for the bathtub case under the wet-drip scenario and for the moist-continuous scenario. In addition, several parametric variations on the moist-continuous data were also used by the PACE-90 analysts.

The wet-drip sources for the bathtub and flow-through models are given in Appendix A, Tables A-1 and A-2, respectively. The data were provided in Ci/yr/package, and were converted to $Ci/m^2/s$ or to $kg/s/m^2$ for use in the analyses. The conversion factors are given in Table 3-8. The release profiles for representative examples of the two source terms are shown in Figures 3-10 through 3-12.

The moist-continuous source terms are given in Appendix A, Tables A-3 through A-6. Four parametric variations are listed: a base case (Case 1), a larger diffusion coefficient (Case 2), a higher reaction rate (Case 3) and a higher fractional-alteration rate, consisting of increased reaction rate and increased fuel surface area (Case 4). These sources were generated separately by PNL using the AREST code (Apted et al., 1989) and were not part of the WG 2 summary report. Table 3-9 lists the parametric variations for the four cases.

TABLE 3-8

CONVERSION FACTORS FOR SOURCE TERMS

Area of Repository: 5.61×10^6 m^2 (1)

Number of Containers in Repository: 35,000

Conversion factor for Ci/yr/pkg to Ci/sec/m^2: 1.977×10^{10}

Nuclide	Specific Activity (2) (Ci/kg)	Conversion Factor to kg/s/m^2
^{99}Tc	17.0	1.163×10^{-11}
^{135}Cs	0.882	2.241×10^{-11}
^{129}I	0.174	1.136×10^{-09}
^{237}Np	0.705	2.804×10^{-10}

(1) Rautman *et al.* (1987)
(2) DOE (1986)

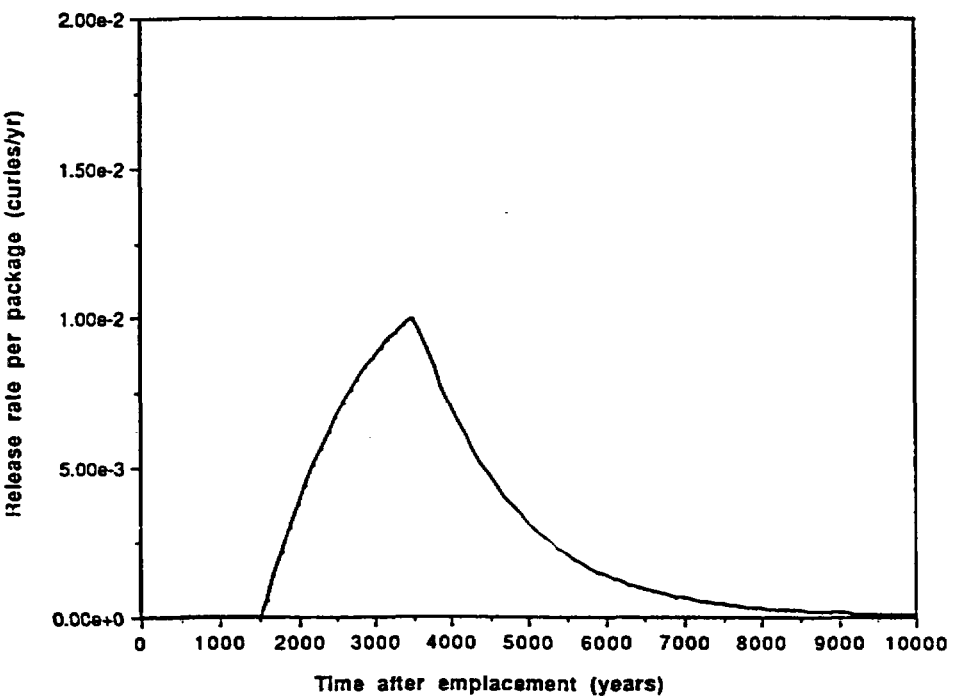

Figure 3-10
Release of ^{99}Tc for Total Repository
From Wet-Drip, Bathtub Source
(from Apted et al., in preparation)

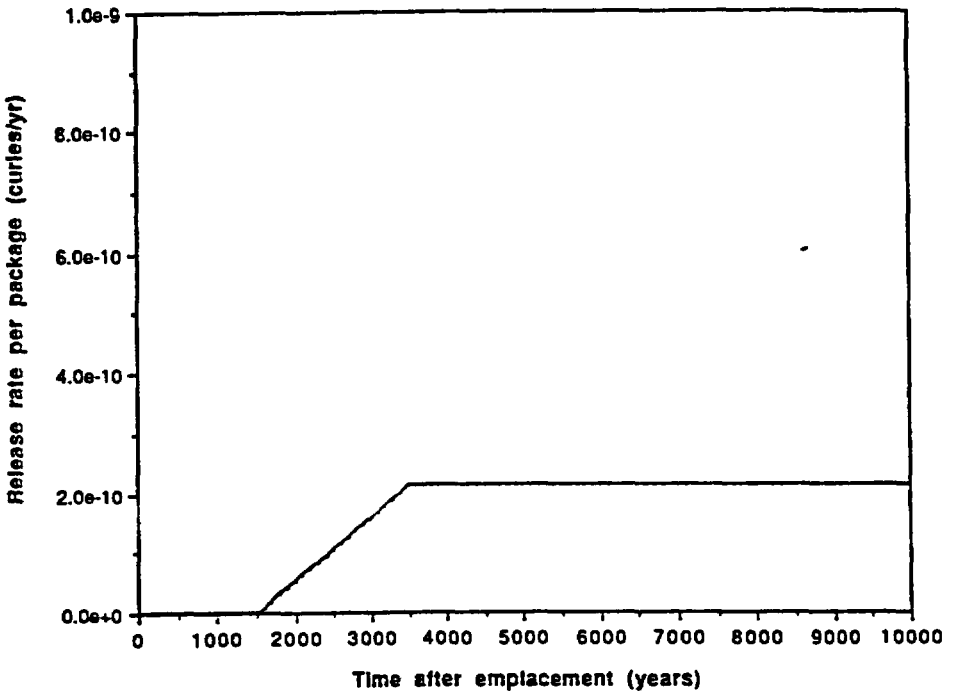

Figure 3-11
Release of ^{237}Np for Total Repository
From Wet-Drip, Bathtub Source

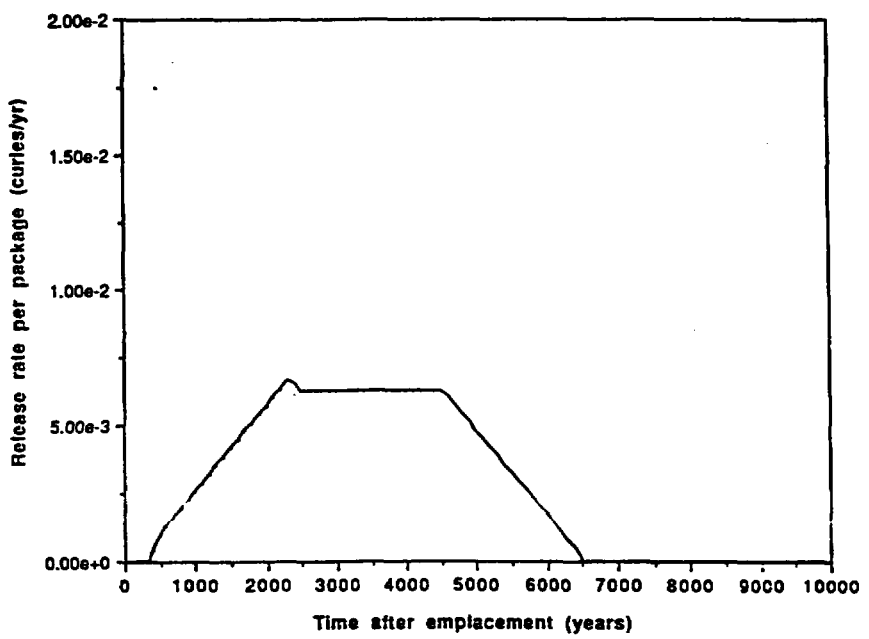

Figure 3-12
Release of ^{99}Tc for Total Repository
From Wet-Drip, Flow-Through Source
(from Apted et al., in preparation)

TABLE 3-9

MOIST-CONTINUOUS SOURCE TERM

PARAMETRIC VARIATIONS

Case	Diffusion Coefficient (cm^2/s)	Reaction Rate ($g/m^2/d$)	Surface Area (cm^2)	Alteration Rate (/yr)
1	1.0×10^{-8}	0.01	4.64×10^{4}	5.3×10^{-6}
2	1.0×10^{-5}	0.01	4.64×10^{4}	5.3×10^{-6}
3	1.0×10^{-8}	10.00	4.64×10^{4}	5.3×10^{-6}
4	1.0×10^{-8}	0.01	9.27×10^{4}	1.1×10^{-5}

Note: The same parameters were used for all nuclides.

Case 2 used a diffusion coefficient that was three orders of magnitude greater than that for Case 1. This variation caused source releases to start sooner (but did not cause higher release rates) from the EBS for the reaction-rate-limited nuclides (Tc, I, Cs) once they were mobilized from the spent fuel. Upon mobilization from the spent fuel, the contaminants moved faster because of the higher diffusion rate. The diffusion rate had no effect on the rate at which the contaminants were mobilized from the fuel. For solubility-limited Np, the release rate was three orders of magnitude higher than Case 1 because of the direct relationship between the diffusion coefficient and the release rate.

Case 3 showed the effect on release of increasing the reaction rate of the UO_2 matrix by a factor of 1000. This caused ^{99}Tc and ^{129}I to be more rapidly released. The increase in ^{135}Cs releases was much less because of its large retardation and the low diffusion coefficient. The cumulative releases for ^{99}Tc, ^{129}I, and ^{135}Cs were relatively higher than Case 1 by factors of 4.0, 2.5, and 1.0, respectively.

Case 4 showed the results of assuming an increase in surface area of the spent fuel by a factor of two. This did not affect solubility-limited nuclides (such as ^{237}Np), but the release rates of the other three elements were a factor of two higher than Case 1. Release profiles for the four source-term Cases are shown in Figures 3-13 through 3-16.

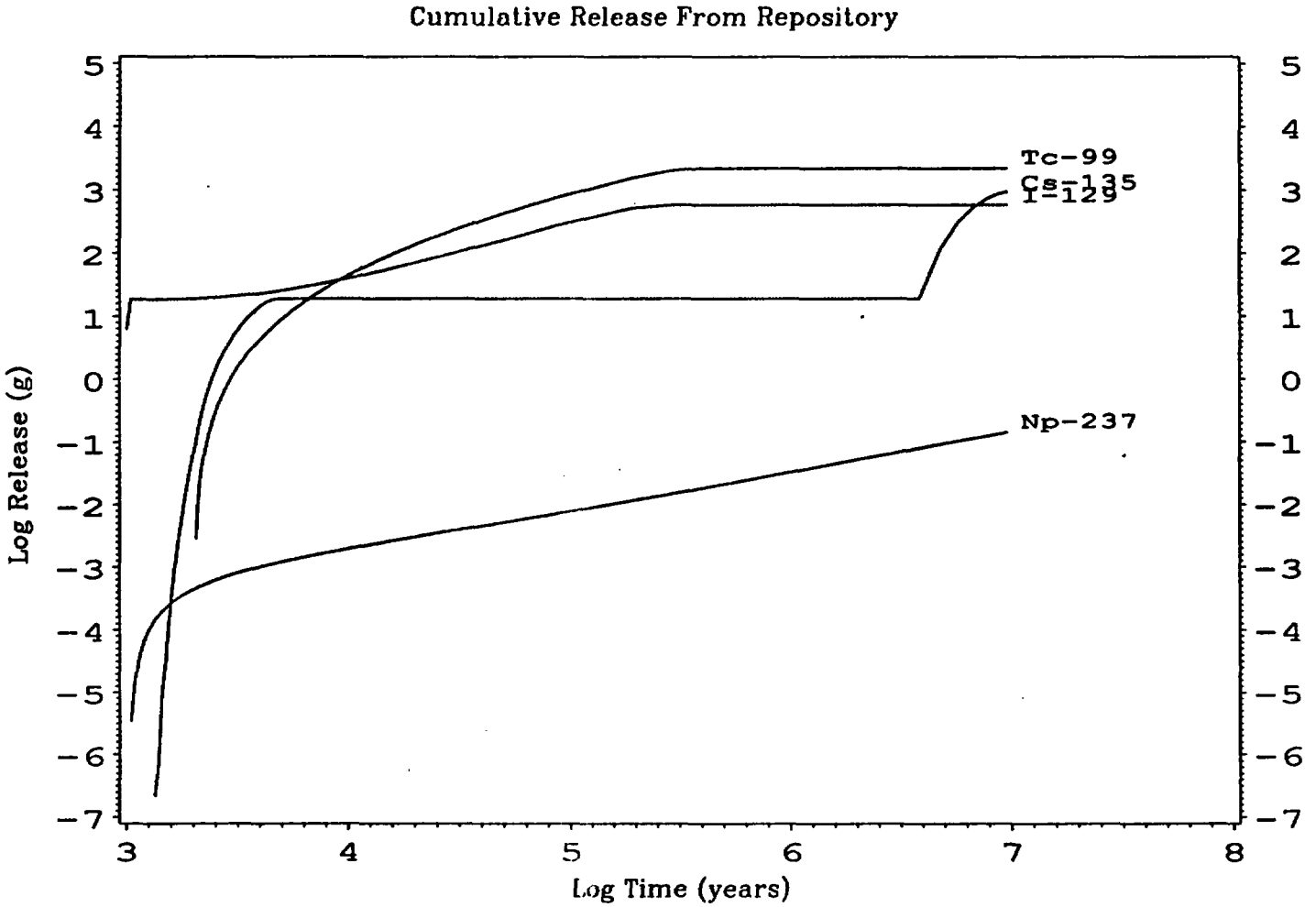

Figure 3-13
Moist-Continuous Release for Case 1
(Base Case)

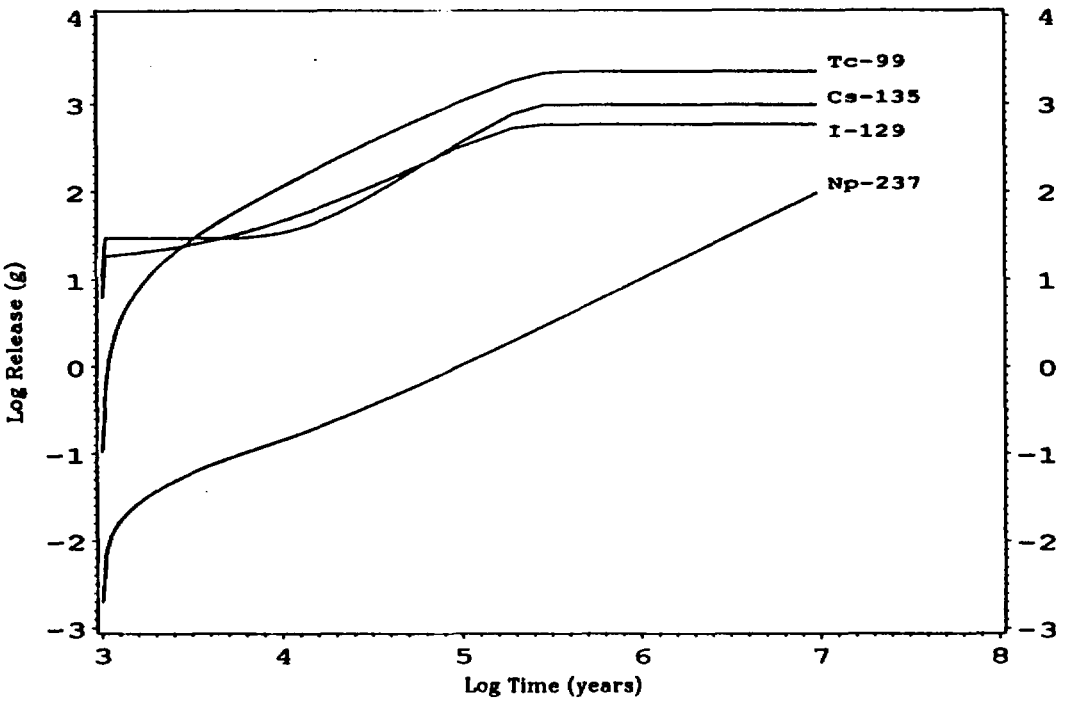

Figure 3-14
Moist-Continuous Release for Case 2
(Enhanced Diffusion Coefficient)

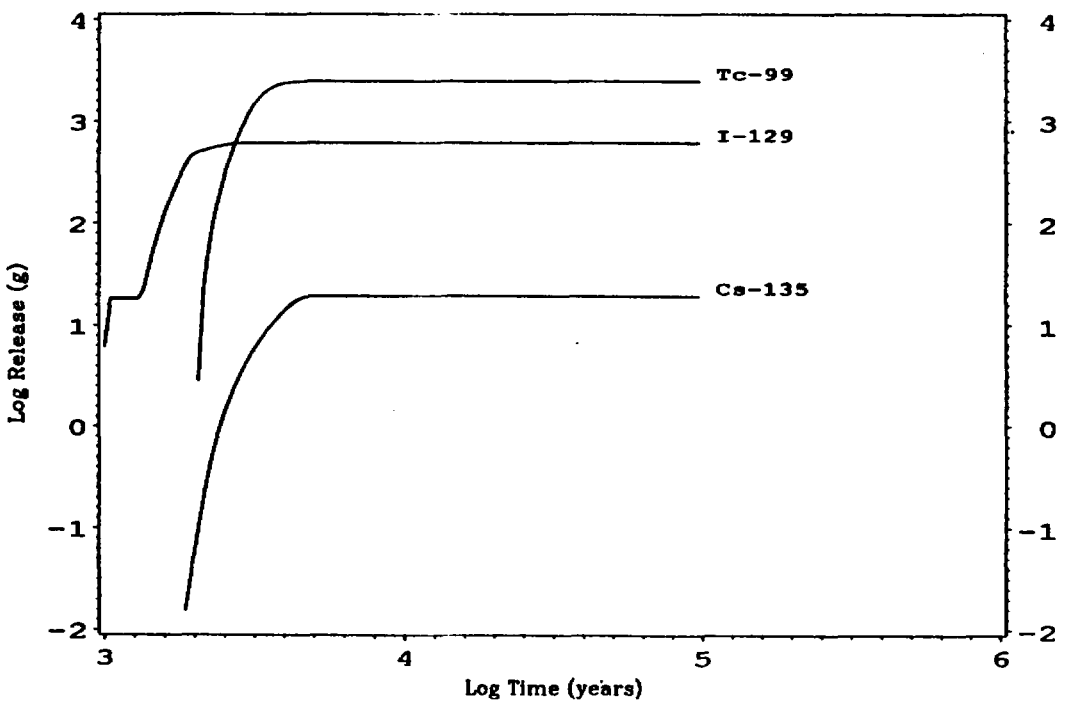

Figure 3-15
Moist-Continuous Release for Case 3
(Increased Reaction Rate)

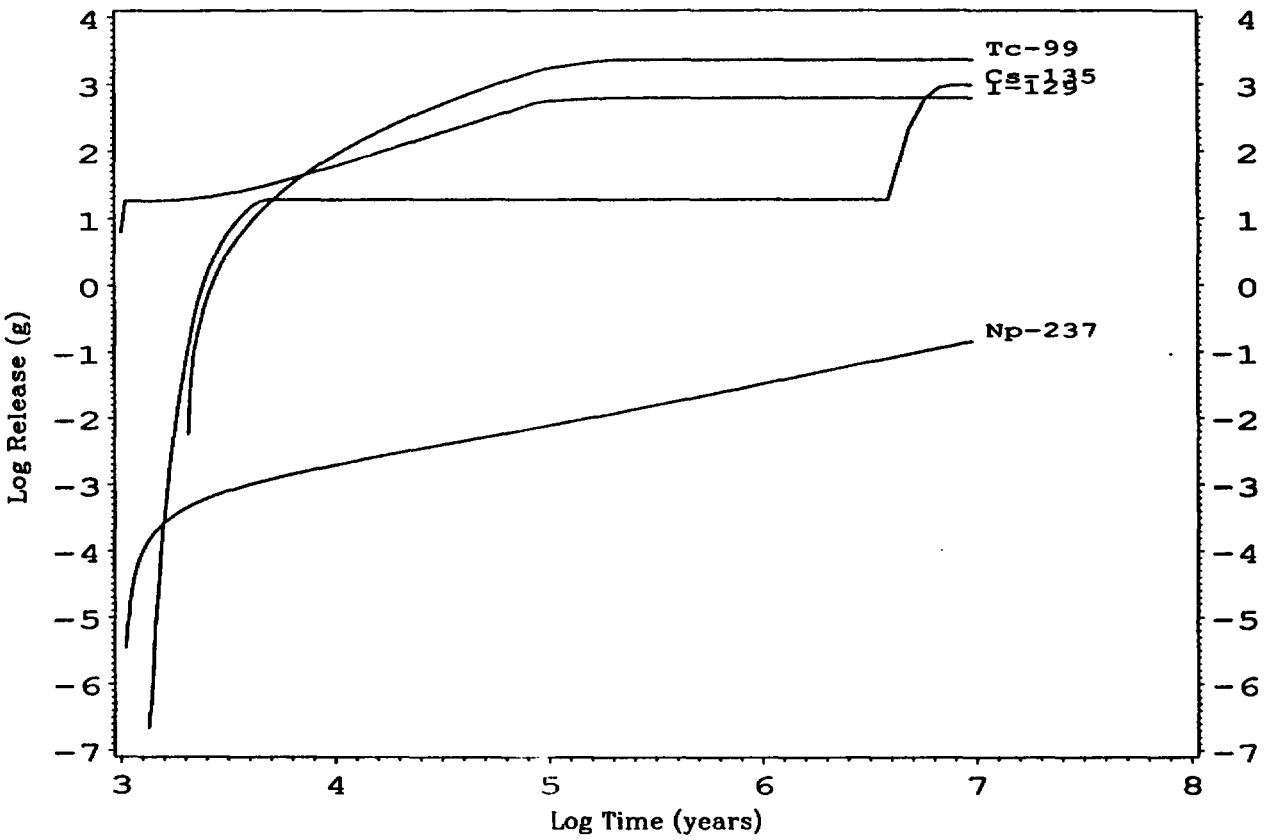

Figure 3-16
Moist-Continuous Release for Case 4
(Increased Surface Area)

3.4 Geochemical and Retardation Data

The sorption parameters from which the PACE nominal configuration values were derived are given in Table 3-10. These parameters were distribution coefficients (K_ds) and are listed for the thermal/mechanical units described by Ortiz et al. (1985). They were based on Thomas (1987) and Daniels et al. (1982). Shown in the table are the K_ds for the four elements of interest, plus those for several other elements.

The sorption ratios in Table 3-10 were obtained from batch sorption experiments conducted using crushed tuff. Details of the experimental procedures were provided by Thomas (1987). The experiments were conducted at room temperature and ambient air pressure using water from the J-13 drill hole (located near Yucca Mountain). The water was pretreated by being in contact with the

crushed tuff for at least two weeks. For sorption of alkalis and alkali earths, results using crushed tuff were shown to differ only slightly from those for intact tuff. However, the effect of crushed versus intact tuff on sorption of transuranic wastes is unknown. These batch experiments might not have been at equilibrium, in the sense that the reaction might not have proceeded to completion. Therefore, the measured K_ds would reflect less sorption of the radionuclides (or less potential for sorption) than at completion. The amount of retardation inferred from the experiments would be less than the value at completion, which would make the values shown here conservative. The values presented in Table 3-10 are assumed to be for the rock matrix. Where "NA" appears, the value was not available; where zero appears as the K_d, an experimental result was represented.

TABLE 3-10

AVERAGE SORPTION PARAMETERS (IN ml/g)

	Thermomechanical Units						
Element	TSw2	TSw3	CHnz	CHnv	PPw	CFUn	BFw
Cs	100.0	100.00	3000.0	NA	200.0	400.0	100.0
Tc	0.1	0.05	0.0	NA	NA	0.2	NA
I	NA	0.00	NA	NA	NA	NA	0
Np	5.0	0.50	3.0	NA	5.0	5.0	NA
Am	10000.0	1000.00	1500.0	NA	4000.0	2500.0	40.0
Ba	250.0	350.00	10000.0	NA	150.0	200.0	200.0
Ce	1200.0	50.00	300.0	NA	150.0	500.0	50.0
Eu	50.0	25.00	1000.0	NA	100.0	50.0	50.0
Pu	100.0	200.00	40.0	NA	50.0	100.0	100.0
U	1.0	0.00	2.5	20.0	2.0	2.5	1.0
Sr	25.0	20.00	1500.0	NA	20.0	35.0	40.0

Values chosen for use in the PACE exercises were generally taken from the thermal/mechanical units most like the geohydrologic zones used here. In general, conservative values (low K_ds) were chosen. Where there is no value in Table 3-10, a very conservative

value of zero has been used for those radionuclides in those geohydrologic units. The K_d values that were assigned to the PACE-90 geohydrologic units are shown in Table 3-11. Application of these values to the PACE problems is subject to the assumption that the experimental conditions under which they were obtained are applicable to the conditions under which transport would occur at Yucca Mountain. Validity of this overall assumption is still the subject of research as part of the Geochemistry Program at the Yucca Mountain Project.

TABLE 3-11
SORPTION COEFFICIENTS
FOR HYDROSTRATIGRAPHIC ZONES (IN ml/g)

Hydrogeologic Zone	Element			
	Cs	Tc	I	Np
Tpt-TM	100	0.1	0.0	5.0
Tpt-TD	100	0.1	0.0	5.0
Tpt-TDL	100	0.1	0.0	5.0
Tpt-TML	100	0.1	0.0	5.0
Tpt-TM	100	0.1	0.0	5.0
Tpt-TV	100	0.05	0.0	0.5
Tpt-TNV	0.0	0.0	0.0	0.0
Tpt-TN	3000	0.0	0.0	3.0
Tpt-BT	3000	0.0	0.0	3.0
Tcb-TN	3000	0.0	0.0	3.0
Tcb-BT	3000	0.0	0.0	3.0
Tcb-TN	3000	0.0	0.0	3.0
Tcb-BT	3000	0.0	0.0	3.0
Tcb-TN	3000	0.0	0.0	3.0
Tcb-BT	3000	0.0	0.0	3.0
Tcb-TN	3000	0.0	0.0	3.0
Tcb-BT	3000	0.0	0.0	3.0
Tcpp-TN	200	0.0	0.0	5.0
Tcpp-TN	200	0.0	0.0	5.0
Tcpp-TP	200	0.0	0.0	5.0

4.0 SUMMARY OF PARTICIPANTS' ANALYSES

The participants listed in Table 2-1 each used the input data provided to model the PACE-90 nominal configuration problem using the computer codes noted there. The computer programs used different mathematical techniques, which could influence the results; they are discussed briefly in the following subsections.

Input for the analyses is described in Section 3. Most participants had to make additional modeling decisions; e.g., simplification of the problem because of computer code restrictions, mesh-point spacing for the calculational mesh, dispersivity factors, water-velocity correlation factors, tortuosity factors, matrix-diffusion factors, etc. These decisions influenced the results; they are discussed for each participant in the Problem Setup subsections.

The following subsections describe the computer codes, the results, and the applicability of the techniques used by the participants to model the radionuclide transport problem.

4.1 SUMO

4.1.1 Code Description

The Performance Assessment Scientific Support program at PNL has developed a model and computer code (SUMO, for system unsaturated model) for performance- and risk-assessment analyses of the potential high-level-nuclear-waste disposal sites. The SUMO model consists of component models embedded in a Monte Carlo framework that allow computation of a complementary cumulative distribution function of releases to the accessible environment. The output is in a form consistent with the current Environmental Protection Agency (EPA) release criterion (EPA, 1985).

The SUMO code provides answers to two major performance objectives. First, it evaluates the performance of a potential nuclear-waste repository by comparison of cumulative radionuclide release to the limits established by EPA. Second, it can predict the population health risk from the repository. The following specific solutions are available from SUMO: (1) radionuclide flux across a surface, (2) cumulative radionuclide flux across a surface, (3) radionuclide concentration at a location, and (4) individual or population dose.

SUMO can implement radionuclide source terms based on a reaction-rate model contained in the AREST code. The implementation in SUMO allows a choice between three possible EBS release models: (1) a steady-state advective model, (2) a steady-state diffusive model, and (3) a transient diffusive model. In addition, assumptions of congruent or incongruent release of radionuclides from the waste form are implemented.

SUMO is an integrated-finite-difference code that is designed to solve 3-D problems. However, it can be adapted to solve 1-D and 2-D problems by specifying a grid size of three in the directions that are to be omitted. SUMO can solve problems with either fully or partially saturated geologic media, or with geologic media in which some parts are fully saturated while others are partially saturated. In the partially saturated case, liquid (water) and gas (air) are assumed to exist, but the movement of only the liquid phase is addressed. Consideration of mass transfer is also restricted to the liquid phase; i.e., vapor transport is not considered. Three governing equations describe fluid flow, heat transfer, and mass transport. The state variables in these equations are the hydraulic head, temperature, and concentration, respectively. These equations can be solved either independently or in various coupled modes.

4.1.2 Problem Setup

The 2-D problem domain modeled was the cross-section between drill holes G-1 and G-4. The problem hydrologic data set contained about 20 distinct hydrologic zones, but this analysis used only four distinct geologic units. The units, the Calico Hills nonwelded, (Tcb-TN), the Prow Pass nonwelded, (Tcpp-TN), the Topopah Spring nonwelded, (Tpt-TN), and the Tpt-TM, were made thicker than the values listed in Tables 3-2 and 3-3 to match the elevational difference from the repository to the water table. The tilting of the beds was represented by stair-stepping the units. The modeling domain was divided into five distinct zones: the four geologic units and the repository (embedded in the Tpt-TM unit). The cross-section for this model can be seen in Figure 4-1.

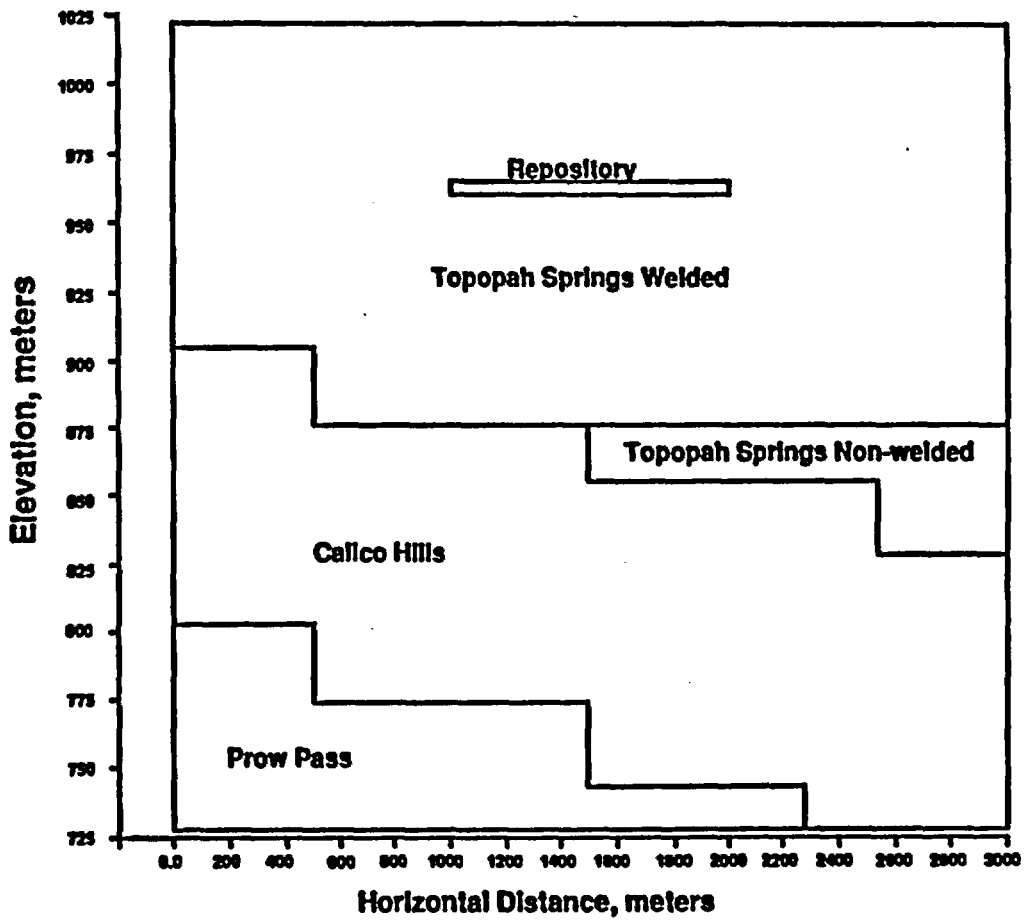

Figure 4-1
SUMO Analysis - Problem Zoning and Boundaries

The stratigraphy was extended 1000 m beyond the northwestern and southeastern edges of the repository, to more closely approximate transport to the accessible environment. The repository was assumed to be 1000 m in lateral extent and 5 m in vertical extent. The northwestern edge of the repository was the horizontal (x) direction reference point and has an x-coordinate of 1000. The x-coordinates ranged from 0 m to 3000 m. The stratigraphic units were arbitrarily extended horizontally using the same unit thicknesses as between the two boreholes.

The vertical (z) coordinates used for the water table were at the approximate elevation of the water table at drill hole G-4. The water table was assumed to be at a constant elevation of 730 m throughout the model domain. The top of the domain was 50 m above the top of the repository at elevation 1020 m. The Tpt-TM was the "host rock" for the repository, and the repository was assumed to have the same rock properties as the surrounding unit. The elevation of the repository at G-4 was 960-965 m. For the sake of simplicity, the repository was assumed to have a constant elevation of 960 m and a thickness of 5 m.

The top of the Tpt-TN unit was also assumed to have a constant elevation. Its elevation at G-4 was approximately 875 m. This value was used as the average elevation of the unit. The unit was assumed to be located between the Tpt-TM and the Tcb-TN units. The Tpt-TN began at x-coordinate 1500 m and stepped downward by 30 m at x-coordinate 2550 m. The 5- to 15-degree eastward dip of the beds was represented by a stair-stepped grid.

The grid for the PACE-90 exercises was designed so that cells were considerably smaller near zone interfaces. The minimum distance between nodes in the x direction was 5 m, but was 1 m in the z direction. The maximum distance between nodes in the x-direction was 50 m and was 5 m in the z-direction. The grid size was 92 in the x-direction, 3 in the y-direction, and 77 in the z-direction, resulting in a grid of approximately 7000 nodes.

Three different boundary conditions were specified for the steady-state pressure equation. The top of the domain had a constant flux boundary of 0.01 mm/yr. The bottom of the domain was the water table, which was held at a constant pressure of zero. The sides of the domain were a Neumann (no-flow) boundary condition.

The grain density, total porosity, and saturated hydraulic conductivity for each of the four zones were taken from Tables 3-2 and 3-3. Effective porosity was estimated as 90 percent of total porosity. Specific storativity was set equal to effective porosity. The molecular diffusion coefficient was 3.15×10^{-3} m/yr for all material types, and the longitudinal dispersivity was taken as 10 percent of the smallest cell thickness. Transverse dispersivity was taken as 10 percent of the longitudinal.

The pressure equation was solved using the van Genuchten (1980) relation for moisture retention and the Mualem (1976) relation for relative hydraulic conductivity. The pressure equation was solved by time-stepping with constant boundary conditions for 1.5 million years. The solution obtained was assumed to represent steady-state conditions. The four moist-continuous source term cases were used for the transport analysis.

4.1.3 Results

Figures 4-2 and 4-3 show the solution of the hydraulic head and relative saturation, respectively. The two figures emphasize that a slight change in the saturation significantly affected the pressure. There was a sharp change in saturation at x-coordinate 1500 m, the end of the Tpt-TN unit. The saturation changed from 83% at the southeast end of the repository to 56% at the northwest end. This caused a sharp pressure front that affected contaminant transport. Vectors representing groundwater flow velocities are shown in Figure 4-4. This figure shows that although the general flow direction was downward, there was some lateral diversion below the repository. This was due to the lower hydraulic conductivity in the Tpt-TN unit, and also to the selection of layers such that

the Tpt-TN did not extend across the entire model domain. The conductivity specified for this zone differed by an order of magnitude from the other zones and acted as a groundwater flow barrier. Groundwater ponded slightly above this layer, resulting in high saturations and the diversion in the flow field.

Travel-time calculations were performed using a particle-tracking algorithm. Discrete particles were released at 500-m horizontal intervals from the plane of the repository. Each particle was monitored until it reached the water table. The results can be seen in Figure 4-5. The average travel time was approximately 2.8 million years, and the paths lengths were about about 230 m (the distance to the water table) for paths away from the Tpt-TN unit. Paths that started in the middle of the repository above the Tpt-TN unit (at x-coordinates greater than 1500 m) had to divert around the pinched-out end of the zone, resulting in a longer path length. Travel times for these paths are lower because of the ponding, as seen in Figure 4-3.

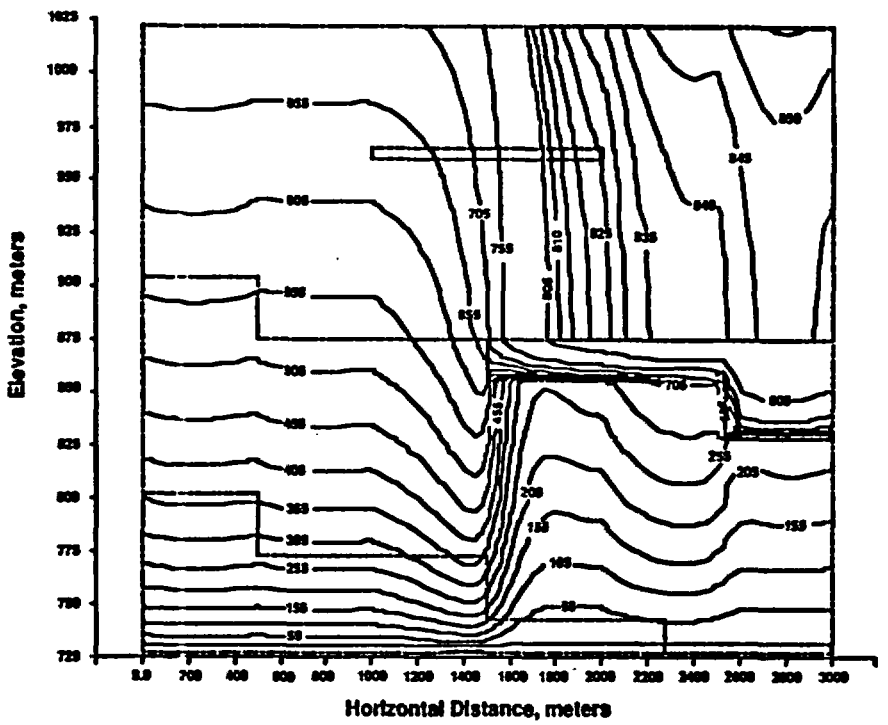

Figure 4-2
SUMO Analysis - Hydraulic Head Contours

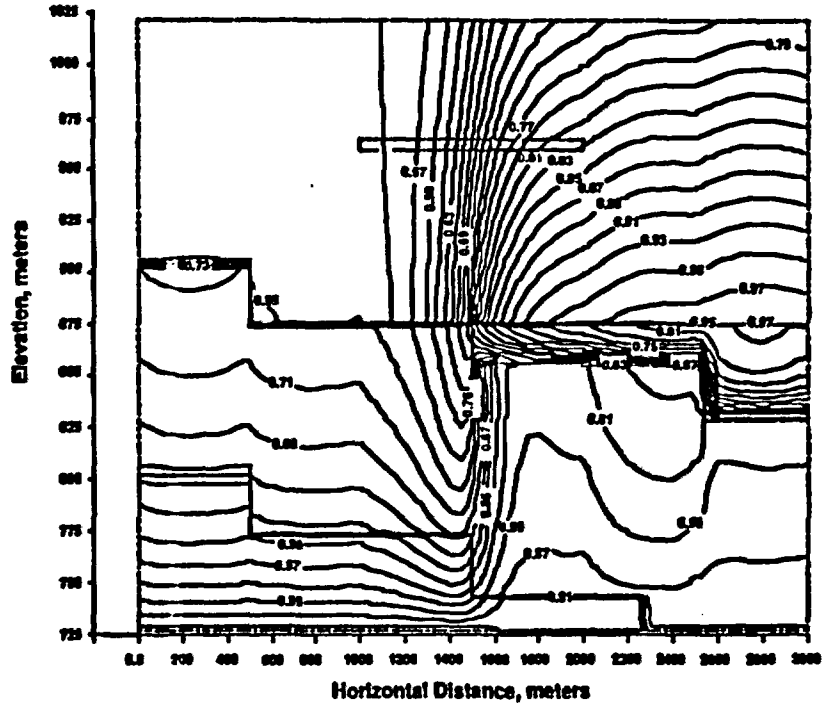

Figure 4-3
SUMO Analysis - Relative Saturations

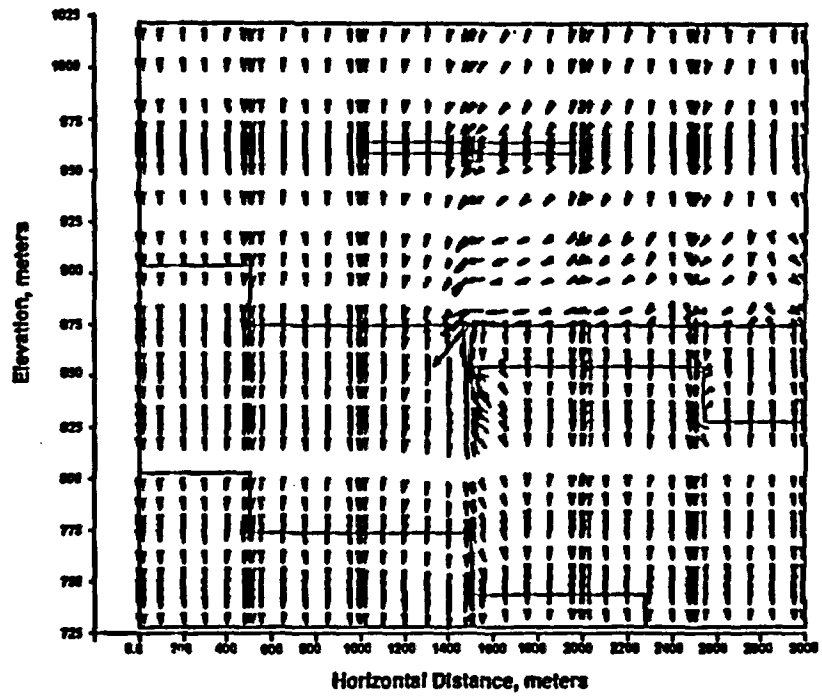

Figure 4-4
SUMO Analysis - Water-Velocity Vectors

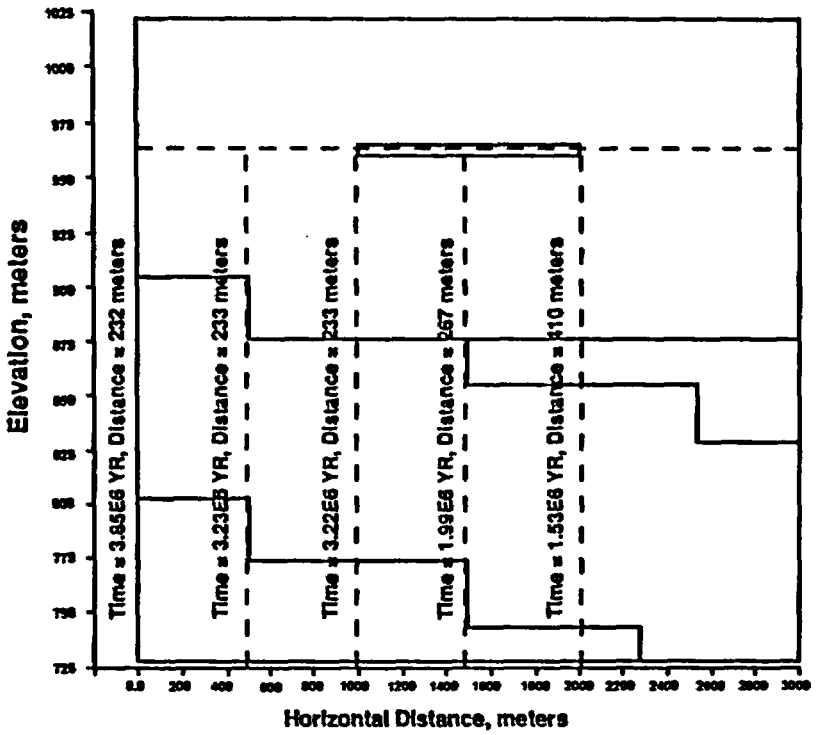

Figure 4-5
SUMO Analysis - Groundwater Travel Times

The transport modeling indicated that significant fluxes of the radionuclides did not reach the water table. Figures 4-6, 4-7, 4-8, and 4-9 show the concentration of ^{135}Cs, ^{99}Tc, ^{129}I, and ^{237}Np, respectively, after 100,000 years of transport for the moist-continuous Case 1 source term. All four figures indicate that the radionuclide movement was affected by both advection and diffusion, with diffusion being dominant. The leading edge of the ^{237}Np plume did not exit the Tpt-TM unit. The ^{99}Tc plume reached the Tcb-TN, but did not reach the water table or enter the Tcpp-TN unit. The ^{129}I plume was transported the furthest, primarily because the K_d for ^{129}I was zero. (Note that the concentration of the leading edge for ^{129}I in Figure 4-8 was ten times higher than for ^{99}Tc). The leading edge of the plume for ^{135}Cs entered the Tpt-TN unit but did not proceed any further into the Tcb-TN after 100,000 years. In contrast to analyses done by other participants, the K_d for ^{135}Cs was set to zero in the Tpt-TM unit.

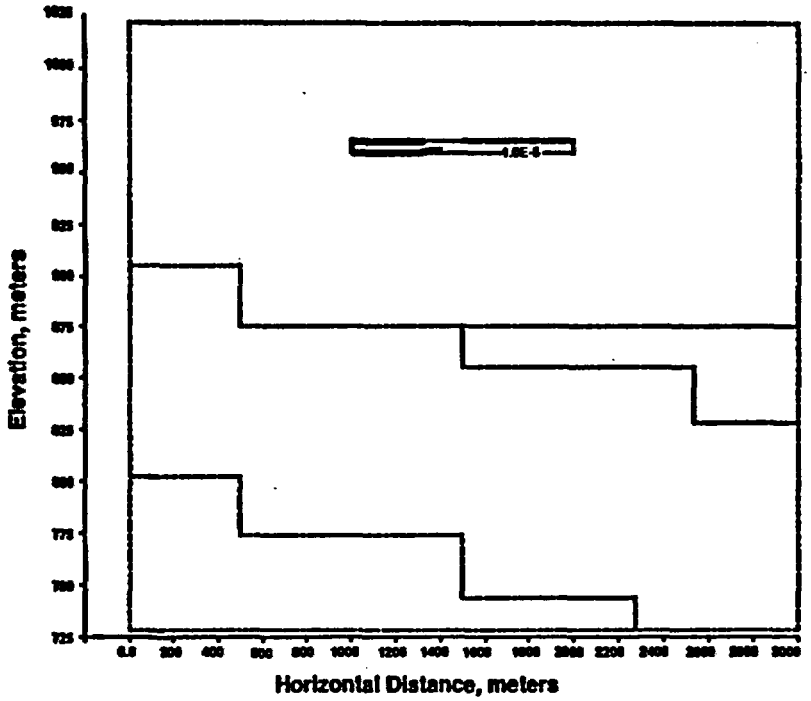

Figure 4-6
SUMO Analysis - Transport Distribution of ^{237}Np (Ci/m^3)

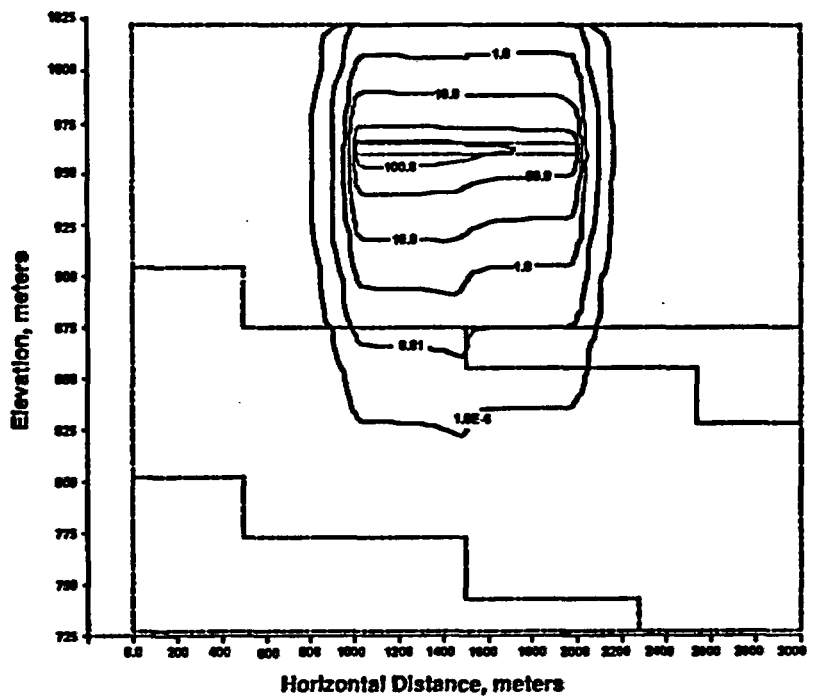

Figure 4-7
SUMO Analysis - Transport Distribution of ^{99}Tc (Ci/m^3)

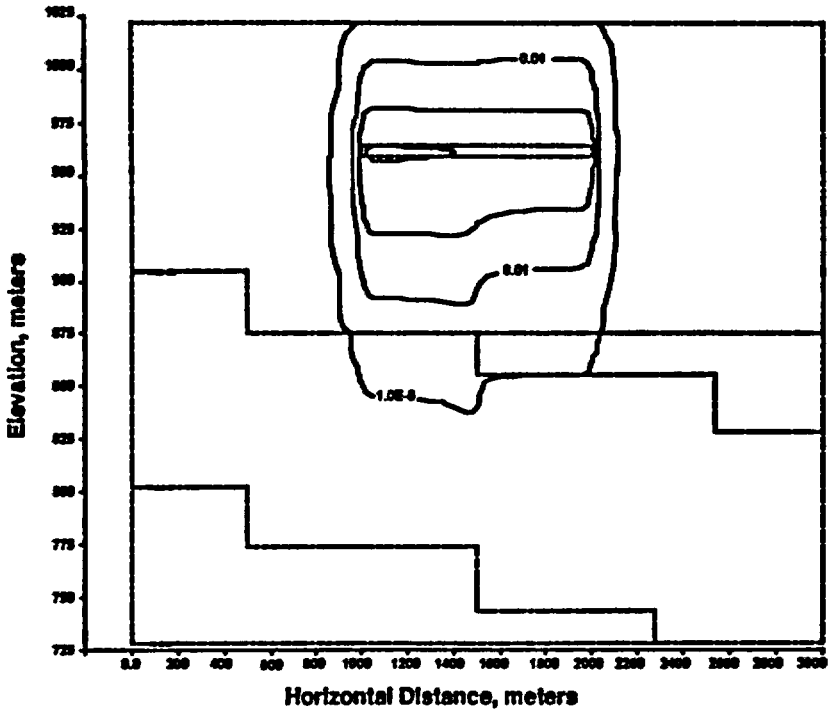

Figure 4-8
SUMO Analysis - Transport Distribution of ^{129}I (Ci/m^3)

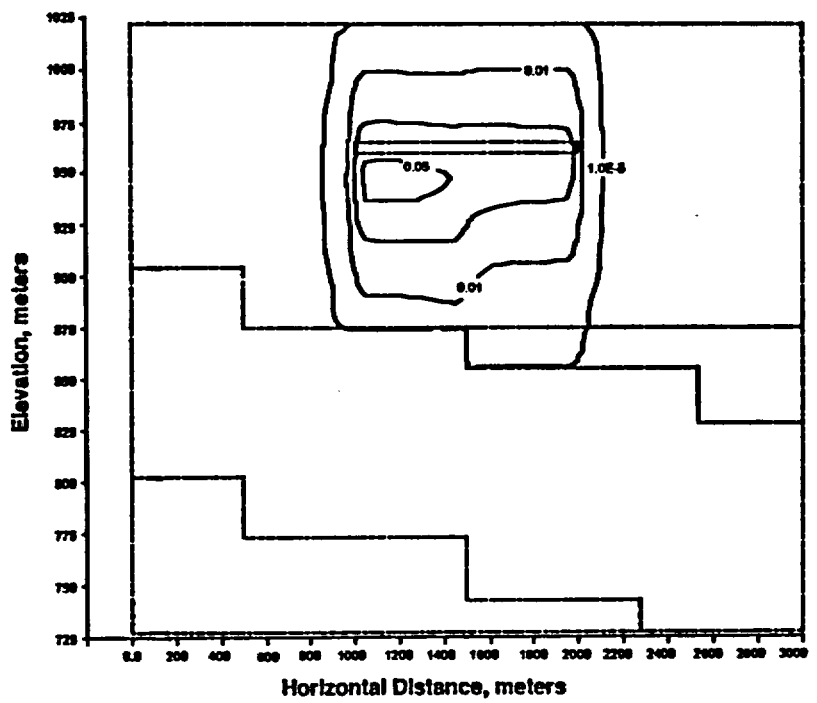

Figure 4-9
SUMO Analysis - Transport Distribution of ^{135}Cs (Ci/m^3)

4.2 TRACRN

4.2.1 Code description

The LANL analysis used TRACRN, a finite-difference code for solving time-dependent reactive flow in porous media in one to three dimensions (Birdsell and Travis, 1990). The subset of equations from TRACRN that were used for these nominal-case calculations included conservation of water mass, conservation of momentum for water using Darcy's Law, and conservation of contaminant. The latter included radioactive decay and equilibrium sorption of species to the rock matrix. These equations were solved using an implicit finite-difference scheme with full upwind differencing (Peyret and Taylor, 1986). The matrix equations were solved using a preconditioned conjugate-gradient method. The first step in solving a contaminant transport problem was to obtain a steady-state water flow field. Once obtained, the contaminant was introduced, and the contaminant conservation equation was solved alone.

4.2.2 Problem Setup

The first step in this problem set was to do 1-D simulations of drill holes G-4 and UE-25a using the hydrologic data as described in Section 3. Relative permeability and capillary pressure curves as functions of water saturation were derived using van Genuchten's formulation with the parameters provided in the hydrologic data set. Matrix and fracture properties were combined by weighting each according to their respective porosities. This resulted in a composite model for relative permeability and capillary pressure that accounted for the transition from matrix flow to fracture flow as saturation was approached.

For each drill hole, 164 finite-difference cells were used. The top cell corresponded to the repository and had a constant downward water flux of 0.01 mm/yr. Three contaminant source terms were used: (1) the moist-continuous Case 1; (2) the wet-drip bath-

tub source; and (3) the wet-drip flow-through source. The bottom boundary was specified by constant pressure and contaminant concentration.

4.2.3 Results

Pressure-head and water-saturation profiles for drill hole G-4 are shown in Figures 4-10 and 4-11. These profiles matched very well with 1-D results of other PACE-90 participants for drill hole G-4. Minimum saturations were around 0.75. Spikes in the saturation profiles corresponded to the locations of thin stratigraphic layers.

Transport results for drill hole G-4 are shown in Figures 4-12 through 4-15 for ^{135}Cs, ^{99}Tc, ^{129}I and ^{237}Np, respectively, after 100,000 years, using the moist-continuous Case 1 source term. (Concentration units are shown as powers of ten). At this low net infiltration rate, the transport was strongly influenced by molecular diffusion, which limited the maximum transport distance. ^{129}I, the only nonsorbing species in this problem set, had a concentration of 10^{-13} Ci/m^3 at a distance of 100 m below the repository after 100,000 years (Figure 4-14). The other three transported species (^{99}Tc, ^{135}Cs, and ^{237}Np) traveled shorter distances. The concentration profiles differed between the moist-continuous case and the two wet-drip cases. The two wet-drip cases were similar. The results for the flow-through case are shown in Figures 4-16 through 4-19. The most transport occurred for ^{129}I (Figure 4-18). After 100,000 years, the concentration 70 m below the repository was 10^{-13} Ci/m^3, but the highest concentration moved only 10 m below the repository. The basic result for all three cases was that transport is governed by diffusion and retardation; thus, the travel distances of all species were very small in the 100,000 year time frame. None of the four contaminants reached the water table.

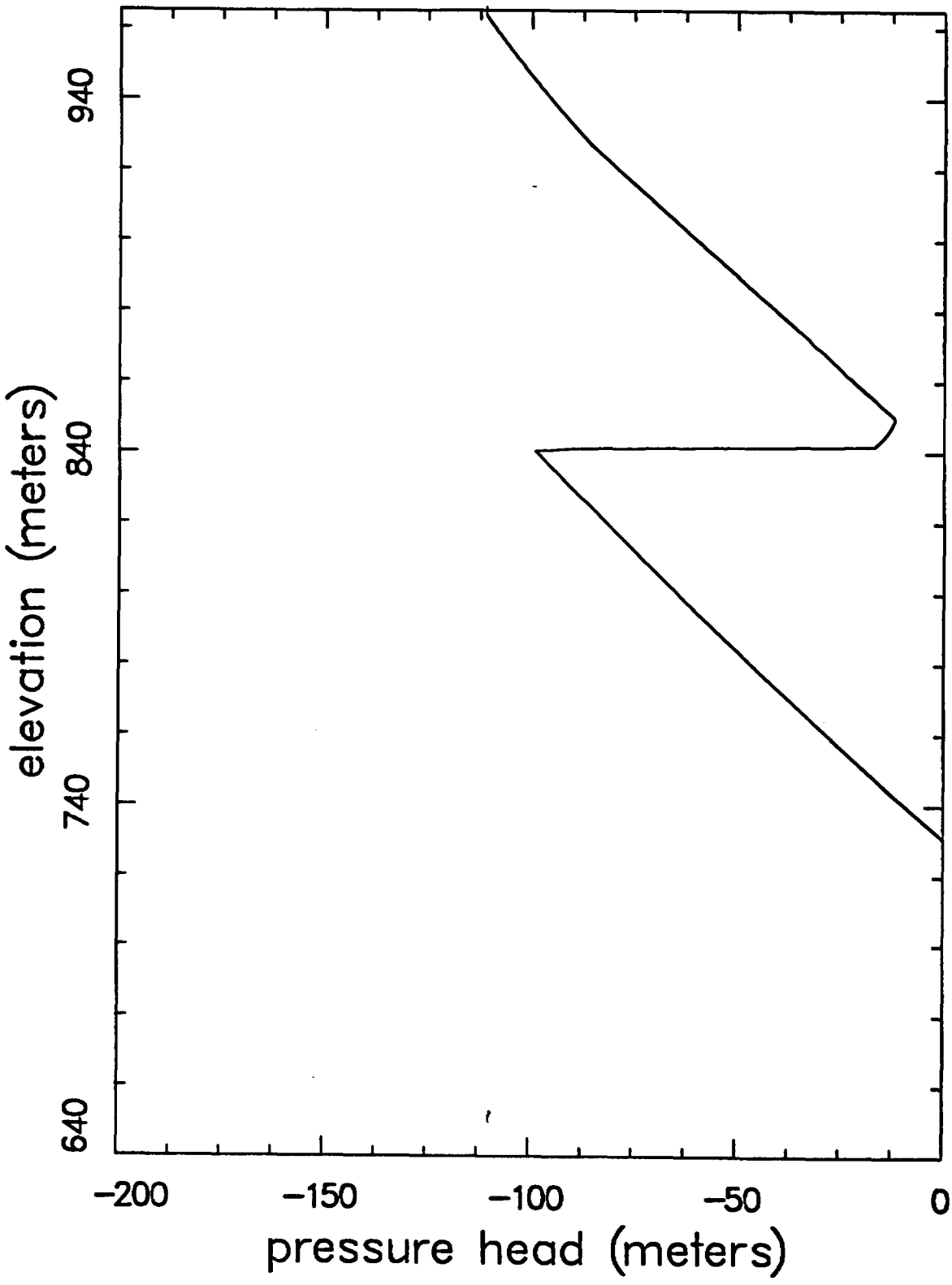

Figure 4-10
TRACRN Analysis - Water Pressure Head for Drill Hole G-4

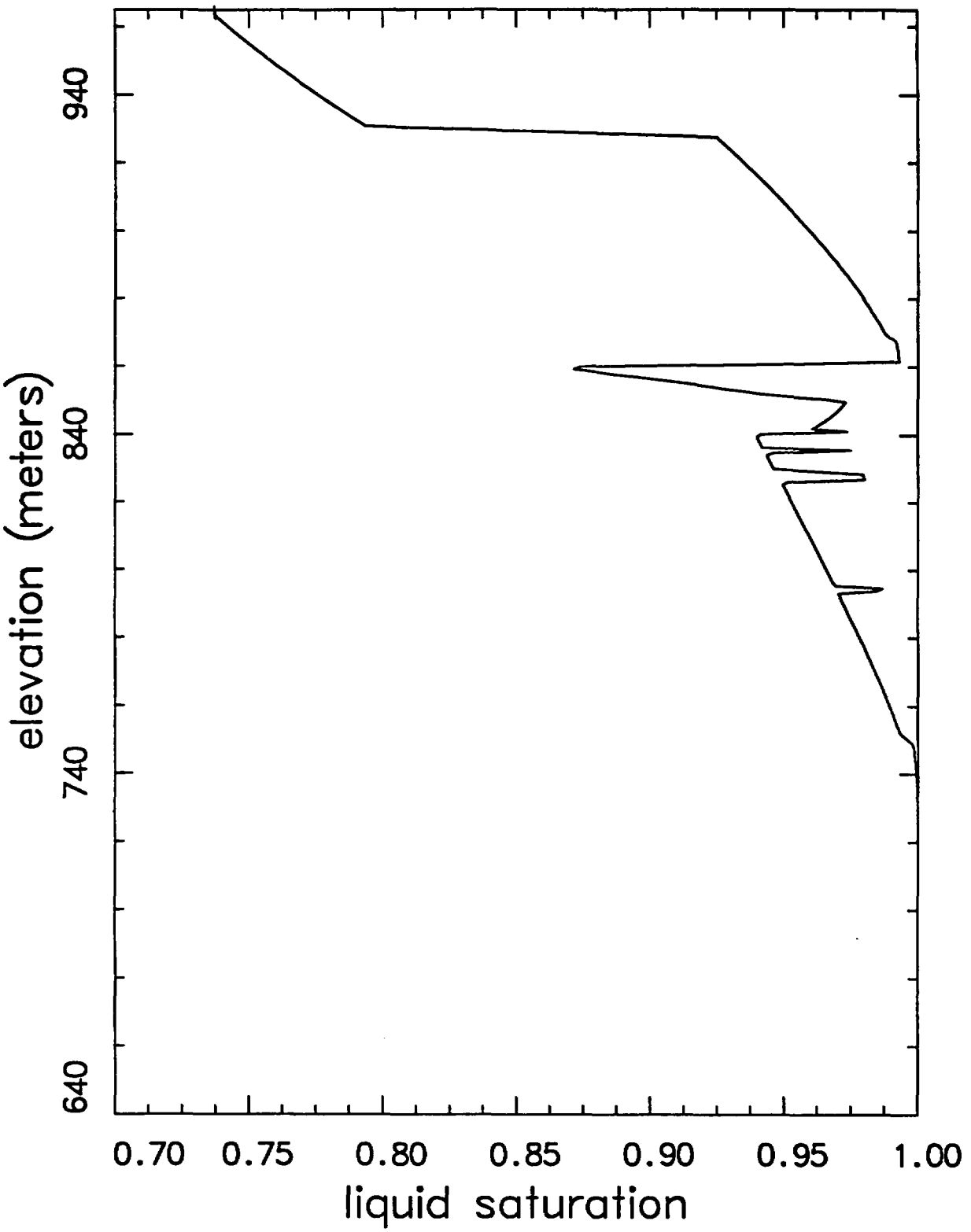

Figure 4-11
TRACRN Analysis - Equilibrium Saturation Profile for Drill Hole G-4

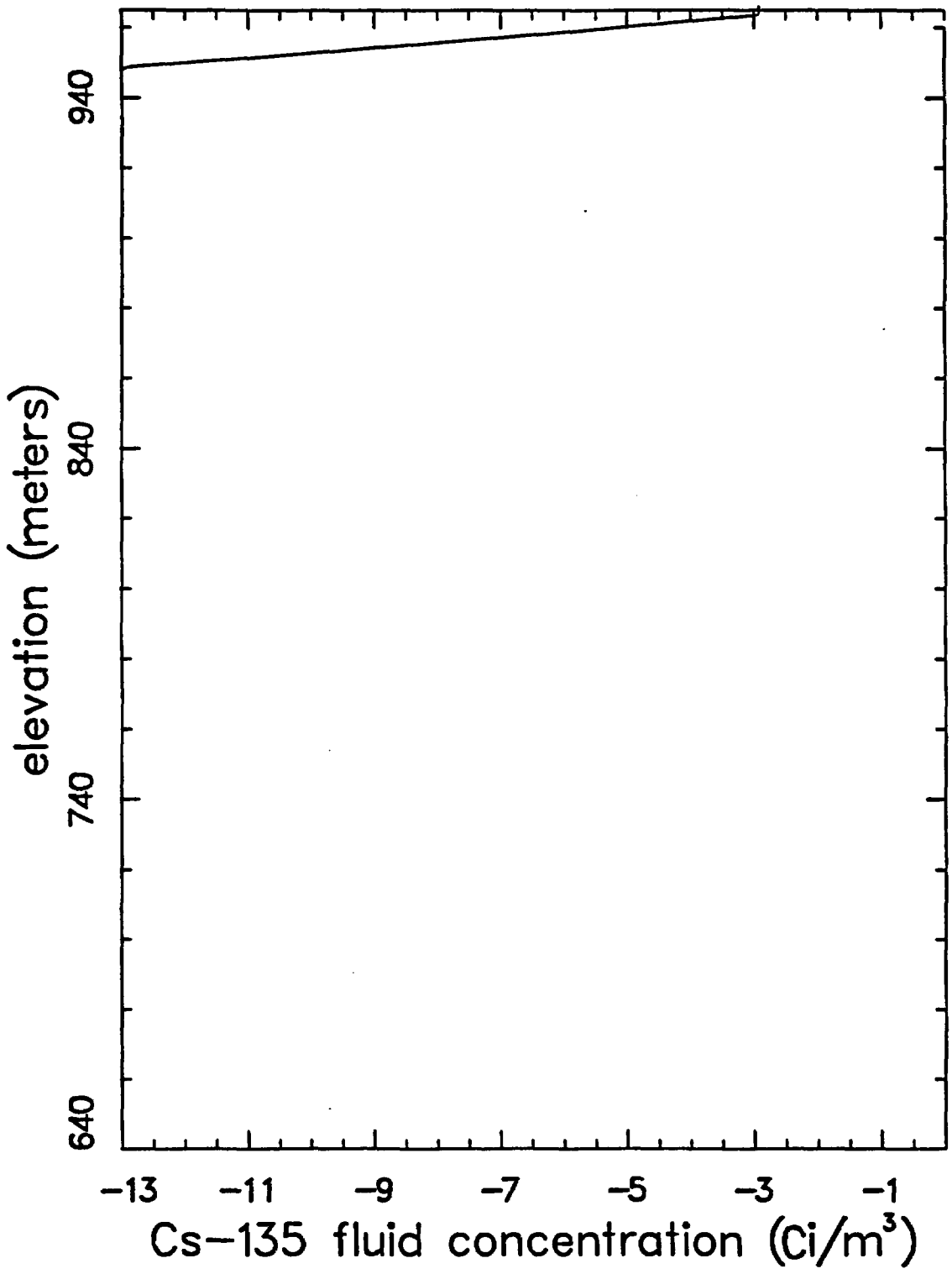

Figure 4-12
TRACRN Analysis - Transport Distribution of ^{135}Cs
Moist-Continuous, Case-1 Source Term
(Logarithm of concentration)

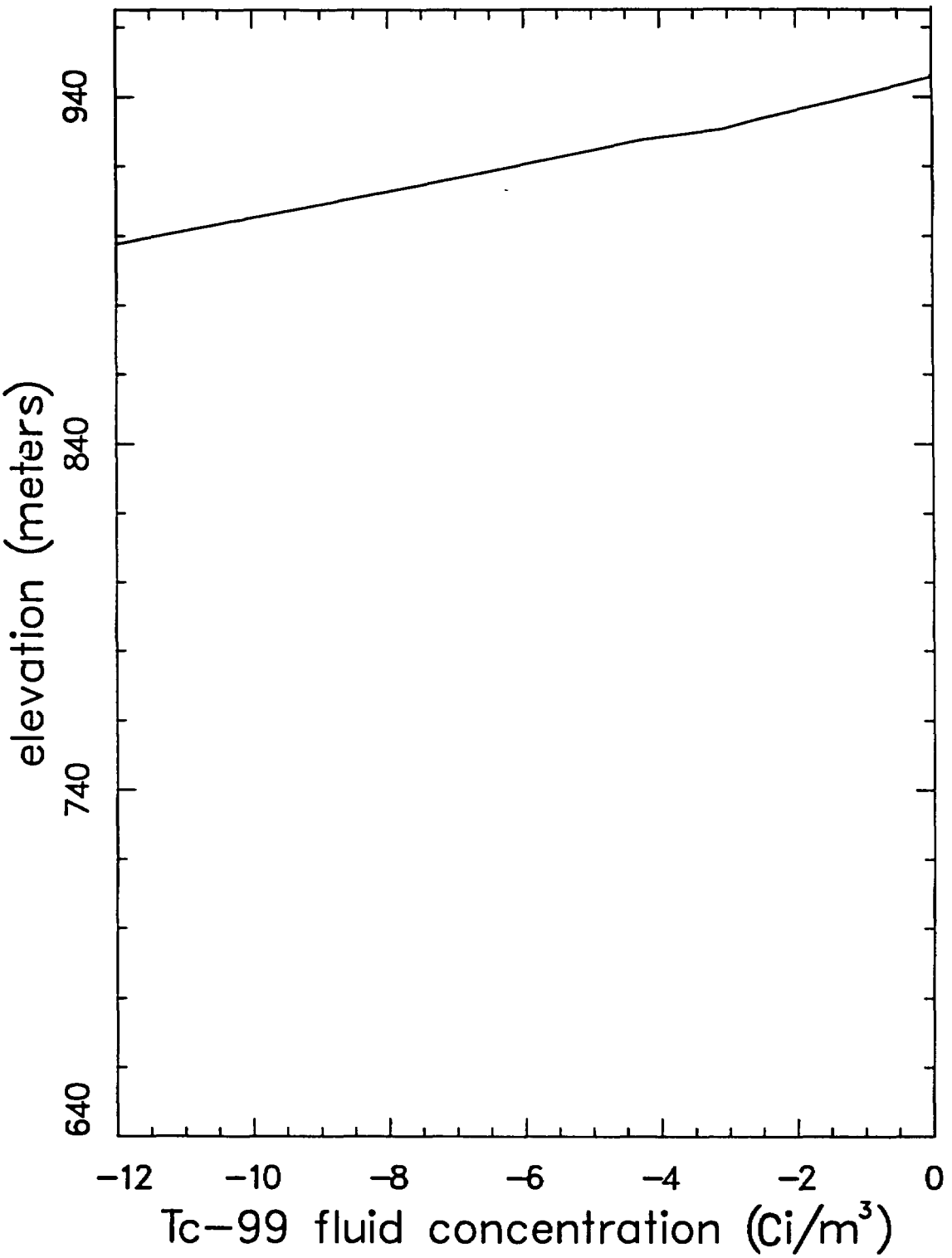

Figure 4-13
TRACRN Analysis - Transport Distribution of ^{99}Tc
Moist-Continuous, Case-1 Source Term
(Logarithm of concentration)

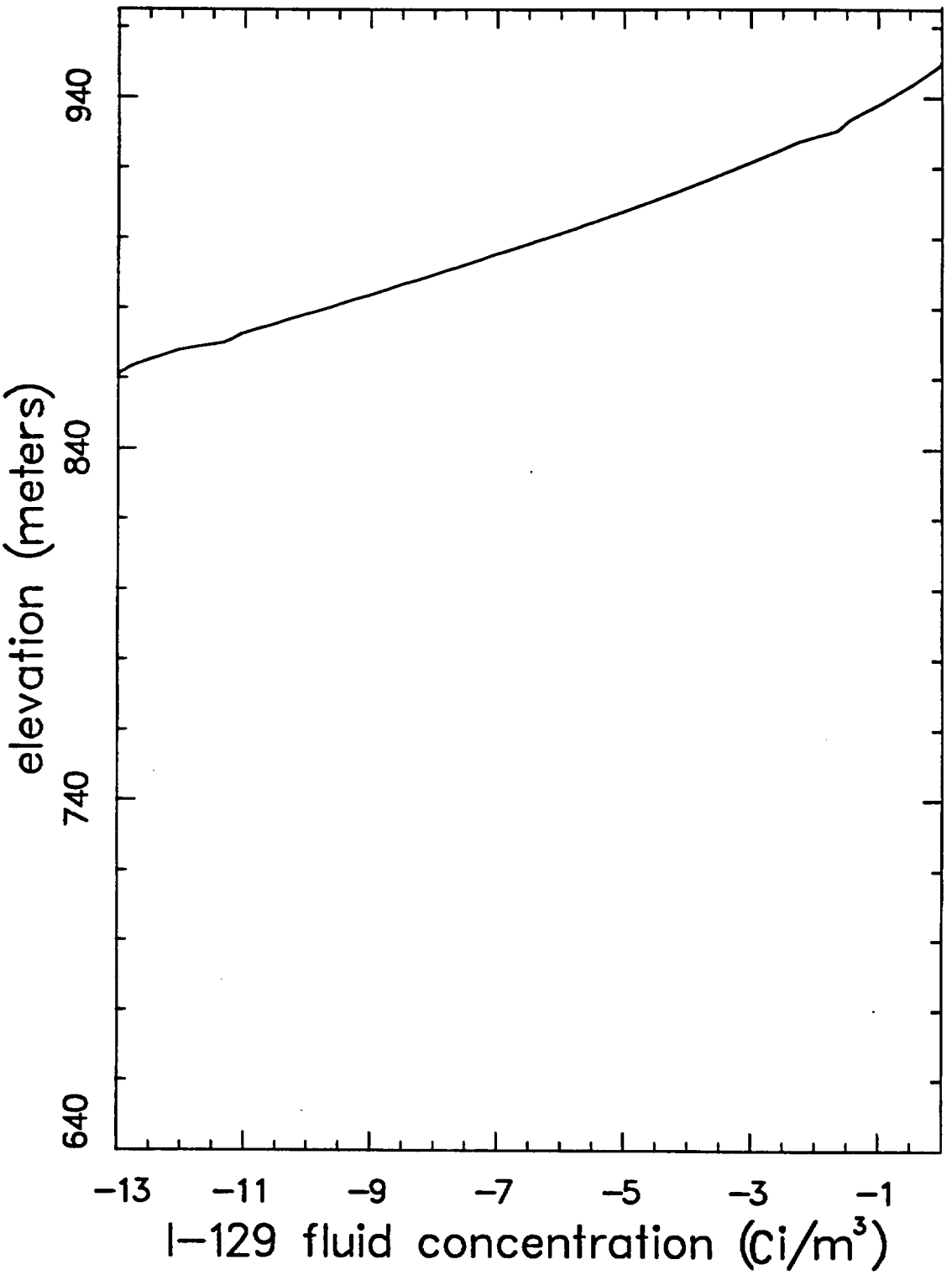

Figure 4-14
TRACRN Analysis - Transport Distribution of ^{129}I
Moist-Continuous, Case-1 Source Term
(Logarithm of concentration)

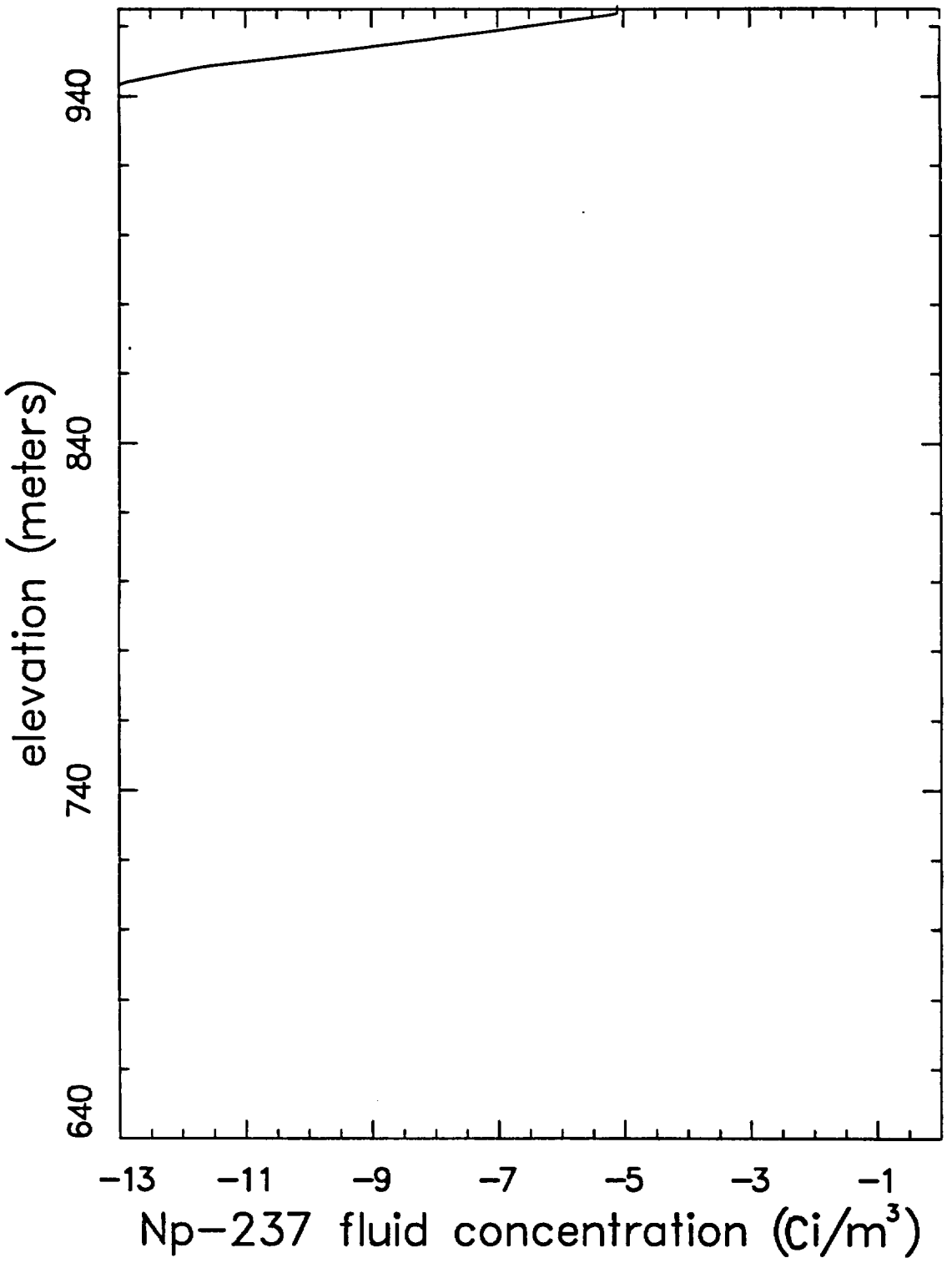

Figure 4-15
TRACRN Analysis - Transport Distribution of ^{237}Np
Moist-Continuous, Case-1 Source Term
(Logarithm of concentration)

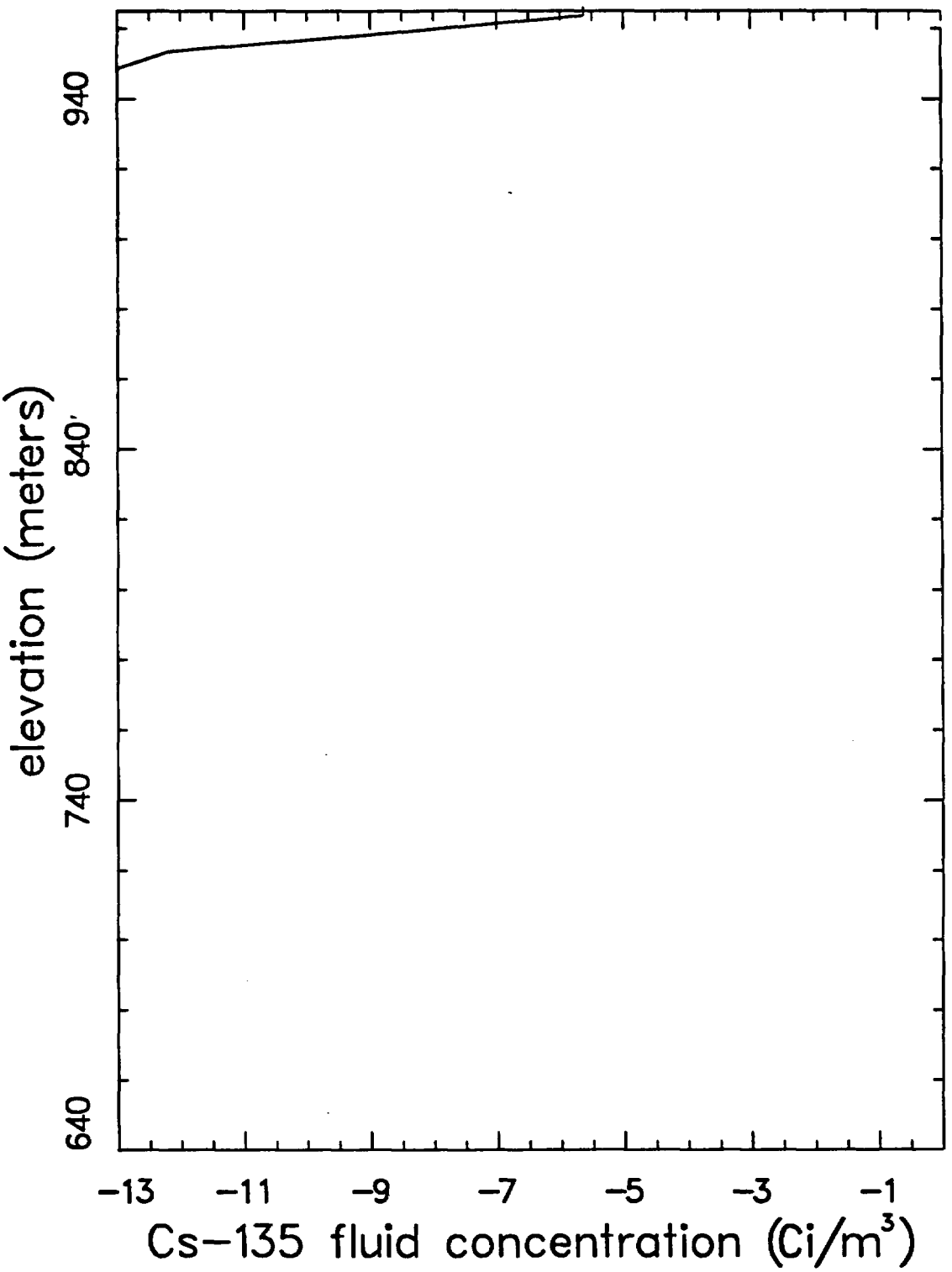

Figure 4-16
TRACRN Analysis - Transport Distribution of ^{135}Cs
Wet-Drip, Flow-Through Source Term
(Logarithm of concentration)

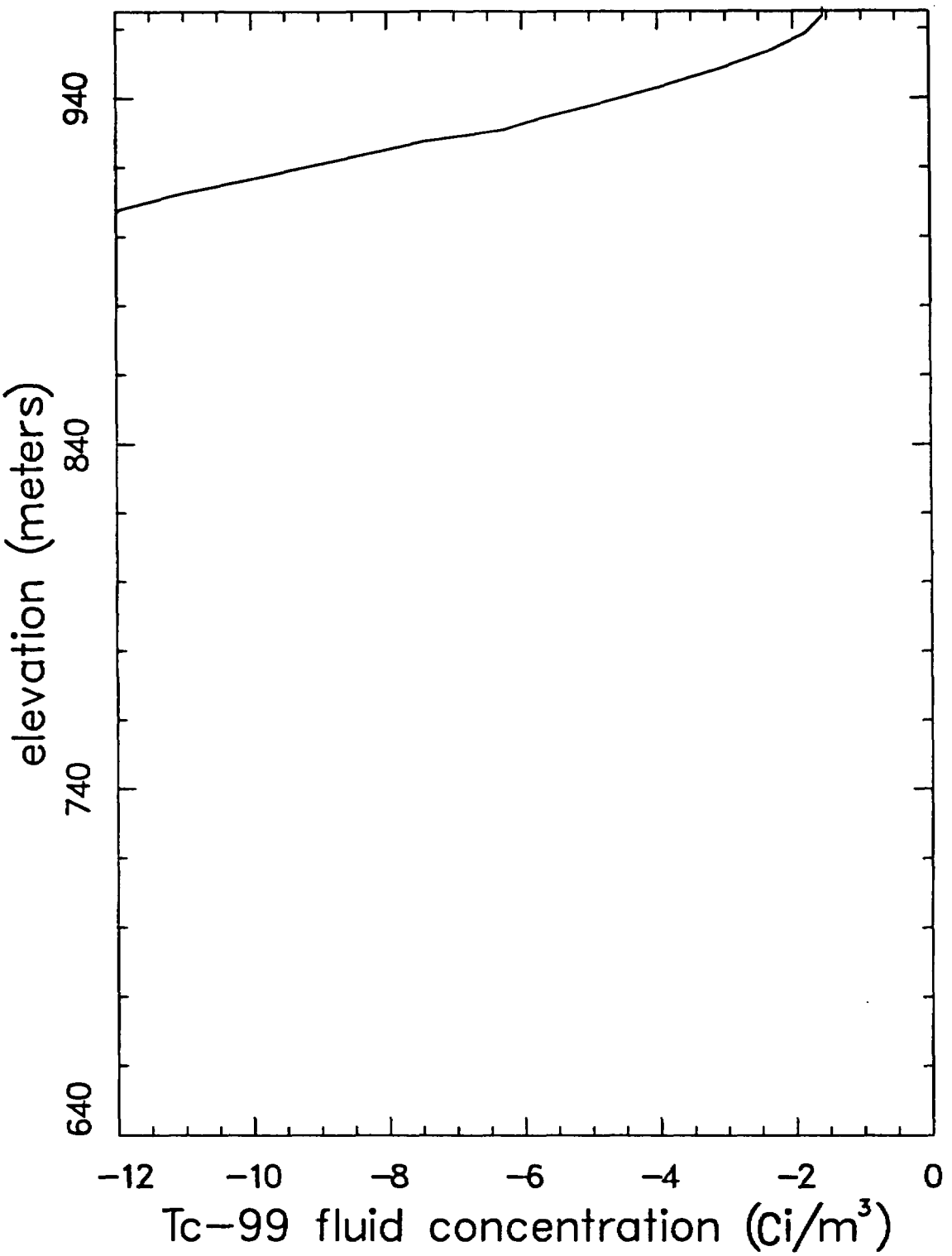

Figure 4-17
TRACRN Analysis - Transport Distribution of ^{99}Tc
Wet-Drip, Flow-Through Source Term
(Logarithm of concentration)

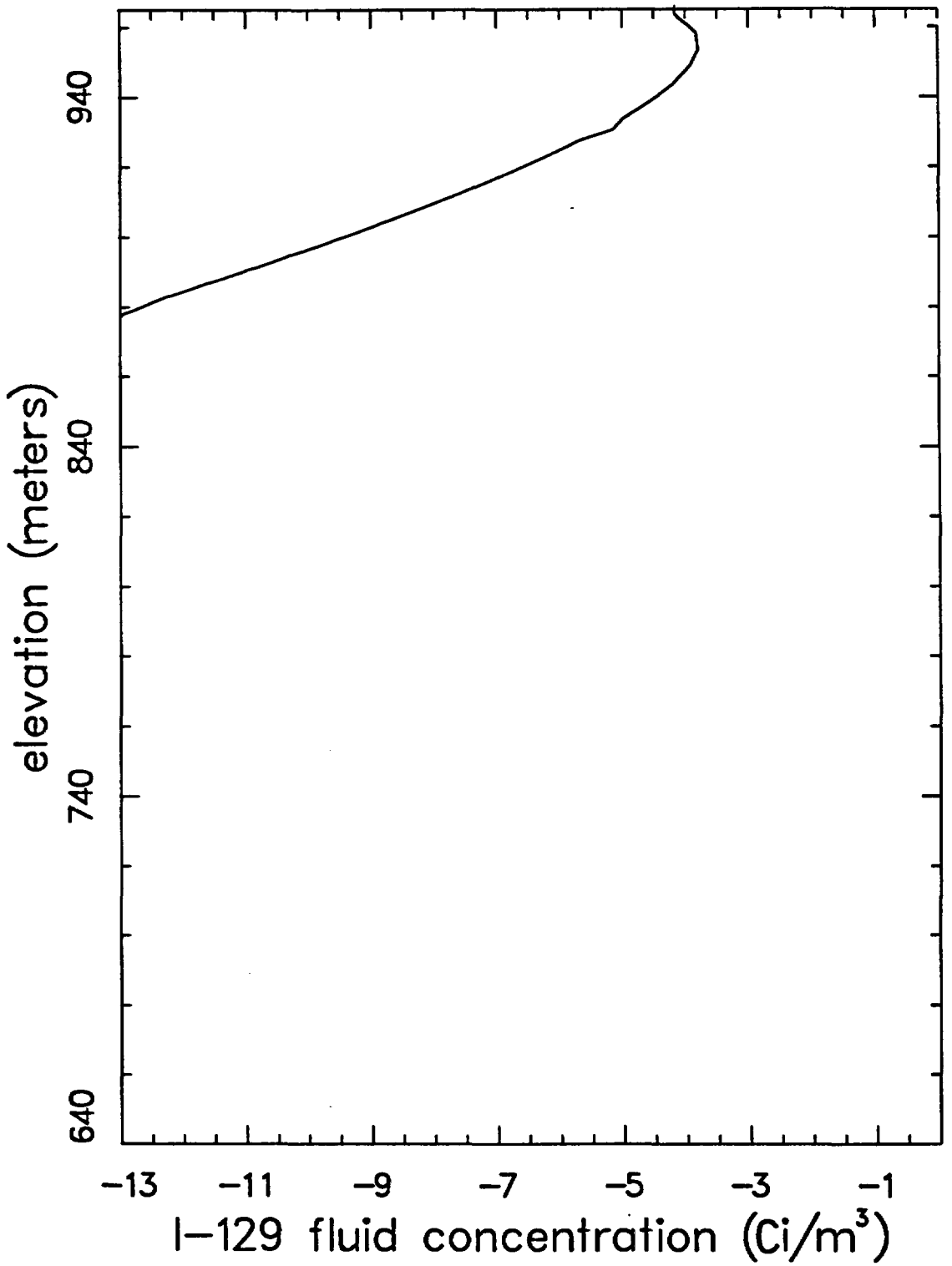

Figure 4-18
TRACRN Analysis - Transport Distribution of ^{129}I
Wet-Drip, Flow-Through Source Term
(Logarithm of concentration)

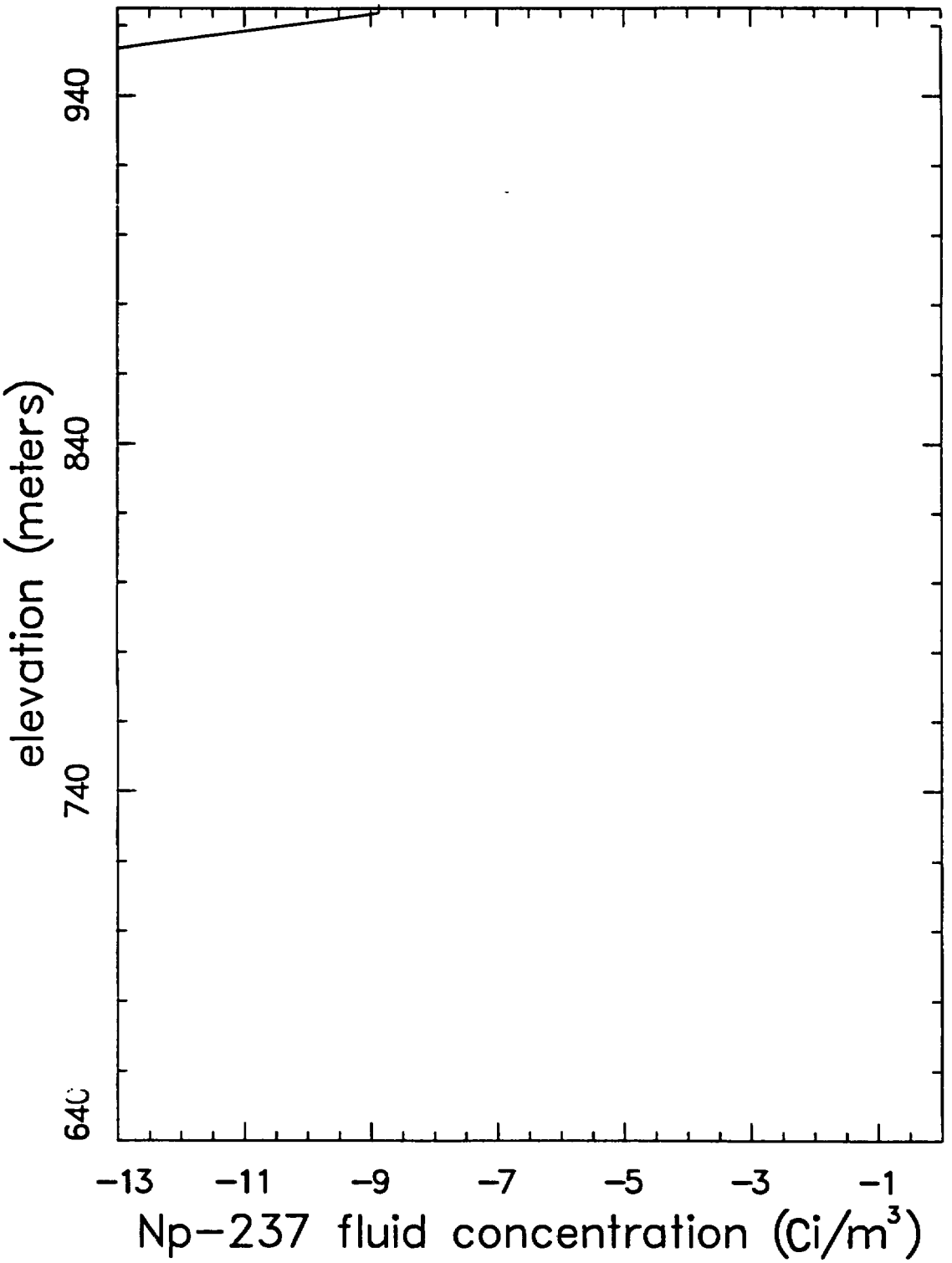

Figure 4-19
TRACRN Analysis - Transport Distribution of ^{237}Np
Wet-Drip, Flow-Through Source Term
(Logarithm of concentration)

Experience with high-resolution 2-D simulations that were started for the perturbed-configuration problems showed that the approach to steady-state flow field was extremely computationally intensive. For a given net infiltration rate it might take several tens of hours of computer CPU time on a large computer such as a Cray Y-MP. Because the 1-D results discussed above indicated that contaminants did not approach the water table at the given infiltration flux, a 2-D simulation would provide little new insight relative to the cost and effort that would be required. Therefore one was not done for this problem.

4.3 TOSPAC

4.3.1 Code Description

TOSPAC is a computer program that calculates groundwater flow and contaminant transport in one dimension (Dudley et al., 1988). TOSPAC consists of three calculational modules: (1) STEADY, which uses Darcy's law to solve for steady-state groundwater flow, (2) DYNAMICS, which uses Richards' equation to solve for transient groundwater flow, and (3) TRANS, which uses a generalized advection-dispersion equation to solve for time-dependent movement of contaminants.

All three modules used the finite-difference method on an Eulerian mesh to solve the differential equations. TOSPAC calculated groundwater flow through partially saturated, fractured, porous media using the composite-porosity model (Peters and Klavetter, 1988). The composite-porosity model provided a description of fractured materials in a manner simple enough to permit site-scale computations. STEADY and DYNAMICS solved for pressure head, then calculated flux, velocity, and saturation for both the matrix and the fractures.

The TRANS module of TOSPAC solved for the time-varying movement of water-soluble contaminants in a flow field supplied by STEADY. TRANS includes terms that accounted for advection, diffus-

ion, hydrodynamic dispersion, contaminant source, contaminant decay, and matrix-fracture coupling (e.g., matrix diffusion). The advective and dispersive terms included a retardation factor (for modeling adsorption), and factors for water-velocity correlation and tortuosity.

The dispersive term in TRANS included both diffusion and hydrodynamic dispersion components. Both upstream and downstream diffusion were allowed, but hydrodynamic dispersion was restricted to the direction of flow. Both the advective and the dispersive terms contained factors for retardation, e.g., adsorption of contaminants onto material surfaces. The input data for retardation are discussed in Section 3.4.

The matrix-fracture coupling term allowed diffusive or advective transfer of contaminants from the water in the matrix to the water in the fractures, and vice versa. Unless there was a barrier to flow between the matrix and the fractures (e.g., a coating on the walls of the fractures), the transfer between matrix and fractures should occur at a much shorter time scale than longitudinal transport. When the time scale was shorter, the matrix and the fractures were said to be tightly coupled.

TRANS can solve for the transport of up to 50 contaminants. Radionuclides can be specified as chains, so that their daughter products are automatically accounted for as they decay. Three different source terms are allowed: calculated source terms based on solubility limitations of the waste, or calculated source terms based on congruent leaching of the source radionuclides from the waste, or arbitrary source terms provided explicitly. The physical and mathematical models used in TOSPAC are described in detail in Dudley et al. (1988). A comprehensive users' guide is in preparation*.

* Gauthier, J. H., M. L. Wilson, R. R. Peters, and A. L. Dudley, in preparation. "Total System Performance Assessment Code (TOSPAC) Volume 2: User's Guide," SAND85-0004, Sandia National Laboratories, Albuquerque, NM.

4.3.2 Problem Setup

TOSPAC was used to analyze flow in columns with stratigraphy representative of the four drill holes defining the boundary of the problem domain. Transport calculations were only performed for the G-4 stratigraphy; this drill hole was the only one which intersected the potential repository. The calculational mesh and geologic-unit assignments for the G-4 stratigraphy are shown in Figure 4-20.

A calculational mesh containing 1361 mesh points was created for the problem set. The mesh points were spaced approximately every 0.5 m through the column, with closer spacing in the neighborhood of the interfaces between geologic units. This spacing was chosen both to ensure a close agreement between the calculated flux and the imposed flux for the flow calculations and to minimize numerical dispersion in the transport calculations.

For the transport calculations, a number of input parameters had not been specified for the exercise, so it was necessary to define them. Dispersivities of approximately ten percent of a path length were reported in the literature (de Marsily, 1986); therefore, a dispersivity factor of 10 m was used (which should return the approximate ten percent value). Diffusion coefficients of 1.0×10^{-9} m^2/s (for ^{99}Tc, ^{129}I, and ^{237}Np) and 2.0×10^{-9} m^2/s for ^{135}Cs, were used. Water-velocity correlation lengths were unavailable. A value of zero was used for the calculations, first because zero was conservative, and second because other participants were either using this value or did not take correlation lengths into consideration. Tortuosity of the matrix was set to ten; tortuosity of the fractures was set to zero. The matrix-fracture-coupling factor was set to one. In TRANS, this setting implied a strong link between the matrix and fractures, e.g., no coating on the fracture walls, and therefore allowed considerable matrix diffusion. For groundwater flow predominantly in the matrix, the coupling factor had no effect; only if fracture flow existed would the results be sensitive to the coupling factor.

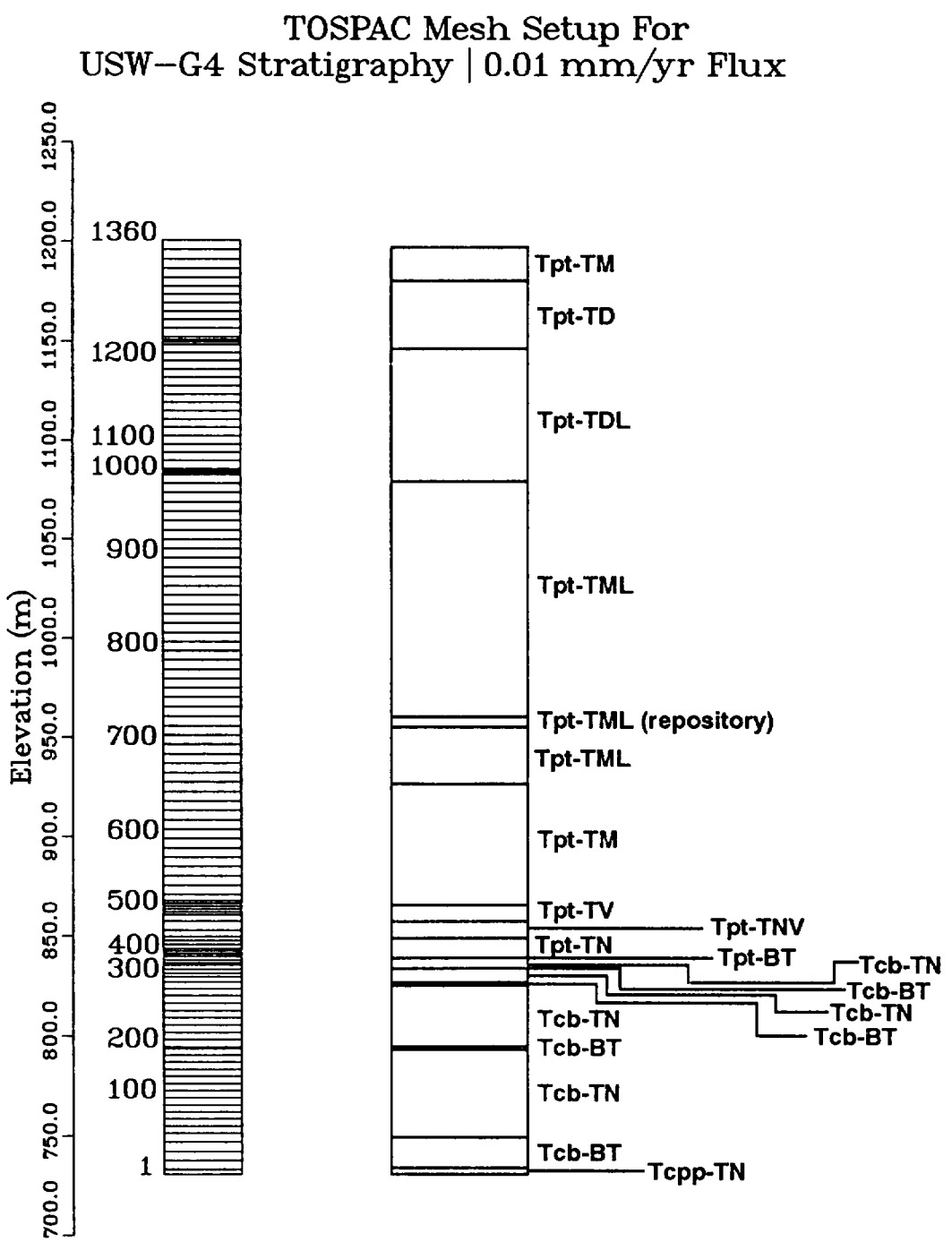

Figure 4-20
TOSPAC Analysis - Problem Geometry for G-4 Stratigraphy

Contaminant half-lives, activities, release limits, and diffusion coefficients were taken from the Environmental Assessment (DOE, 1986). The solubility limit for ^{237}Np was taken from DOE (1986). Solubility limits for ^{99}Tc, ^{129}I, and ^{135}Cs were only known to be large, and were set to values that would not be reached in the calculations (greater than 100 kg/m^3).

Calculations were made using all the source terms given in Section 3.2. The source provided was for the entire repository. It was divided by the design-area of the repository (5.61×10^6 m^2) to provide source-release per square meter. This scaling allowed comparison of one-dimensional and multi-dimensional calculations.

4.3.3 Results

4.3.3.1 Flow Calculations

Steady-state flow calculations were performed using the stratigraphies of the four drill holes defining the problem. The stratigraphies were not simplified: all geologic strata were included, and material properties were used as stated. The flow field calculated for drill hole G-4 was used in the contaminant-transport calculations (Section 4.3.3.2).

For the specified net infiltration of 0.01 mm/yr, Figure 4-21 presents the pressure-head profiles calculated for the four stratigraphies. Typically, the lower the pressure head, the drier the material. A hydrostatic or no-flow condition occurred when the negative pressure head equaled the elevation ($-P = z$). The nominal condition was nearly hydrostatic. Regions where the pressure-head curves became less negative (e.g., in Tpt-TN) were of very low hydraulic conductivity, and large pressures had to be maintained to support flow. The material properties in the G-4 and UE-25a stratigraphies were somewhat different from those used in the G-1 and H-1 stratigraphies, and, as was evident in Tpt-TDL, the pressure-head curves behaved differently.

Figure 4-22 presents the saturation of the matrix for the four stratigraphies. Once the pressure head was known, the saturation could be calculated using the characteristic curves. The characteristic curves for most of the matrix materials used in this exercise had small pores with accompanying large capillary pressures. Even at low pressure heads, the saturation was well above 60 percent. The exception was for Tpt-TNV, which was specified as highly porous and highly conductive.

The saturation of the fractures is presented in Figure 4-23. The fractures were at residual saturation everywhere except in the neighborhood of the lower boundary, where the boundary condition imposed increased saturation. The characteristic curves specified for the fractures indicated that the fractures desaturated at approximately -1 m of pressure head, a value much higher than the pressure profile shown in Figure 4-21.

Figure 4-24 presents the composite flux for the four stratigraphies. Composite flux is the combination of the flux in the matrix and fractures. (In one dimension it is also the same as the Darcy velocity or the percolation rate.) A flux of 0.01 mm/yr is the same as 3.17×10^{-13} m/s, which are the units reported on the plot. For 1-D flow at steady state, the calculated flux should equal the imposed flux. As shown in the figures, the calculated flux deviated by at most one percent. The deviations occurred at interfaces where material properties were discontinuous and STEADY had the most difficulty finding a solution.

The velocity of water in the matrix is shown in Figure 4-25. As mentioned above, velocity was calculated as the flux divided by the effective area available for flow. Velocities were greater than the flux because the area available for flow was less than one m^2. Velocities decreased near the water table because the boundary condition had saturated the fractures in this region.

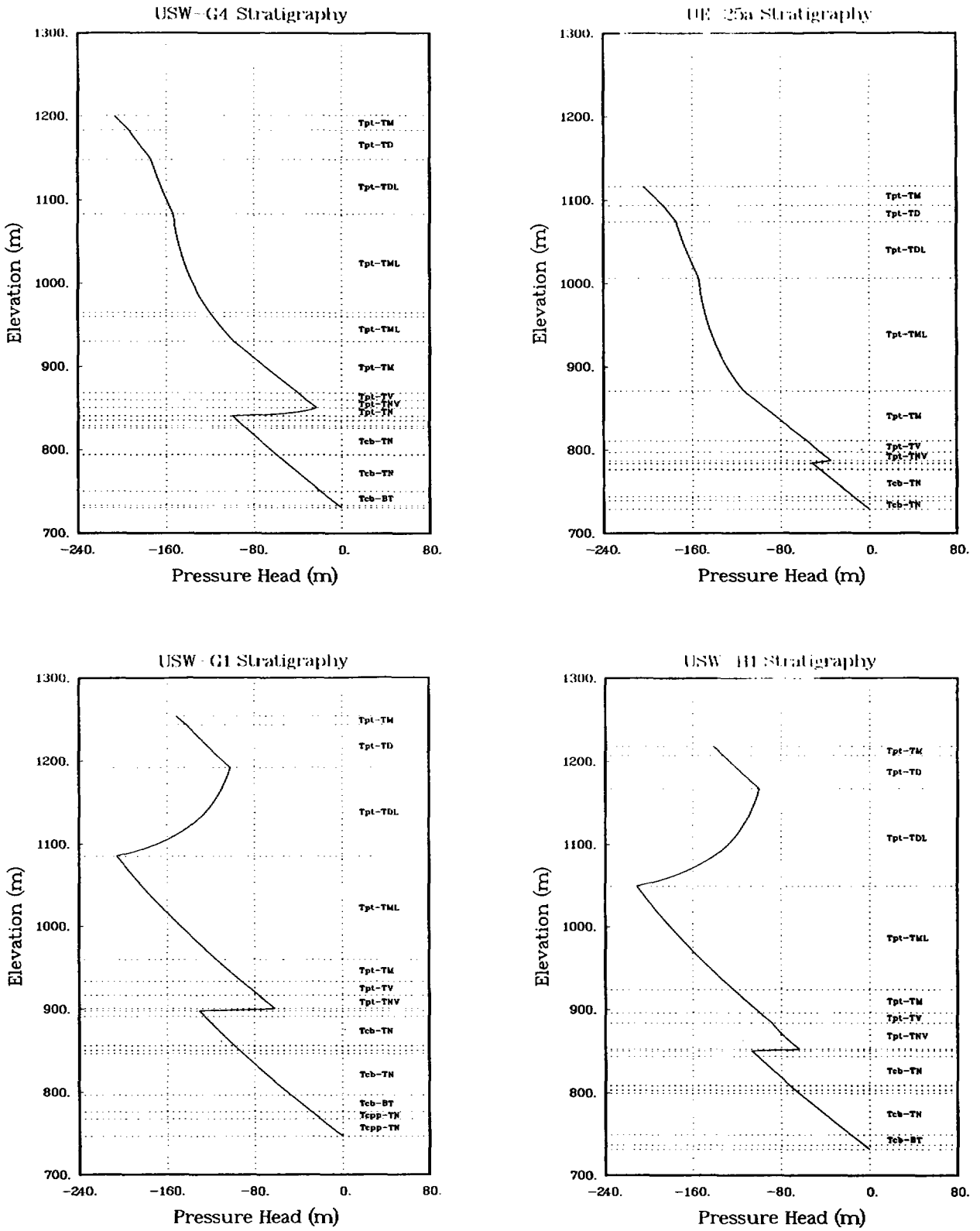

Figure 4-21
TOSPAC Analysis - Pressure-Head Profiles

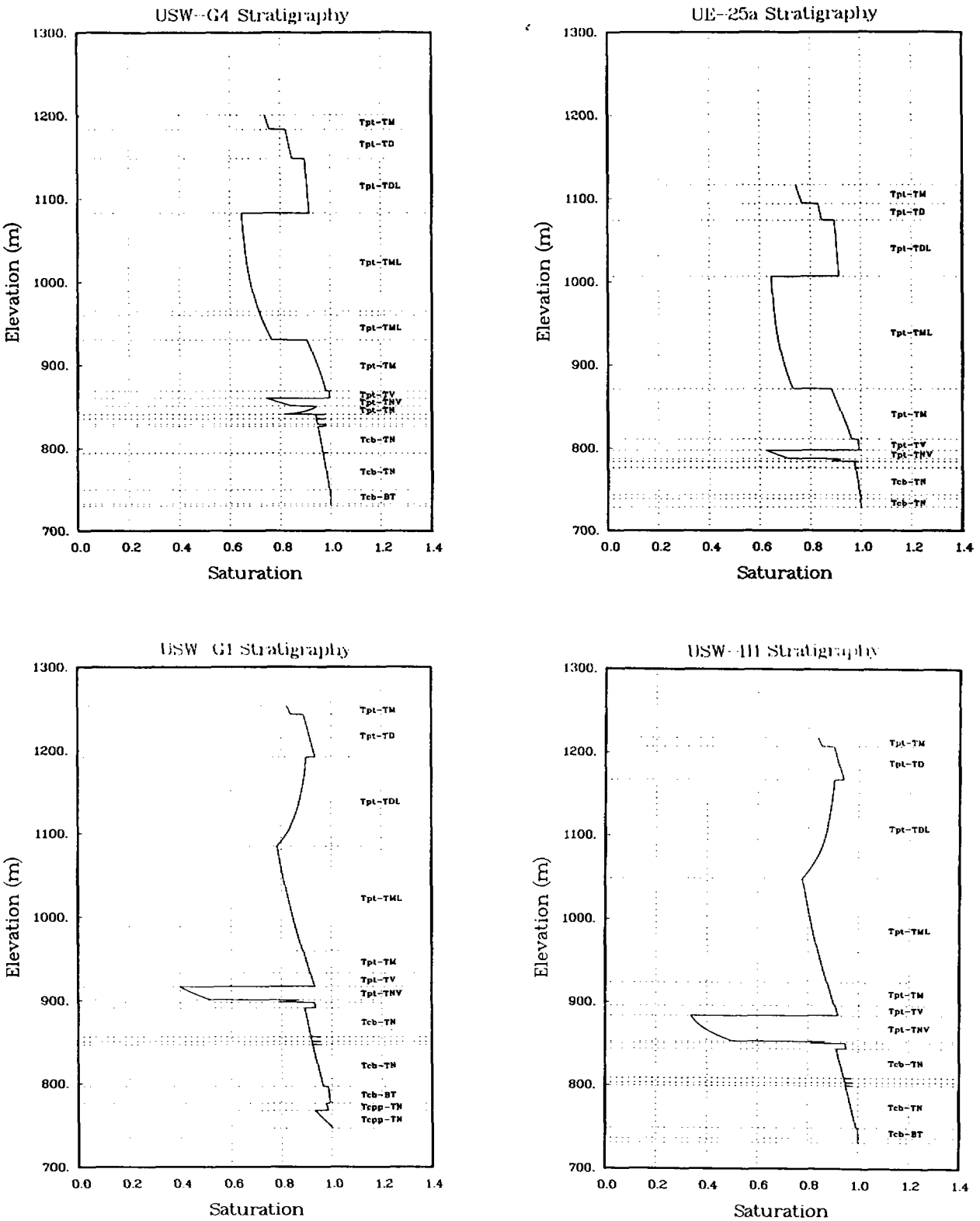

Figure 4-22
TOSPAC Analysis - Matrix-Saturation Profiles

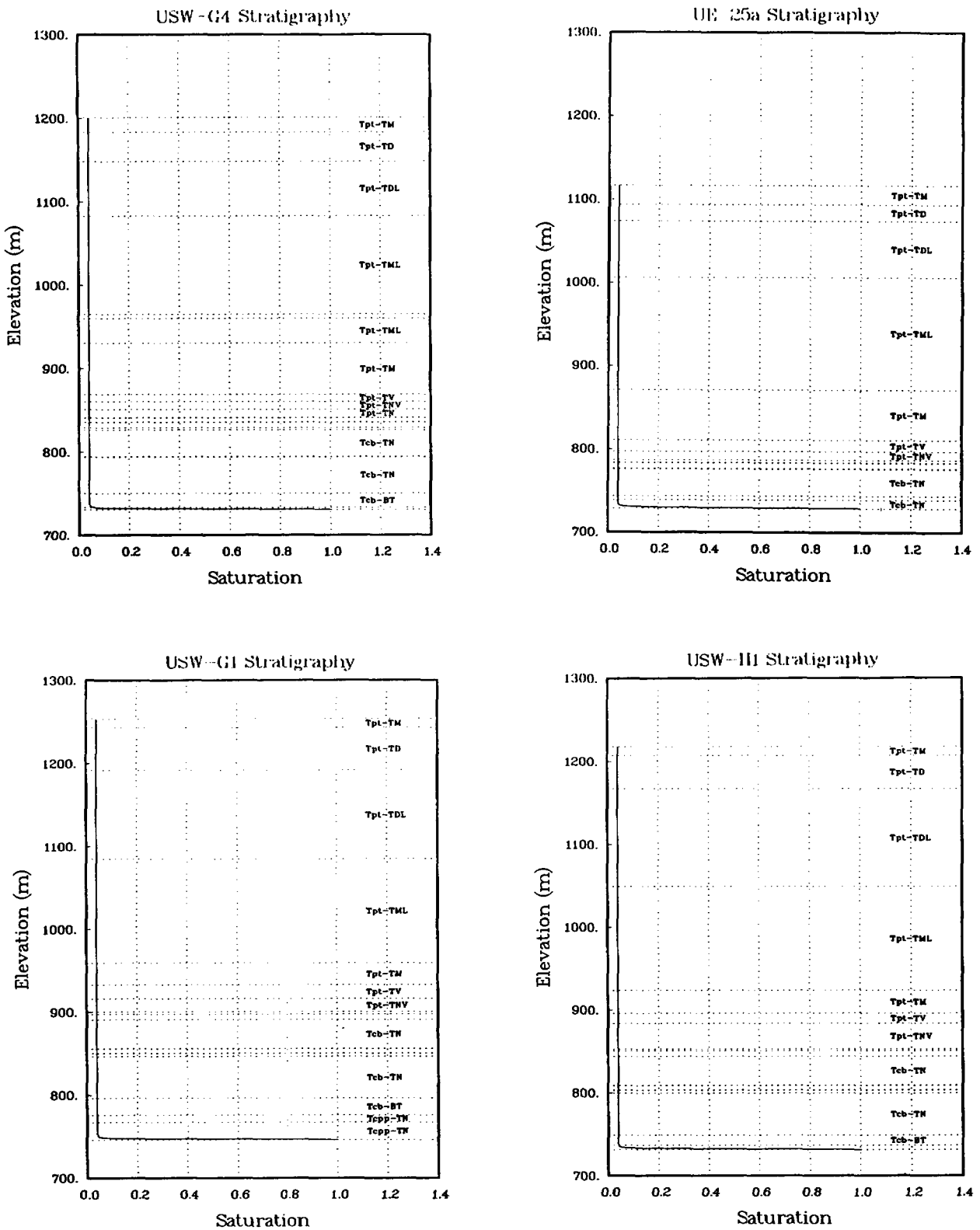

Figure 4-23
TOSPAC Analysis - Fracture-Saturation Profiles

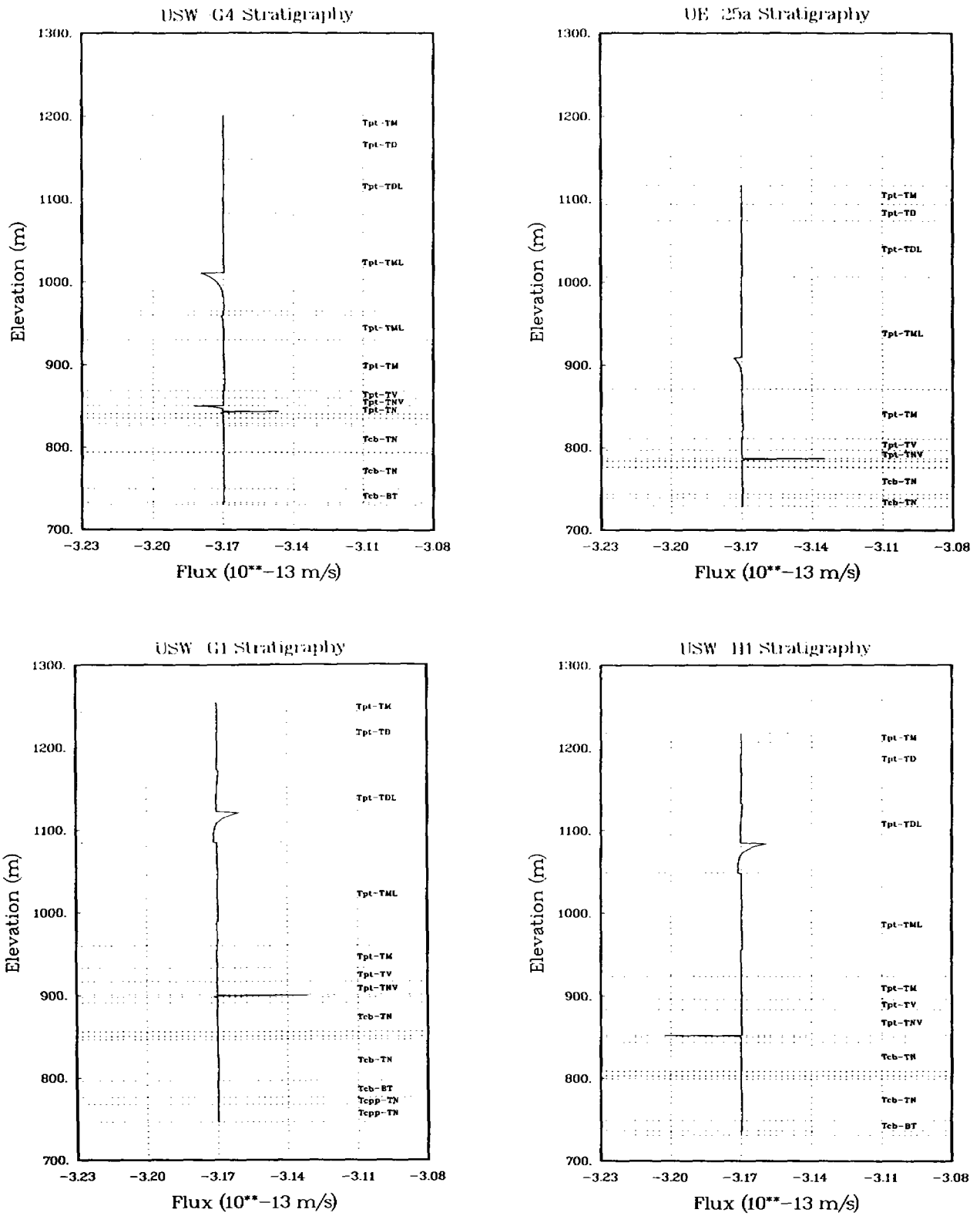

Figure 4-24
TOSPAC Analysis - Composite-Flux Profiles

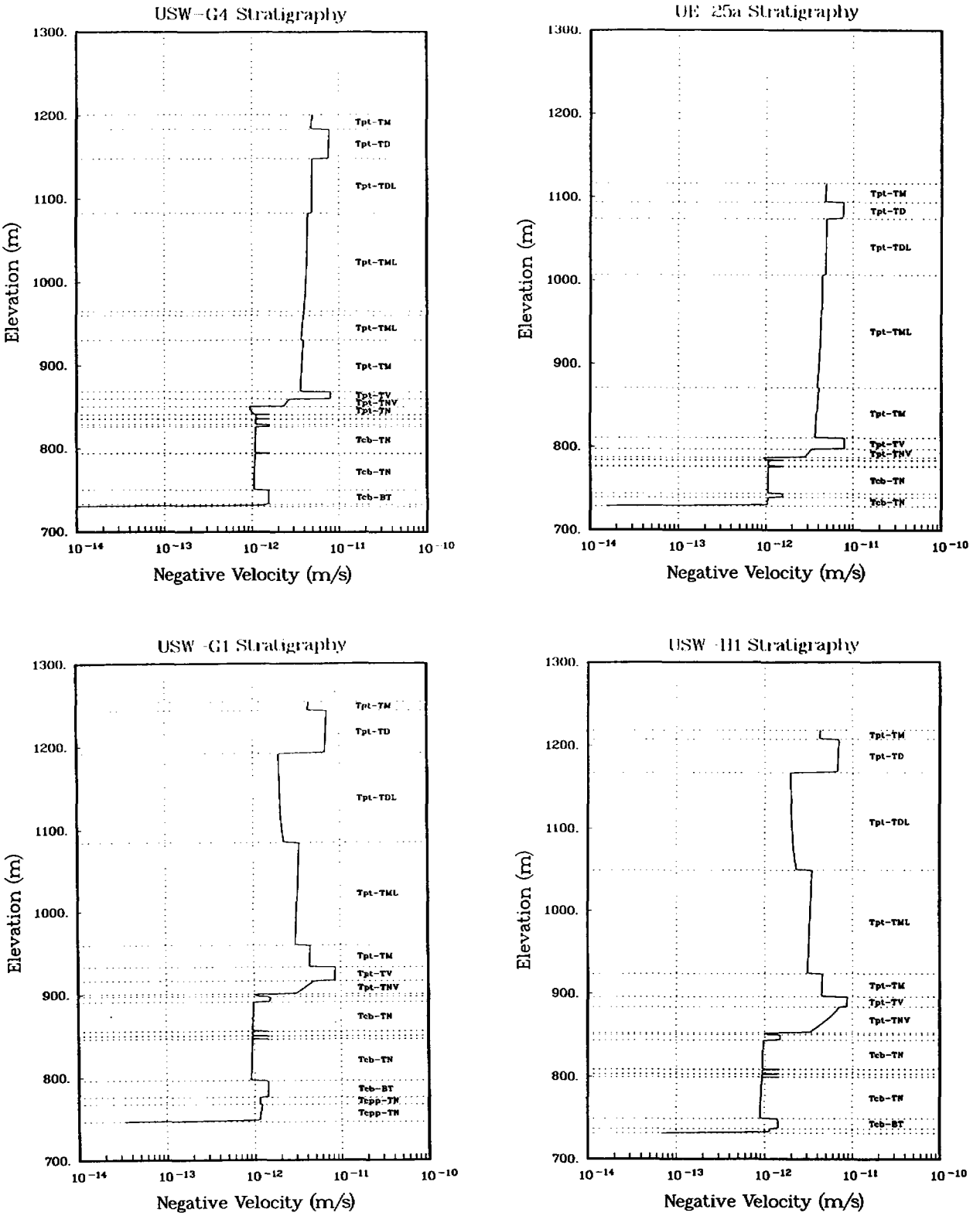

Figure 4-25
TOSPAC Analysis - Matrix Water-Velocity Profiles

Figure 4-26 shows the velocity of water in the fractures. Significant velocities were only evident near the water table where the fractures contained water (as shown in Figure 4-23). Two units in the G-4 stratigraphy were sufficiently nonconductive to show incipient flow in the fractures, even at this low flux. Given the assumptions in the model for groundwater flow, no significant flow could occur in the fractures.

Figure 4-27 presents the groundwater travel times calculated in the four drill holes. These were an important measure by which to compare different calculations, especially those done in one dimension and those done in multiple dimensions. Travel times were calculated by the average-fastest-particle method. The "fastest" particle was the one which traveled the fastest path, either through the matrix or the fractures, provided that path carried at least one percent of the total flow. The figure also shows the travel times that resulted if a particle was restricted to the matrix or the fractures, with a note telling over how much of the distance the result was applicable (e.g., how much of the distance carried at least one percent of the flow). The travel times were from an elevation of 960 m to the water table. Because the elevation of the water table varied for each stratigraphy, this distance varied for each drill hole. The 960-m elevation was chosen because it corresponded to the bottom of the repository at drill hole G-4.

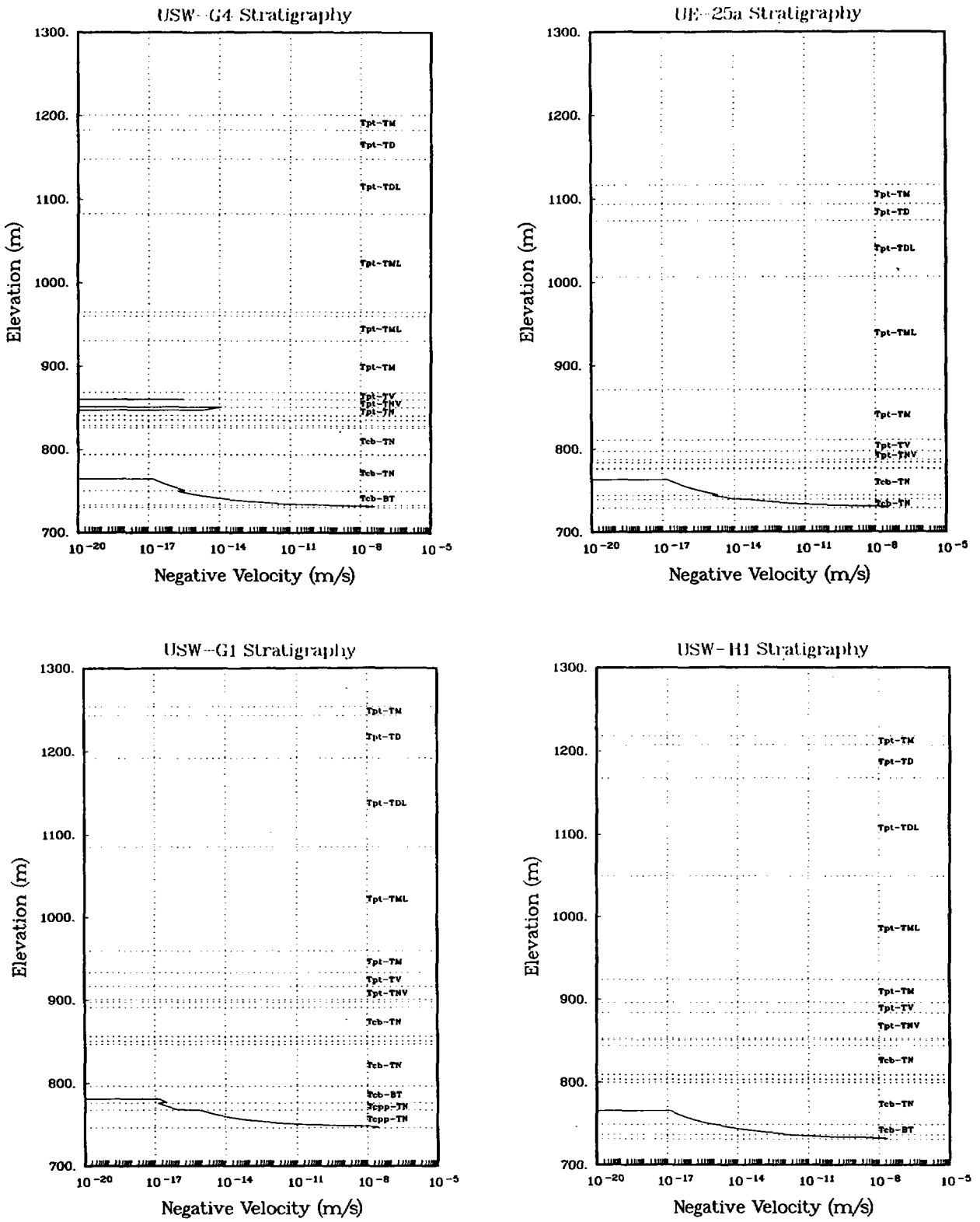

Figure 4-26
TOSPAC Analysis - Fracture Water-Velocity Profiles

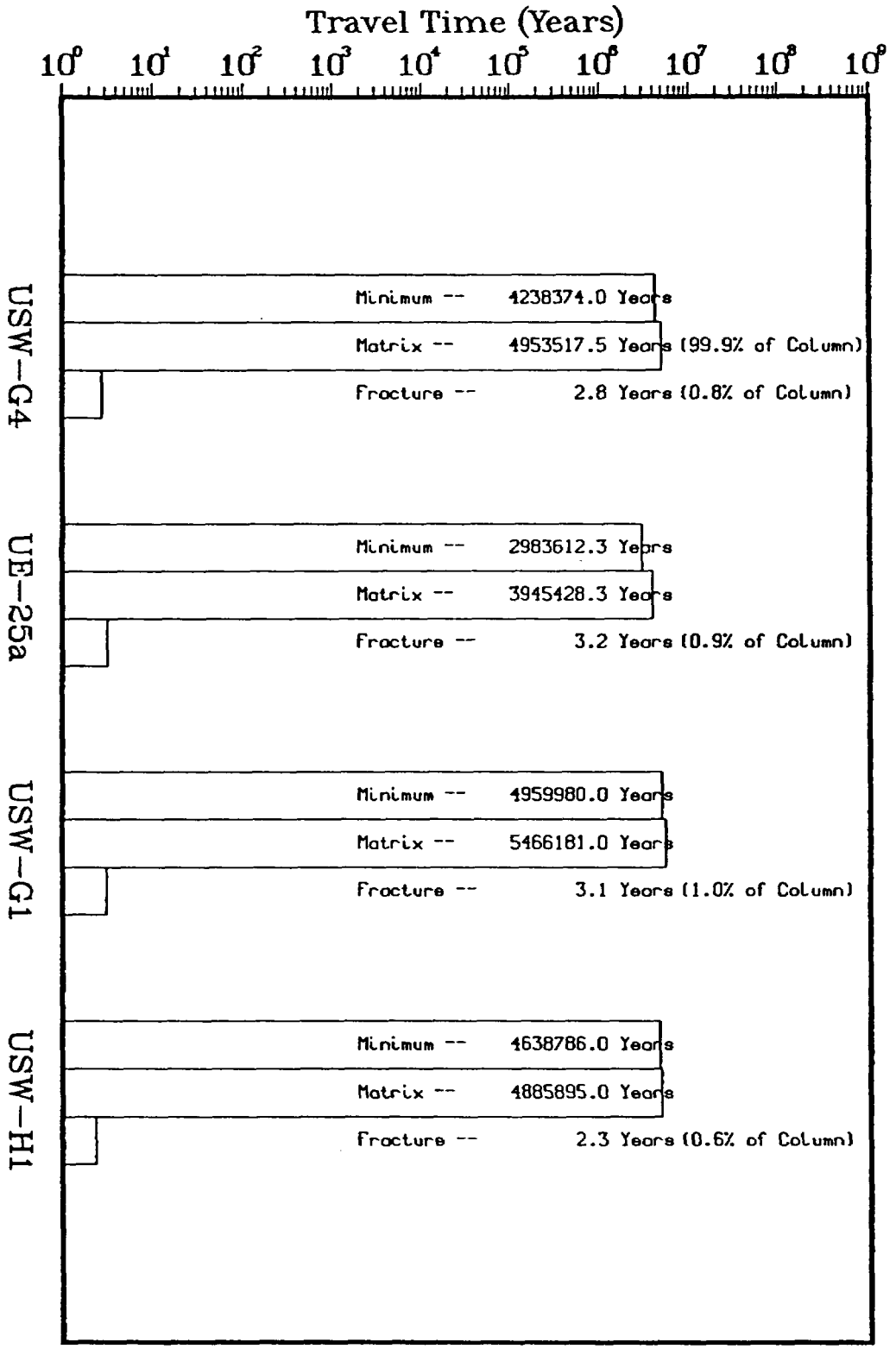

Figure 4-27
TOSPAC Analysis - Groundwater Travel Times From the Repository for the Four Stratigraphies

4.3.3.2 Transport Calculations

Calculations with TOSPAC indicated that only ^{129}I would reach the water table in 100,000 years for these input parameters. Therefore, in this section the contaminant concentration levels in the groundwater are used to describe the results.

Figure 4-28 presents the concentration profiles of the four nuclides, as supplied by the moist-continuous Case-1 source. In this, and all the other plots in this section, the smooth shapes of the profiles are a consequence of using constant dispersivity and diffusion coefficients on the transport equation. At the repository elevation, the amounts of ^{99}Tc, ^{129}I, and ^{237}Np increased steadily with time. ^{99}Tc and ^{129}I showed a spreading of concentration over distance and time. Since ^{135}Cs and ^{237}Np were highly retarded species, they adsorbed to the matrix material near the repository. They were not expected to move far.

^{99}Tc showed spreading of approximately 40 m upstream from the repository and 50 m downstream at 100,000 years. At a steady-state water flux of 0.01 mm/yr, by advection alone a contaminant particle could be expected to travel 10 m in 100,000 years. This fact, plus analysis of the transport equation showed that approximately 10 m of the downstream spreading was caused by advection, 40 m was caused by diffusion, and less than 1 m was caused by hydrodynamic dispersion. These proportions held also for the other nuclides, and they were independent of the source term used.

The spreading of the concentration curves over elevation differed because the retardation factors differed among nuclides. For instance, ^{129}I showed greater spreading than ^{99}Tc; ^{129}I was specified to have no retardation in any of the geologic units, while ^{99}Tc was specified to have a retardation of 0.1 in the Tpt-TML. The retardation of ^{99}Tc was small, but it was not zero. In contrast, retardations of ^{135}Cs and ^{237}Np were specified as 100 and 5, respectively, for Tpt-TML. ^{135}Cs and ^{237}Np showed minimal transport.

Figure 4-29 presents concentration surfaces for the four nuclides using the moist-continuous Case-1 source. Concentration surfaces indicate how the concentration behaved over both time and distance. On the plots, the top of the column (1200.6 m) is to the right; the bottom (730.6 m) is to the left. Early time (zero years) is in the background; late time (100,000 yr) is in the foreground. The concentration scale differs for each nuclide; therefore some care must be taken when interpreting the surface. The concentration surfaces indicate how the source term influenced the results. In the plots, the repository region is the highest part of the surface. The concentrations in this region are the amounts released by the source term dissolved in the available water.

For the Case-1 source, the ^{99}Tc and ^{237}Np concentrations in the source region were monotonically increasing over time (they were released at a relatively constant rate). The ^{135}Cs concentration reached a maximum almost immediately, then stayed at approximately this level. The ^{129}I concentration had a peculiar dip in it at early time. The dip was caused by the transport of the readily releasable fraction of ^{129}I in the waste container; after this release was transported out of the source region, the concentration dropped until the remaining ^{129}I was released. Other nuclides also had a ready-release fraction (e.g., ^{135}Cs), but because of retardation, they did not move away fast enough to cause a dip in the concentration in the source region.

Figure 4-30 shows the concentration profiles of the four nuclides from moist-continuous Case-2 source. The profiles for ^{99}Tc and ^{129}I were very similar to those presented in Figure 4-28. The profiles for ^{135}Cs and ^{237}Np were similar in shape to those presented in Figure 4-28, but the concentrations were two orders of magnitude greater. Figure 4-31 presents the concentration surfaces for the four nuclides using the Case-2 source. Other than a difference in quantity, the major dissimilarity was with the shape of the ^{135}Cs surface in the source region. With the Case-1 source, ^{135}Cs reached its maximum concentration almost immediately; with the Case-2 source, the concentration increased over time.

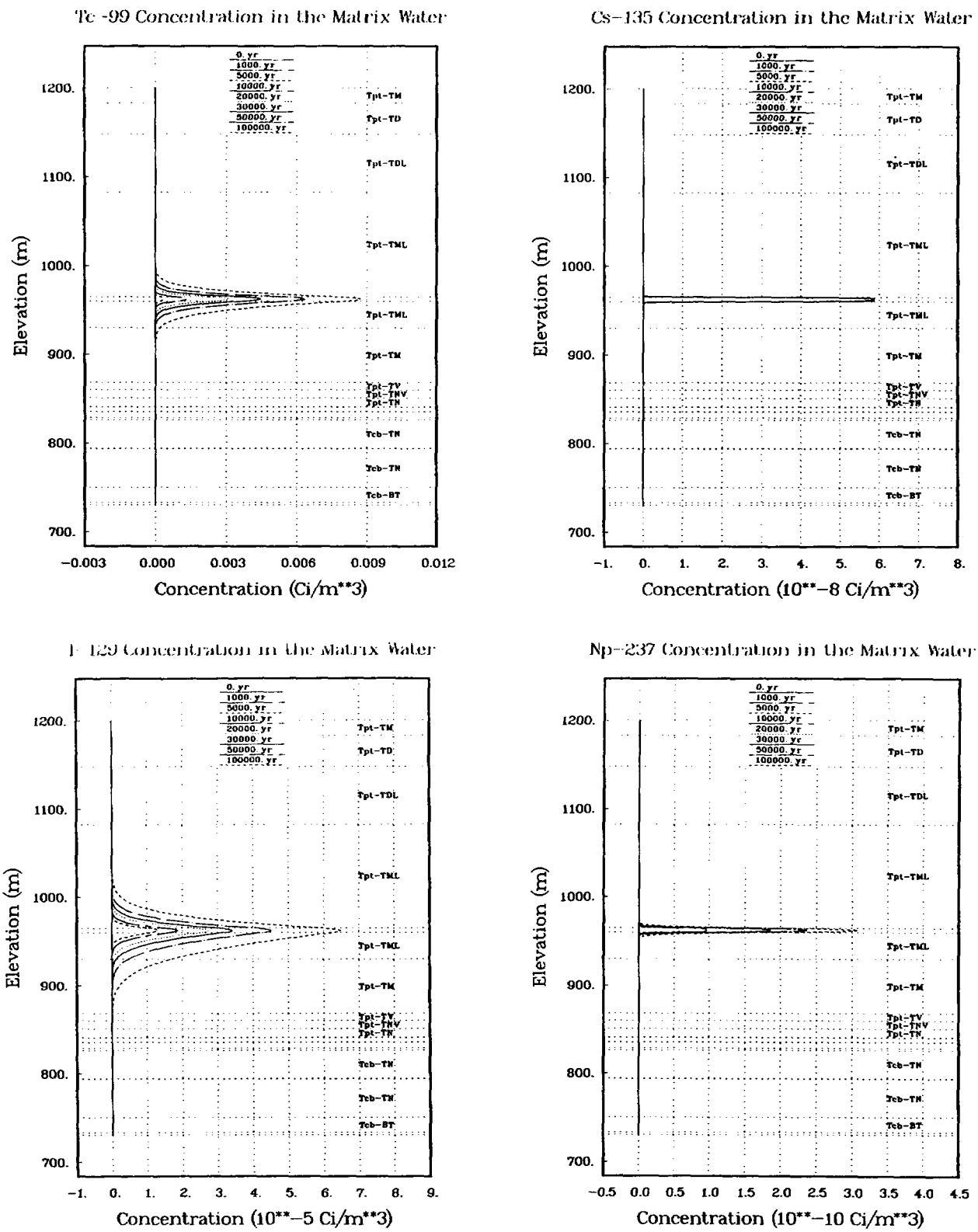

Figure 4-28
TOSPAC Analysis - Concentration Profiles Using Moist-Continuous, Case-1 Source

USW–G4 Stratigraphy; 0.01 mm/yr Flux
Moist–Continuous Source (Case 1)
Tc–99 Concentration in the Matrix Water

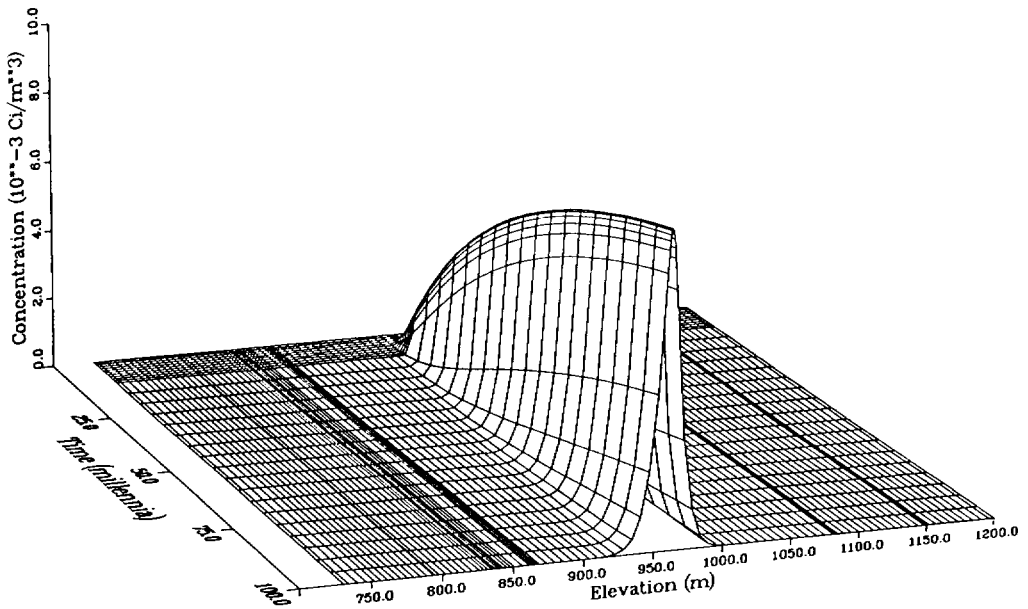

USW–G4 Stratigraphy; 0.01 mm/yr Flux
Moist–Continuous Source (Case 1)
Cs–135 Concentration in the Matrix Water

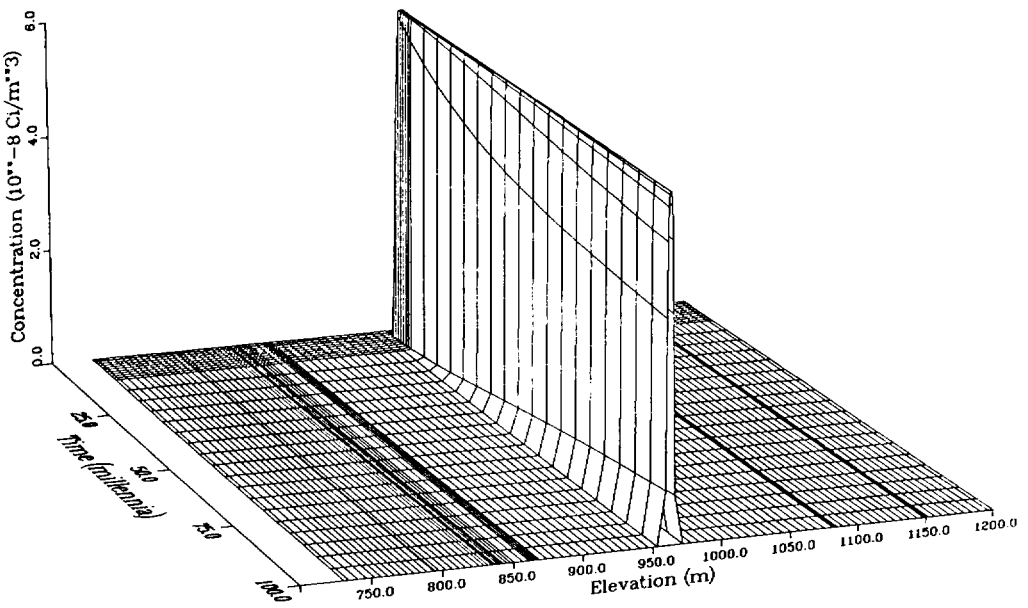

Figure 4-29
TOSPAC Analysis - Concentration Surfaces Using
Moist-Continuous, Case-1 Source

USW–G4 Stratigraphy; 0.01 mm/yr Flux
Moist–Continuous Source (Case 1)
I–129 Concentration in the Matrix Water

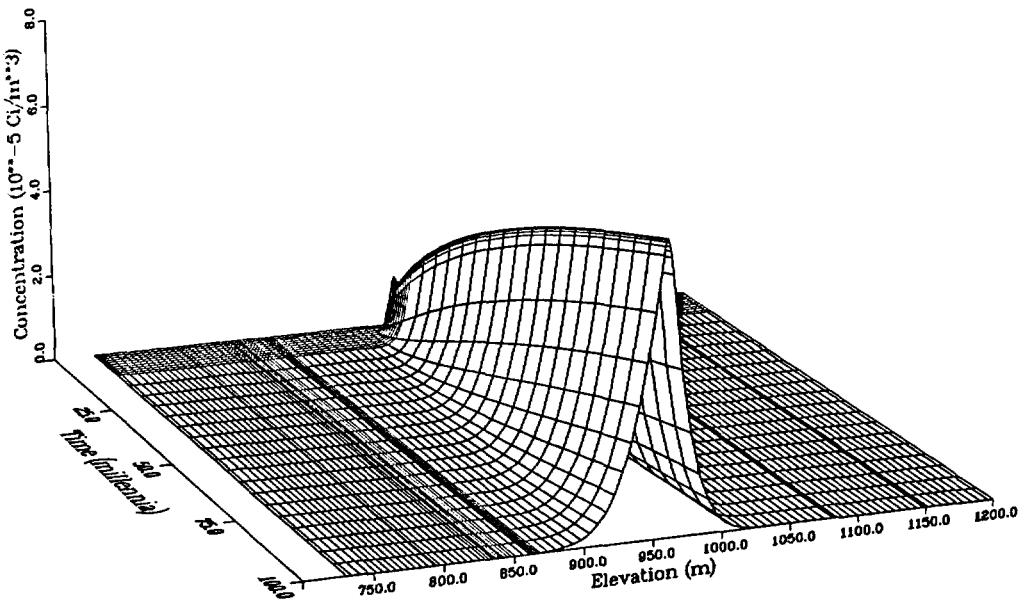

USW–G4 Stratigraphy; 0.01 mm/yr Flux
Moist–Continuous Source (Case 1)
Np–237 Concentration in the Matrix Water

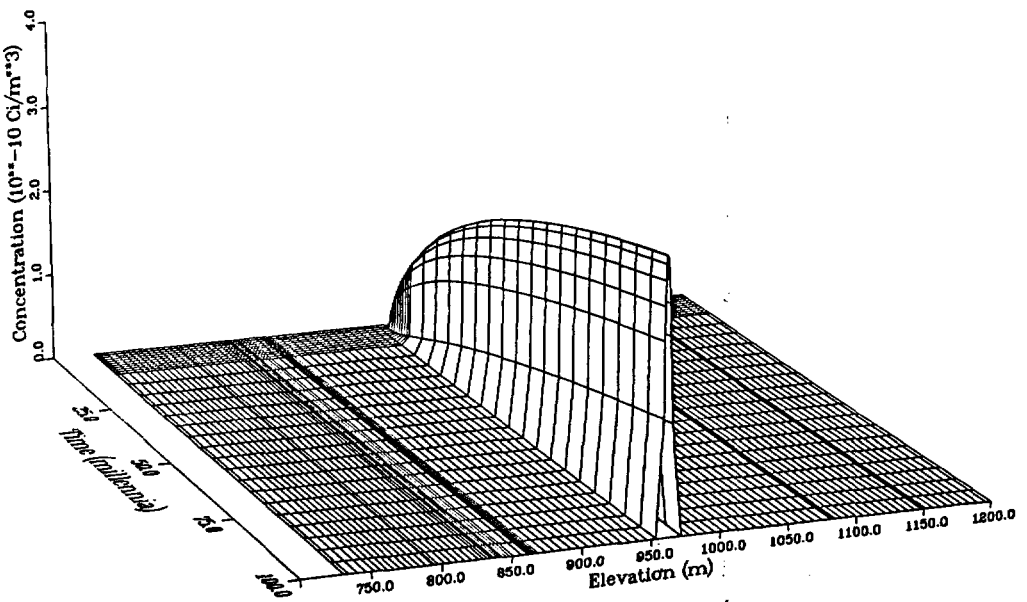

Figure 4-29, Continued

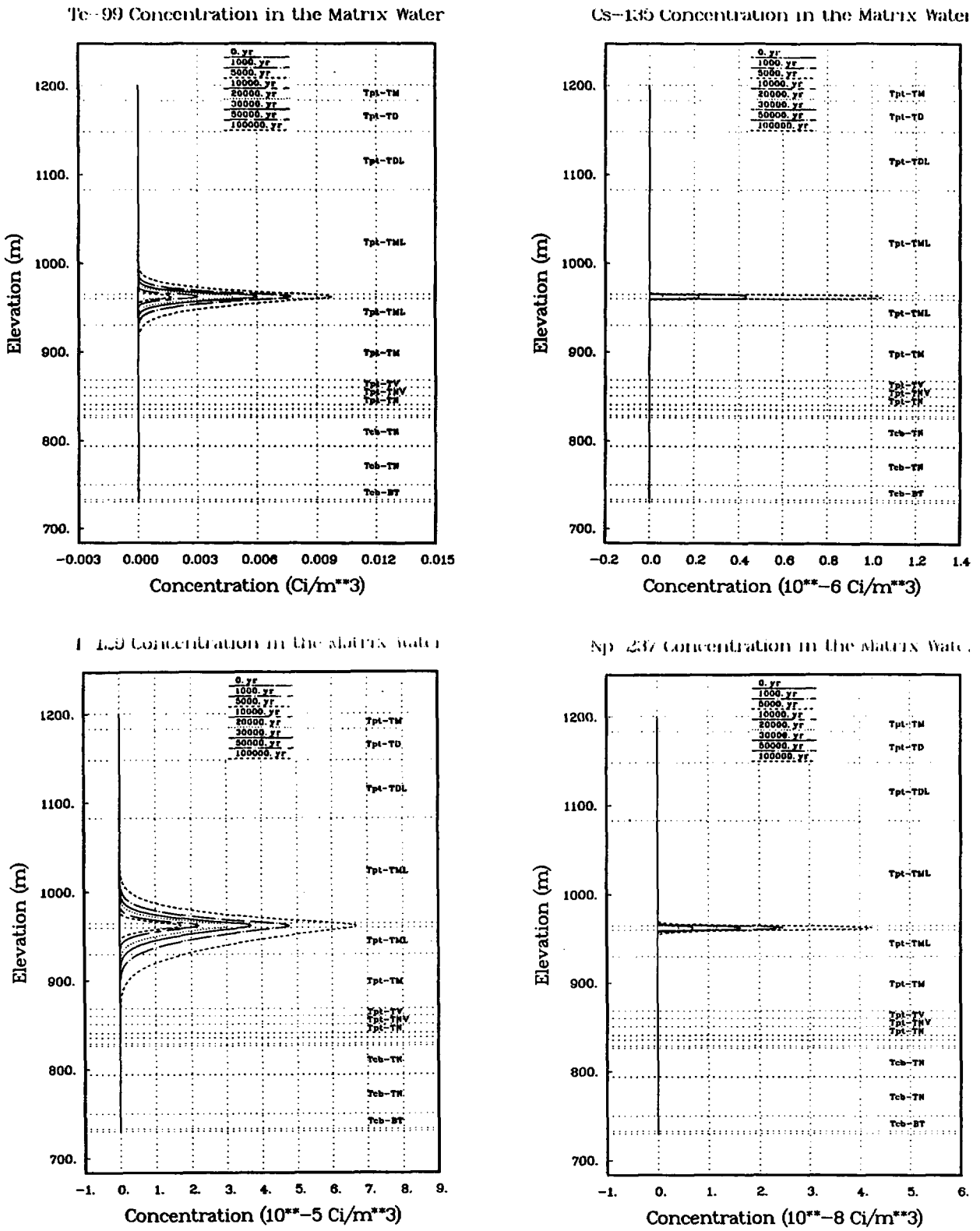

Figure 4-30
TOSPAC Analysis - Concentration Profiles Using Moist-Continuous, Case-2 Source

USW–G4 Stratigraphy; 0.01 mm/yr Flux
Moist–Continuous Source (Case 2)
Tc–99 Concentration in the Matrix Water

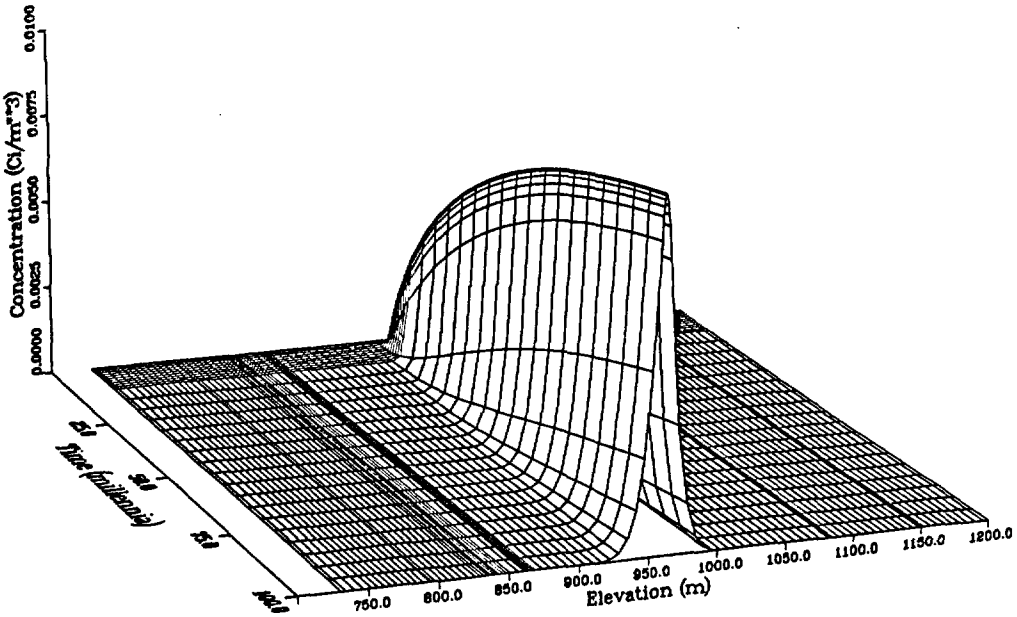

USW–G4 Stratigraphy; 0.01 mm/yr Flux
Moist–Continuous Source (Case 2)
Cs–135 Concentration in the Matrix Water

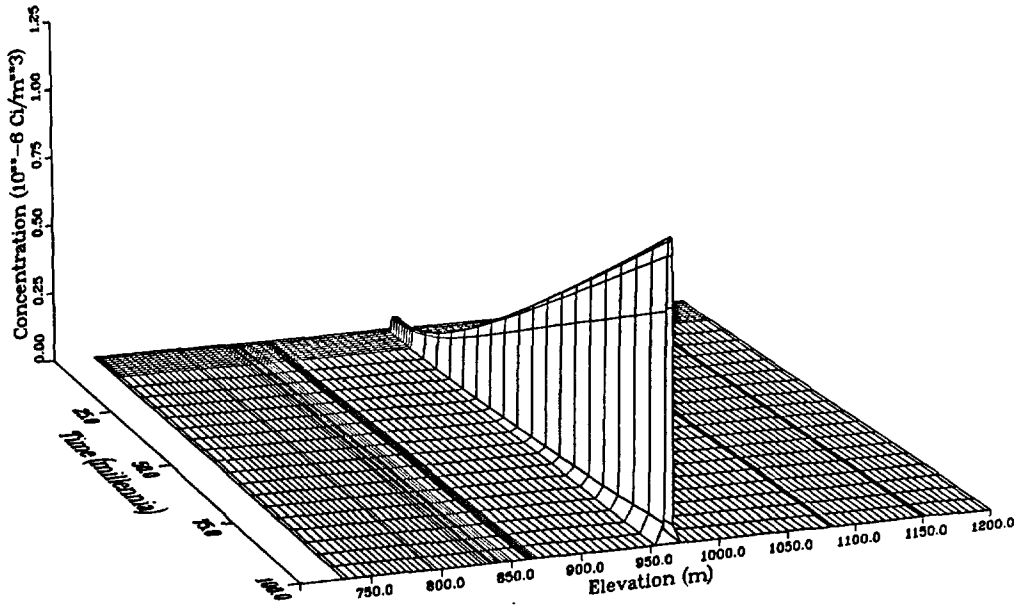

Figure 4-31
TOSPAC Analysis - Concentration Surfaces Using
Moist-Continuous, Case-2 Source

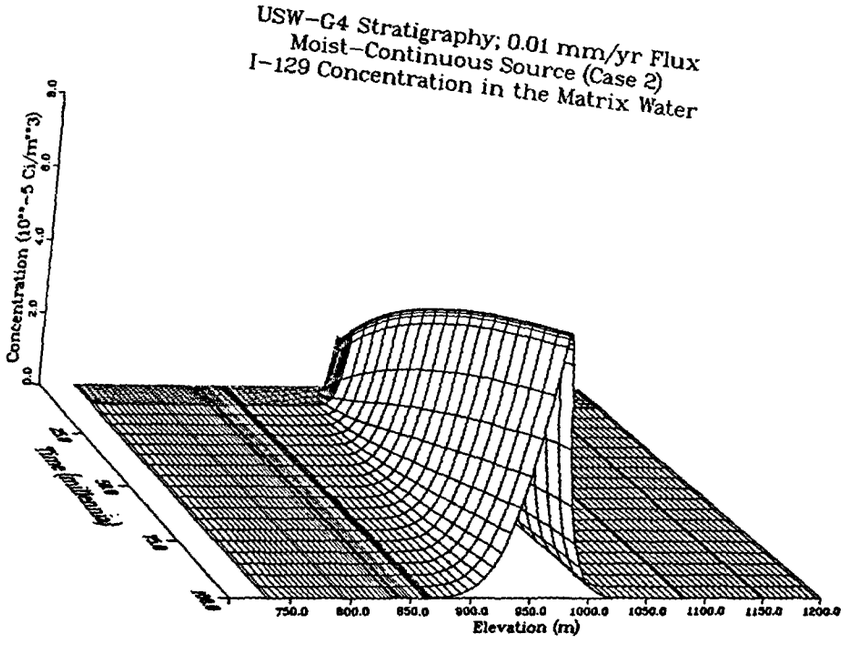

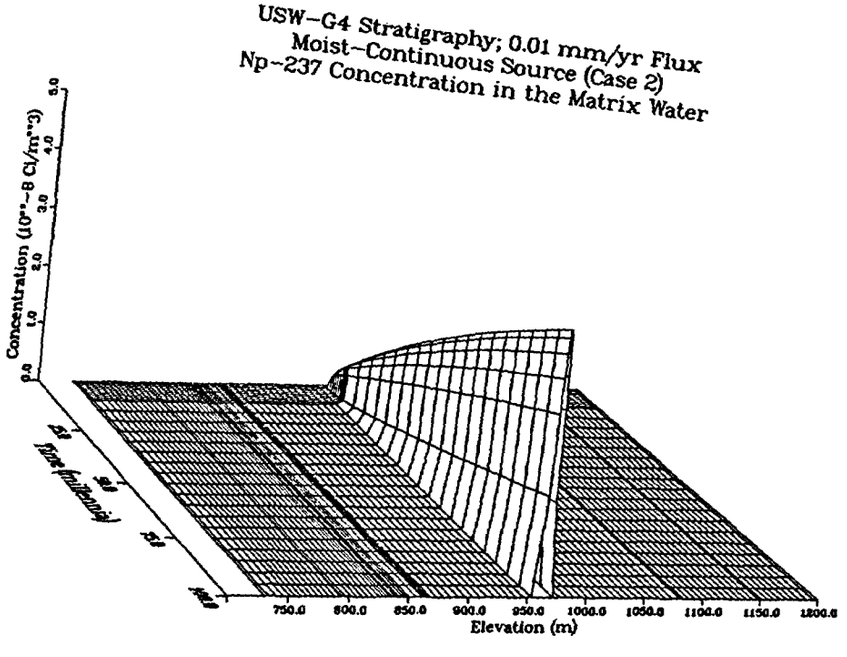

Figure 4-31, Continued

The concentration profiles for the moist-continuous Case-3 source are presented in Figure 4-32. Concentrations for nuclides ^{135}Cs and ^{237}Np appeared similar to those shown for the Case-1 source; even the scales were similar. However, concentrations for ^{99}Tc and ^{129}I were markedly different. For these two nuclides, a spike in the concentrations appeared at early time and was damped as time progressed. The concentration spike was approximately two orders of magnitude greater than the maximum levels reached in the Case-1 and Case-2 sources. Spreading of the nuclides was also greater and was caused by the larger concentrations in the source region at early time. The concentration of ^{129}I extended 100 m downstream before it fell to zero. Figure 4-33 presents the concentration surfaces for the four nuclides using the Case-3 source. The ^{135}Cs and ^{237}Np surfaces were almost identical to those shown for the Case-1 source. The ^{99}Tc and ^{129}I surfaces showed the early release. Notice that the concentrations in the source region were greater for these two nuclides than the values shown in Figure 4-32.

Figure 4-34 presents the concentration profiles resulting from moist-continuous Case-4 source. The profiles are similar to those shown for the Case-1 source. ^{99}Tc showed a twofold increase in concentration when compared with the ^{99}Tc released by the Case-1 source. The concentration surfaces for the four nuclides using the Case-4 source are shown in Figure 4-35. Again, they were quite similar to those shown for the Case-1 source; however, ^{99}Tc and ^{129}I showed a drop in concentration in the source region at 100,000 years. ^{99}Tc and ^{129}I were both released in approximately the same manner, only faster, in the Case-4 source when compared with the Case-1 source. The drop at 100,000 years was caused primarily by transport out of the source region after release ceased. For ^{99}Tc, radioactive decay also contributed to the drop in concentration, but only slightly.

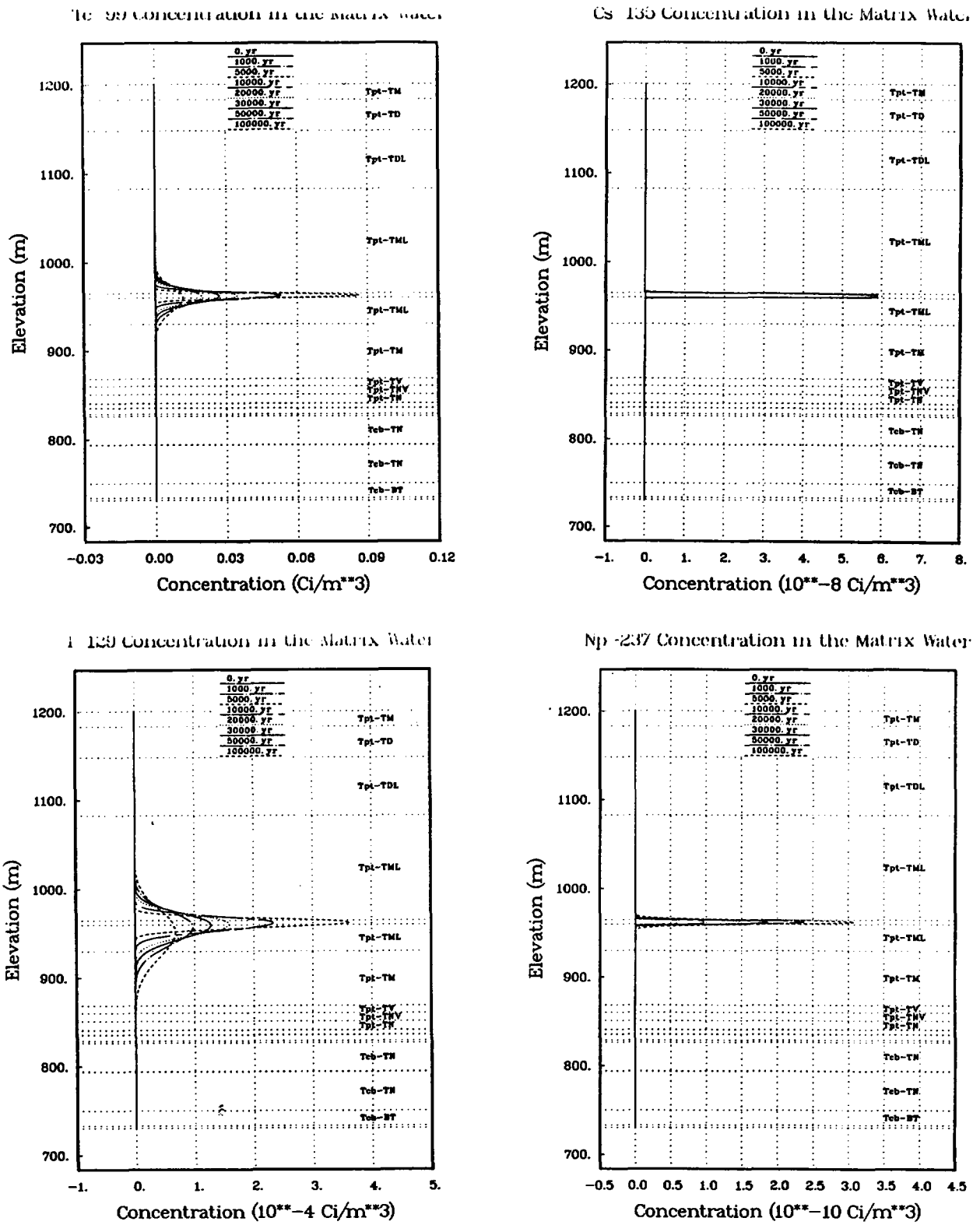

Figure 4-32
TOSPAC Analysis - Concentration Profiles Using
Moist-Continuous, Case-3 Source

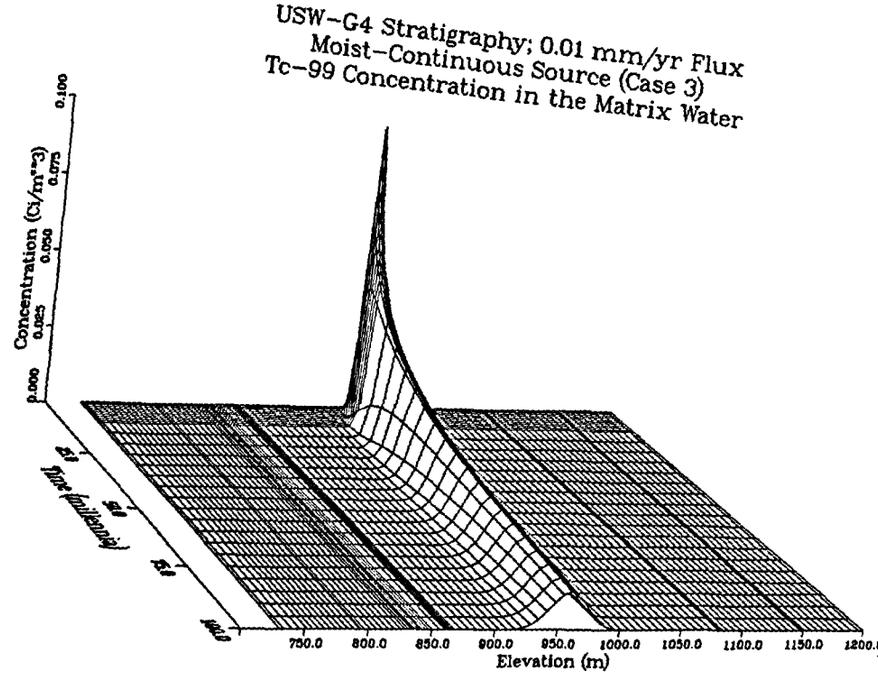

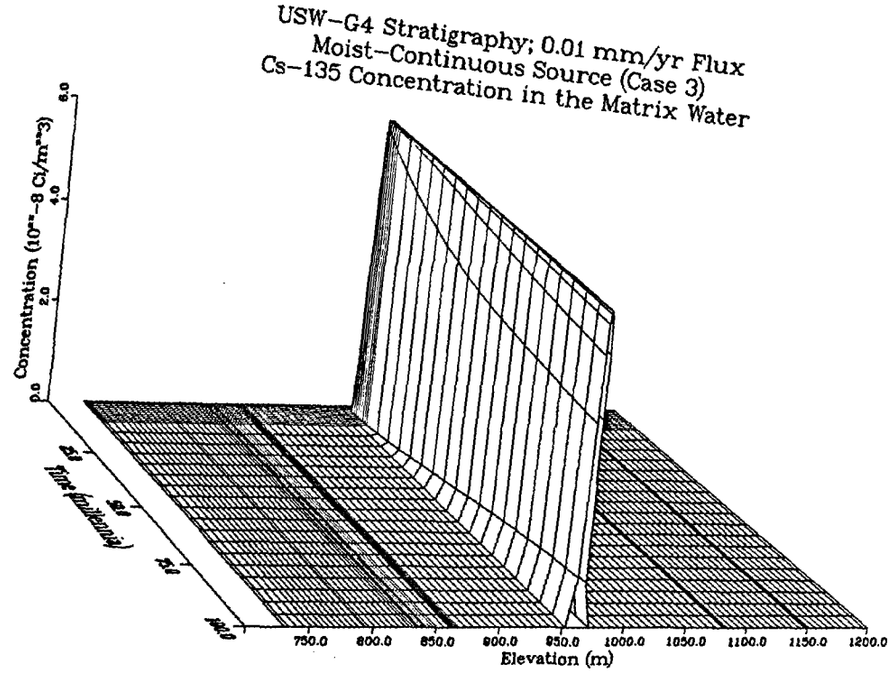

Figure 4-33
TOSPAC Analysis - Concentration Surfaces Using
Moist-Continuous, Case-3 Source

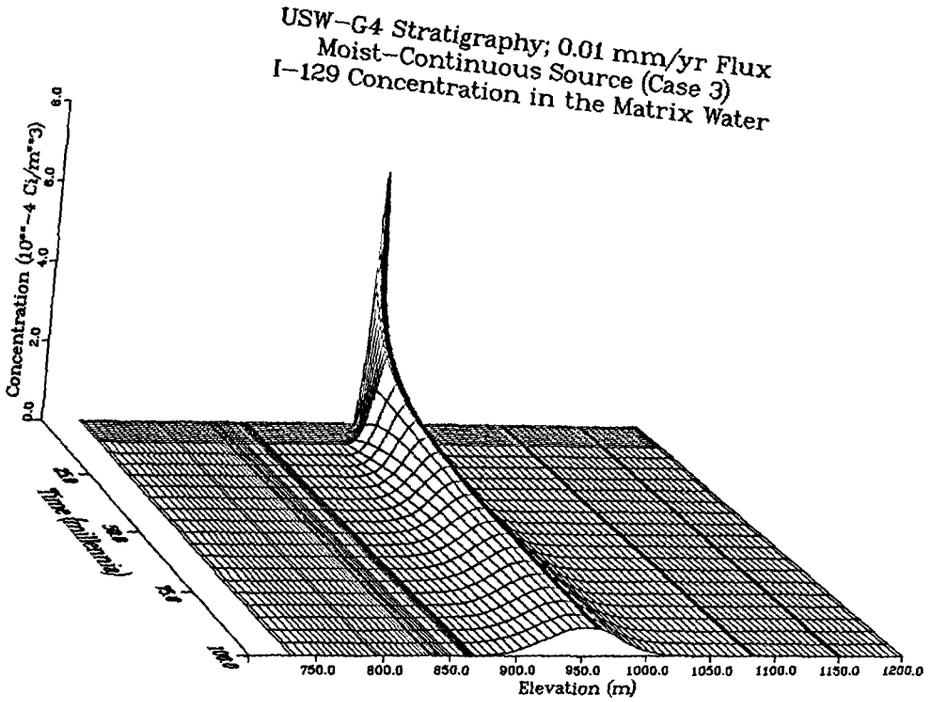

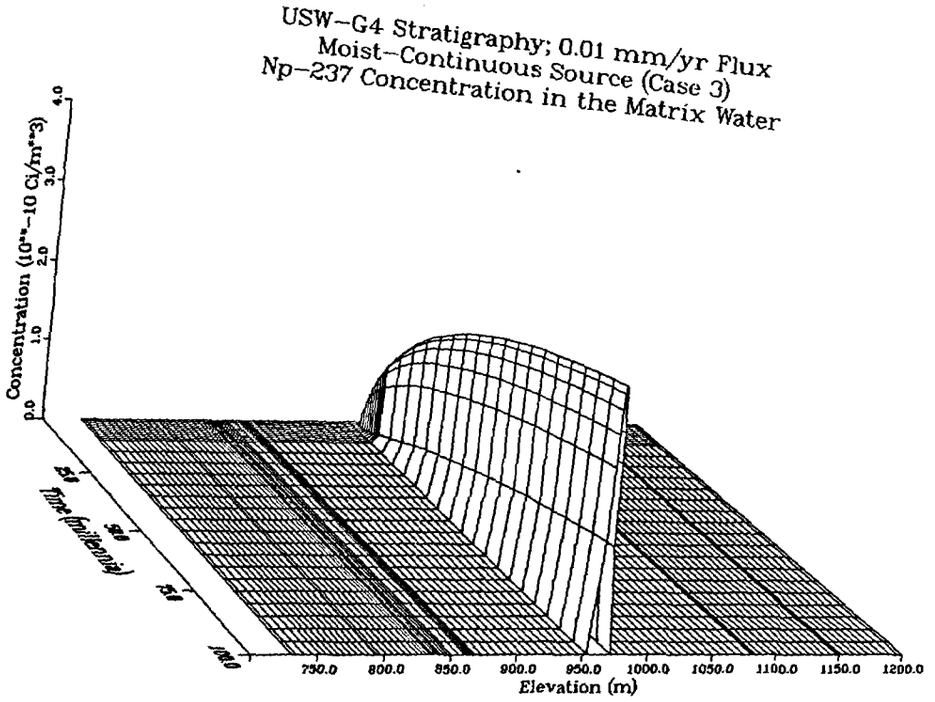

Figure 4-33, Continued

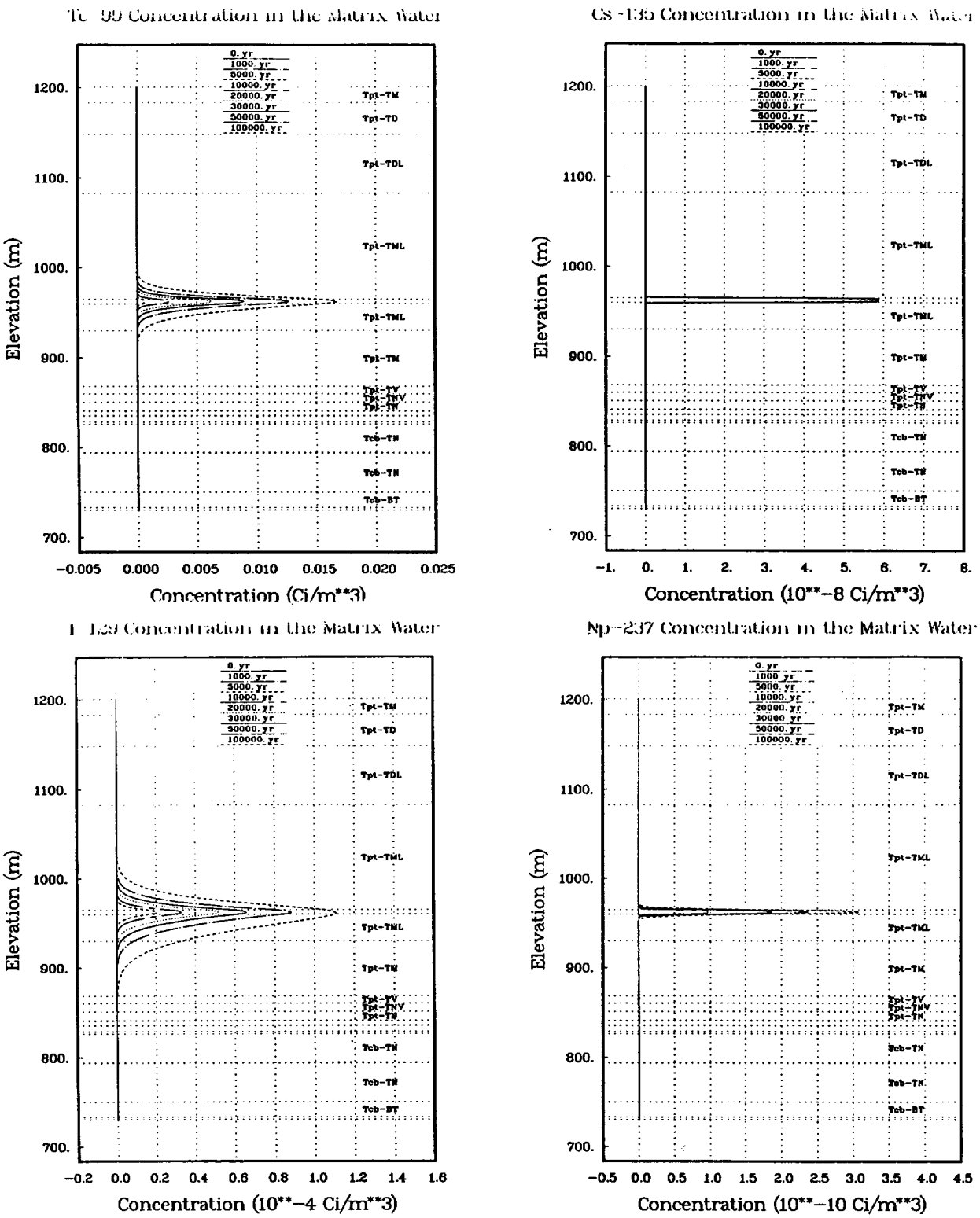

Figure 4-34
TOSPAC Analysis - Concentration Profiles Using Moist-Continuous, Case-4 Source

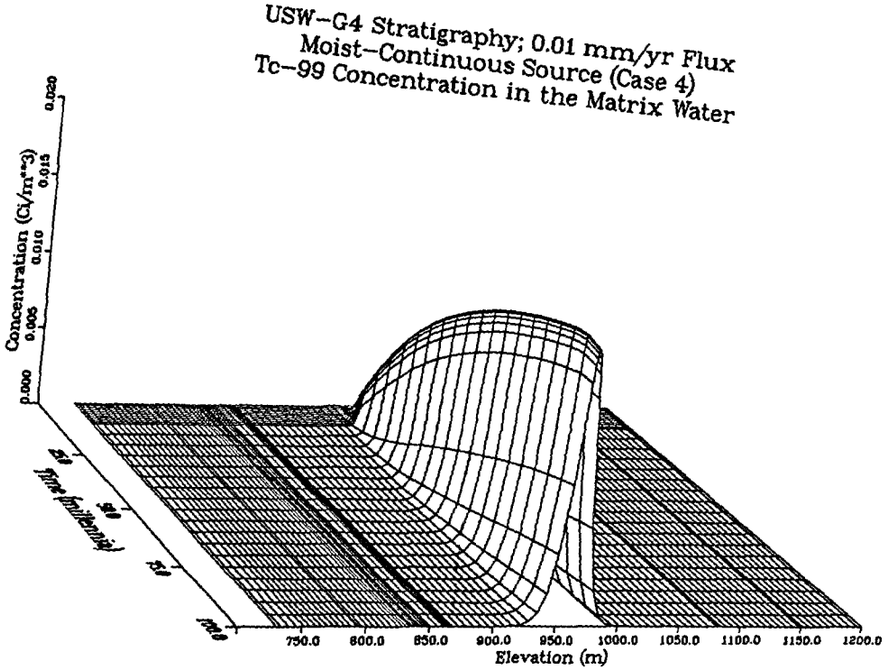

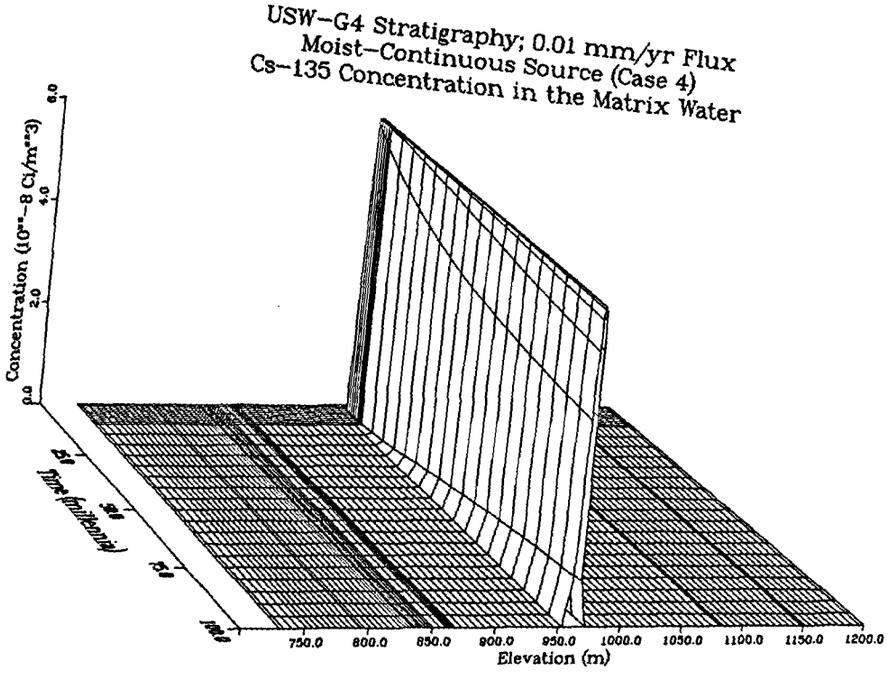

Figure 4-35
TOSPAC Analysis - Concentration Surfaces Using
Moist-Continuous, Case-4 Source

USW–G4 Stratigraphy; 0.01 mm/yr Flux
Moist–Continuous Source (Case 4)
I–129 Concentration in the Matrix Water

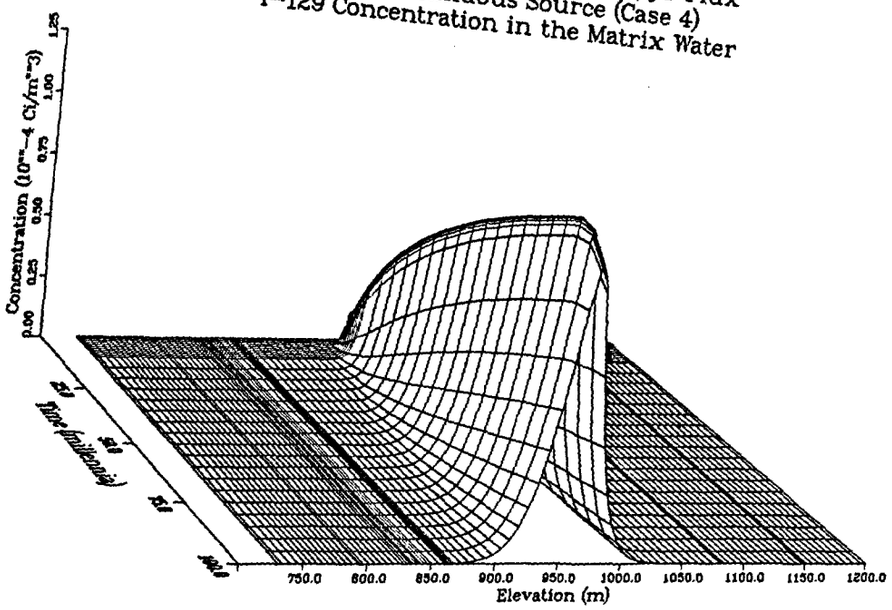

USW–G4 Stratigraphy; 0.01 mm/yr Flux
Moist–Continuous Source (Case 4)
Np–237 Concentration in the Matrix Water

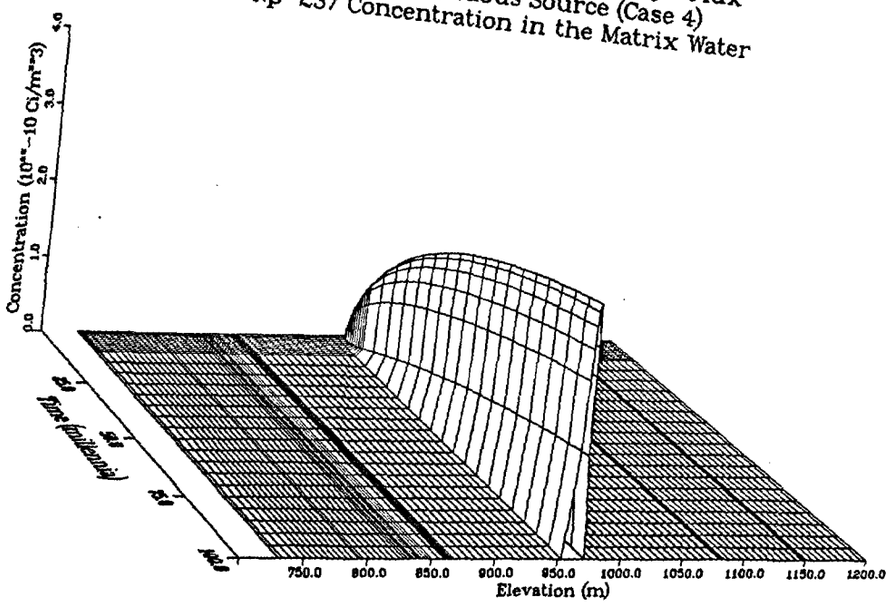

Figure 4-35, Continued

Figure 4-36 presents the concentration profiles resulting from the wet-drip flow-through source. The curves for ^{99}Tc and ^{129}I are quite similar to those shown for the Case-3 source. As with the Case-3 source, the rise in concentration was rapid. Initially the rise was not quite as rapid as with the Case-3 source; however, the release did all occur within the first 10,000 years. At late time, concentration levels and spread of ^{99}Tc and ^{129}I were virtually identical with those shown for the Case-3 source. The curves for ^{135}Cs showed an immediate jump to the maximum concentration, similar to the jump seen in the sources for Cases 1, 3, and 4, although for the flow-through source the concentration was between two and four orders of magnitude greater. ^{135}Cs did show negligible transport, however. The curves for ^{237}Np showed a gradual, nearly-linear rise in concentration, consistent with the nearly constant release. Transport of ^{237}Np was also negligible.

The concentration surfaces for the four nuclides using the wet-drip flow-through source are presented in Figure 4-37. Notable were the spikes in concentration of ^{99}Tc and ^{129}I. These spikes were of less magnitude than those shown for the Case-3 source. At late time, the magnitude and spread of these nuclides were again almost identical with those released by the Case-3 source.

Figure 4-38 presents the concentration profiles derived from the wet-drip bathtub source. The most notable characteristic of this set of plots is that it is indistinguishable from the set shown for the flow-though source. This observation also applies to Figure 4-39, which shows the concentration surfaces for the four nuclides using the bathtub source. From the viewpoint of a 1-D transport calculation, the flow-through and bathtub sources were the same.

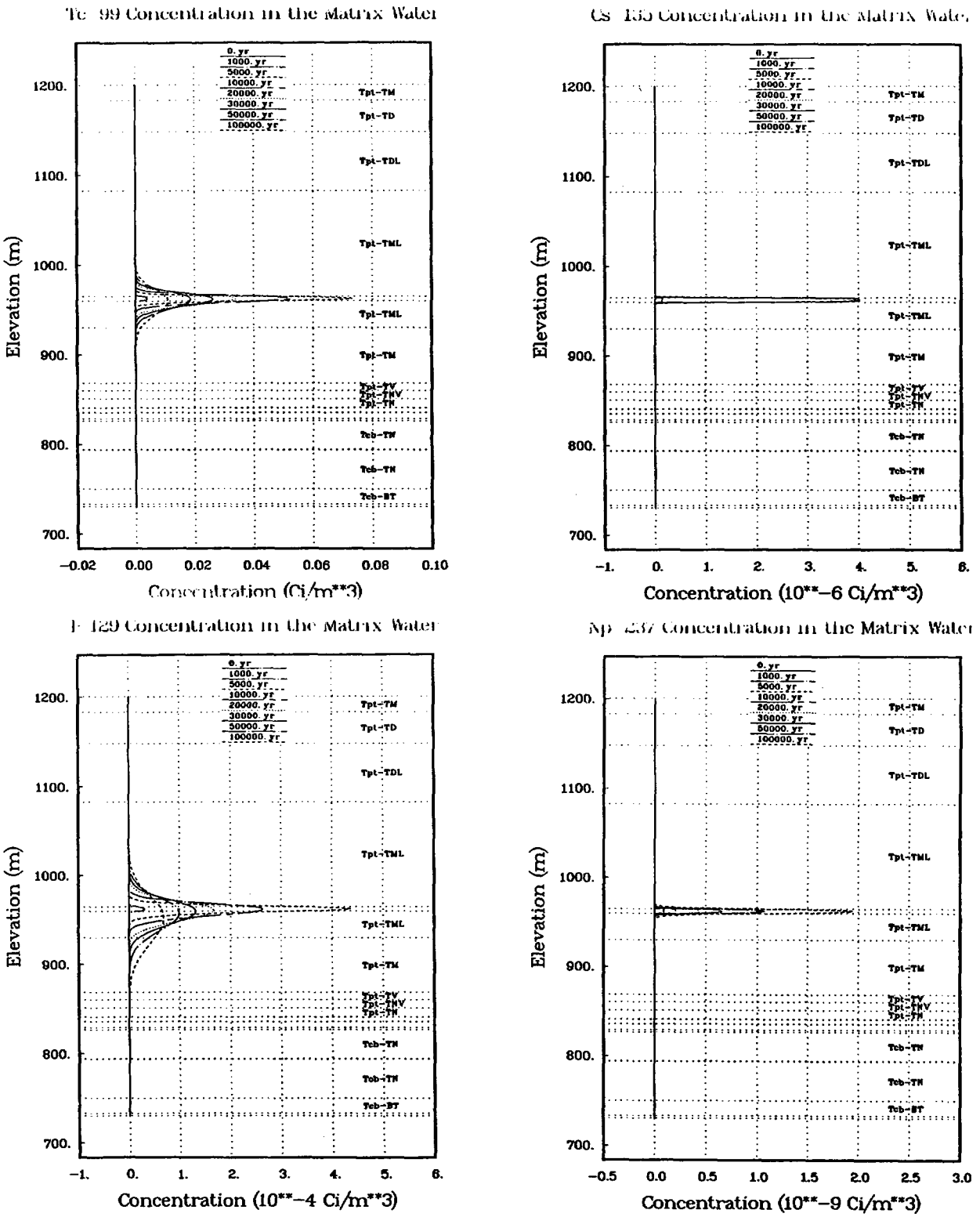

Figure 4-36
TOSPAC Analysis - Concentration Profiles Using Wet-Drip, Flow-Through Source

USW–G4 Stratigraphy; 0.01 mm/yr Flux
Wet–Drip Flow–Through Source
Tc–99 Concentration in the Matrix Water

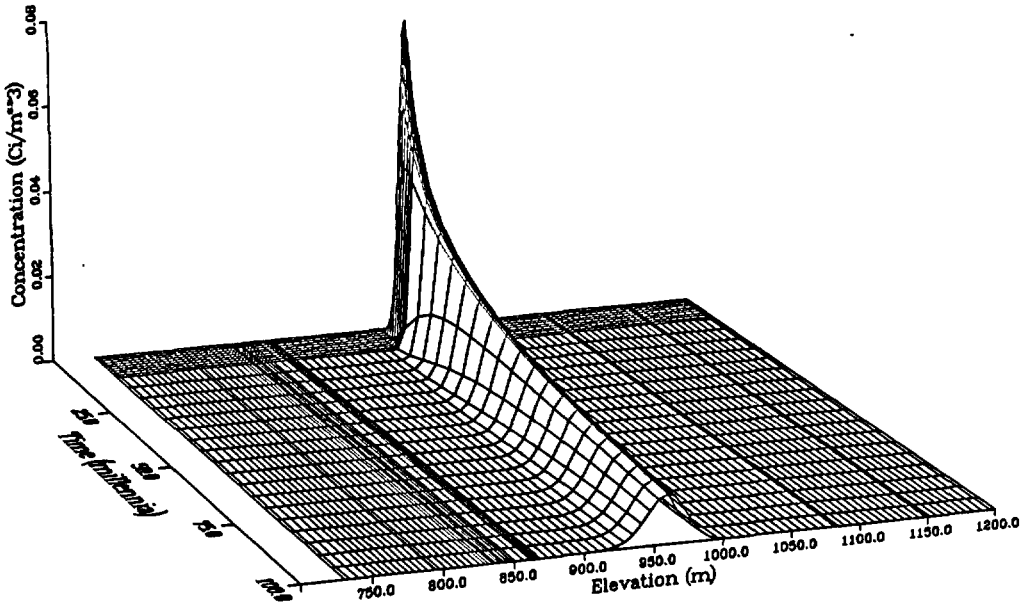

USW–G4 Stratigraphy; 0.01 mm/yr Flux
Wet–Drip Flow–Through Source
Cs–135 Concentration in the Matrix Water

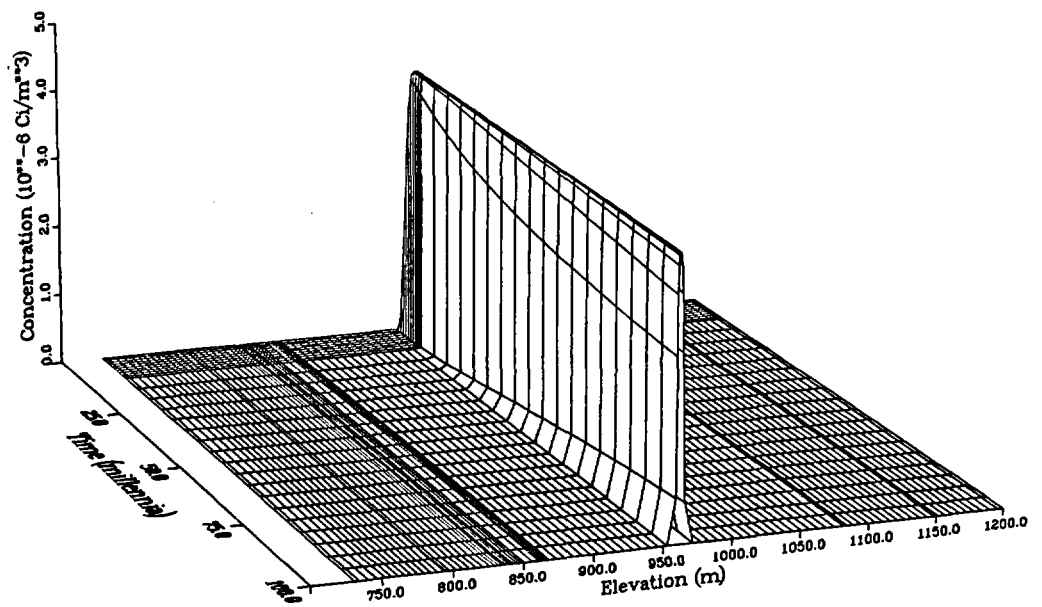

Figure 4-37
TOSPAC Analysis - Concentration Surfaces Using
Wet-Drip, Flow-Through Source

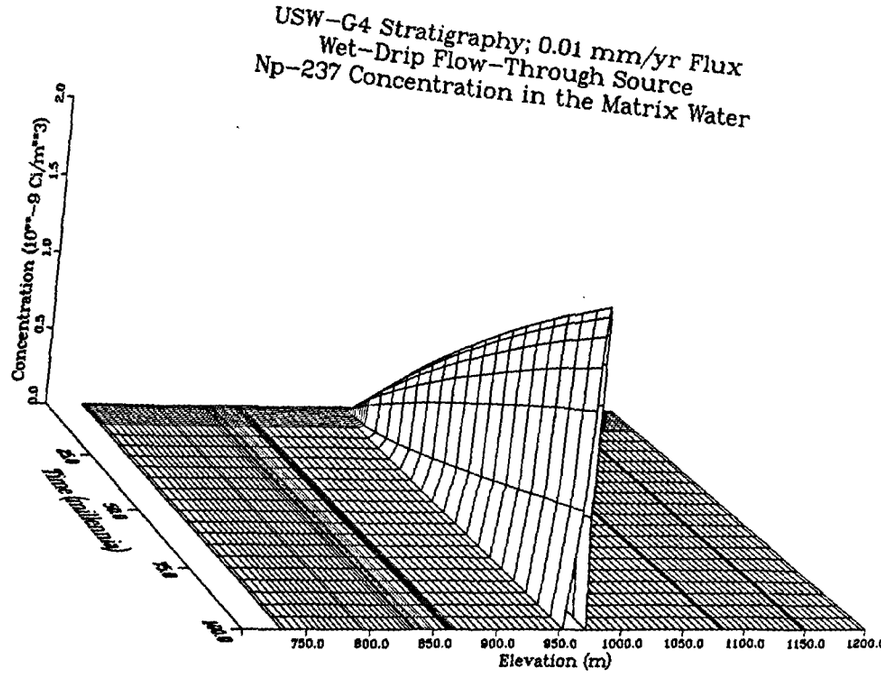

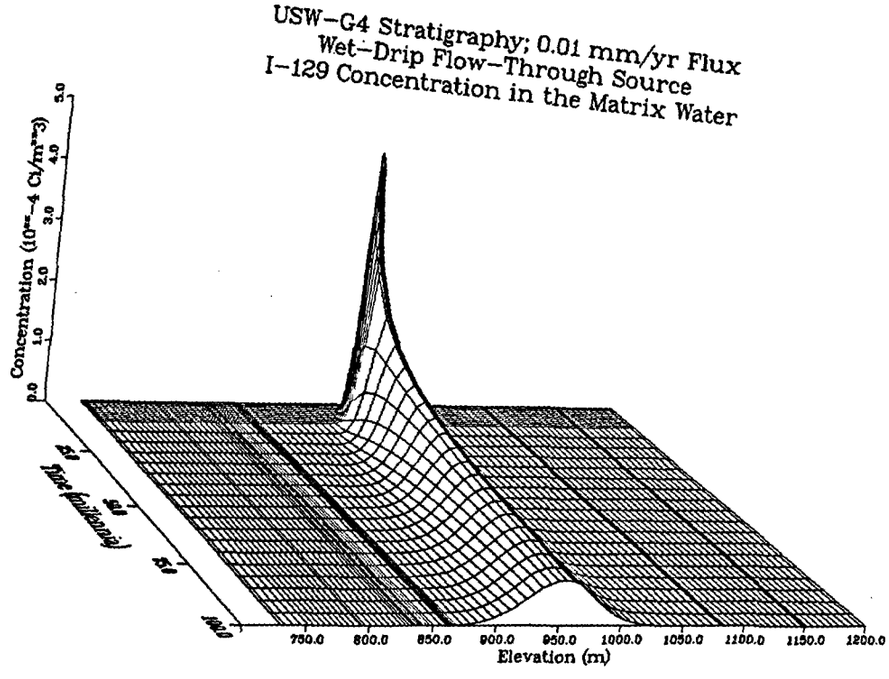

Figure 4-37, Continued

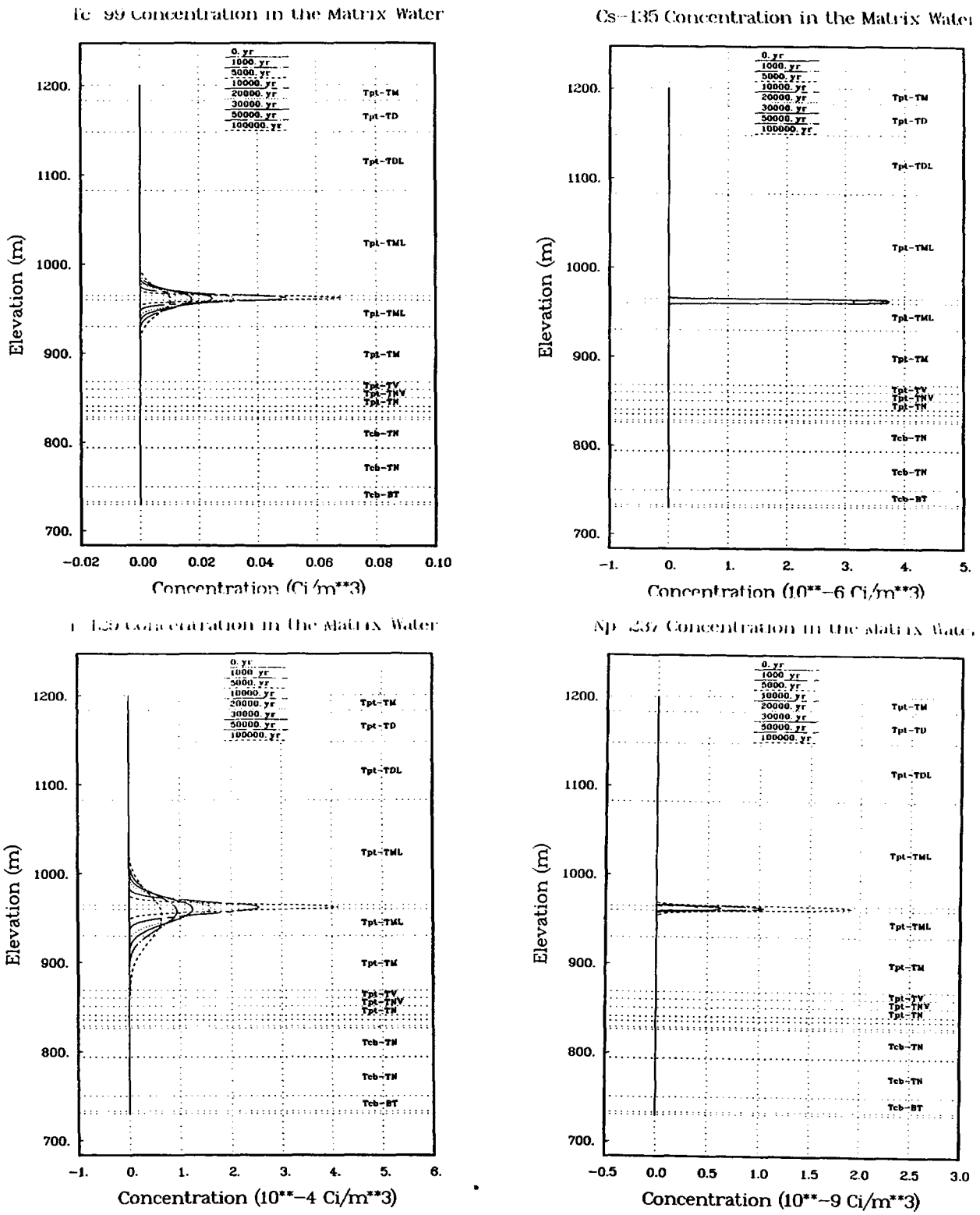

Figure 4-38
TOSPAC Analysis - Concentration Profiles Using
Wet-Drip, Bathtub Source

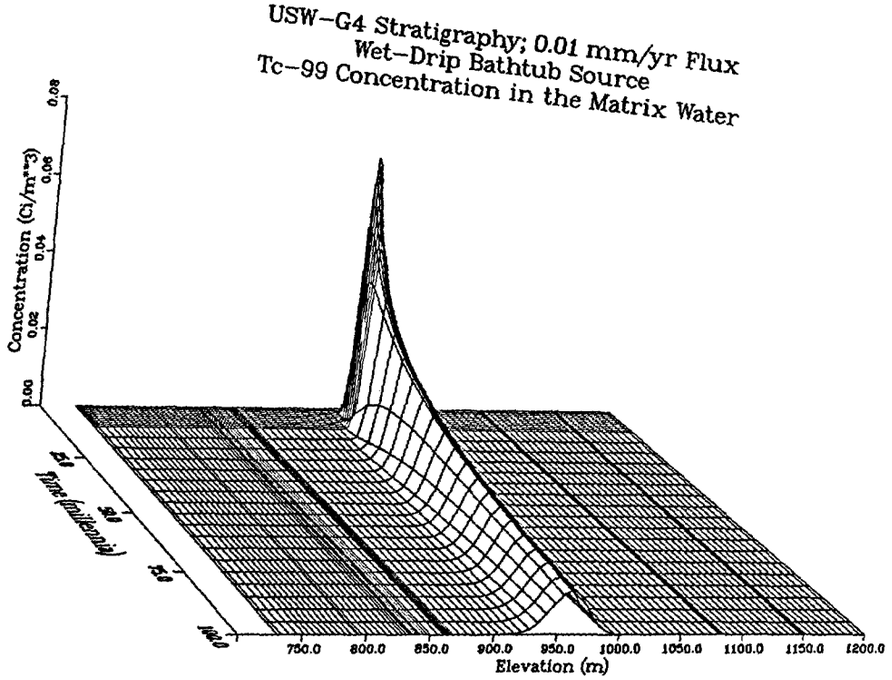

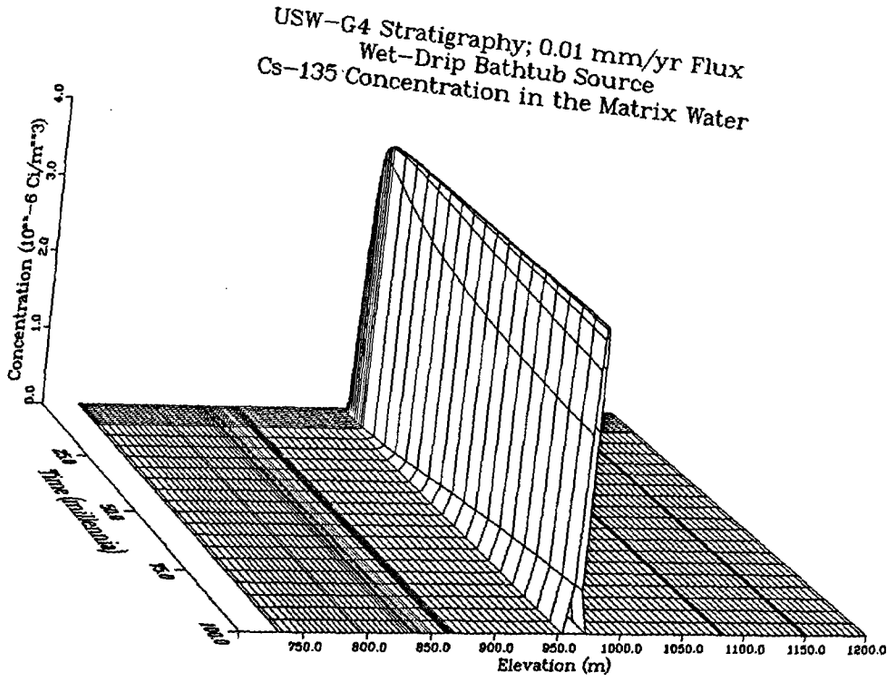

Figure 4-39
TOSPAC Analysis - Concentration Surfaces Using Wet-Drip, Bathtub Source

USW-G4 Stratigraphy; 0.01 mm/yr Flux
Wet-Drip Bathtub Source
I-129 Concentration in the Matrix Water

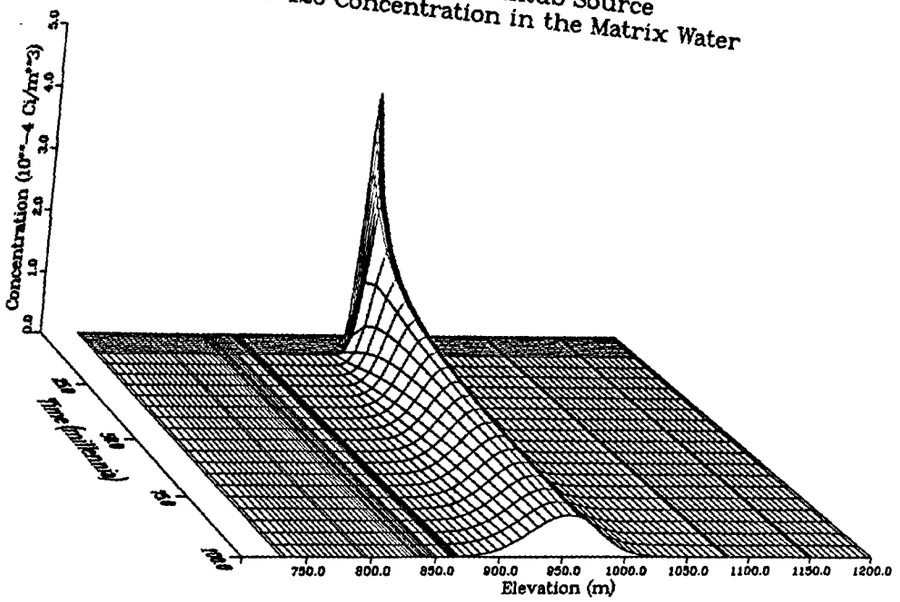

USW-G4 Stratigraphy; 0.01 mm/yr Flux
Wet-Drip Bathtub Source
Np-237 Concentration in the Matrix Water

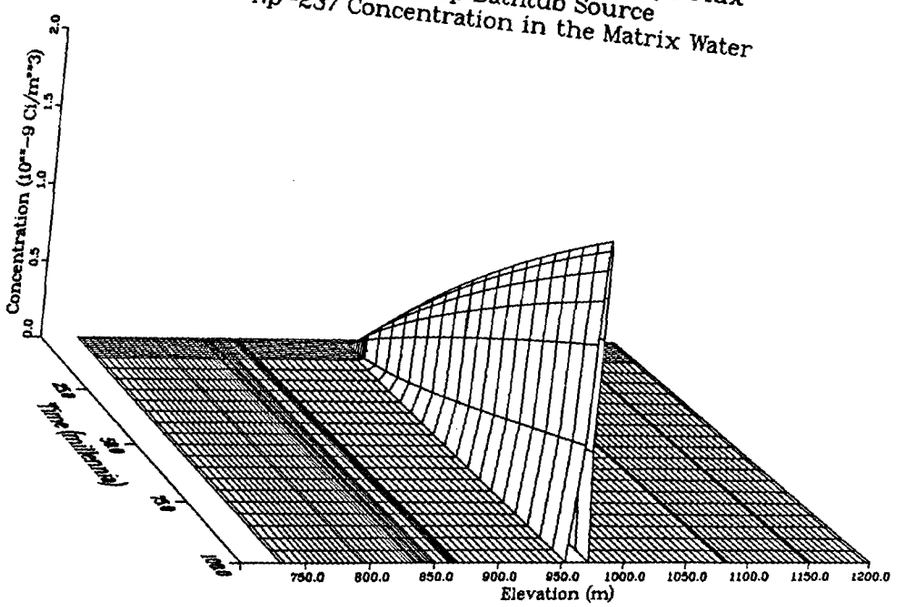

Figure 4-39, Continued

4.4 DCM-3D and NEFTRAN

4.4.1 Code Description

4.4.1.1 DCM-3D

DCM-3D is a groundwater-flow code capable of modeling saturated and unsaturated flow in a fractured porous medium*. The model implemented in the code uses a double-continuum approach similar to that used in petroleum reservoir engineering (van Golf-Racht, 1982). The matrix continuum and the fracture continuum each have their own flow equations which are coupled by a matrix-to-fracture transfer term. The transfer term depends on the pressure difference between the matrix continuum and the fracture continuum and the degree of saturation of the matrix continuum.

The governing equations are numerically differentiated spatially with a block-centered, finite-difference approach. For steady-state calculations, the time derivative is not differentiated. The resulting set of finite-difference equations are solved with a general differential equation solver, LSODES. LSODES is designed to solve a set of sparse, stiff ordinary differential equations by means of backwards difference formulas (Hindmarsh, 1983; Press et al., 1989).

DCM-3D is capable of modeling either a single-continuum or double-continuum problem. It is capable of handling spatially and temporally varying flux and pressure boundary conditions and source terms. The boundary flux and the source term for the matrix or the fracture continua can be prescribed by the user for each continuum. They can also depend on the mobility ratio between the two continua. The van Genuchten equations (van Genuchten, 1980) are used to describe the characteristic curves of each continuum.

* Updegraff, C. D. and Lee, C. E., in preparation. "DCM-3D - A Dual-Continuum, 3-D, Groundwater Flow Code for Unsaturated, Fractured, Porous Media," SAND90-7015, Sandia National Laboratories, Albuquerque, NM.

4.4.1.2 NEFTRAN

NEFTRAN (network flow and transport) is a performance-assessment code designed to do computationally efficient simulations of transport of multiple, n-membered radionuclide chains across large distances over long periods of time (Longsine et al., 1987). The NEFTRAN computer code is capable of simulating groundwater flow and radionuclide transport in saturated, fractured, porous media, and simulating radionuclide transport in partially-saturated, fractured, porous media.

NEFTRAN models advective/dispersive transport of radionuclides through a series of 1-D legs (stream tubes) using the distributed velocity method (DVM) (Campbell et al., 1981). For unsaturated-zone transport, the transport migration path, mean pore velocities for each leg along the path, and saturations for each leg along the path are each determined from an external flow calculation (in this case, from DCM-3D).

The DVM partitions the radionuclides within each leg into discrete packets and determines a distribution of velocities for the packets based on the mean retarded particle velocity and a dispersivity for each leg. Mean retarded particle velocity within a leg is the mean pore flow velocity divided by the particle retardation factor for that leg. Legs along the migration path can be either single-porosity matrix, single-porosity fracture, or dual-porosity fracture. Within the dual-porosity fracture legs, transport of radionuclides into and out of stationary matrix fluid is simulated. Included in the transport calculation is radionuclide decay and production.

Because the spatial orientation of the transport legs in NEFTRAN is neither specified by the user nor implied within the code, the orientation of the legs can be arbitrary. As a result, if a dominant, non-branching, migration path can be defined in multiple dimensions by a flow calculation external to NEFTRAN, it can simulate quasi-multi-dimensional transport along this path.

NEFTRAN has the capability to either generate its own source term internally or read an arbitrary source term from an external file. The source term module and transport module within NEFTRAN are decoupled. As a result, selected decay chains can be used for source calculations only and not be transported. Internal source term models within NEFTRAN include leach-limited with either constant or exponential leach rates, solubility-limited, or mixing cell.

Specific output from NEFTRAN includes integrated or cumulative release (Ci) of each radionuclide at a discharge point, discharge rate (Ci/yr) at the discharge point as a function of time, and concentration (Ci/m^3) at the discharge point as a function of time.

Further discussion of the conceptual, mathematical, and numerical models used in NEFTRAN can be found in Longsine et al. (1987).

4.4.2 Problem Setup

4.4.2.1 DCM-3D

DCM-3D was used to simulate unsaturated flow in a 1-D column. The column extended from the bottom of the repository to the water table at the G-4 drill hole. Flow in both matrix and fractures was modeled. Fifteen materials with varying hydrological properties and thicknesses were used in the simulation (see Section 3.1). A total of 122 grid blocks were used to simulate the 229.4-m distance between the water table and the repository. Grid block sizes varied from 0.5 m to 6.9 m.

The upper boundary net infiltration rate was 0.01 mm/yr. The infiltration into the upper boundary was divided between the matrix and the fractures based on the mobility ratio between the two. At the upper boundary, nearly all the infiltration occurred in the matrix as a result of the steepness of the fracture hydraulic conductivity curves compared to those for the matrix. The lower boundary condition was set to zero pressure for both the matrix and

the fractures, representing the water table at the bottom of the grid. The initial pressure heads were set to the negative of the distance above the water table for both the matrix and the fractures. This corresponded to a zero flux initial condition in both the matrix and the fractures.

To reach steady-state, the code was run until the Darcy fluxes at each grid block boundary reached steady-state. This occurred when the Darcy fluxes at the grid-block boundaries became equal to the specified net infiltration rate.

4.4.2.2 NEFTRAN

Transport simulations were based on the 1-D, steady-state flow calculations. Transport from the base of the repository to the water table for each of the four radionuclides (^{99}Tc, ^{129}I, ^{135}Cs, ^{237}Np) was simulated. Mean flow velocities, transport leg lengths, number of legs, nature of legs (i.e., fracture or matrix), and moisture contents were determined by a flow code post-processor and supplied to NEFTRAN. The length and number of transport legs were based on the hydrologic and geochemical properties of the system. Hydrologically, a new leg was defined whenever the transport reached a new material. Different hydrostratigraphic units in this problem corresponded to the different materials. Geochemically, a new leg was defined when sorption distribution coefficients changed. As a result, the mean transport velocity within a leg was constant. A new leg would also be defined if flow switched from matrix to fracture, or vice versa.

The problem input data defined 17 transport legs. For these 17 legs, a number ranging from 3246 (for ^{129}I) to 2546 (for ^{135}Cs) grid blocks was used. The size of the transport grid blocks was constant within a leg, but could vary from leg to leg. The transport migration path is summarized in Table 4-1. Dispersivity values within each leg were chosen to be ten percent of the leg length. Assigning a different dispersivity to each leg was possible because DVM was applied to each leg separately, with each leg being assigned a unique mean velocity. Time steps, as determined

internally in NEFTRAN, were 7000 years for ^{99}Tc and ^{129}I, and 5×10^4 years for ^{135}Cs and ^{237}Np.

TABLE 4-1

NEFTRAN TRANSPORT MIGRATION PATH SUMMARY

Leg	Length (m)	Type	Dispers. (m)	Mean Pore Vel. (m/yr)
0 (Tpt-TML)	4.6	source	0.46	1.12×10^{-4}
1 (Tpt-TML)	29.8	m	2.98	1.12×10^{-4}
2 (Tpt-TM)	61.6	m	6.16	1.06×10^{-4}
3 (Tpt-TV)	8.5	m	0.85	2.51×10^{-4}
4 (Tpt-TNV)	9.2	m	0.92	6.26×10^{-5}
5 (Tpt-TN)	9.7	m	0.97	3.08×10^{-5}
6 (Tpt-BT)	0.6	m	0.06	4.35×10^{-5}
7 (Tcb-TN)	4.6	m	0.46	2.96×10^{-5}
8 (Tcb-BT)	0.6	m	0.06	4.45×10^{-5}
9 (Tcb-TN)	6.4	m	0.64	2.94×10^{-5}
10 (Tcb-BT)	2.7	m	0.27	4.44×10^{-5}
11 (Tcb-TN)	31.7	m	3.17	2.90×10^{-5}
12 (Tcb-BT)	0.9	m	0.09	4.40×10^{-5}
13 (Tcb-TN)	43.3	m	4.33	2.83×10^{-5}
14 (Tcb-BT)	15.2	m	1.52	4.35×10^{-5}
15 (Tcb-BT)	1.9	f	0.19	1.12×10^{-3}
16 (Tcpp-TN)	2.7	f	0.27	6.48×10^{-1}

m = matrix; f = fracture

Radionuclide retardation factors were calculated from the sorption coefficients specified in Section 3.4 and by the moisture-content values from the flow simulations. Transport calculations were performed for only the G-4 drill hole. This drill hole was the only one in the problem set that intersects the repository.

Calculations were made using the two wet-drip source terms given in Section 3.3. Discharge rates and cumulative release were calculated directly. Calculations of concentrations were based on the repository area multiplied by the moisture content at the release point.

4.4.3 Results

4.4.3.1 DCM-3D

Results from the DCM-3D simulation consisted of pressure heads, moisture contents, and Darcy velocities for both the matrix and fractures. The moisture-content values were converted to saturations.

The matrix pressure head decreased with distance above the water table (Figure 4-40). From the water table to approximately 110 m above the water table, the matrix pressure head closely tracked the initial values. However, at a distance between 110 m and 120 m above the water table, the matrix pressure head increased steeply from approximately -100 m to approximately -23 m. This steep increase occurred in a unit with low matrix hydraulic conductivity, which underlay a unit with extremely high matrix hydraulic conductivity. A steep gradient had to form in the unit with low matrix hydraulic conductivity in order for water to flow through it at a flux equal to the infiltration rate. Between 120 m above the water table and the repository, the matrix pressure head again decreased along a line nearly parallel to the initial matrix pressure head.

The total matrix head, referenced to sea level, showed a positive upward gradient (Figure 4-41). This indicated a downward flux of water. The gradient was not steep except between I10 m and 120 m above the water table, as was discussed above.

Fracture pressures mirrored the matrix pressures. This was caused by the relatively large transfer factor used in the transfer term. As a result, near equality of the matrix and fracture pressures was expected. Since the fracture pressure heads were almost equal to the matrix pressure heads, they are not presented.

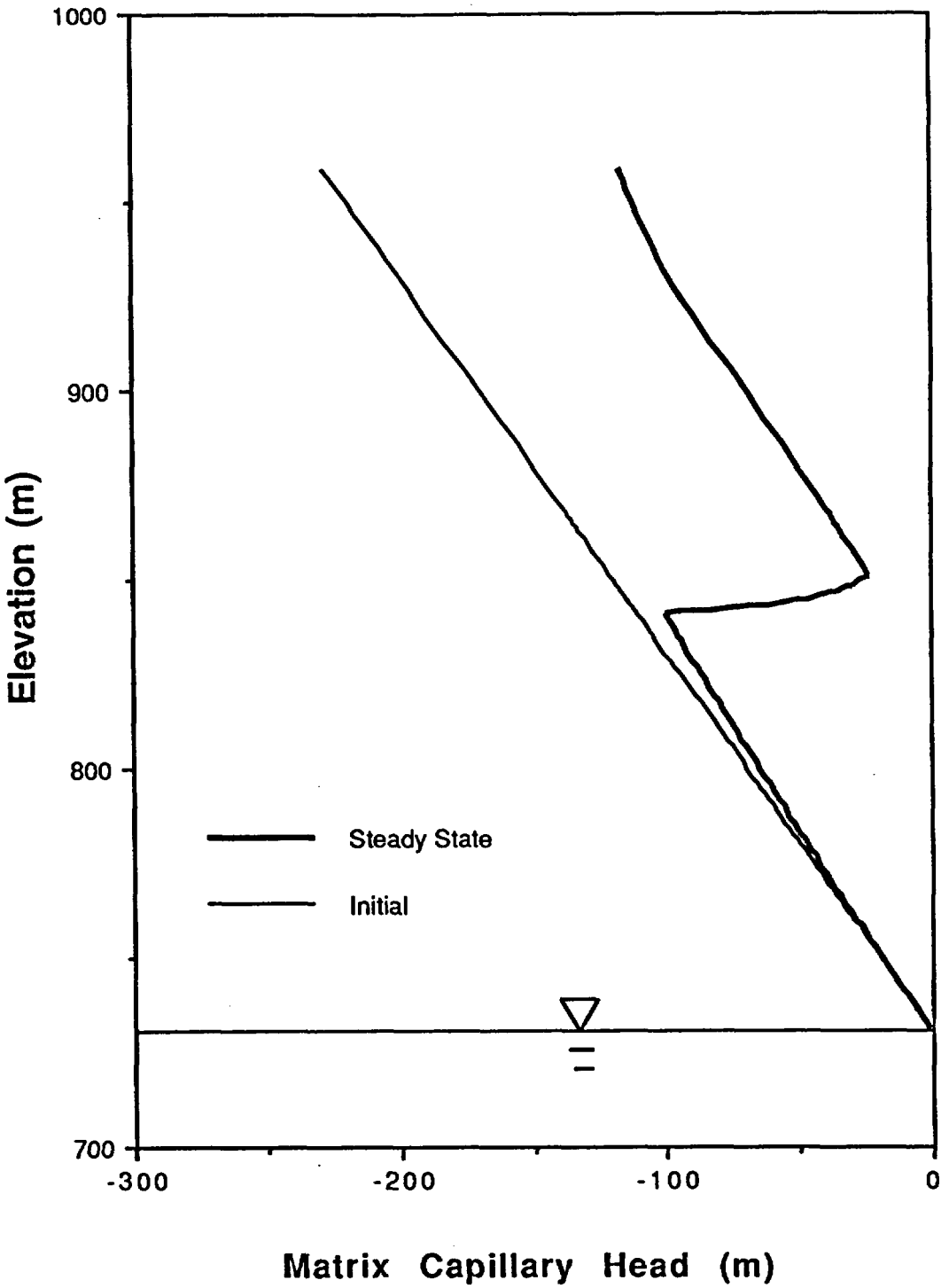

Figure 4-40
DCM-3D Analysis - Matrix Pressure Head

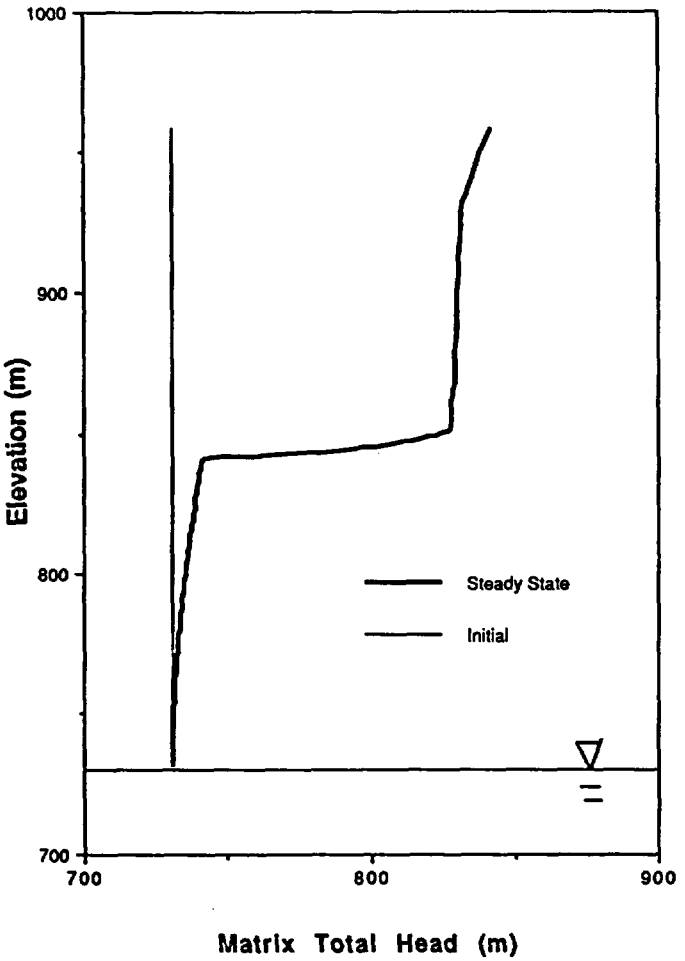

Figure 4-41
DCM-3D Analysis - Matrix Total Pressure Head

Degree of saturation for the matrix was quite variable (Figure 4-42). At distances between the water table and 110 m above the water table, the steady-state saturations were similar to the initial ones. At elevations higher than 110 m above the water table, the matrix saturations showed significant changes from the initial values. The low-hydraulic-conductivity unit that underlay the high-hydraulic-conductivity unit caused a significant impact on the saturations in this region. The peaks in the steady-state curve reflected the different hydrologic properties of the various geologic units, because most of the flow occurred in the matrix.

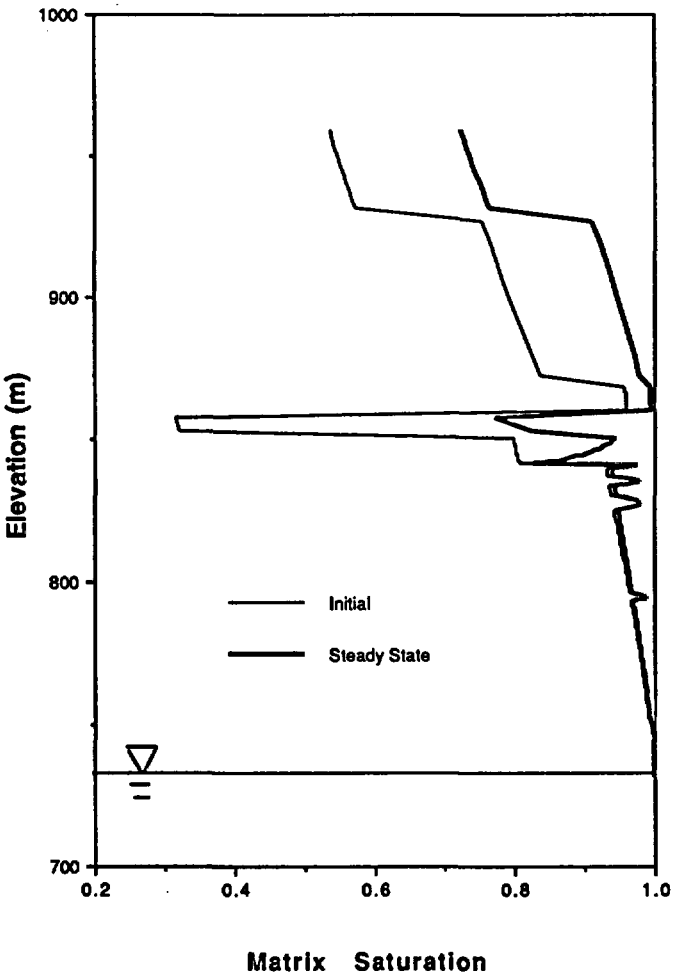

Figure 4-42
DCM-3D Analysis - Matrix Water Saturation

The degree of saturation for the fracture continuum showed almost no change from its initial values between the water table and the repository (Figure 4-43). Because of the steepness of the fracture-saturation characteristic curve, even large fracture pressure-head changes kept the fractures extremely dry. Near the water table the fracture saturations approached 1.0 as a consequence of the boundary conditions placed on the pressure head.

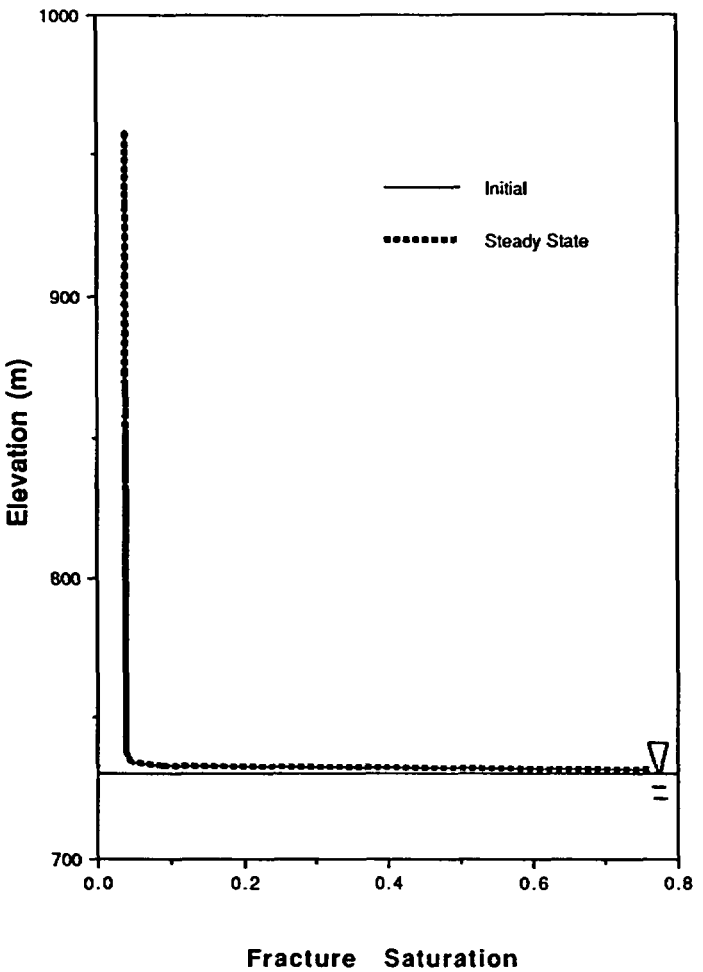

Figure 4-43
DCM-3D Analysis - Fracture Water Saturation

The Darcy velocities in the matrix were proportional to the infiltration rate everywhere except within 2 m of the water table (Figure 4-44). In this region, significant flow in fractures began and flow in the matrix decreased. An expanded plot of the Darcy velocities near the water table shows this more clearly (Figure 4-45). The crossover in the Darcy velocities represented a significant exchange of water from the matrix to the fractures near the water table, as was expected from the boundary conditions.

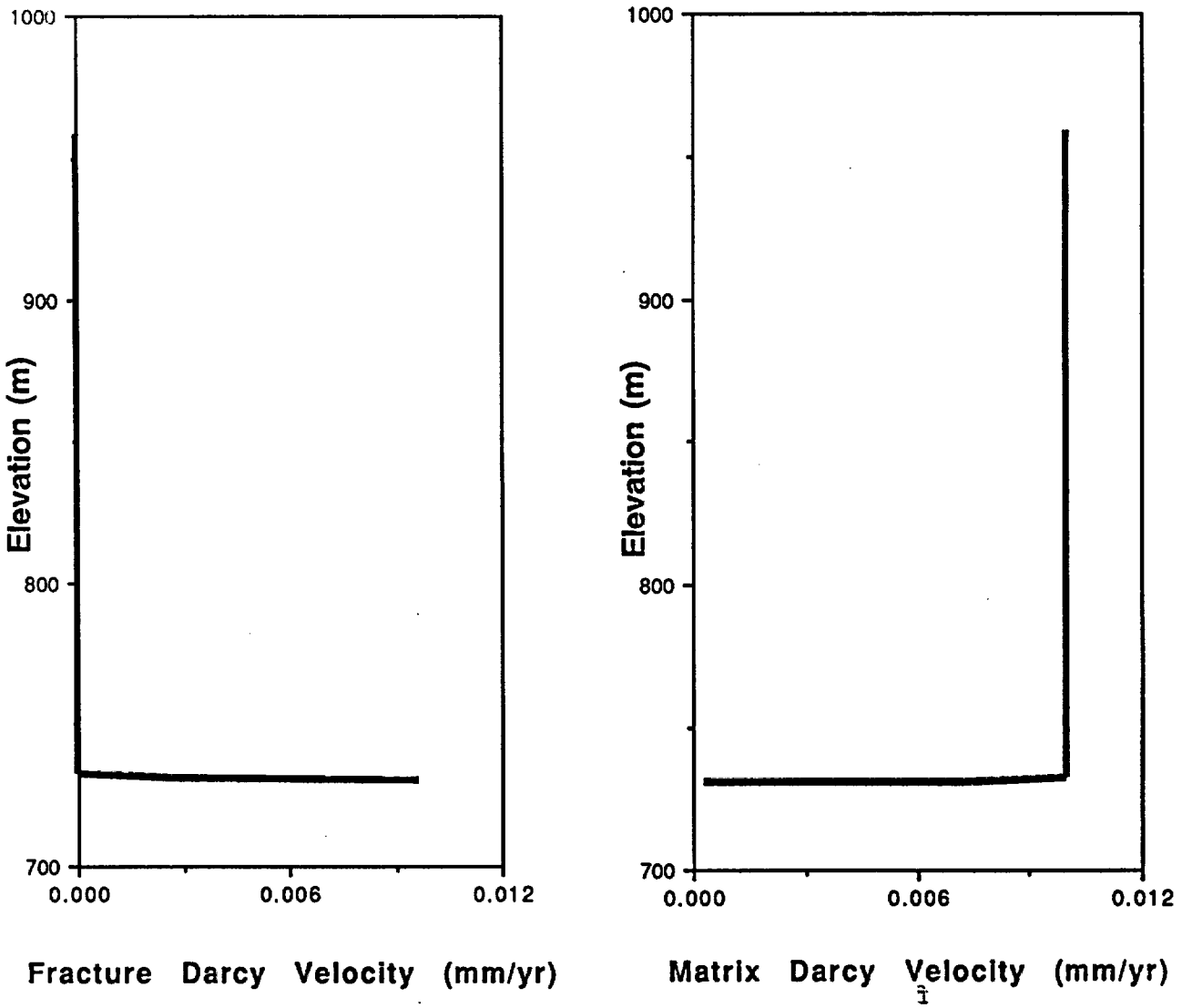

Figure 4-44
DCM-3D Analysis - Darcy Velocities for Fractures and Matrix

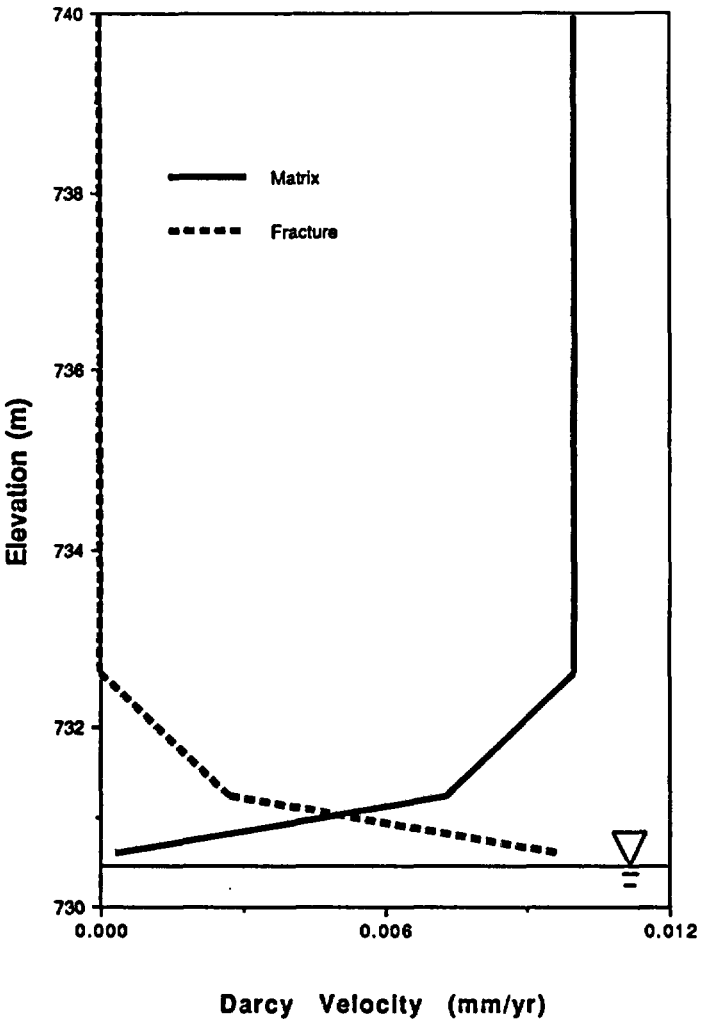

Figure 4-45
DCM-3D Analysis - Darcy Velocities Near the Water Table

4.4.3.2 NEFTRAN

Results from the NEFTRAN simulations included release rates, concentrations, and cumulative release for each of the radionuclides. The two wet-drip source terms were used. Because none of the radionuclides reached the water table, releases from legs for which there was transport are reported here. Simulation times were continued up to 10^6 years because little (^{129}I) or no (^{99}Tc, ^{135}Cs, and ^{237}Np) release from even the first leg occurred at 100,000 years.

The average retarded velocities of ^{99}Tc, ^{135}Cs, and ^{237}Np in this exercise were very low, based on the given infiltration rate and retardation values. Consequently, very little transport for each of these radionuclides was observed. At 10^6 years, zero release of ^{135}Cs and ^{237}Np from the first transport leg occurred, so transport calculations for these nuclides through subsequent legs were not done. Cumulative releases from each leg for all radionuclides are shown in Tables 4-2 and 4-3.

^{99}Tc was released from the first transport leg, beginning at about 700,000 years (Figure 4-46). However, the cumulative release from Leg 1 at 10^6 years was about seven orders of magnitude less than the cumulative release from either of the source terms at the repository horizon after 10,000 years. There were no discernible differences in the release rates from the first leg due to differences in source terms. Release of ^{99}Tc from Leg 2 had not occurred at 10^6 years.

Releases of ^{129}I were relatively much larger than for the other three radionuclides, because ^{129}I was not retarded. Figure 4-47 shows that almost all of the ^{129}I released from the source had passed through Leg 1 at 10^6 years. Figure 4-48 and Tables 4-2 and 4-3 also illustrate this. At 10^5 years there was little release from Leg 1. Because of the very long half-life for ^{129}I (1.6×10^7 years), very little of the isotope decayed, even after 10^6 years. The effect of dispersion can be seen in the increase in the spread of the release profile in Figure 4-47 as compared to source-term release profiles. The only distinction between the releases for the two source terms was a small difference in the magnitude of the peak release rate. Other small differences resulting from differences in source terms were obscured because of the large time scale over which the curve is displayed.

TABLE 4-2

CUMULATIVE RELEASE AT 10^6 YEARS (Ci)

WET-DRIP BATHTUB SOURCE TERM

Leg	^{99}Tc	^{129}I	^{135}Cs	^{237}Np
Source	626460	1511.5	16782	0.4861
1	2.3×10^{-2}	1475.0	0	0
2	0	1022.3	0	0
3	0	966.3	0	0
4	0	656.6	0	0
5	0	114.1	0	0
6	0	85.6	0	0
7	0	17.1	0	0
8	0	12.5	0	0
9	0	0.59	0	0
10	0	0.18	0	0
11	0	2.6×10^{-9}	0	0
12	0	9.3×10^{-10}	0	0
13	0	0	0	0
14	0	0	0	0
15	0	0	0	0
16 (water table)	0	0	0	0

TABLE 4-3

CUMULATIVE RELEASE AT 10^6 YEARS (Ci)

WET-DRIP FLOW-THROUGH SOURCE TERM

Leg	^{99}Tc	^{129}I	^{135}Cs	^{237}Np
Source	580270	1422.3	15573	4.8×10^{-1}
1	2.1×10^{-2}	1388.0	0	0
2	0	961.5	0	0
3	0	908.8	0	0
4	0	617.2	0	0
5	0	107.1	0	0
6	0	80.3	0	0
7	0	16.1	0	0
8	0	11.7	0	0
9	0	0.55	0	0
10	0	0.17	0	0
11	0	2.4×10^{-9}	0	0
12	0	8.6×10^{-10}	0	0
13	0	0	0	0
14	0	0	0	0
15	0	0	0	0
16 (water table)	0	0	0	0

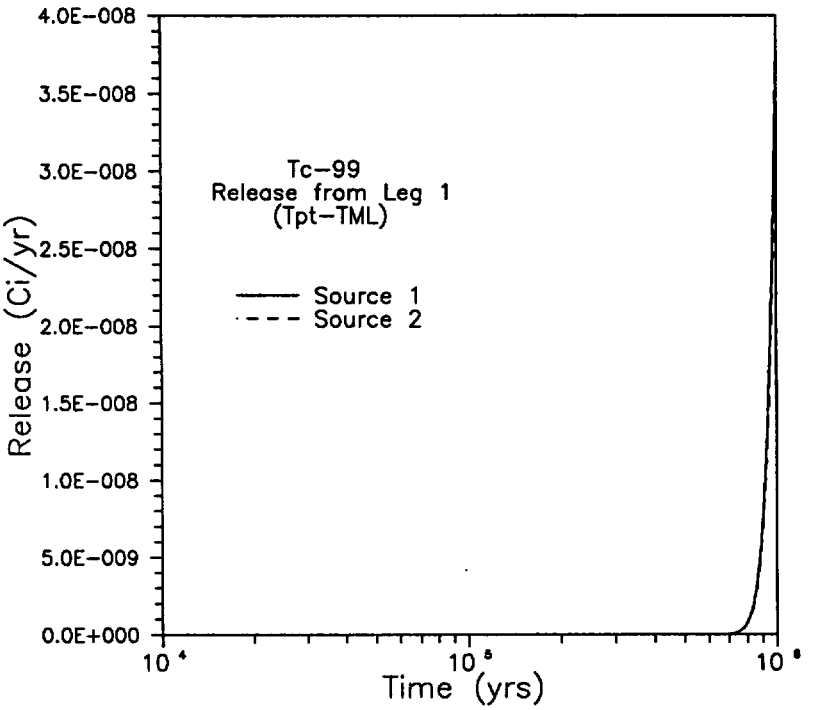

Figure 4-46
NEFTRAN Analysis - Release Rate for ^{99}Tc from Leg 1

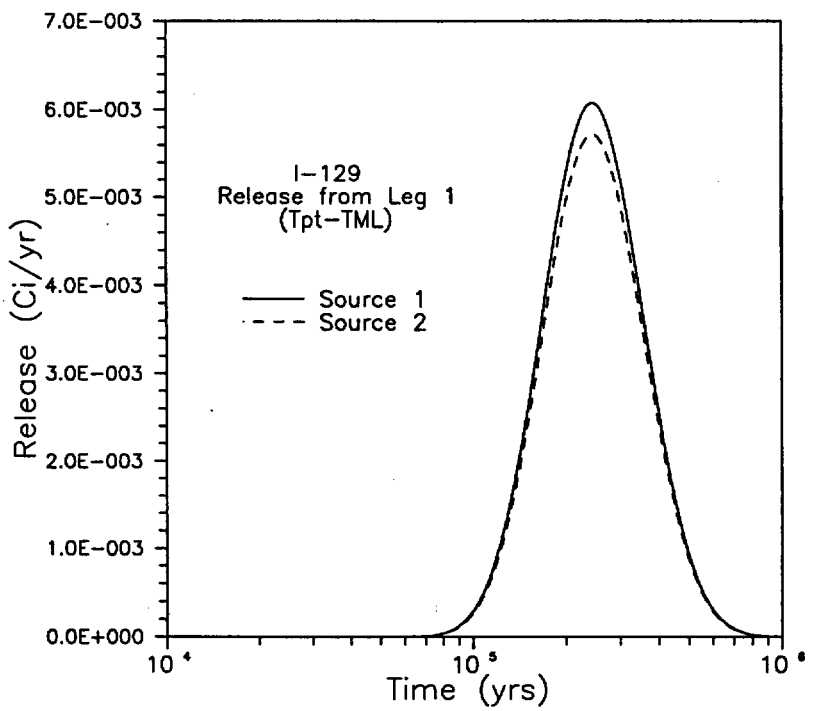

Figure 4-47
NEFTRAN Analysis - Release Rate for ^{129}I from Leg 1

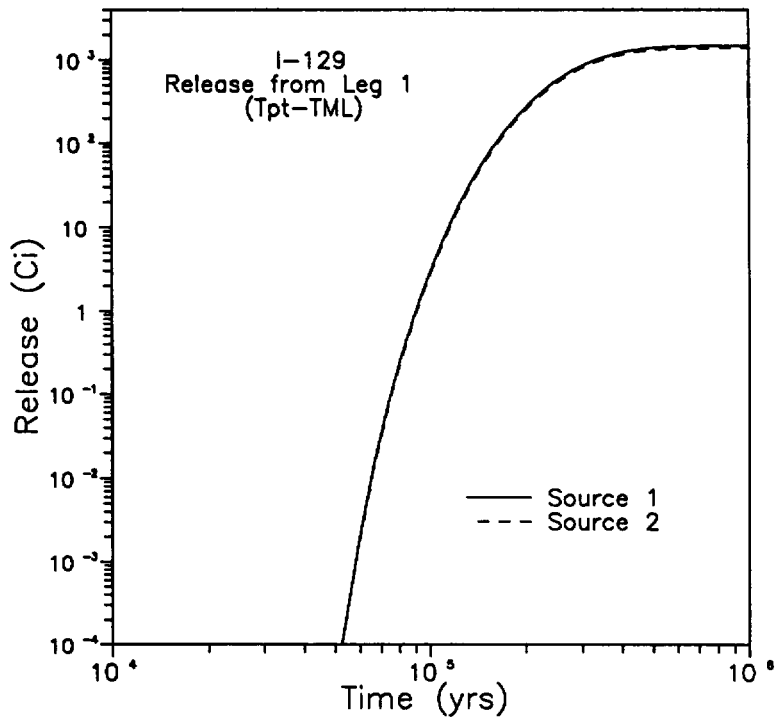

Figure 4-48
NEFTRAN Analysis - Cumulative Release for ^{129}I from Leg 1

The release rate and cumulative release of ^{129}I from Leg 2 are shown in Figures 4-49 and 4-50. An obvious decrease in the release rate was noted. The cumulative release at 10^6 years decreased by about 30 percent from the release out of the first leg. Release rates and cumulative release curves for the remaining legs are not shown here. At 10^6 years, no release of ^{129}I beyond the twelfth leg occurred (the water table was at the bottom of Leg 16).

Concentrations were calculated from the release rates, mean pore velocity, and the pore area containing water at the end of each leg (i.e., base of each unit). The pore area containing water was based on the moisture contents calculated using DCM-3D and a repository area of 5.61×10^6 m^2. The concentration at the lower boundary of the source at 100,000 years and later was specified by the source term models being set to zero.

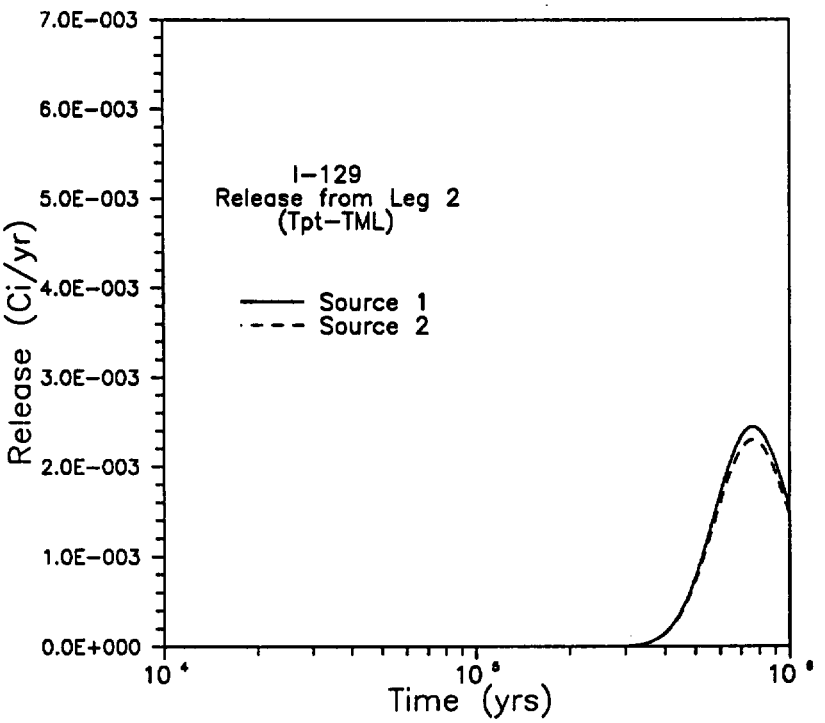

Figure 4-49
NEFTRAN Analysis - Release Rate for ^{129}I from Leg 2

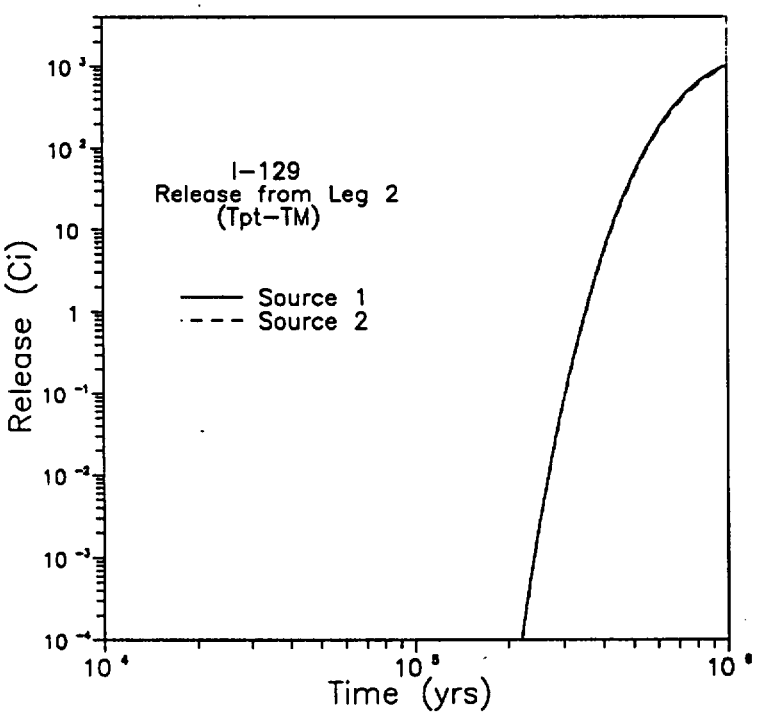

Figure 4-50
NEFTRAN Analysis - Cumulative Release for ^{129}I from Leg 2

Concentration profiles for ^{129}I at 100,000, 500,000, and 10^6 years for the two wet-drip sources are given in Figures 4-51 and 4-52. The profiles for the two sources were virtually identical. With NEFTRAN, an actual profile was somewhat difficult to display because the shapes of the profiles were controlled in part by the spatial points at which the concentrations were calculated. Concentrations were not calculated at the interior points of each unit. The profile across the second leg at 500,000 years is an example in which the profile is probably misleading. Leg 2 is the longest leg in the transport path, extending from 868 m to 930 m elevation. The release rates from Leg 1 (top of Leg 2; Figure 4-47) and Leg 2 (bottom of Leg 2; Figure 4-49) at 500,000 years, as well as the moisture contents at these two points were very similar. Therefore the concentrations at the top and bottom of Leg 2 were almost the same. However, the release rate from Leg 1 was at the end of the curve and release rate from Leg 2 was at the head of the curve. This implied that the concentration at the interior of Leg 2 at 500,000 years was higher than at the boundaries.

At 10^6 years, the plume was still 100 m above the water table. It was difficult to see the increase in the spread in the curve because of the concentration cutoff on the plot of 10^{-6} Ci/m^3. A better perspective of absolute release may be gained from Figure 4-53, which shows cumulative release as a function of elevation at 10^6 years.

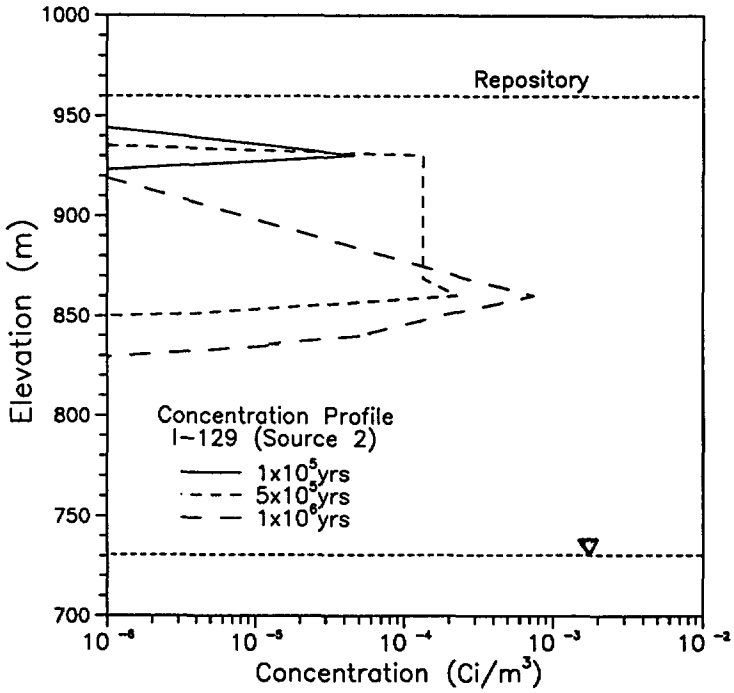

Figure 4-51
NEFTRAN Analysis - Concentration Profiles for ^{129}I, Wet-Drip, Bathtub Source

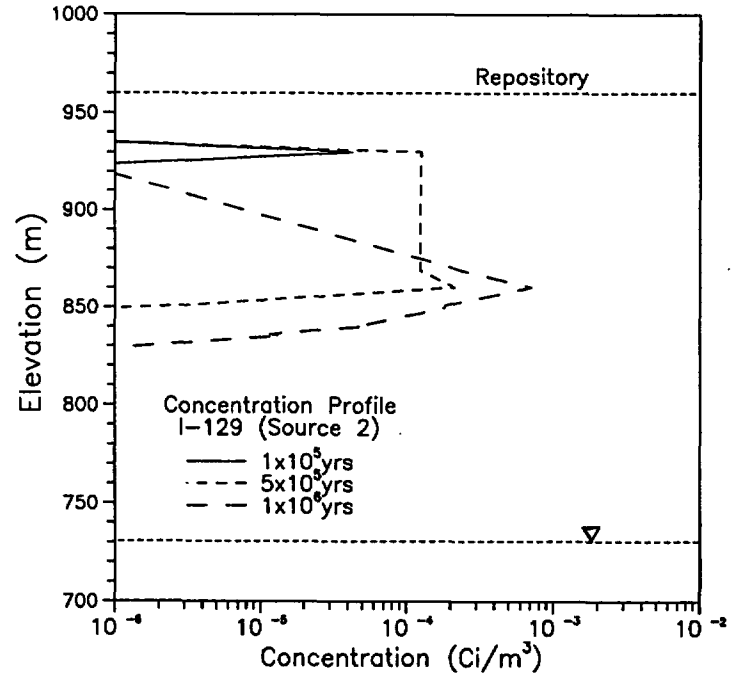

Figure 4-52
NEFTRAN Analysis - Concentration Profiles for ^{129}I, Wet-Drip, Flow-Through Source

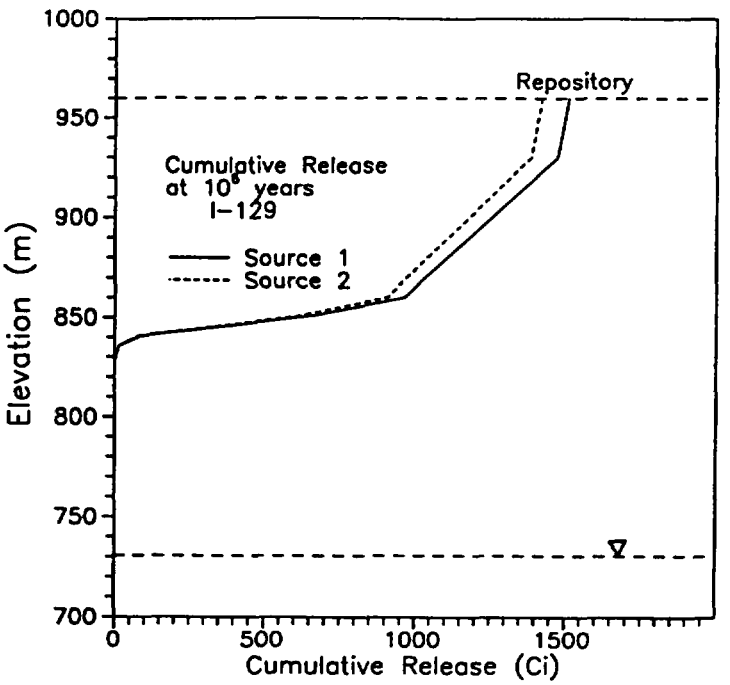

Figure 4-53
NEFTRAN Analysis - Cumulative Release Profiles for ^{129}I

4.5 LLUVIA, NORIA, and FEMTRAN

4.5.1 Code Description

4.5.1.1 One-Dimensional Codes

LLUVIA (Hopkins and Eaton, 1990) was used to do the PACE-90 1-D, steady flow analyses. LLUVIA was developed to efficiently solve this class of flow problems. The problem involved the steady flux of an incompressible, Newtonian fluid through a 1-D domain of saturated or partially saturated layers of porous media. The media may contain fractures whose properties vary from those of the matrix. The composite matrix-fracture model representation treats the material as a single continuum in solving for the pressure field. The first-order differential equation describing such a flow is Darcy's equation. Conservation of mass is ensured by the imposed steady-state condition, and Darcy's equation is a statement of momentum balance. The implicit solution procedure, DEBDF (Sham-

pine and Watts, 1980), uses a backward differentiation formula of orders one through five, and is interval-oriented. It is particularly well-suited to the solution of nonlinear problems. The specified flux or net infiltration rate was an imposed condition and was constant throughout the domain. The pressure field computed by the solution of Darcy's equation was subsequently used to compute the hydraulic conductivity, saturation, and water velocities in both the matrix and fractures. In these calculations, the matrix and fractures were treated as separate continua.

4.5.1.2 Two-Dimensional Codes

The single-phase version of the finite-element code NORIA (Bixler, 1985) was used. This code solves the nonlinear, parabolic, partial differential equation for conservation of mass and momentum (Richards' equation). Steady-state problems are solved by calculating a transient solution until a steady-state solution is reached. The numerical procedure uses the standard Galerkin finite-element method to handle spatial discretization of 2-D domains with either planar symmetry or axisymmetry. Time integration is performed by a second-order predictor-corrector scheme that uses error estimates to automatically adjust time-step size to maintain uniform local time truncation error throughout the calculation. Nearly all material properties, such as permeability, can either be set to constant values or can be defined as functions of the dependent and independent variables by user-supplied subroutines.

The 2-D finite element code FEMTRAN (Martinez, 1985) was used to compute the transport of solutes using the steady 1-D and 2-D flow fields computed with LLUVIA and NORIA, respectively. The 1-D solution was computed as a check on the 2-D solution. FEMTRAN uses bilinear basis functions defined on four-point quadrilaterals for discretizing the spatial terms in the transport equation via Galerkin's method of weighted residuals. Element calculation of the coefficient matrices are computed with four-point Gauss-Legendre quadrature. The resulting system of ordinary differential equations describing the time history at all basis points is integrated with the implicit second-order (Crank-Nicolson) trapezoid rule.

4.5.2 Problem Setup

4.5.2.1 One-Dimensional Analyses

The stratigraphy described in Section 3 was used for the four drill holes. The domain modeled for each hole was from the given water table location to the top of the Tpt unit. The number of nodes used in the model ranged from 268 (UE-25a) to 357 (G-1). These nodes were evenly spaced within each unit and were approximately 1.5 m apart.

The solute-transport calculations were not as well defined. Each participant was free to specify the diffusion, the dispersion, and the matrix-fracture coupling models. A 1-D solute transport code (Dykhuizen, 1987) was modified to accept the hydrologic output from LLUVIA, which ensured internal consistency. The code was further modified to use the more accurate matrix-fracture coupling model recently developed (Dykhuizen, 1990).

Groundwater flows near the repository elevation, at the specified infiltration rate, occurred through the matrix pore system. The fracture system was essentially dry. Therefore, only matrix transport was used for the transport calculation.

To solve the solute-transport equation, boundary conditions had to be provided. The domain modeled was from the water table up to the repository elevation. The repository was located 30 m above the lower interface of the Tpt-TML geologic unit. A zero concentration was imposed at the lower boundary. This conservatively assumed that the water table had an infinite capacity with good mixing. A flux boundary condition was imposed at the upper boundary equal to the release rates provided. This eliminated any diffusion of the solute upward from the repository.

4.5.2.2 Two-Dimensional Analyses

A 2-D solution of the cross-section lying between drill holes G-4 and UE-25a was obtained for the specified net infiltration rate. Nine different material regions were included in this problem. All of the material layers defined in Section 3.1 were used down through the Tpt-TN layer. This was the layer that resulted in appreciable lateral flow. The nine layers below that interface were combined into a single layer by averaging the material properties. Unnecessary complexity would have been added to the problem by inclusion of these layers, some of which were less than 1 m thick. A total of 1,260 quadrilateral elements were used, as is shown in Figure 4-54. A no-flux initial condition was used, and the right and left boundaries were no-flow boundaries. The bottom boundary was held at a pore pressure of zero m to represent the water table. The top boundary was held at the specified problem net infiltration flux. Approximately three Cray XMP hours were required to reach the steady-state condition.

Because of the low net infiltration flux for the nominal case, preliminary estimates of advective travel distance indicated that only nonsorbing radionuclides needed to be considered. The transport of ^{129}I, which was nonsorbing, along the vertical at drill hole G-4 for the 1-D problem and in the plane of the cross-section from G-4 to UE-25a was computed. Only the moist-continuous source term, Case 3, was considered because it offered the potential for greatest transport.

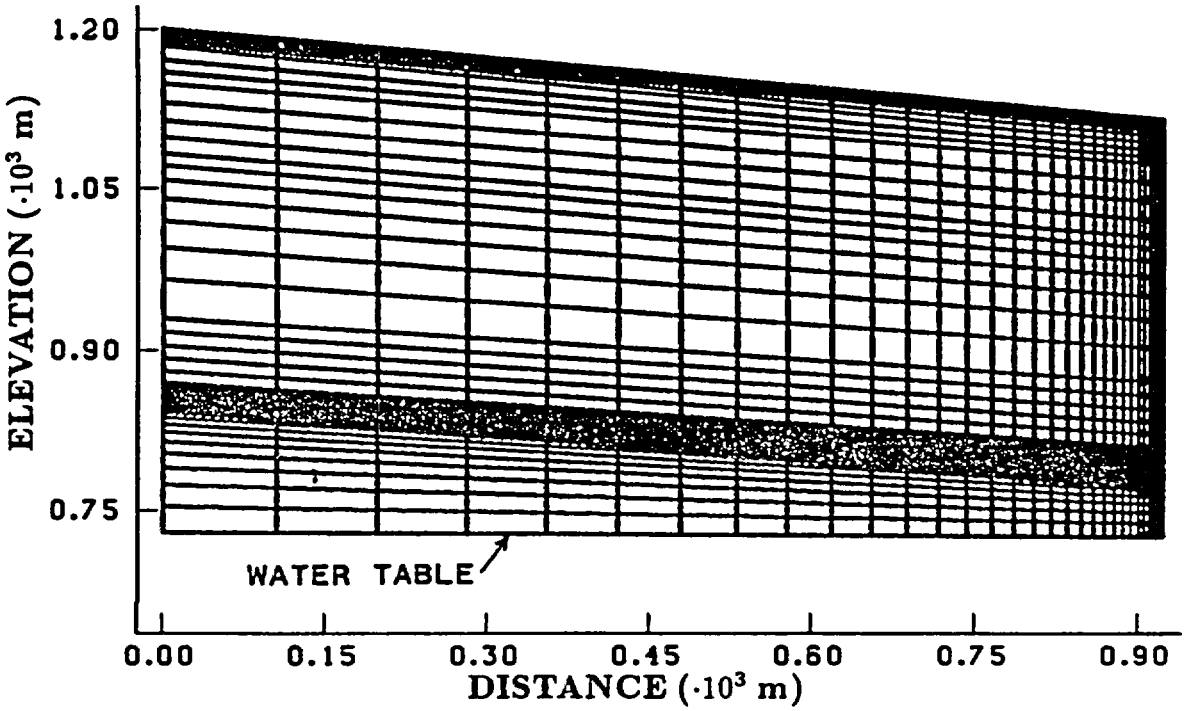

Figure 4-54
NORIA Analysis - 2-D Finite-Element Geometry

Because of the small solute-transport distance for the specified infiltration rate and the nature of the hydrologic solution generated by NORIA, the 2-D transport was computed on a smaller mesh. Given the travel distance computed in the 1-D problem, the mesh used for the hydrology was too coarse to resolve the transport properly. Furthermore, the hydrologic solution showed that the fluxes in the first 100 m below the repository departed only slightly from vertical, and the moisture contents varied between 0.085 and 0.1. Hence, the 2-D transport was computed on the mesh shown in Figure 4-55. This included the first 100 m below the repository and the two drill holes (G-4 and UE-25a) defining the cross-section. This mesh included 552 elements, each about 8.3 m high by 20 m wide, for a total of 611 node points. The NORIA hydrology was approximated in FEMTRAN by specifying a uniform moisture content in the region equal to 0.095, and by specifying a downward flux of 0.01 mm/yr and a horizontal flux of 0 mm/yr.

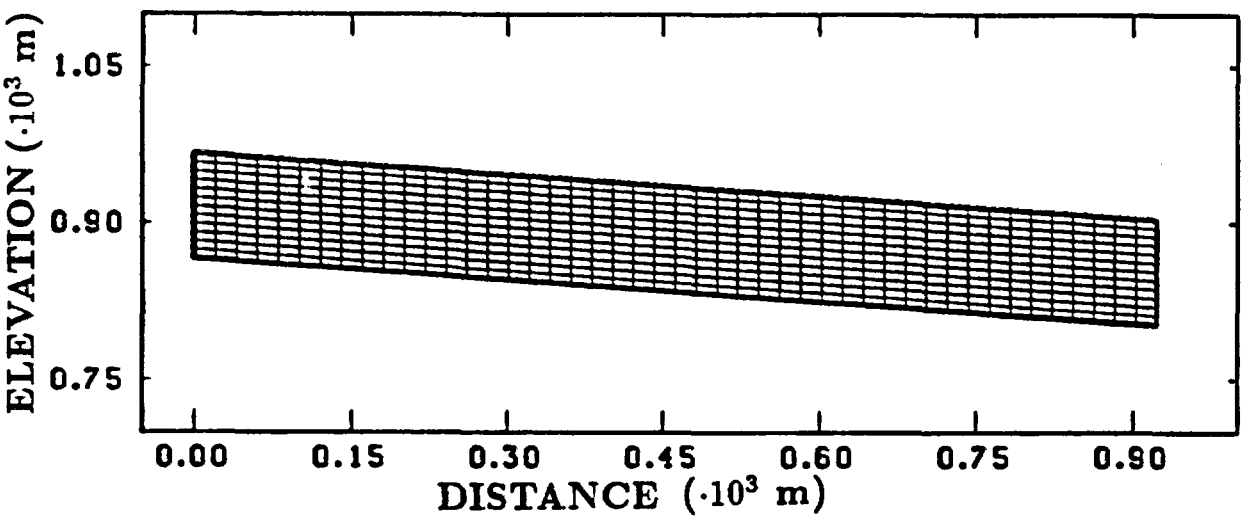

Figure 4-55
NORIA Analysis - 2-D Finite-Element Mesh for Transport

The hydrology solution computed by LLUVIA was used for the 1-D problem. The 1-D mesh at drill hole G-4, defined by LLUVIA and including all material layers, consisted of 178 four-node elements.

For both the 1-D and 2-D problems, no-flux boundaries were specified along the vertical sides of the mesh (at 0 and 923 m) and the concentration was specified as zero along the bottom of the mesh. A mixed boundary condition, equal to the release rate provided, was specified along the first 680 m of the top of the 2-D mesh extending from G-4 (representing the repository), with the remainder specified as no-flux. In order to obtain comparable concentrations between 1-D and 2-D results, the release rates were converted to flux rates by dividing the total release rates by the repository area, 5.61×10^2 m^2. The simulations for 1-D and 2-D used 151 time steps of varying size. The 2-D case was run on the CRAY-XMP and required 100 CPU seconds. The 1-D case was run on the VAX 8600 and required about 300 CPU seconds.

4.5.3 Results

4.5.3.1 One-Dimensional Results

The requested output quantities are plotted in Figures 4-56 through 4-63. In each figure, results from holes G-1 and H-1 are shown together, as are those from holes G-4 and UE-25a. These combinations were chosen because the material properties of the paired holes were similar. Figures 4-56 and 4-57 show the pressure-head profiles for the four drill holes. The similarities in material properties and differences in elevations of the units are apparent in these figures. Matrix saturations are shown in Figures 4-58 and 4-59. Similar trends in matrix saturation are seen between holes G-1 and H-1. However, hole UE-25a showed a thin layer of low matrix saturation at an elevation of 780 m that did not appear in G-4. Comparison of the units for these two holes that were between the water table and this elevation revealed a low-conductivity layer in G-4 that did not appear in UE-25a. The fracture saturations for all holes were near their residual values except very close to the water table. Water velocities in the matrix and in the fractures are shown in Figures 4-60 through 4-63 (positive values indicate a downward velocity). The matrix water velocities were all of the same order of magnitude throughout most of the domain. The fracture velocities all showed a significant increase near the Tpt-TNV unit where there was an order of magnitude change in fracture porosity and bulk conductivity.

The 1-D solute transport calculations were performed for the 0.01 mm/yr net infiltration condition. The output requested was the integrated amount of each of the representative radionuclides that reached the water table in 100,000 years. Because of the low flow rate and the reactive nature of the solutes, this produced a zero result. This was shown analytically by expressing the solute concentration as a function of the groundwater velocity, density, moisture content, and retardation coefficients. Using a moisture content of 0.2 and a matrix density of 2.0 g/cc, the solute travel distances after 100,000 years as a function of K_d for several assumed infiltration rates were calculated (Table 4-4). From this we

see that only the nonreactive radionuclides at higher infiltration rates were advected to the water table within the 100,000-year time period.

TABLE 4-4
SOLUTE TRAVEL DISTANCES (IN METERS)

Sorption Coefficient (K_d)	Infiltration Rate (mm/yr) 0.01	0.1	0.5
0	5	50	250
1	0.45	4.5	22
10	0.05	0.5	2.5
100	0.005	0.05	0.25

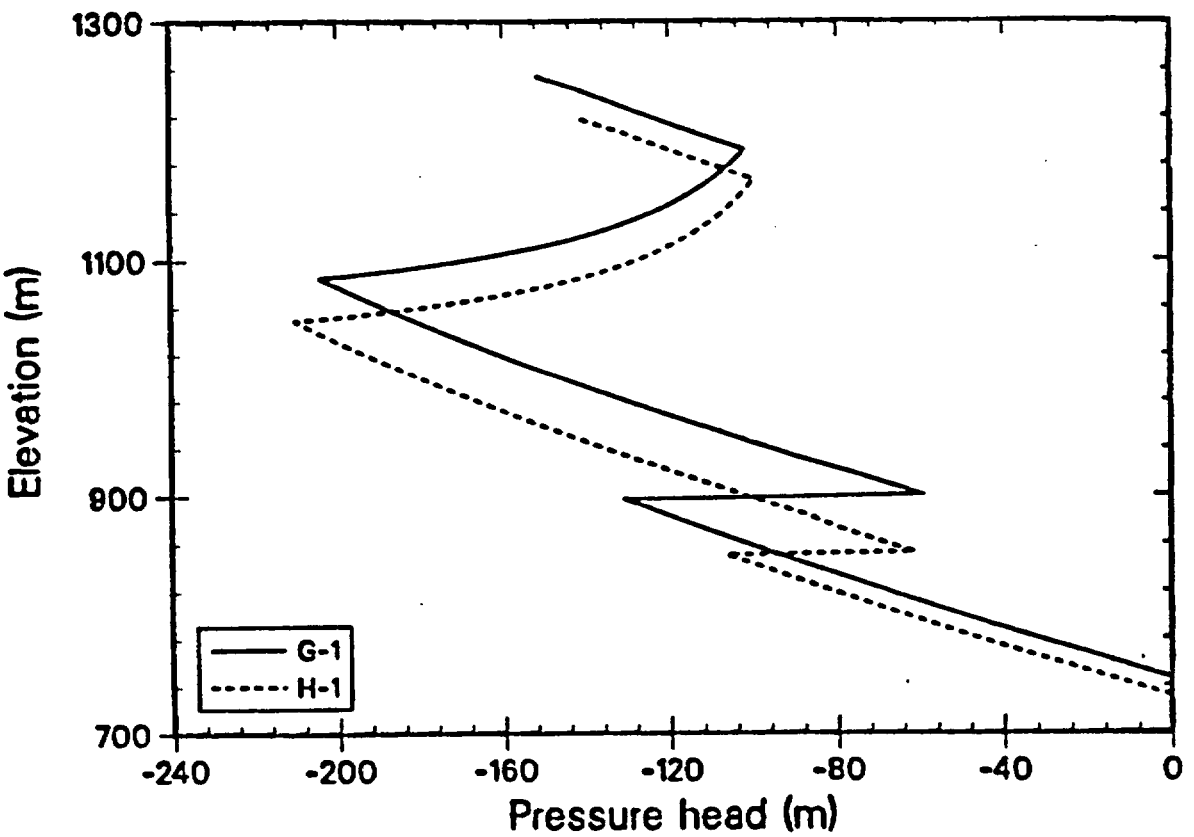

Figure 4-56
LLUVIA Analysis - Pressure Head for Drill Holes G-1 and H-1

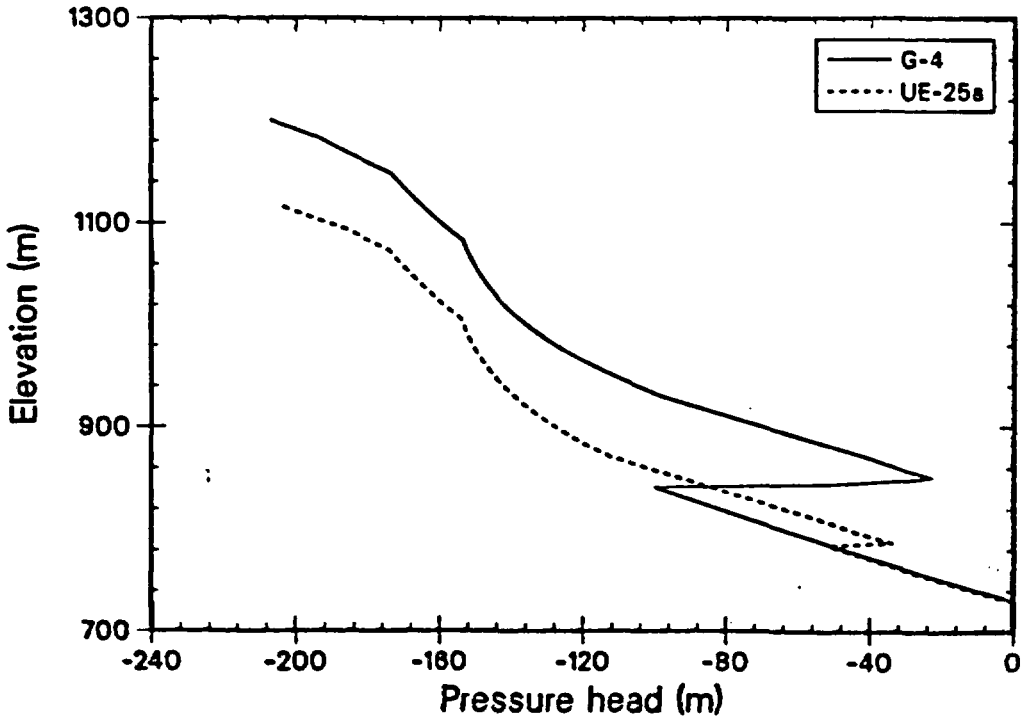

Figure 4-57
LLUVIA Analysis - Pressure Head for Drill Holes G-4 and UE-25a

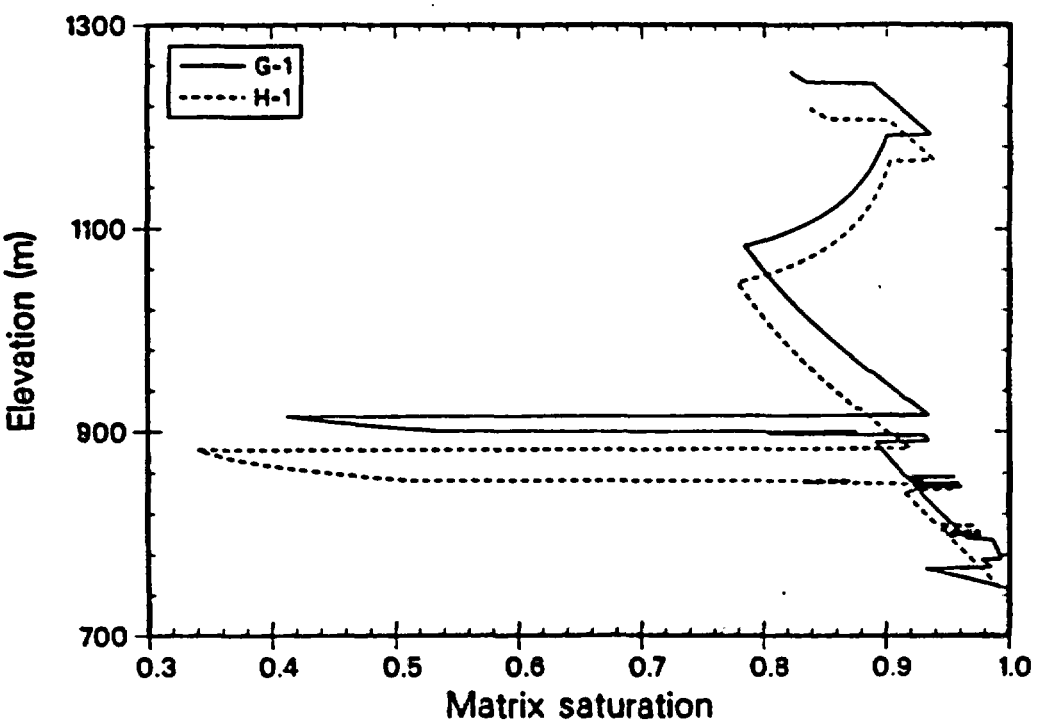

Figure 4-58
LLUVIA Analysis - Matrix Saturation for Drill Holes G-1 and H-1

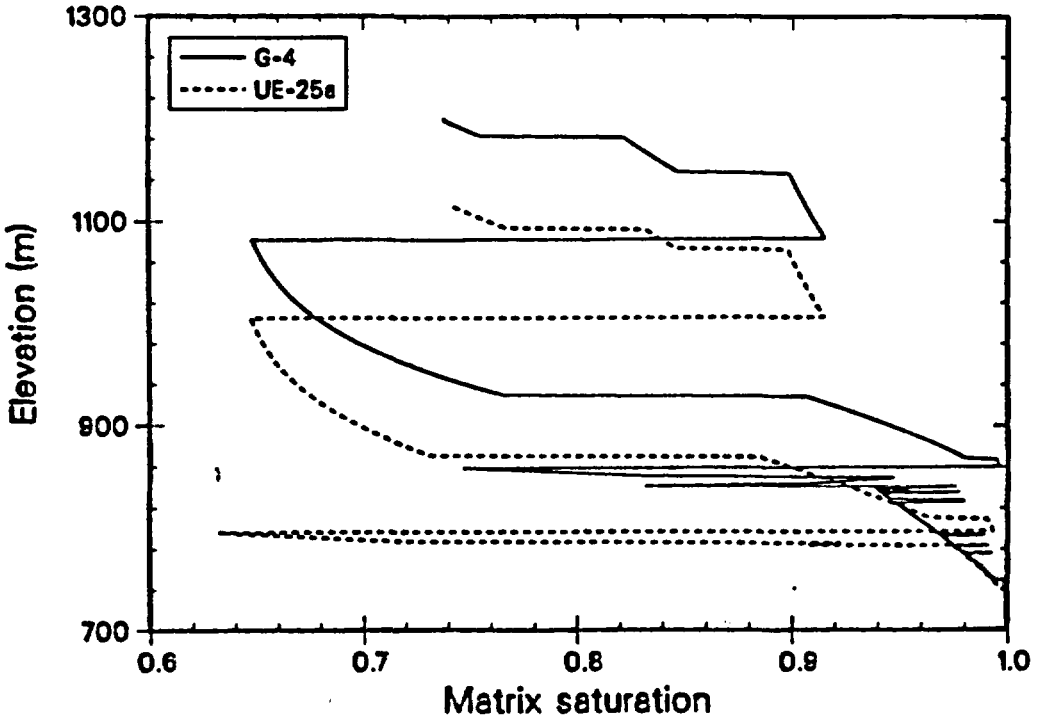

Figure 4-59
LLUVIA Analysis - Matrix Saturation for Drill Holes G-4 and UE-25a

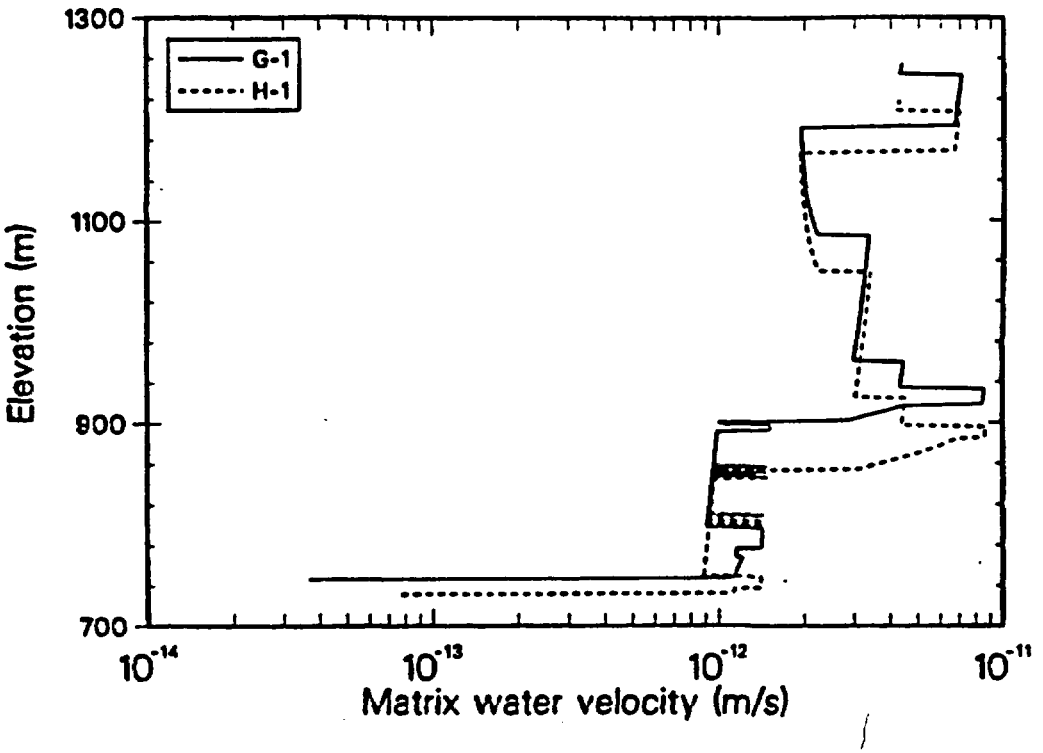

Figure 4-60
LLUVIA Analysis - Matrix Water Velocities for G-1 and H-1

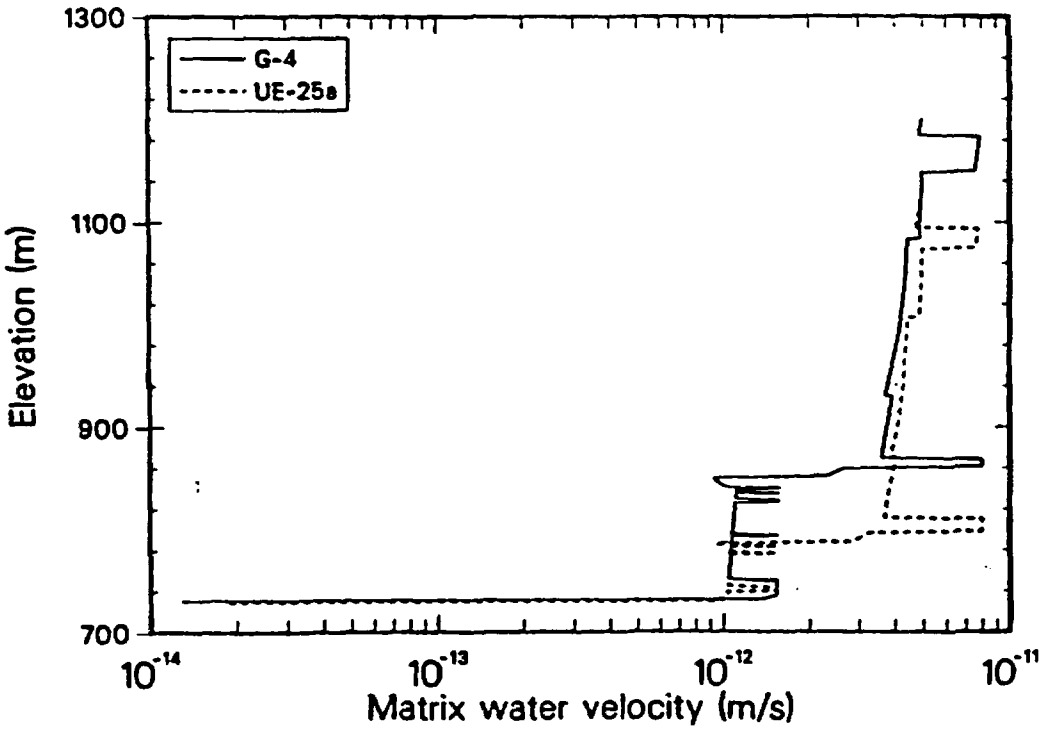

Figure 4-61
LLUVIA Analysis - Matrix Water Velocities for G-4 and UE-25a

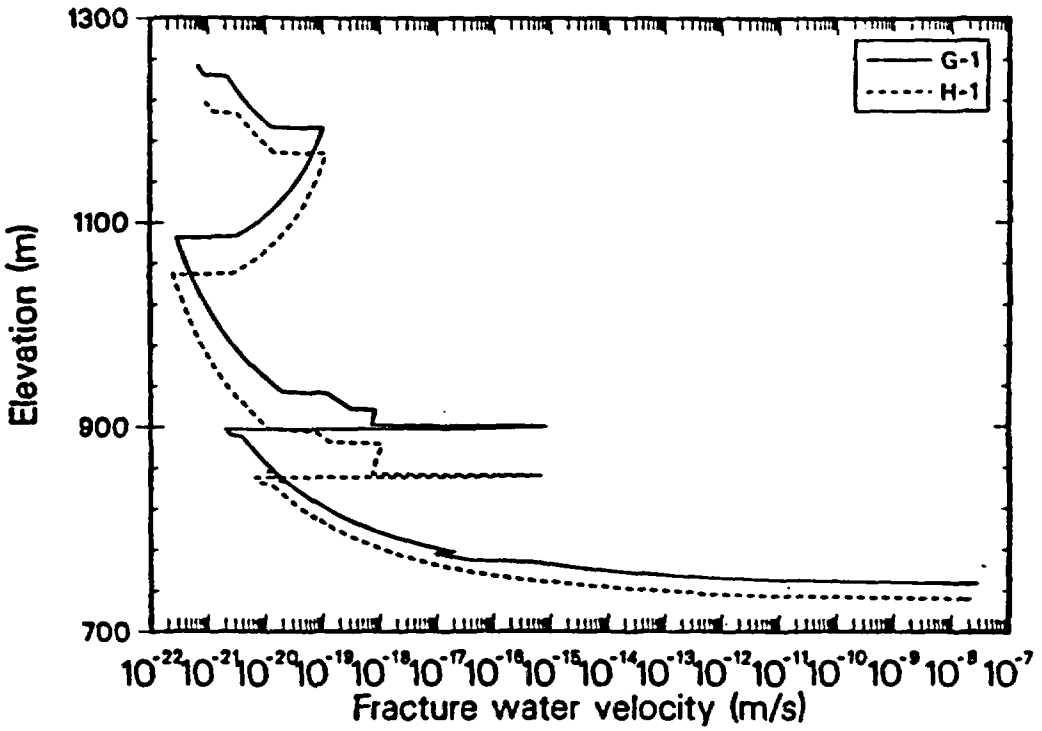

Figure 4-62
LLUVIA Analysis - Fracture Water Velocities for G-1 and H-1

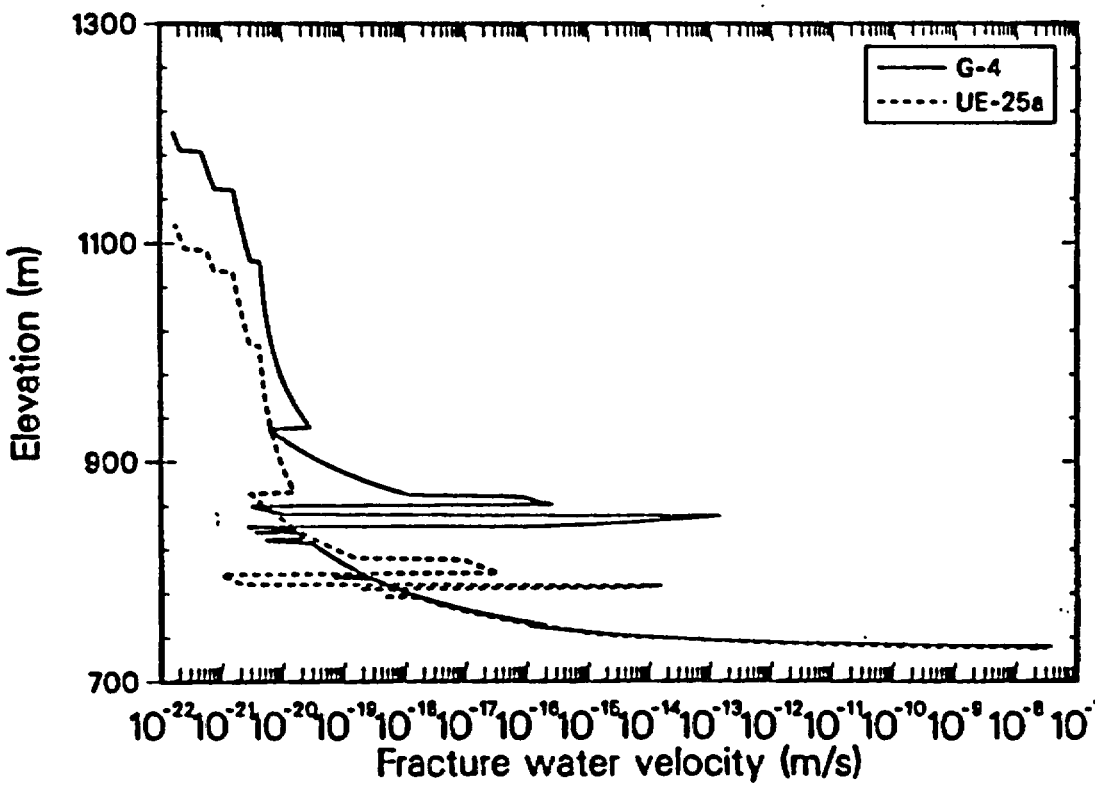

Figure 4-63
LLUVIA Analysis - Fracture Water Velocities for G-4 and UE-25a

Table 4-4 only indicates the distance that the solute would advect in 100,000 years. The diffusion/dispersion of the solute resulted in some solute traveling farther than the advected distance. To determine the relative importance of the advection versus the diffusion motion, the Peclet number was formed. The Peclet number is double the square of the ratio of the advected distance over the diffused distance:

$$P_e = 2\ (X_a/X_d)^2,$$

where $X_a = v_a t$, and $X_d = (2D_e t)^{1/2}$. Note that this Peclet number is based on the advected distance. Because this distance increased with time, all flows were eventually advection-dominated in the limit of large times and distances. All flows analyzed here were strongly influenced by diffusion, if not totally diffusion-dominated, because of the low infiltrations.

Figures 4-64 and 4-65 show the transport of ^{129}I and ^{99}Tc through the G-4 stratigraphy after 100,000 years. All four of the moist-continuous source-term variation cases are presented on these plots. As can be seen, the ^{99}Tc was somewhat retarded as a result of the sorption coefficients provided. In both plots it is shown that the moist-continuous Case-3 source-term variation resulted in the most movement of the solute. This is because this case released more solute earlier in the 100,000-year period. However, all four source-term variation cases resulted in similar movement of the solute for this low infiltration. Furthermore, results from the other three drill holes showed very similar solute distribution, when compared on a basis of distance traveled from the repository horizon.

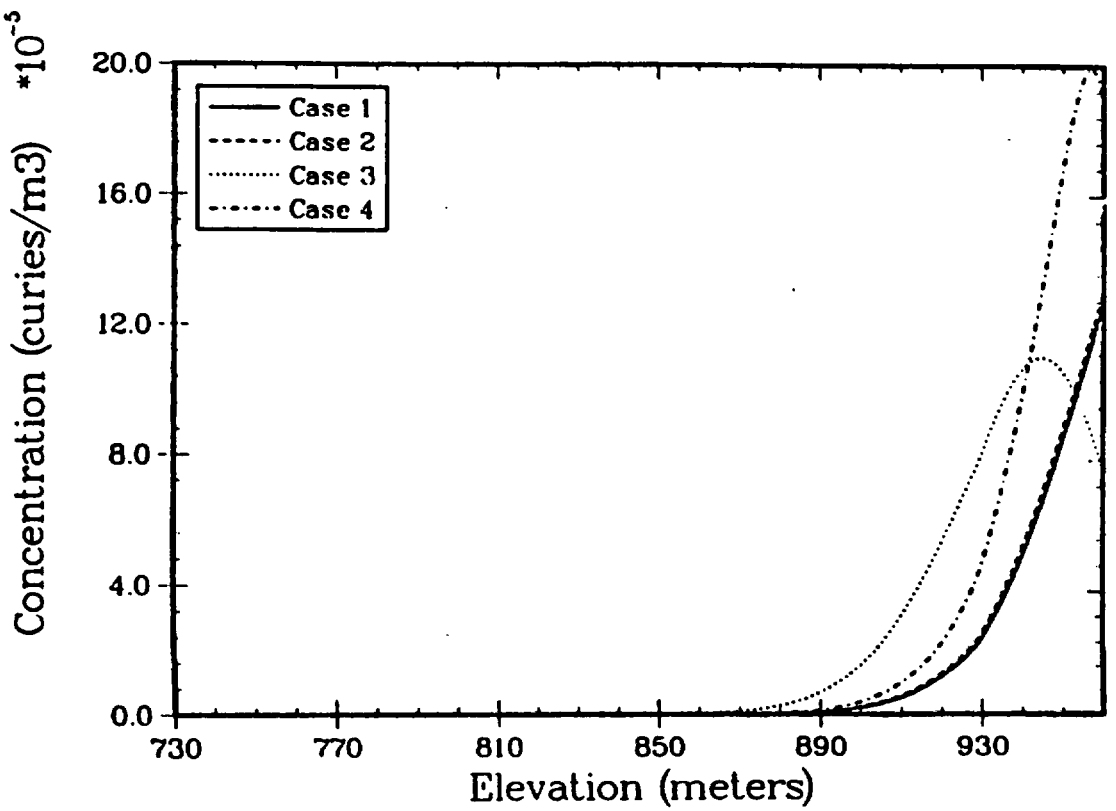

Figure 4-64
LLUVIA Analysis - ^{129}I Transport at G-4 After 100,000 Years

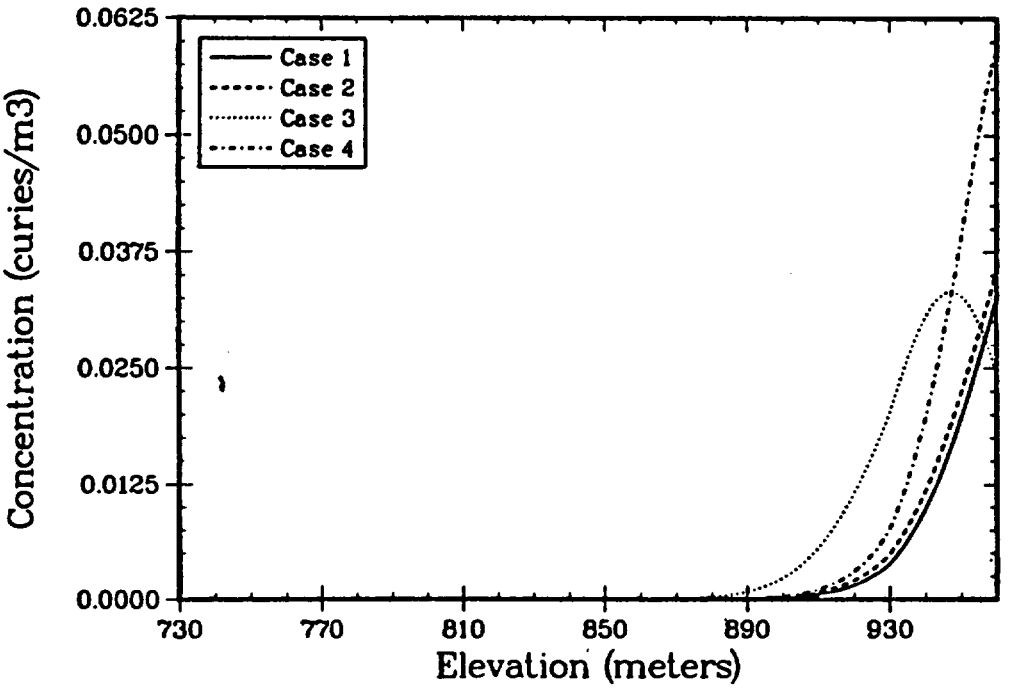

Figure 4-65
LLUVIA Analysis - ^{99}Tc Transport at G-4 After 100,000 Years

All of the plots presented are in units of curies per cubic meter of groundwater. These plots do not directly show the amount of solute sorbed onto the geologic media. These units were chosen to be consistent with those of the other PACE-90 participants.

4.5.3.2 Two-Dimensional Results

Figures 4-66 and 4-67 show the steady-state material saturation from the water table to the top of the computed region. These distributions agree well with the 1-D results given in Figure 4-59. As would be expected, the 2-D results showed a slightly drier profile below the Tpt-TNV zone at hole G-1 and a wetter profile in the down-dip direction, toward hole UE-25a, as a result of lateral water flow. Figures 4-68 and 4-69 show that there is a small gradient in matrix saturation in the top half of the region. The matrix saturation along the bottom was defined to be one by the nature of the applied boundary condition. Figure 4-70 compares the

vertical Darcy flux at three vertical locations. There was no appreciable lateral flow above the Tpt-TNV unit. Below this level, the flux near the right boundary was an order of magnitude larger on the down-dip side. Figure 4-71 shows contours of matrix saturation. The water flux vectors and pathlines shown in Figures 4-72 and 4-73, respectively, show that there was little water diversion through the region above the Tpt-TNV. Considerable lateral diversion of the infiltrating water was calculated in the Tpt-TNV unit, even for this relatively low infiltration condition. This was a direct result of the variation between layers of the saturated conductivity being six orders of magnitude. It appeared that the six-order variation in hydraulic conductivity between the Tpt-TV, Tpt-TNV, and Tpt-TN units was the dominating hydrologic property. Earlier studies done by Prindle and Hopkins (1989) showed a similar diversion phenomena at the Tpc/Tpt interface.

Figure 4-74 shows the concentration of ^{129}I (in Ci/m^3) along the vertical at drill hole G-4 for the 1-D and 2-D geometries at 100,000 years. The water table at G-4 was specified at 730 m and the repository at 960 m. As expected, the transport distance was small. The peak concentration traveled less than 20 m below the repository and entire solute body traveled less than about 50 m below the repository. The comparison between the 1-D and 2-D solutions was excellent, indicating transport was essentially 1-D over this time span. This is further illustrated in Figures 4-75 and 4-76 showing contour maps of concentration in the 2-D problem at 50,000 years and 100,000 years, respectively. The contours show that the transport was 1-D except for the region around the edge of the repository and that none of the solute was transported to the water table over the first 100,000 years.

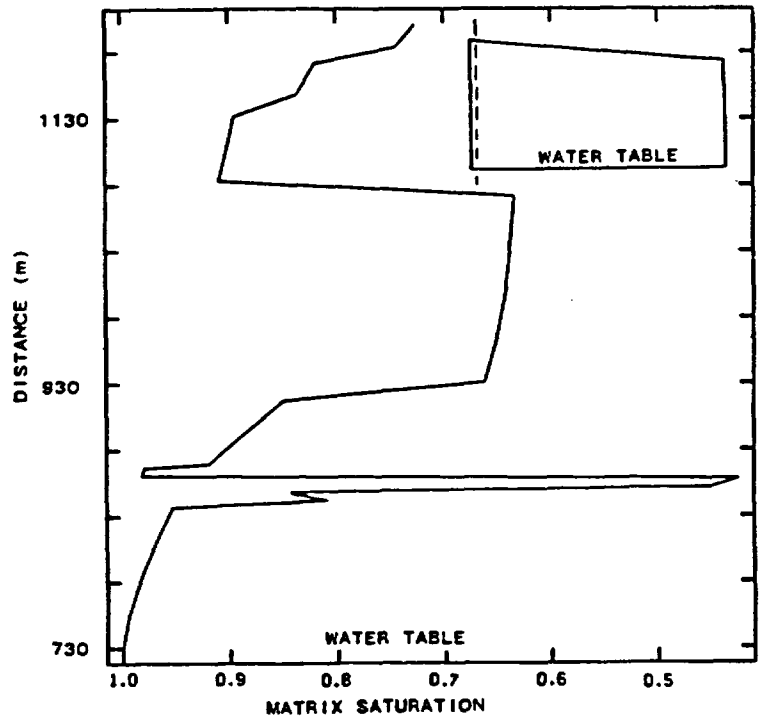

Figure 4-66
NORIA Analysis - Matrix Saturation Profile at Drill Hole G-4

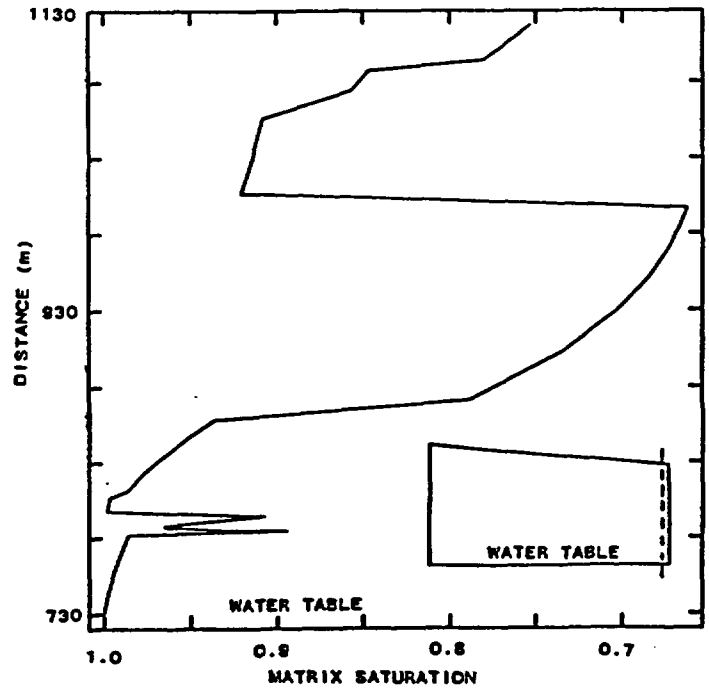

Figure 4-67
NORIA Analysis - Matrix Saturation Profile at Drill Hole UE-25a

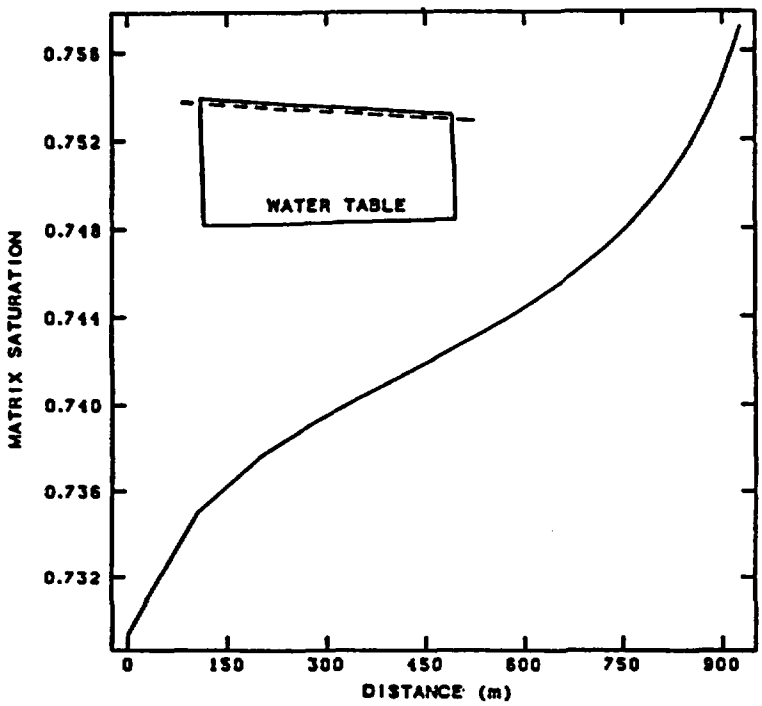

Figure 4-68
NORIA Analysis - Matrix Saturation Profile at Top

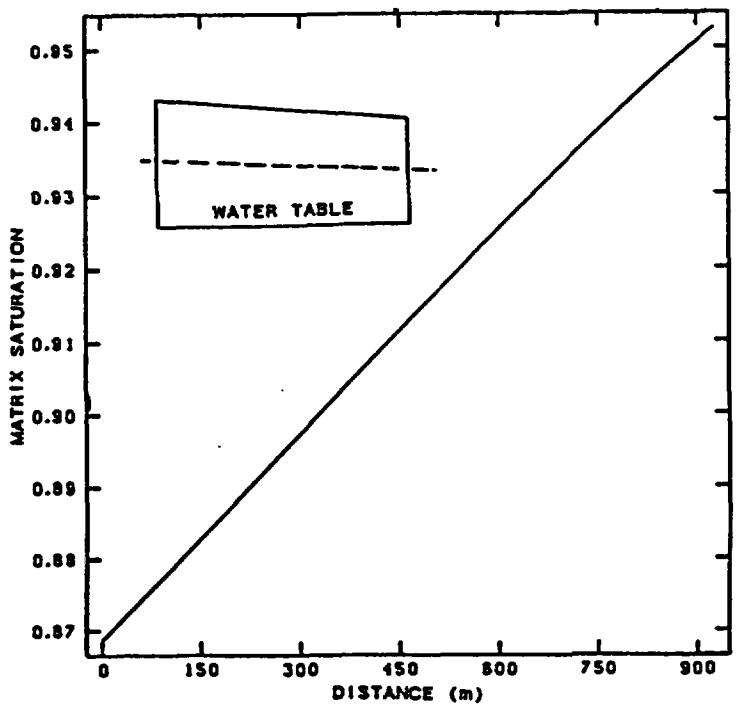

Figure 4-69
NORIA Analysis - Matrix Saturation Profile at Middle

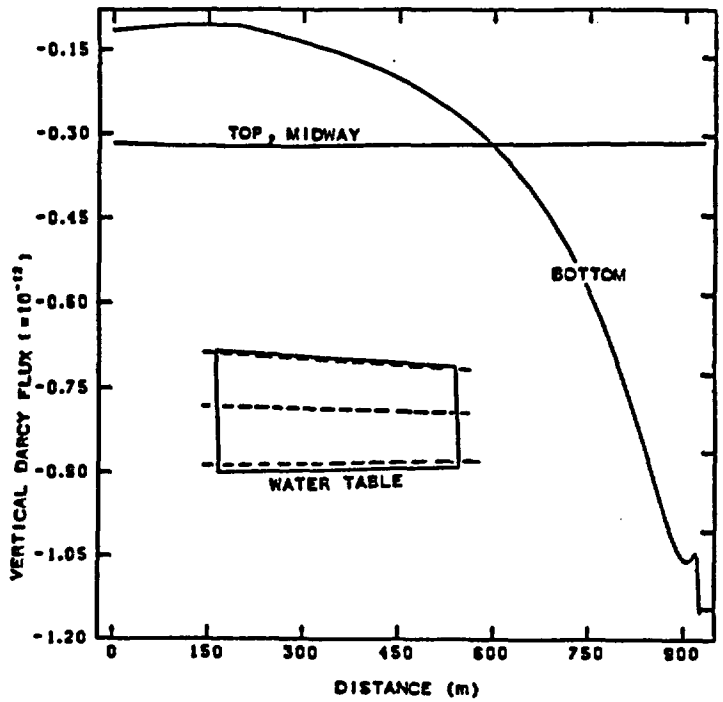

Figure 4-70
NORIA Analysis - Vertical Water Flux Profiles at Locations in Inset

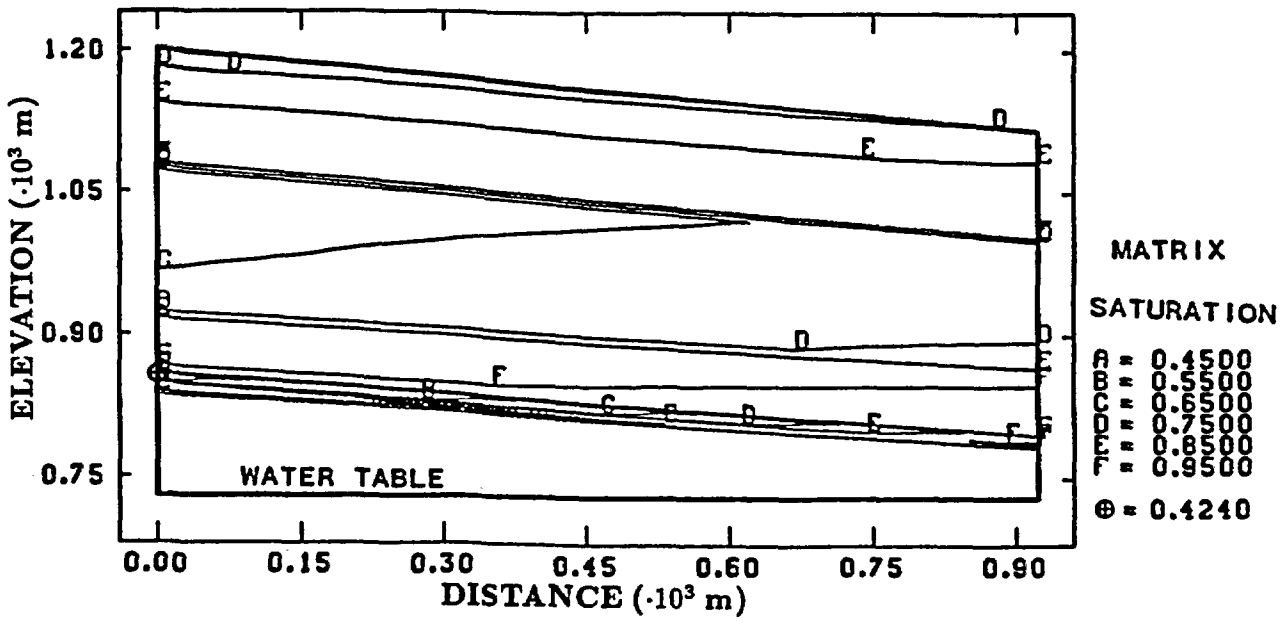

Figure 4-71
NORIA Analysis - Matrix Saturation Contours

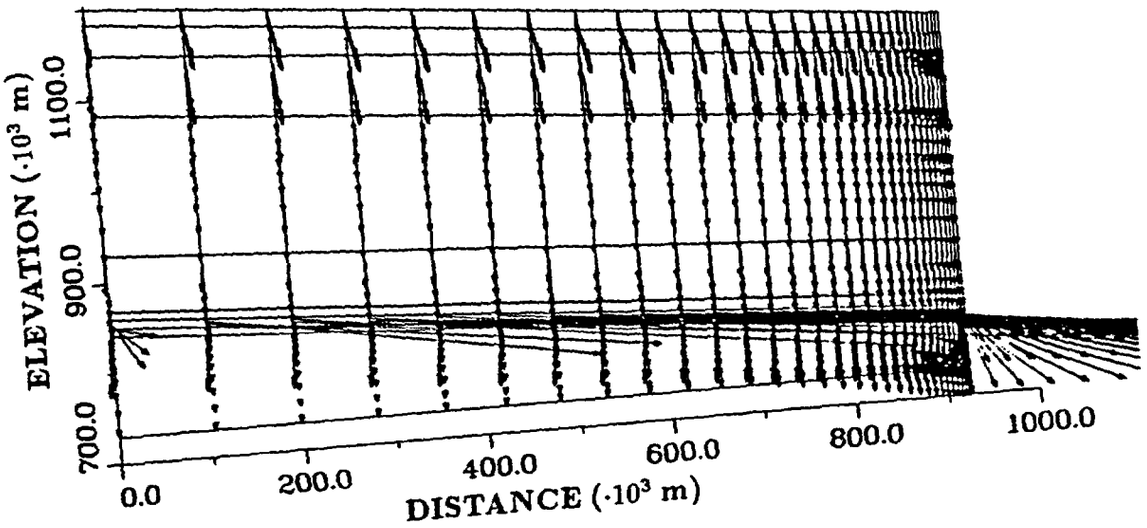

Figure 4-72
NORIA Analysis - Darcy Flux Vectors

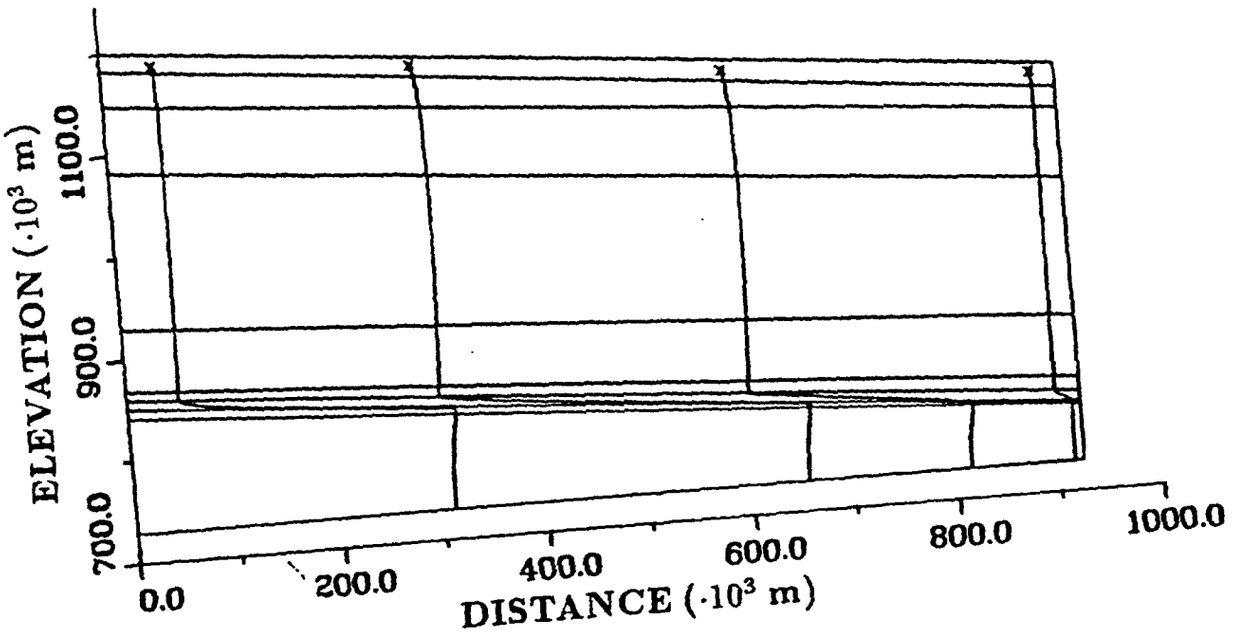

Figure 4-73
NORIA Analysis - Water Particle Pathlines

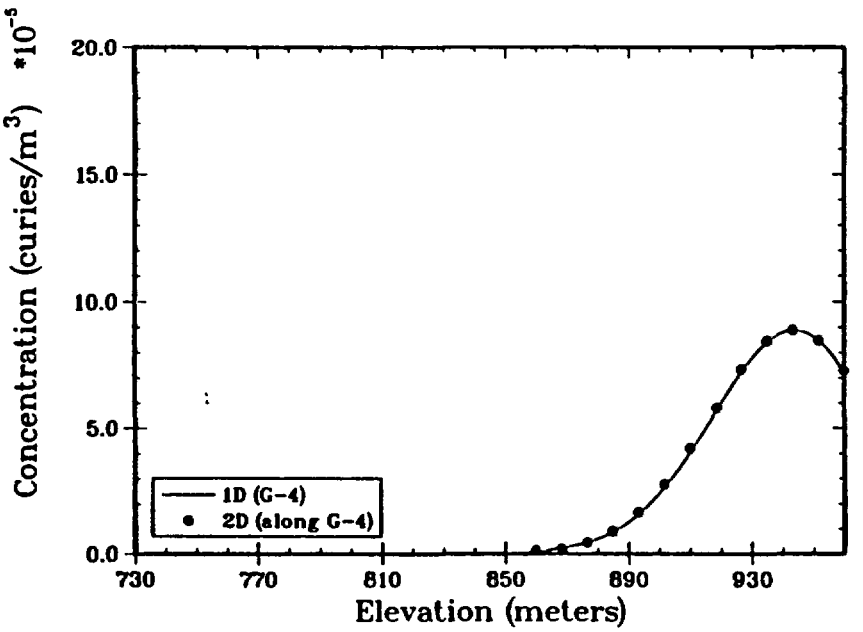

Figure 4-74
FEMTRAN Analysis - Comparison of 1-D and 2-D Calculations for Concentration of ^{129}I

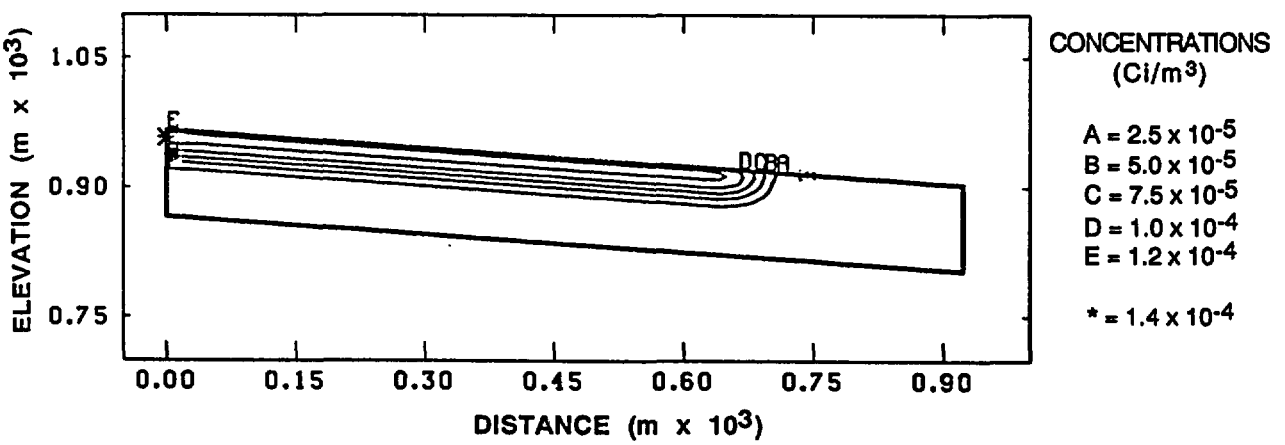

Figure 4-75
FEMTRAN Analysis - Concentration Contours for ^{129}I at 50,000 years

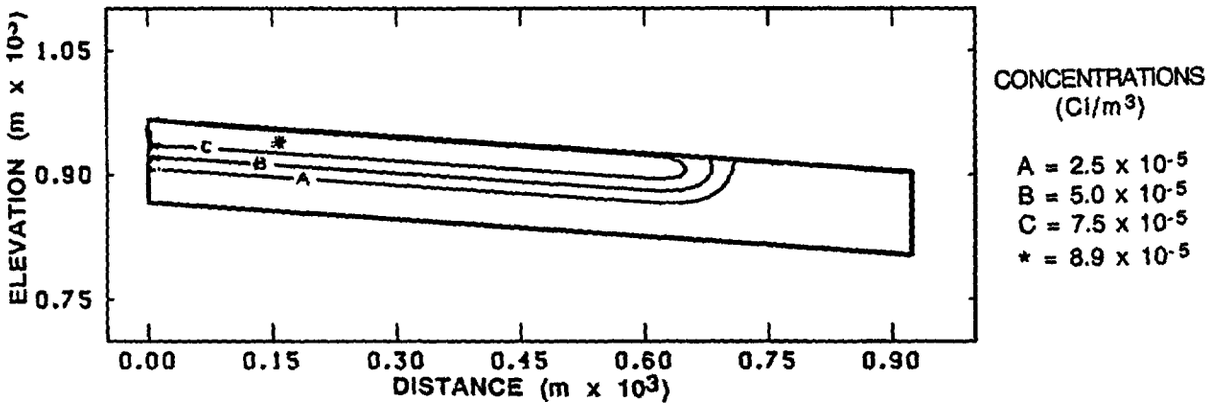

Figure 4-76
FEMTRAN Analysis - Concentration Contours for
^{129}I at 100,000 years

5.0 SUMMARY AND DISCUSSION

5.1 Summary and Comparison of Results

Calculation of the PACE-90 nominal-case problem was accomplished in three steps. First, a complex hydrostratigraphy and associated data for a site-scale groundwater radionuclide transport problem were developed. Next, radionuclide source-terms appropriate for the nominal case were defined. Finally, liquid-phase transport of selected radionuclides was calculated using both 1-D and 2-D models to solve for the hydrologic flow and transport fields.

The radionuclide release profiles fell into two general classes: those with a large initial release, followed by a decreasing profile (the wet-drip and moist-continuous, Case-3 sources), and those with an increasing release profile (moist-continuous, Cases 1, 2, and 4 sources). Figures 5-1 and 5-2 (taken from the TOSPAC analyses) summarize the source characteristics. The differences in the releases were due to the release-rate behavior of the sources.

The codes used to address the 1-D hydrologic problem were LLUVIA, TOSPAC, TRACRN, and DCM-3D. Two basic approaches were used for the 1-D codes. LLUVIA, TOSPAC, and TRACRN used a single-continuum, finite-difference procedure, while DCM-3D used a dual-continuum, finite-difference approach. All four models used a minimum of fifteen hydrostratigraphic units from the repository to the water table. Some participants did a more extensive suite of calculations than others. These extensions included modeling varying numbers of drill holes, incorporating layers above the repository into the problem domain, or calculating groundwater travel time. Table 5-1 summarizes the 1-D hydrology results.

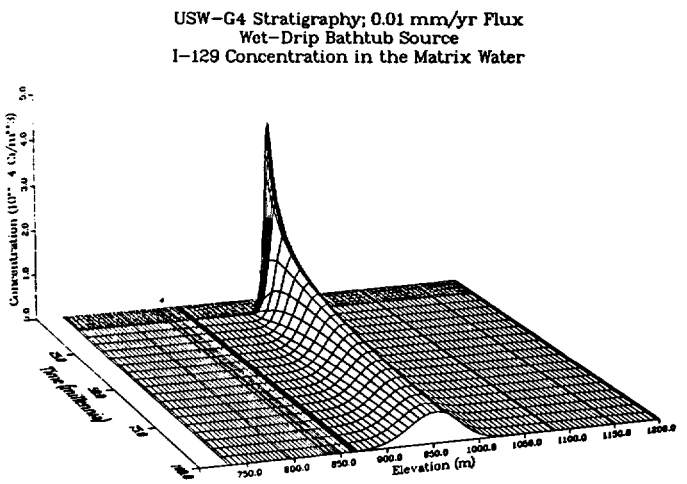

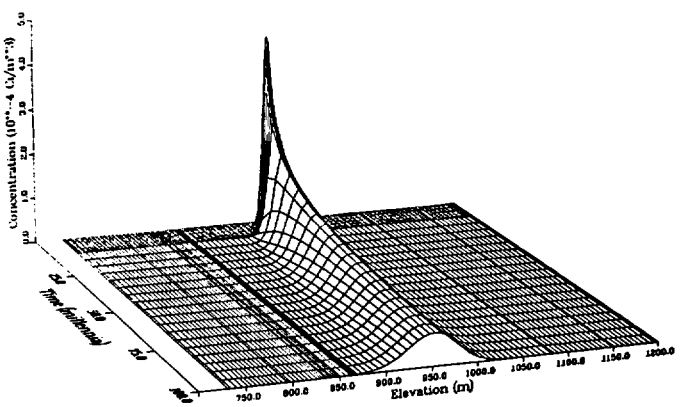

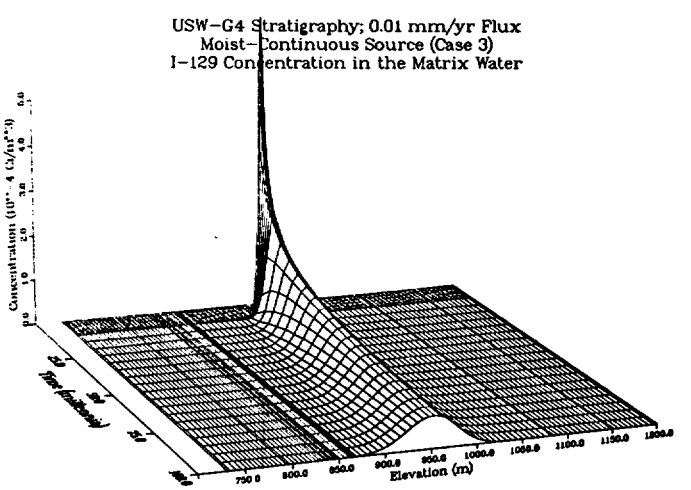

Figure 5-1
Comparison of Source Profiles for ^{129}I
(Wet-Drip, Moist-Continuous, Case 3)

USW-G4 Stratigraphy; 0.01 mm/yr Flux
Moist-Continuous Source (Case 1)
I-129 Concentration in the Matrix Water

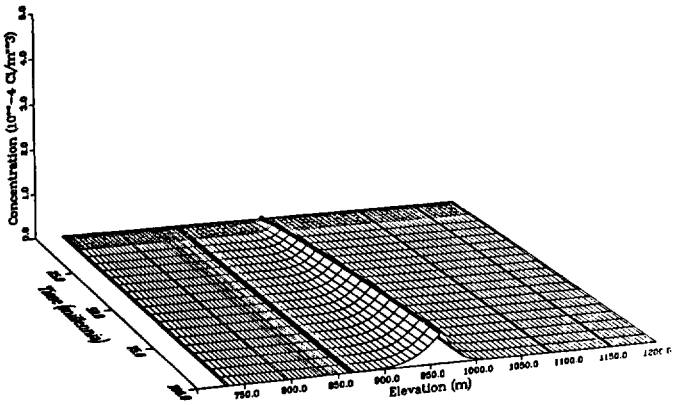

USW-G4 Stratigraphy; 0.01 mm/yr Flux
Moist-Continuous Source (Case 2)
I-129 Concentration in the Matrix Water

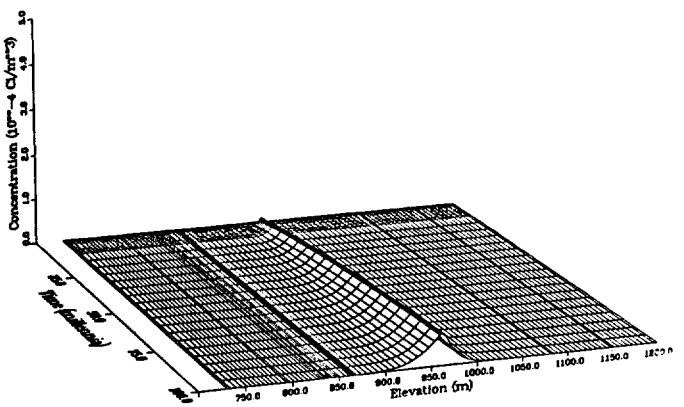

USW-G4 Stratigraphy; 0.01 mm/yr Flux
Moist-Continuous Source (Case 4)
I-129 Concentration in the Matrix Water

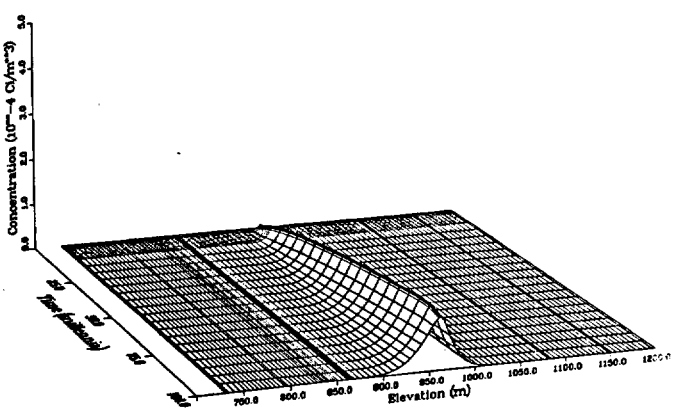

Figure 5-2
Comparison of Source Profiles for ^{129}I
(Moist-Continuous, Cases 1, 2, and 4)

TABLE 5-1

SUMMARY OF RESULTS FOR 1-D HYDROLOGIC CODES

Code	Drill Hole Modeled	Elevations Modeled (m)	Zones Used	Groundwater Travel Time (yr)
TRACRN	G-4	640 - 965	17	—
	UE-25a	640 - 965	17	—
TOSPAC	G-4	730 - 1200	20	4.2×10^6
	G-1	730 - 1200	20	4.9×10^6
	H-1	730 - 1200	20	4.6×10^6
	UE-25a	730 - 1200	20	3.0×10^6
DCM-3D	G-4	730 - 960	15	—
LLUVIA	G-4	730 - 1200	18	4.2×10^6
	G-1	730 - 1200	18	5.0×10^6
	H-1	730 - 1200	18	4.6×10^6
	UE-25a	730 - 1200	18	2.9×10^6

For the 1-D solute-transport simulations, all but NEFTRAN used a finite-difference method with a two-equation, coupled fracture/matrix model. NEFTRAN used the distributed velocity method to simulate transport in a series of path legs that were specified as being either fracture or matrix. All 1-D codes but TOSPAC constrained the problem to allow no upward transport of radionuclides. The TOSPAC model allowed for diffusion of radionuclides. Table 5-2 summarizes the 1-D transport results.

Regardless of the water-flow and solute-transport modeling differences, all four 1-D modeling approaches produced very similar velocity, saturation, pressure, and radionuclide release profiles, although the magnitudes of the curves were not always comparable. These results are detailed in Section 4. Table 5-2 is a summary of the calculated elevations of the 10^{-5} Ci/m^3 concentration of each of the four nuclides for all 1-D calculations, compared with the source elevation of 965 m and water table elevation of 730 m. None of the 1-D codes used large amounts of computer time. It is therefore reasonable to consider using these codes for multiple-realization statistical studies.

TABLE 5-2

SUMMARY OF RESULTS FOR 1-D TRANSPORT CODES

Code	Drill Hole Modeled	Source Term	100,000-year 10^{-5} Ci/m^3 Concentration Elevations			
			Cs	Tc	I	Np
TRACRN	G-4	Case 1	960	920	890	965
	G-4	Flow-Through	965	935	925	965
TOSPAC	G-4	Case 1	965	930	920	965
	G-4	Case 2	965	930	920	965
	G-4	Case 3	965	920	890	965
	G-4	Case 4	965	925	910	965
	G-4	Flow-Through	965	920	900	965
	G-4	Bathtub	965	915	900	965
NEFTRAN	G-4	Flow-Through	965	965	930	965
	G-4	Bathtub	965	965	925	965
LLUVIA	G-4	Case 1	965	910	920	965
	G-4	Case 2	965	910	920	965
	G-4	Case 3	965	880	870	965
	G-4	Case 4	965	910	910	965

SUMO and NORIA addressed the problem using 2-D geometries. SUMO modeled a total system extending vertically from the water table to 50 m above the repository and 3000 m horizontally along a line including drill holes G-1 and G-4. SUMO used four hydrostratigraphic layers to represent the geologic section. The NORIA model included the region between drill holes G-4 and UE-25a, and from the water table to the top of the Tpt-TM unit. NORIA modeled the geologic section using nine of the PACE-90 hydrostratigraphic zones. One of the nine units used in the NORIA simulations was the Tpt-TNV unit, which had a permeability six orders of magnitude greater than its neighboring units. The inclusion of this unit provided a conduit for considerable lateral water diversion. This was the most evident difference resulting from different assumptions used in these two 2-D analyses. However, the lateral diversion of flow occured approximately 100 m below the repository. Since the predicted solute transport never reached distances greater than 40 m below the repository, this difference in modeling had little effect on the radionuclide-transport results. Table 5-3 compares the hydrologic results for the 2-D modeling.

TABLE 5-3

SUMMARY OF 2-D HYDROLOGIC RESULTS

Code	Cross Section Modeled	Domain Modeled (m)	# Zones Used	x Location (m)	Groundwater Travel Times (yr)
SUMO	G-1 - G-4	730 - 1020 (z)	4	0	3.8×10^6
		0 - 2000 (x)		500	3.2×10^6
				1000	3.2×10^6
				1500	2.0×10^6
				2000	1.5×10^4
NORIA	G-4 - UE-25	730 - 1200 (z)	9	0	4.2×10^6
		0 - 923 (x)		200	6.4×10^6
				400	2.3×10^6
				600	1.7×10^6
				800	1.5×10^6
				923	2.9×10^6

5.2 Discussion of Model and Parameter Uncertainties

For any natural system, such as Yucca Mountain, there will be uncertainties in our knowledge of the values for parameters such as the physical, material, and hydrologic properties. Consequently, calculations must use data sampled from the ranges of values assumed for those parameters. The PACE-90 calculations used only one of many parameter samplings consistent with the conceptual model for Yucca Mountain. Although the PACE-90 outcomes did not predict any radionuclide transport to the accessible environment, other parameter realizations could predict releases. For example, the use of a low net infiltration rate for this problem made it not unexpected that there was no predicted radionuclide release to the water table. For the hydraulic conductivity specified, the net infiltration rate was limited to 0.01 mm/year to maintain unsaturated conditions (consistent with values observed in the core samples). Other combinations of matrix-fracture hydraulic conductivities and net infiltration rates could also produce unsaturated flow, but would probably result in considerably different transport results.

The problem that was solved was one of many descriptions of the nominal flow system at Yucca Mountain. A complete description

of all the nominal flow systems, comprising the expected conditions at Yucca Mountain, would require a comprehensive review of all the features, events, and processes associated with the hydrologic system of Yucca Mountain. Such a review would link PA problems with scenarios describing all the processes expected to occur at Yucca Mountain. This review will be done by means of event tree diagrams describing the flow processes.

5.3 Discussion of Simplifications in the Modeling

Several simplifications were made in order to model the expected conditions at Yucca Mountain. The effect of these simplifications was to limit the applicability of the PACE-90 analyses. These simplifications included (1) the assumptions of uniform water infiltration; (2) homogeneous, isotropic geologic zones; (3) isothermal conditions at the repository and surrounding rock; (4) a source term with a limited number of radionuclides; (5) boundary conditions that permitted ponding of water within units; (6) considering sorption to occur in the matrix, when it might instead preferentially occur in the fractures; (7) a water flow rate so low that vapor transport might be important; (8) a highly conservative source term, which assumes that the release from the EBS occurs at the container-emplacement-borehole wall; and (9) the use of the composite-porosity model for describing hydraulic behavior.

The first five simplifications listed above were parametric. By providing more detailed or different parameters to the existing models, the results might better reflect the actual complexity of the site. The remaining simplifications were conceptual. The analyses could not be improved until the models of the site were refined with additional data. For example, the sorbing minerals in the Tpt-TN unit are thought to be distributed on the fractures (Carlos, 1987). However, in the PACE-90 analyses the sorbing minerals were modeled as being contained in the matrix. Secondly, the downward infiltration rate was specified as 0.01 mm/yr (10^{-13} m/s), which was smaller than the isotropic water-diffusion coefficient used in these problems. The diffusion effects modeled here considered only molecular diffusion of liquid water, ignoring the vapor

phase. If the net infiltration rate was as small as was specified, downward movement of the liquid water might not be the dominant transport process. Next, treating the source-term release as if it occured at the borehole wall did not take into account the mechanisms involved in transporting the contaminants from the container to the borehole wall. Finally, the composite-porosity model simplified unsaturated-zone calculations to the point where site-scale calculations were possible. However, this model assumes that the pressure heads in the matrix and in the fractures are equal, an assumption that is not always valid. A dual-porosity model, which uses separate equations for matrix flow and fracture flow and joins the equations with a transfer term, might be a more realistic model of flow behavior.

5.4 Future Work

The effort reported here raises several issues that should be addressed in future work and in site-data collection efforts in order to assess the performance of the potential Yucca Mountain repository. These issues fall into three main categories (1) hydrologic considerations, (2) contaminant transport, and (3) contaminant releases from the repository (source terms).

Hydrology: In the PACE-90 calculations, the hydrologic properties of individual layers were assumed to be laterally homogeneous. If different statistical realizations of properties were used to represent the natural variability of geologic materials more accurately, the results might be substantially different. Many thin layers of materials were used to indicate vertical variability in the problem definition. This detailed stratigraphy was geologically realistic. However, the question remains whether this amount of detail strongly affected the overall flow field in a manner that is important for performance assessment. Sensitivity analyses need to be carried out to address both of these problems.

All calculations reported here used isotropic hydrologic properties within individual layers. In reality, the rocks at Yucca Mountain have directional fabrics that may have a strong influence

on flow. For example, in welded tuffs the rock commonly has a strong horizontal fabric, while fractures are dominantly vertical. The properties of fractures and faults are also not well understood. Are the faults best characterized as rubble zones? If so, how far into the surrounding units do the effects of brecciation extend? What is the effect of mineralization? Are clay and/or zeolitic minerals present in abundance? Have the fractures been filled in with silica or carbonate cements? What are the apertures of the fractures? What is the density and the degree of connectivity of the fracture systems? Finally, what is the effect of offset of units along the fault planes on the diversion of flow? Any of these features may provide lateral variations that may have a significant effect on groundwater flow. These types of information need to be obtained from site-specific data.

In addition to physical constraints on flow fields, several aspects of modeling are still poorly understood. One of these is the effect of boundary conditions. What would be the effect of nonuniform distribution of infiltration along the top boundary, as opposed to the uniform distributions that were used in the current 2-D models? Side boundaries may have a strong effect on the entire flow field. What boundary types give more accurate representations: impermeable, constant-pressure, or some other types? How far must the side boundaries be extended to reduce their effects to insignificance? What types of problems require 2-D or 3-D modeling? Under what conditions is it sufficient to do 1-D calculations? If the 0.01-mm/year net infiltration rate is realistic, should we be looking at vapor flow as well as liquid flow? Since fracture flow is not substantial at the 0.01-mm/yr infiltration rate, should we investigate other infiltration rates that will result in fracture flow? How should we handle locally saturated fields?

Transport: Sorption coefficients need to be better defined and understood. One aspect of this need is whether sorbing minerals are preferentially distributed at Yucca Mountain, either on fracture walls or within the matrix. The nature of this distribution will strongly determine whether or not contaminants have access to the sorbing minerals under a given flow regime (matrix or frac-

ture). Finally, since colloids can be transported much faster than can dissolved species, the possibility that radionuclides could be transported by means of colloids needs to be addressed.

Source Terms: Source terms for release of contaminants need to be closely coupled with the infiltration rates predicted for the repository horizon. The spatial distribution of the source terms should be treated in more detail. At what distance from the repository might the individual plumes from containers merge so that the "far-field" can be rigorously defined?

All of the future work proposed above expresses our uncertainties regarding the system. To properly accommodate these uncertainties, future PA analyses must follow specific steps: (1) the use of event trees (or other logic diagrams) to relate the PA analysis (the problem being done) to scenarios describing the overall processes that are occurring; (2) assignment of probabilities of occurrence to the elements of the event tree describing the problem; (3) identification of conceptual-model assumptions and alternative conceptual models pertinent to the problem; (4) assignment of ranges and probabilities of occurrence to parameter values; (5) performance of the calculations, recognizing the impacts of boundary and initial conditions on the calculation; and (6) expression of the outcomes of the analysis in terms of the uncertainties of the inputs. By better structuring the method of performing PA calculations, analyses can better identify the types of information needed from site-characterization activities and will ultimately provide a more meaningful and comprehensive set of analyses on which to base total-system PA.

6.0 CONCLUSIONS

The PACE-90 nominal-case exercise modeled one set of parameters and conceptual model assumptions thought to be representative of a set of conditions at Yucca Mountain. For the conditions and assumptions specified, there was no calculated release of radionuclides from the repository either to the water table directly below, or to the accessible environment beyond the repository boundaries. The problem description yielded flow regimes where the diffusion of solutes was the dominant process. At least one calculation indicated that there was a minor, but not insignificant, contribution from advection. The concentration contours for the transported nuclides produced were similar for all analyses. However, the problem was not defined with parameters that stressed the models or the codes sufficiently to illustrate any potential differences.

This exercise has emphasized that obtaining site-characterization data from the Yucca Mountain site is of paramount importance. Without site-specific data, our conceptual models and parameter values are only speculative. Future performance-assessment analyses must better reflect the uncertainties in our knowledge of the site. The ability of these analyses to guide site characterization will improve as more data become available. For example, assigning priorities to the surface-based testing program requires guidance from performance assessment exercises such as these.

The PACE-90 problem analyzed one of many nominal configurations. Other nominal configurations might yield significantly different results. All nominal configurations consistent with our uncertainties in the conceptual model and parameters are constituents of the expected conditions. For this reason, it is important to emphasize that, because of the limitations of the available data and the analyses, the results obtained by PACE-90 do not adequately describe conditions "expected" to occur at Yucca

Mountain. More comprehensive PA analyses must examine the uncertainties in the conceptual models and parameter values. Sensitivity studies, which are an initial attempt at addressing uncertainties, will be discussed in Volume 2 of this report.

The PACE-90 participants were able to interact readily to produce useful work in a short time frame. Because each participating organization had different strengths, the combined effort benefitted from numerous viewpoints and contributions.

7.0 REFERENCES

Apted, M. J., A.M. Liebetrau, and D.W. Engel, 1989. "The Analytical Repository Source-Term (AREST) Model: Analysis of Spent Fuel as a Nuclear Waste Form," PNL-6347, Pacific Northwest Laboratory, Richland, WA. (NNA.890510.0023)

Bentley, C. B., 1984. "Geologic Data for Test Well USW G-4, Yucca Mountain Area, Nye County, Nevada," USGS Open-File Report 84-063. (NNA.870519.0100)

Birdsell, K. H. and B. J. Travis, 1991. "Results of the COVE2a Benchmarking Calculations Run with TRACR3D," LA-11513-MS, Los Alamos National Laboratory, Los Alamos, NM. (NNA.900213.0043)

Bish, D. L., F. A. Caporuscio, J. F. Copp, B. M. Crowe, J. D. Purson, J. R. Smyth, and R. G. Warren, 1981. "Preliminary Stratigraphic and Petrologic Characterization of Core Samples from USW G-1, Yucca Mountain, NV," LA-8840-MS, Los Alamos National Laboratory, Los Alamos, NM. (NNA.870406.0158)

Bish, D. L. and S. J. Chipera, 1989. "Revised Mineralogic Summary of Yucca Mountain, Nevada," LA-11497-MS, Los Alamos National Laboratory, Los Alamos, NM. (NNA.891019.0029)

Bixler, N. E., 1985. "NORIA---A Finite Element Computer Program for Analyzing Water, Vapor, Air, and Energy Transport in Porous Media," SAND84-2057, Sandia National Laboratories, Albuquerque, NM. (NNA.870721.0002)

Burdine, N. T., 1953. "Relative Permeability Calculations from Pore Size Distribution Data," American Institute of Mining Engineers, Petroleum Transactions, 198, pp. 71-77. (NNA.890522.0241)

Byers, F. M., Jr., W. J. Carr, P. P. Orkild, W. D. Quinlivan, and K. A. Sargent, 1976. "Volcanic Suites and Related Cauldrons of Timber Mountain-Oasis Valley Caldera Complex of Southern Nevada," USGS Prof. Paper 919. (NNA.870406.0239)

Campbell, J. E., Longsine, D. E., and Reeves, M., 1981. "Distributed Velocity Method of Solving the Convective-Dispersion Equation: 1. Introduction, Mathematical Theory, and Numerical Implementation," Advances Water Resources, 4, pp. 102-108. (NNA.910128.0149)

Carlos, B. A., 1987. "Minerals in Fractures of the Saturated Zone from Drill Core USW G-4, Yucca Mountain, Nye County, Nevada," LA-10927-MS, Los Alamos National Laboratory, Los Alamos, NM. (NNA.870708.0026)

Carr, W. J., 1984. "Regional Structural Setting of Yucca Mountain, Southeastern Nevada, and Late Cenozoic Rates of Tectonic Activity in Part of the Southwestern Great Basin, Nevada and California," USGS Open-File Report 84-854. (HQS.880517.2634)

Daniels, W. R., K. Wolfsberg, R. S. Rundberg, A. E. Ogard, J. F. Kerrisk, C. J. Duffy, T. W. Newton, J. L. Thompson, B. P. Bayhurst, D. L. Bish, J. D. Blacic, B. M. Crowe, B. R. Erdal, J. F. Griffith, S. D. Knight F. O. Lawrence, V. L. Rundberg, M. L. Sykes, G. M. Thompson, B. J. Travis, E. N. Treher, R. J. Vidale, G. R. Walter, R. D. Aguilar, M. R. Cisneros, S. Maestas, A. J. Mitchell, P. Q. Oliver, N. A. Raybold, and P. L. Wanek, 1982. "Summary Report on the Geochemistry of Yucca Mountain and Environs," LA-9328-MS, Los Alamos National Laboratory, Los Alamos, NM. (HQS.880517.1974)

de Marsily, G., 1986. Quantitative Hydrogeology, Academic Press, Orlando, FL. (NNA.910207.0116)

DOE, 1986. "Nuclear Waste Policy Act (Section 112) Environmental Assessment, Yucca Mountain Site, Nevada Research and Development Area, Nevada," DOE/RW-0073, U. S. Department of Energy, Washington, DC. (NNA.890327.0062-.0064)

Dudley, A. L., R. R. Peters, J. H. Gauthier, M. L. Wilson, M. S. Tierney, and E. A. Klavetter, 1988. "Total System Performance Assessment Code (TOSPAC) Volume 1: Physical and Mathematical Bases," SAND85-0002, Sandia National Laboratories, Albuquerque, NM. (NNA.881202.0211)

Dykhuizen, R. C., 1987. "Transport of Solutes Through Unsaturated Fractured Media," Water Resour. Res., 21 (12), pp. 1531-1539. (NNA.890327.0047)

Dykhuizen, R. C., 1990. "A New Coupling Term for Dual Porosity Models," Water Resour. Res., 26, (2), pp. 351-356. (NNA.910328.0058)

EPA, 1985. "Environmental Standards for the Management and Disposal of Spent Nuclear Fuel, High-Level and Transuranic Radioactive Wastes: Final Rule," U. S. Environmental Protection Agency, (10 CFR 40 Part 191), Washington, D.C. (HQS.880517.3264)

Eslinger, P. W., P. G. Doctor, D. M. Elwood, D. W. Engel, M. D. Freshley, A. M. Liebetrau, P. W. Reimus, D. L. Strenge, J. E. Tanner, and A. E. van Luik, 1989. "Preliminary Post-Closure Risk Assessment, Yucca Mountain, Nevada, Candidate Repository Site," PNL-SA-17573, Pacific Northwest Laboratory, Richland, WA. (NNA.910328.0047)

Freeze, R. A., and J. A. Cherry, 1979. Groundwater, Prentice Hall, Englewood Cliffs, NJ. (NNA.870406.0444)

Hindmarsh, A. C., 1983. "ODEPACK, A Systematized Collection of ODE Solvers," Scientific Computing, R. S. Stepleman, et al., Eds., North-Holland, Amsterdam, pp. 55-64. (NNA.910328.0065)

Hopkins, P. L., and R. R. Eaton, 1990. "LLUVIA: A Program for One-Dimensional, Steady-State Flow Through Partially Saturated Porous Media," SAND88-0558, Sandia National Laboratories, Albuquerque, NM. (NNA.900406.0001)

Longsine, D. E., Bonano, E. J., and Harlan, C. P., 1987. "User's Manual for the NEFTRAN Computer Code," U.S. Nuclear Regulatory Commission, NUREG/CR-4766, Washington, D.C., and Sandia National Laboratories, SAND86-2405, Albuquerque, NM. (NNA.910328.0045)

Martinez, M. J., 1985. "FEMTRAN -- A Finite Element Computer Program for Simulating Radionuclide Transport Through Porous Media," SAND84-0747, Sandia National Laboratories, Albuquerque, NM. (NNA.870728.0029)

Mualem, Y., 1976. "A New Model for Predicting the Hydraulic Conductivity of Unsaturated Porous Materials," Water Resour. Res.,12 (3), pp. 513-522. (HQS.880517.1803)

O'Connell, W. J., 1990. "Status of Integrated Performance Assessment of the Waste Packages and Engineered Barrier System," UCRL-10214, Lawrence Livermore National Laboratory, Livermore, CA. (NNA.900607.0215)

Ortiz, T. S., R. L. Williams, F. B. Nimick, B. C. Whittet, and D. L. South, 1985. "A Three-Dimensional Model of Reference Thermal/Mechanical and Hydrological Stratigraphy at Yucca Mountain, Southern Nevada," SAND84-1076, Sandia National Laboratories, Albuquerque, NM. (NNA.890315.0013)

Peters, R. R., E. A. Klavetter, I. J. Hall, S. C. Blair, P. R. Heller, and G. W. Gee, 1984. "Fracture and Matrix Hydrologic Characteristics of Tuffaceous Materials from Yucca Mountain, Nye County, Nevada," SAND84-1471, Sandia National Laboratories, Albuquerque, NM. (NNA.870407.0036)

Peters, R. R. and E. A. Klavetter, 1988. "A Continuum Model for Water Movement in an Unsaturated Fractured Rock Mass," Water Resor. Res., 24 (3), pp. 416-430. (NNA.890523.0139)

Peyret, R. and T. D. Taylor, 1990. Computational Methods for Fluid Flow, Springer-Verlag, New York. (NNA.910522.0048)

Pigford, T. H. and W. W.-L. Lee, 1989. "Waste Package Performance in Unsaturated Rock," Proceedings of FOCUS '89, Nuclear Waste Isolation in the Unsaturated Zone, Las Vegas, NV, September 1989. (NNA.910429.0152)

Press, W. H., Flannery, B. P., Teukolsky, S. A., and Flannery, W. T., 1989. Numerical Recipes, The Art of Scientific Computing, FORTRAN Version, Cambridge University Press, New York. (NNA.910522.0006)

Prindle, R. and P. Hopkins, 1990. "On Conditions and Parameters Important to Model Sensitivity for Unsaturated Flow Through Layered, Fractured Tuff: Results of Analyses for HYDROCOIN Level 3 Case 2," SAND89-0652, Sandia National Laboratories, Albuquerque, NM. (NNA.900523.0211)

Rautman, C. A., B. C. Whittet, D. L. South, 1987. "Definitions of Reference Boundaries for the Proposed Geologic Repository at Yucca Mountain, Nevada," SAND86-2157, Sandia National Laboratories, Albuquerque, NM. (HQS.880517.2833)

Richards, L. A., 1931. "Capillary Conduction of Liquids Through Porous Mediums," Physics 1, pp. 318-333. (NNA.890522.0282)

Rush, F. E., W. Thordarson, and L. Bruckheimer, 1983. "Geologic and Drill-Hole Data for Test Well USW H-1 Adjacent to Nevada Test Site, Nye County, NV," USGS Open-File Report 83-141. (NNA.870519.0103)

SEPDB, 1989. Yucca Mountain Project Site and Engineering Properties Database Product No. SEP0070, Sandia National Laboratories, Albuquerque, NM. (NNA.910306.0145)

SNL, 1987. "Site Characterization Plan Conceptual Design Report," compiled by MacDougall, H. R., L. W. Scully, and J. R. Tillerson, SAND84-2641, Sandia National Laboratories, Albuquerque, NM. (NN1.880902.0014-.0019)

Sadeghi, M. M., W. W.-L. Lee, T. H. Pigford, and P. L. Chambre, 1990. "Release Rates of Radionuclides in to Dripping Ground Water," LBL-28430, Paper submitted to the 1990 ANS Annual Meeting. (NNA.910328.0048)

Sadeghi, M. M., W. W.-L. Lee, T. H. Pigford, and P. L. Chambre, 1990. "Diffusive Release of Radionuclides into Saturated and Unsaturated Tuff," LBL-28428, Lawrence Berkeley Laboratory, Berkeley, CA. (NNA.910328.0049)

Scott, R. B. and J. Bonk, 1984. "Preliminary Geologic Map of Yucca Mountain, Nevada, with Geologic Sections," USGS Open-File Report 84-494. (HQS.880517.1443)

Shampine, L. F. and H. A. Watts, 1980. "DEPAC--Design of a User Oriented Package of ODE Solvers," SAND79-2374, Sandia National Laboratories, Albuquerque, NM. (NNA.900122.0001)

Spengler, R. W., D. C. Muller, and R. B. Livermore, 1979. "Preliminary Report on the Geology and Geophysics of Drill Hole UE-25a #1, Yucca Mountain, Nevada Test Site," USGS Open-File Report 79-1244. (HQS.880517.1491)

Thomas, K. W., 1987. "Summary of Sorption Measurements Performed with Yucca Mountain, Nevada, Tuff Samples and Water from Well J-13," LA-10960-MS, Los Alamos National Laboratory, Los Alamos, NM. (NNA.890602.0026)

van Genuchten, M. Th., 1980. "A Closed-Form Equation for Predicting the Hydraulic Conductivity of Unsaturated Soils," Soil Science, 44 (5), pp. 892-898. (NNA.890522.0287)

van Golf-Racht, T. D., 1982. Fundamentals of Fractured Reservoir Engineering, Elsevier/North-Holland, New York. (NNA.910328.0078)

APPENDIX A

Source Terms used for
PACE-90 Nominal Configuration Analyses

TABLE A-1
WET-DRIP SCENARIO,
BATHTUB MODEL

Time (yrs)	Total Releases (Ci/yr/pkg) Tc-99	I-129	Cs-135	Np-237
0	0	0	0	0
300	0	0	0	0
1520	0	0	0	0
1521	7.325E-06	1.789E-08	1.959E-07	1.061E-13
1600	5.865E-04	1.432E-06	1.568E-05	8.489E-12
1700	1.360E-03	3.321E-06	3.638E-05	1.910E-11
1800	2.191E-03	5.352E-06	5.862E-05	2.972E-11
1900	2.992E-03	7.307E-06	8.004E-05	4.034E-11
2000	3.736E-03	9.127E-06	9.996E-05	5.097E-11
2500	6.696E-03	1.637E-05	1.793E-04	1.042E-10
3000	8.664E-03	2.119E-05	2.321E-04	1.575E-10
3500	9.969E-03	2.439E-05	2.671E-04	2.109E-10
4000	7.096E-03	1.739E-05	1.904E-04	2.135E-10
4500	4.710E-03	1.156E-05	1.265E-04	2.138E-10
5000	3.121E-03	7.672E-06	8.399E-05	2.140E-10
5500	2.068E-03	5.092E-06	5.574E-05	2.141E-10
6000	1.371E-03	3.379E-06	3.699E-05	2.141E-10
6500	9.084E-04	2.243E-06	2.455E-05	2.141E-10
7000	6.020E-04	1.489E-06	1.629E-05	2.141E-10
7500	3.989E-04	9.882E-07	1.081E-05	2.141E-10
8000	2.644E-04	6.558E-07	7.176E-06	2.141E-10
8500	1.752E-04	4.354E-07	4.763E-06	2.141E-10
9000	1.164E-04	2.898E-07	3.170E-06	2.141E-10
9500	7.863E-05	1.960E-07	2.144E-06	2.141E-10
10000	5.370E-05	1.341E-07	1.466E-06	2.141E-10
20000	0	0	0	2.141E-10
100000	0	0	0	2.141E-10

TABLE A-2
WET-DRIP SCENARIO,
FLOW-THROUGH MODEL

Time (yrs)	Total Releases (Ci/yr/pkg) Tc-99	I-129	Cs-135	Np-237
0	0	0	0	0
300	0	0	0	0
350	0	0	0	0
351	8.320E-06	2.016E-08	2.208E-07	1.0928E-13
400	4.109E-04	9.9541E-07	1.090E-05	5.4643E-12
500	9.905E-04	2.3946E-06	2.629E-05	1.6399E-11
600	1.308E-03	3.1519E-06	3.470E-05	2.7363E-11
700	1.625E-03	3.9091E-06	4.312E-05	3.8402E-11
800	1.942E-03	4.6663E-06	5.153E-05	4.9515E-11
900	2.258E-03	5.4236E-06	5.995E-05	6.0665E-11
1000	2.575E-03	6.1808E-06	6.836E-05	7.1854E-11
1500	4.154E-03	9.967E-06	1.104E-04	1.2832E-10
2000	5.727E-03	1.3753E-05	1.525E-04	1.8465E-10
2500	6.307E-03	1.5145E-05	1.683E-04	2.2176E-10
3000	6.289E-03	1.5145E-05	1.683E-04	2.1963E-10
3500	6.274E-03	1.5145E-05	1.683E-04	2.1661E-10
4000	6.262E-03	1.5145E-05	1.683E-04	2.138E-10
4500	6.247E-03	1.5137E-05	1.682E-04	2.1382E-10
5000	4.839E-03	1.1737E-05	1.304E-04	2.1403E-10
5500	3.275E-03	7.951E-06	8.833E-05	2.1411E-10
6000	1.714E-03	4.1648E-06	4.626E-05	2.1412E-10
6500	1.557E-04	3.7862E-07	4.205E-06	2.1412E-10
7000	0	0	0	2.1412E-10
7500	0	0	0	2.1412E-10
8000	0	0	0	2.1412E-10
8500	0	0	0	2.1412E-10
9000	0	0	0	2.1412E-10
9500	0	0	0	2.1412E-10
10000	0	0	0	2.1412E-10
20000	0	0	0	2.1412E-10
100000	0	0	0	2.1412E-10

TABLE A-3
MOIST-CONTINUOUS SCENARIO,

BASE CASE (CASE 1)

Total Releases (Ci/yr)

Time (yrs)	Tc-99
2000	0.00E+00
3000	8.22E-01
4000	1.43E+00
5000	1.91E+00
6000	2.29E+00
7000	2.60E+00
8000	2.84E+00
9000	3.03E+00
10000	3.18E+00
11000	3.32E+00
21000	3.85E+00
31000	3.93E+00
41000	3.89E+00
51000	3.82E+00
61000	3.74E+00
71000	3.64E+00
81000	3.54E+00
91000	3.45E+00
101000	3.35E+00
201000	2.47E+00
301000	1.50E+00
401000	0.00E+00

Time (yrs)	Cs-135
1070	0.00E+00
1080	9.02E-40
1090	3.45E-35
1100	1.58E-31
1200	3.49E-15
1300	7.71E-10
1400	3.21E-07
1500	1.11E-05
1600	1.12E-04
1700	5.66E-04
1800	1.86E-03
1900	4.56E-03
2000	9.26E-03
3000	1.59E-01
4000	2.07E-01
5000	0.00E+00
801000	0.00E+00
901000	9.05E-06
1001000	2.00E-05
1101000	3.83E-05
2101000	8.03E-04
3101000	2.15E-03
4101000	3.28E-03
5101000	3.92E-03
6101000	4.13E-03
7101000	3.96E-03
8101000	0.00E+00

Total Releases (Ci/yr)

Time (yrs)	I-129
1000.07	0.00E+00
1000.08	8.11E-38
1000.09	1.53E-33
1000.10	3.98E-30
1000.20	8.56E-15
1000.30	1.01E-09
1000.40	3.33E-07
1000.50	1.05E-05
1000.60	1.03E-04
1000.70	5.21E-04

Time (yrs)	Np-237
1010.00	0.00E+00
1020.00	5.47E-08
1030.00	4.33E-07
1040.00	1.17E-06
1050.00	2.07E-06
1060.00	2.97E-06
1070.00	3.80E-06
1080.00	4.54E-06
1090.00	5.17E-06
1100.00	5.70E-06

TABLE A-3, Continued

Total Releases (Ci/yr)

Time (yrs)	I-129	Time (yrs)	Np-237
1000.80	1.74E-03	1200.00	8.01E-06
1000.90	4.43E-03	1300.00	8.20E-06
1001.00	9.23E-03	1400.00	7.91E-06
1002.00	2.29E-01	1500.00	7.51E-06
1003.00	6.06E-01	1600.00	7.10E-06
1004.00	9.49E-01	1700.00	6.72E-06
1005.00	1.20E+00	1800.00	6.39E-06
1006.00	1.38E+00	1900.00	6.08E-06
1007.00	1.51E+00	2000.00	5.82E-06
1008.00	1.59E+00	3000.00	4.21E-06
1009.00	1.73E+00	4000.00	3.45E-06
1010.00	1.77E+00	5000.00	3.02E-06
1020.00	1.84E+00	6000.00	2.70E-06
1030.00	8.22E-01	7000.00	2.47E-06
1040.00	0.00E+00	8000.00	2.31E-06
1300.00	0.00E+00	9000.00	2.17E-06
1400.00	1.22E-03	10000.00	2.05E-06
1500.00	1.89E-03	11000.00	1.96E-06
1600.00	2.55E-03	21000.00	1.43E-06
1700.00	3.17E-03	31000.00	1.19E-06
1800.00	3.76E-03	41000.00	1.06E-06
1900.00	4.24E-03	51000.00	9.62E-07
2000.00	4.80E-03	61000.00	8.94E-07
3000.00	8.00E-03	71000.00	8.40E-07
4000.00	9.49E-03	81000.00	7.98E-07
5000.00	1.02E-02	91000.00	7.61E-07
6000.00	1.06E-02	101000.00	7.33E-07
7000.00	1.09E-02	201000.00	5.73E-07
8000.00	1.11E-02	301000.00	5.04E-07
9000.00	1.12E-02	401000.00	4.63E-07
10000.00	1.12E-02	501000.00	4.34E-07
11000.00	1.13E-02	601000.00	4.13E-07
21000.00	1.16E-02	701000.00	3.95E-07
31000.00	1.17E-02	801000.00	3.80E-07
41000.00	1.18E-02	901000.00	3.66E-07
51000.00	1.18E-02	1001000.00	3.54E-07
61000.00	1.18E-02	2001000.00	2.76E-07
71000.00	1.18E-02	3001000.00	2.34E-07
81000.00	1.18E-02	4001000.00	2.07E-07
91000.00	1.18E-02	5001000.00	1.90E-07
101000.00	1.19E-02	6001000.00	1.79E-07
201000.00	4.91E-03	7001000.00	1.72E-07
301000.00	0.00E+00	8001000.00	1.67E-07
		9001000.00	1.63E-07

TABLE A-4
MOIST-CONTINUOUS SCENARIO,

HIGHER DIFFUSION COEFFICIENT (CASE 2)

Total Releases (Ci/yr)

Time (yrs)	Tc-99	Time (yrs)	Cs-135
1001.00	0.00E+00	1000.07	0.00E+00
1002.00	8.29E-01	1000.08	9.05E-37
1003.00	1.45E+00	1000.09	3.45E-32
1004.00	1.94E+00	1000.10	1.58E-28
1005.00	2.33E+00	1000.20	3.49E-12
1006.00	2.64E+00	1000.30	7.71E-07
1007.00	2.90E+00	1000.40	3.21E-04
1008.00	3.11E+00	1000.50	1.11E-02
1009.00	3.28E+00	1000.60	1.12E-01
1010.00	3.42E+00	1000.70	5.66E-01
1020.00	4.11E+00	1000.80	1.86E+00
1030.00	4.33E+00	1000.90	4.58E+00
1040.00	4.44E+00	1001.00	9.26E+00
1050.00	4.47E+00	1002.00	1.59E+02
1060.00	4.54E+00	1003.00	2.07E+02
1070.00	4.54E+00	1004.00	0.00E+00
1080.00	4.58E+00	5000.00	0.00E+00
1090.00	4.62E+00	6000.00	1.22E-02
1100.00	4.62E+00	7000.00	1.61E-02
1200.00	4.69E+00	8000.00	2.00E-02
1300.00	4.73E+00	9000.00	2.38E-02
1400.00	4.76E+00	10000.00	2.72E-02
1500.00	4.76E+00	11000.00	3.04E-02
1600.00	4.80E+00	21000.00	5.15E-02
1700.00	4.80E+00	31000.00	6.22E-02
1800.00	4.80E+00	41000.00	6.87E-02
1900.00	4.80E+00	51000.00	7.30E-02
2000.00	4.80E+00	61000.00	7.58E-02
3000.00	4.80E+00	71000.00	7.79E-02
4000.00	4.80E+00	81000.00	7.96E-02
5000.00	4.76E+00	91000.00	8.09E-02
6000.00	4.76E+00	101000.00	8.19E-02
7000.00	4.76E+00	201000.00	7.81E-02
8000.00	4.73E+00	301000.00	0.00E+00
9000.00	4.73E+00		
10000.00	4.69E+00		
11000.00	4.69E+00		
21000.00	4.54E+00		
31000.00	4.40E+00		
41000.00	4.25E+00		
51000.00	4.14E+00		
61000.00	4.00E+00		
71000.00	3.85E+00		
81000.00	3.74E+00		
91000.00	3.63E+00		

TABLE A-4, Continued

Total Releases (Ci/yr)

Time (yrs)	Tc-99
101000.00	3.51E+00
201000.00	2.54E+00
301000.00	7.13E-01
401000.00	0.00E+00

Time (yrs)	I-129
1000.00	0.00E+00
1000.01	1.81E+03
1000.02	1.84E+03
1000.03	9.12E+02
1000.04	0.00E+00
1000.30	0.00E+00
1000.40	1.22E-03
1000.50	1.89E-03
1000.60	2.55E-03
1000.70	3.17E-03
1000.80	3.76E-03
1000.90	4.24E-03
1001.00	4.80E-03
1002.00	8.00E-03
1003.00	9.49E-03
1004.00	1.02E-02
1005.00	1.06E-02
1006.00	1.09E-02
1007.00	1.11E-02
1008.00	1.12E-02
1009.00	1.13E-02
1010.00	1.13E-02
1020.00	1.16E-02
1030.00	1.17E-02
1040.00	1.18E-02
1050.00	1.18E-02
1060.00	1.18E-02
1070.00	1.19E-02
1080.00	1.19E-02
1090.00	1.19E-02
1100.00	1.19E-02
1200.00	1.20E-02
1300.00	1.20E-02
1400.00	1.20E-02
1500.00	1.20E-02
1600.00	1.20E-02
1700.00	1.20E-02
1800.00	1.20E-02
1900.00	1.21E-02
2000.00	1.21E-02
3000.00	1.21E-02
4000.00	1.21E-02

Time (yrs)	Np-237
1000.01	0.00E+00
1000.02	5.47E-05
1000.03	4.33E-04
1000.04	1.17E-03
1000.05	2.07E-03
1000.06	2.97E-03
1000.07	3.80E-03
1000.08	4.54E-03
1000.09	5.17E-03
1000.10	5.70E-03
1000.20	8.01E-03
1000.30	8.20E-03
1000.40	7.91E-03
1000.50	7.51E-03
1000.60	7.10E-03
1000.70	6.72E-03
1000.80	6.39E-03
1000.90	6.08E-03
1001.00	5.82E-03
1002.00	4.21E-03
1003.00	3.45E-03
1004.00	3.02E-03
1005.00	2.70E-03
1006.00	2.47E-03
1007.00	2.31E-03
1008.00	2.17E-03
1009.00	2.05E-03
1010.00	1.96E-03
1020.00	1.43E-03
1030.00	1.19E-03
1040.00	1.06E-03
1050.00	9.62E-04
1060.00	8.94E-04
1070.00	8.40E-04
1080.00	7.98E-04
1090.00	7.61E-04
1100.00	7.33E-04
1200.00	5.73E-04
1300.00	5.04E-04
1400.00	4.63E-04
1500.00	4.34E-04
1600.00	4.13E-04

TABLE A-4, Continued

Total Releases (Ci/yr)

Time (yrs)	I-129
5000.00	1.21E-02
6000.00	1.21E-02
7000.00	1.21E-02
8000.00	1.21E-02
9000.00	1.21E-02
10000.00	1.21E-02
11000.00	1.21E-02
21000.00	1.21E-02
31000.00	1.21E-02
41000.00	1.21E-02
51000.00	1.21E-02
61000.00	1.21E-02
71000.00	1.20E-02
81000.00	1.20E-02
91000.00	1.20E-02
101000.00	1.20E-02
201000.00	4.28E-03
301000.00	0.00E+00

Time (yrs)	Np-237
1700.00	3.95E-04
1800.00	3.80E-04
1900.00	3.66E-04
2000.00	3.54E-04
3000.00	2.76E-04
4000.00	2.34E-04
5000.00	2.07E-04
6000.00	1.90E-04
7000.00	1.79E-04
8000.00	1.72E-04
9000.00	1.67E-04
10000.00	1.63E-04
11000.00	1.61E-04
21000.00	1.57E-04
31000.00	1.57E-04
41000.00	1.57E-04
51000.00	1.57E-04
61000.00	1.57E-04
71000.00	1.57E-04
81000.00	1.57E-04
91000.00	1.57E-04
101000.00	1.57E-04
201000.00	1.57E-04
301000.00	1.57E-04
401000.00	1.57E-04
501000.00	1.57E-04
601000.00	1.57E-04
701000.00	1.57E-04
801000.00	1.57E-04
901000.00	1.57E-04
1001000.00	1.57E-04
2001000.00	1.57E-04
3001000.00	1.57E-04
4001000.00	1.57E-04
5001000.00	1.57E-04
6001000.00	1.57E-04
7001000.00	1.57E-04
8001000.00	1.57E-04
9001000.00	1.57E-04

TABLE A-5
MOIST-CONTINUOUS SCENARIO,

HIGHER FUEL ALTERATION RATE (CASE 3)

Total Releases (Ci/yr)

Time (yrs)	Tc-99
1900.00	0.00E+00
2000.00	1.30E+02
3000.00	8.22E+02
4000.00	9.34E+01
5000.00	0.00E+00

Time (yrs)	Cs-135
1070.00	0.00E+00
1080.00	9.02E-40
1090.00	3.45E-35
1100.00	1.58E-31
1200.00	3.49E-15
1300.00	7.71E-10
1400.00	3.21E-07
1500.00	1.11E-05
1600.00	1.12E-04
1700.00	5.66E-04
1800.00	1.86E-03
1900.00	4.56E-03
2000.00	9.26E-03
3000.00	1.59E-01
4000.00	2.07E-01
5000.00	0.00E+00
887000.00	0.00E+00
888000.00	8.05E-03
889000.00	8.13E-03
890000.00	8.20E-03
891000.00	8.28E-03
901000.00	9.05E-03
911000.00	9.88E-03
921000.00	1.08E-02
931000.00	1.17E-02
941000.00	1.27E-02
951000.00	1.37E-02
961000.00	1.49E-02
971000.00	1.61E-02
981000.00	1.73E-02
1081000.00	3.39E-02
1181000.00	5.94E-02
1281000.00	6.92E-02
1381000.00	0.00E+00

Total Releases (Ci/yr)

Time (yrs)	I-129
1000.07	0.00E+00
1000.08	8.11E-38
1000.09	1.53E-33
1000.10	3.98E-30
1000.20	8.56E-15
1000.30	1.01E-09

Time (yrs)	Np-237
1010.00	0.00E+00
1020.00	5.47E-08
1030.00	4.33E-07
1040.00	1.17E-06
1050.00	2.07E-06
1060.00	2.97E-06

TABLE A-5, Continued

Total Releases (Ci/yr)

Time (yrs)	I-129
1000.40	3.33E-07
1000.50	1.05E-05
1000.60	1.03E-04
1000.70	5.21E-04
1000.80	1.74E-03
1000.90	4.43E-03
1001.00	9.23E-03
1002.00	2.29E-01
1003.00	6.06E-01
1004.00	9.49E-01
1005.00	1.20E+00
1006.00	1.38E+00
1007.00	1.51E+00
1008.00	1.59E+00
1009.00	1.73E+00
1010.00	1.77E+00
1020.00	1.84E+00
1030.00	8.22E-01
1040.00	0.00E+00
1300.00	0.00E+00
1400.00	1.22E+00
1500.00	1.89E+00
1600.00	2.55E+00
1700.00	3.17E+00
1800.00	3.76E+00
1900.00	4.24E+00
2000.00	1.00E+00
3000.00	0.00E+00

Time (yrs)	Np-237
1070.00	3.80E-06
1080.00	4.54E-06
1090.00	5.17E-06
1100.00	5.70E-06
1200.00	8.01E-06
1300.00	8.20E-06
1400.00	7.91E-06
1500.00	7.51E-06
1600.00	7.10E-06
1700.00	6.72E-06
1800.00	6.39E-06
1900.00	6.08E-06
2000.00	5.82E-06
3000.00	4.21E-06
4000.00	3.45E-06
5000.00	3.02E-06
6000.00	2.70E-06
7000.00	2.47E-06
8000.00	2.31E-06
9000.00	2.17E-06
10000.00	2.05E-06
11000.00	1.96E-06
21000.00	1.43E-06
31000.00	1.19E-06
41000.00	1.06E-06
51000.00	9.62E-07
61000.00	8.94E-07
71000.00	8.40E-07
81000.00	7.98E-07
91000.00	7.61E-07
101000.00	7.33E-07
201000.00	5.73E-07
301000.00	5.04E-07
401000.00	4.63E-07
501000.00	4.34E-07
601000.00	4.13E-07
701000.00	3.95E-07
801000.00	3.80E-07
901000.00	3.66E-07
1001000.00	3.54E-07
2001000.00	2.76E-07
3001000.00	2.34E-07
4001000.00	2.07E-07
5001000.00	1.90E-07
6001000.00	1.79E-07
7001000.00	1.72E-07
8001000.00	1.67E-07
9001000.00	1.63E-07

TABLE A-6
MOIST-CONTINUOUS SCENARIO,

LARGER FUEL SURFACE AREA (CASE 4)

Total Releases (Ci/yr)

Time (yrs)	Tc-99	Time (yrs)	Cs-135
2000.00	0.00E+00	1070.00	0.00E+00
3000.00	1.64E+00	1080.00	9.02E-40
4000.00	2.86E+00	1090.00	3.45E-35
5000.00	3.82E+00	1100.00	1.58E-31
6000.00	4.58E+00	1200.00	3.49E-15
7000.00	5.20E+00	1300.00	7.71E-10
8000.00	5.67E+00	1400.00	3.21E-07
9000.00	6.03E+00	1500.00	1.11E-05
10000.00	6.36E+00	1600.00	1.12E-04
11000.00	6.62E+00	1700.00	5.66E-04
21000.00	7.67E+00	1800.00	1.86E-03
31000.00	7.82E+00	1900.00	4.56E-03
41000.00	7.74E+00	2000.00	9.26E-03
51000.00	7.63E+00	3000.00	1.59E-01
61000.00	7.45E+00	4000.00	2.07E-01
71000.00	7.27E+00	5000.00	0.00E+00
81000.00	7.09E+00	887000.00	0.00E+00
91000.00	6.87E+00	888000.00	1.61E-05
101000.00	4.51E+00	889000.00	1.62E-05
201000.00	0.00E+00	890000.00	1.64E-05
		891000.00	1.65E-05
		901000.00	1.81E-05
		911000.00	1.98E-05
		921000.00	2.15E-05
		931000.00	2.34E-05
		941000.00	2.53E-05
		951000.00	2.75E-05
		961000.00	2.96E-05
		971000.00	3.21E-05
		981000.00	3.45E-05
		1081000.00	6.79E-05
		1181000.00	1.19E-04
		1281000.00	1.90E-04
		1381000.00	2.85E-04
		1481000.00	4.02E-04
		1581000.00	5.43E-04
		1681000.00	7.07E-04
		1781000.00	8.92E-04
		1881000.00	1.10E-03
		2881000.00	3.72E-03
		3881000.00	6.13E-03
		4881000.00	7.49E-03
		5881000.00	0.00E+00

TABLE A-6, Continued

Total Releases (Ci/yr)

Time (yrs)	I-129	Time (yrs)	Np-237
1000.07	0.00E+00	1010.00	0.00E+00
1000.08	8.11E-38	1020.00	5.47E-08
1000.09	1.53E-33	1030.00	4.33E-07
1000.10	3.98E-30	1040.00	1.17E-06
1000.20	8.56E-15	1050.00	2.07E-06
1000.30	1.01E-09	1060.00	2.97E-06
1000.40	3.33E-07	1070.00	3.80E-06
1000.50	1.05E-05	1080.00	4.54E-06
1000.60	1.03E-04	1090.00	5.17E-06
1000.70	5.21E-04	1100.00	5.70E-06
1000.80	1.74E-03	1200.00	8.01E-06
1000.90	4.43E-03	1300.00	8.20E-06
1001.00	9.23E-03	1400.00	7.91E-06
1002.00	2.29E-01	1500.00	7.51E-06
1003.00	6.06E-01	1600.00	7.10E-06
1004.00	9.49E-01	1700.00	6.72E-06
1005.00	1.20E+00	1800.00	6.39E-06
1006.00	1.38E+00	1900.00	6.08E-06
1007.00	1.51E+00	2000.00	5.82E-06
1008.00	1.59E+00	3000.00	4.21E-06
1009.00	1.73E+00	4000.00	3.45E-06
1010.00	1.77E+00	5000.00	3.02E-06
1020.00	1.84E+00	6000.00	2.70E-06
1030.00	8.22E-01	7000.00	2.47E-06
1040.00	0.00E+00	8000.00	2.31E-06
1300.00	0.00E+00	9000.00	2.17E-06
1400.00	2.43E-03	10000.00	2.05E-06
1500.00	3.76E-03	11000.00	1.96E-06
1600.00	5.10E-03	21000.00	1.43E-06
1700.00	6.33E-03	31000.00	1.19E-06
1800.00	7.48E-03	41000.00	1.06E-06
1900.00	8.52E-03	51000.00	9.62E-07
2000.00	9.56E-03	61000.00	8.94E-07
3000.00	1.60E-02	71000.00	8.40E-07
4000.00	1.90E-02	81000.00	7.98E-07
5000.00	2.05E-02	91000.00	7.61E-07
6000.00	2.13E-02	101000.00	7.33E-07
7000.00	2.18E-02	201000.00	5.73E-07
8000.00	2.21E-02	301000.00	5.04E-07
9000.00	2.23E-02	401000.00	4.63E-07
10000.00	2.25E-02	501000.00	4.34E-07
11000.00	2.26E-02	601000.00	4.13E-07
21000.00	2.32E-02	701000.00	3.95E-07
31000.00	2.34E-02	801000.00	3.80E-07
41000.00	2.35E-02	901000.00	3.66E-07
51000.00	2.36E-02	1001000.00	3.54E-07
61000.00	2.36E-02	2001000.00	2.76E-07
71000.00	2.36E-02	3001000.00	2.34E-07
81000.00	2.37E-02	4001000.00	2.07E-07

TABLE A-6, Continued

Total Releases (Ci/yr)

Time (yrs)	I-129	Time (yrs)	Np-237
91000.00	2.37E-02	5001000.00	1.90E-07
101000.00	9.82E-04	6001000.00	1.79E-07
201000.00	0.00E+00	7001000.00	1.72E-07
		8001000.00	1.67E-07
		9001000.00	1.63E-07

APPENDIX B

Data Relevant to the Reference Information Base and the Site and Engineering Properties Data Base

No data were taken from the Reference Information Base (RIB). Tables 3-2 and 3-3 should be considered for inclusion in the RIB. Some of the data used in the definition of the problem geohydrology came from the Site and Engineering Properties Data Base (SEPDB). Most of the data used to augment the SEPDB data are qualitative and may not be appropriate for inclusion in the SEPDB.

DISTRIBUTION LIST

1 John W. Bartlett, Director (RW-1)
Office of Civilian Radioactive
Waste Management
U.S. Department of Energy
Forrestal Bldg.
Washington, D.C. 20585

1 F. G. Peters, Deputy Director (RW-2)
Office of Civilian Radioactive
Waste Management
U.S. Department of Energy
Forrestal Bldg.
Washington, D.C. 20585

1 D. G. Horton (RW-3)
Office of Quality Assurance
Office of Civilian Radioactive
Waste Management
U.S. Department of Energy
Forrestal Bldg.
Washington, D.C. 20585

1 T. H. Isaacs (RW-4)
Office of Strategic Planning
and International Programs
Office of Civilian Radioactive
Waste Management
U.S. Department of Energy
Forrestal Bldg.
Washington, D.C. 20585

1 J. D. Saltzman (RW-5)
Office of External Relations
Office of Civilian Radioactive
Waste Management
U.S. Department of Energy
Forrestal Bldg.
Washington, D.C. 20585

1 Samuel Rousso (RW-10)
Office of Program and Resources
Management
Office of Civilian Radioactive
Waste Management
U.S. Department of Energy
Forrestal Bldg.
Washington, D.C. 20585

1 Carl P. Gertz (RW-20)
Office of Geologic Disposal
Office of Civilian Radioactive
Waste Management
U.S. Department of Energy
Forrestal Bldg.
Washington, D.C. 20585

1 D. E. Shelor (RW-30)
Office of Systems and Compliance
Office of Civilian Radioactive
Waste Management
U.S. Department of Energy
Forrestal Bldg.
Washington, D.C. 20585

1 L. H. Barrett (RW-40)
Office of Storage and Transportation
Office of Civilian Radioactive
Waste Management
U.S. Department of Energy
Forrestal Bldg.
Washington, D.C. 20585

1 F. G. Peters (RW-50)
Office of Contractor Business
Management
Office of Civilian Radioactive
Waste Management
U.S. Department of Energy
Forrestal Bldg.
Washington, D.C. 20585

1 J. C. Bresee (RW-10)
Office of Civilian Radioactive
Waste Management
U.S. Department of Energy
Forrestal Bldg.
Washington, D.C. 20585

1 S. J. Brocoum (RW-20)
Office of Civilian Radioactive
Waste Management
U.S. Department of Energy
Forrestal Building
Washington, D.C. 20585

1 Gerald Parker (RW-30)
Office of Civilian Radioactive
Waste Management
U.S. Department of Energy
Forrestal Bldg.
Washington, D.C. 20585

1 D. U. Deere, Chairman
Nuclear Waste Technical
Review Board
1100 Wilson Blvd. #910
Arlington, VA 22209-2297

1 C. A. Allen, Member
Nuclear Waste Technical
Review Board
1100 Wilson Blvd. #910
Arlington, VA 22209-2297

1 P. A. Dominico, Member
Nuclear Waste Technical
Review Board
1100 Wilson Blvd. #910
Arlington, VA 22209-2297

1 D. W. North, Member
Nuclear Waste Technical
Review Board
1100 Wilson Blvd. #910
Arlington, VA 22209-2297

1 E. D. Verink, Jr., Member
Nuclear Waste Technical
Review Board
1100 Wilson Blvd. #910
Arlington, VA 22209-2297

5 Carl P. Gertz, Project Manager
Yucca Mountain Project Office
Nevada Operations Office
U.S. Department of Energy
Mail Stop 523
P.O. Box 98518
Las Vegas, NV 89193-8518

1 C. L. West, Director
Office of External Affairs
Nevada Operations Office
U.S. Department of Energy
P.O. Box 98518
Las Vegas, NV 89193-8518

12 Technical Information Office
Nevada Operations Office
U. S. Department of Energy
P.O. Box 98518
Las Vegas, NV 89193-8518

1 P. K. Fitzsimmons, Director
Health Physics & Environmental
Division
Nevada Operations Office
U.S. Department of Energy
P.O. Box 98518
Las Vegas, NV 89193-8518

1 Repository Licensing & Quality
Assurance Project Directorate
Division of Waste Management
U.S. Nuclear Regulatory Commission
Washington, D.C. 20555

1 Senior Project Manager for Yucca
Mountain Repository Project Branch
Division of Waste Management
U.S. Nuclear Regulatory Commission
Washington, D.C. 20555

1 NRC Document Control Desk
Division of Waste Management
U.S. Nuclear Regulatory Commission
Washington, D.C. 20555

1 G. N. Gnugnoli, ACNW
U.S. Nuclear Regulatory Commission
MS P-315
Washington, D.C. 20555

1 E. P. Binnall
Field Systems Group Leader
Building 50B/4235
Lawrence Berkeley Laboratory
Berkeley, CA 94720

1 Center for Nuclear Waste
Regulatory Analyses
6220 Culebra Road
Drawer 28510
San Antonio, TX 78284

3 L. J. Jardine
Technical Project Officer for YMP
Lawrence Livermore National
Laboratory
Mail Stop L-204
P.O. Box 808
Livermore, CA 94550

4 R. J. Herbst
Technical Project Officer for YMP
Los Alamos National Laboratory
N-5, Mail Stop J521
P.O. Box 1663
Los Alamos, NM 87545

1 H. N. Kalia
Exploratory Shaft Test Manager
Los Alamos National Laboratory
Mail Stop 527
101 Convention Center Dr.
Suite 820
Las Vegas, NV 89109

1 J. F. Divine
Assistant Director for
Engineering Geology
U.S. Geological Survey
106 National Center
12201 Sunrise Valley Dr.
Reston, VA 22092

6 L. R. Hayes
Technical Project Officer for YMP
U.S. Geological Survey
P.O. Box 25046
421 Federal Center
Denver, CO 80225

1 D. Zesiger
U.S. Geological Survey
101 Convention Center Dr.
Suite 860 - MS509
Las Vegas, NV 89109

1 DeWayne A. Campbell
YMP Technical Project Officer
Bureau of Reclamation
P.O. Box 25007 Bldg. 67
Denver, CO 80225-0007

1 K. W. Causseaux
NHP Reports Chief
U.S. Geological Survey
P.O. Box 25046
421 Federal Center
Denver, CO 80225

1 R. V. Watkins, Chief
Project Planning and Management
U.S. Geological Survey
P.O. Box 25046
421 Federal Center
Denver, CO 80225

1 V. M. Glanzman
U.S. Geological Survey
P.O. Box 25046
913 Federal Center
Denver, CO 80225

1 J. H. Nelson
Technical Project Officer for YMP
Science Applications International
Corp.
101 Convention Center Dr.
Suite 407
Las Vegas, NV 89109

2 SAIC-T&MSS Library
Science Applications International
Corp.
101 Convention Center Dr.
Suite 407
Las Vegas, NV 89109

1 Elaine Ezra
YMP GIS Project Manager
EG&G Energy Measurements, Inc.
Mail Stop D-12
P.O. Box 1912
Las Vegas, NV 89125

1 W. M. Hewitt, Program Manager
Roy F. Weston, Inc.
955 L'Enfant Plaza, Southwest
Suite 800
Washington, D.C. 20024

1 Technical Information Center
Roy F. Weston, Inc.
955 L'Enfant Plaza, Southwest
Suite 800
Washington, D.C. 20024

1 D. L. Fraser, General Manager
Reynolds Electrical & Engineering Co.
P.O. Box 98521
Mail Stop 555
Las Vegas, NV 89193-8521

1 Robert F. Pritchett
Technical Project Officer for YMP
Reynolds Electrical & Engineering Co.
Mail Stop 615
P.O. Box 98521
Las Vegas, NV 89193-8521

1 A. E. Gurrola
General Manager
Raytheon, Inc.
Mail Stop 580
P.O. Box 93838
Las Vegas, NV 89193-3838

1 James C. Calovini
Raytheon Services, Inc.
101 Convention Center Dr.
Suite P-280
Las Vegas, NV 89109

1 D. L. Lockwood, General Manager
Raytheon Services, Inc.
Mail Stop 514
P.O. Box 93265
Las Vegas, NV 89193-3265

1 Richard L. Bullock
Technical Project Officer for YMP
Raytheon Services, Inc.
101 Convention Center Dr.
Suite P250
Las Vegas, NV 89109

1 R. E. Lowder
Technical Project Officer for YMP
MAC Technical Services
Valley Bank Center
101 Convention Center Drive
Suite 1100
Las Vegas, NV 89109

1 D. J. Bales
Science and Technology Division
Office of Scientific and Technical Information
U.S. Department of Energy
P.O. Box 62
Oak Ridge, TN 37831

1 Carlos G. Bell, Jr.
Professor of Civil Engineering
Civil and Mechanical Engineering Department
University of Nevada, Las Vegas
4505 South Maryland Parkway
Las Vegas, NV 89154

1 C. F. Costa, Director
Nuclear Radiation Assessment Division
U.S. Environmental Protection Agency
Environmental Monitoring Systems Laboratory
P.O. Box 93478
Las Vegas, NV 89193-3478

1 ONWI Library
Battelle Columbus Laboratory
Office of Nuclear Waste Isolation
505 King Avenue
Columbus, OH 43201

1 T. Hay, Executive Assistant
Office of the Governor
State of Nevada
Capitol Complex
Carson City, NV 89710

3 R. R. Loux, Jr.
Executive Director
Nuclear Waste Project Office
State of Nevada
Evergreen Center, Suite 252
1802 North Carson Street
Carson City, NV 89710

1 C. H. Johnson
Technical Program Manager
Nuclear Waste Project Office
State of Nevada
Evergreen Center, Suite 252
1802 North Carson Street
Carson City, NV 89710

1 John Fordham
Water Resources Center
Desert Research Institute
P.O. Box 60220
Reno, NV 89506

1 Dr. Martin Mifflin
Desert Research Institute
Water Resources Center
2505 Chandler Avenue
Suite 1
Las Vegas, NV 89120

1 Eric Anderson
Mountain West Research-Southwest Inc.
2901 N. Central Ave. #1000
Phoenix, AZ 85012-2730

1 Department of Comprehensive Planning
Clark County
225 Bridger Avenue, 7th Floor
Las Vegas, NV 89155

1 Planning Department
Nye County
P.O. Box 153
Tonopah, NV 89049

1 Lincoln County Commission
Lincoln County
P.O. Box 90
Pioche, NV 89043

5 Judy Foremaster
City of Caliente
P.O. Box 158
Caliente, NV 89008

1 Economic Development Department
City of Las Vegas
400 East Stewart Avenue
Las Vegas, NV 89109

1 Community Planning & Development
City of North Las Vegas
P.O. Box 4086
North Las Vegas, NV 89030

1 City Manager
City of Henderson
Henderson, NV 89015

1 Director of Community Planning
City of Boulder City
P.O. Box 367
Boulder City, NV 89005

1 Commission of the European Communities
200 Rue de la Loi
B-1049 Brussels
Belgium

1 D. C. Dobson
Yucca Mountain Project Office
U.S. Department of Energy
P.O. Box 98518
Las Vegas, NV 89193-8518

1 J. M. Boak
Yucca Mountain Project Office
U.S. Department of Energy
P.O. Box 98518
Las Vegas, NV 89193-8518

1 M. B. Blanchard
Yucca Mountain Project Office
U.S. Department of Energy
P.O. Box 98518
Las Vegas, NV 89193-8518

5 J. R. Dyer
Yucca Mountain Project Office
U.S. Department of Energy
P.O. Box 98518
Las Vegas, NV 89193-8518

1 A. T. MacIntyre
Lawrence Livermore National Laboratory
Mail Stop L-440
P.O. Box 808
Livermore, CA 94550

1 D. A. Chesnut
Lawrence Livermore National Laboratory
Mail Stop L-204
P.O. Box 808
Livermore, CA 94550

1 W. E. Grassley
Lawrence Livermore National Laboratory
Mail Stop L-204
P.O. Box 808
Livermore, CA 94550

1 W. J. O'Connell
Lawrence Livermore National Laboratory
Mail Stop L-195
P.O. Box 808
Livermore, CA 94550

1 G. A. Valentine
Los Alamos National Laboratory
Mail Stop F-665
P.O. Box 1663
Los Alamos, NM 87545

1 G. Zyvoloski
Los Alamos National Laboratory
Mail Stop F-665
P.O. Box 1663
Los Alamos, NM 87545

1 K. G. Eggert
Los Alamos National Laboratory
Mail Stop F-665
P.O. Box 1663
Los Alamos, NM 87545

1 J. A. Canepa
Los Alamos National Laboratory
Mail Stop J-521
P.O. Box 1663
Los Alamos, NM 87545

1 K. H. Birdsell
Los Alamos National Laboratory
Mail Stop J-665
P.O. Box 1663
Los Alamos, NM 87545

1 P. Cloke
SAIC
101 Convention Center Drive
Las Vegas, NV 89109

1 J. M. Younker
SAIC
101 Convention Center Drive
Las Vegas, NV 89109

1 U-S. Park
SAIC
101 Convention Center Drive
Las Vegas, NV 89109

1 K. M. Kersch
SAIC
101 Convention Center Drive
Las Vegas, NV 89109

1 D. Hoxie
U.S. Geological Survey
P.O. Box 25046
Denver Federal Center, MS 425
Denver, CO 80225

1 W. W.-L. Lee
Lawrence Berkeley Laboratory
Earth Sciences Division
1 Cyclotron Road
Berkeley, CA 94720

1 T. Narasimhan
Lawrence Berkeley Laboratory
Earth Sciences Division
1 Cyclotron Road
Berkeley, CA 94720

1 J. Wang
Lawrence Berkeley Laboratory
Earth Sciences Division
1 Cyclotron Road
Berkeley, CA 94720

1 C. K. Hastings
Pacific Northwest Laboratories
P.O. Box 999, MS K6-96
Richland, WA 99352

1 T. Miley
Pacific Northwest Laboratories
P.O. Box 999, MS K2-92
Richland, WA 99352

1 P. W. Eslinger
Pacific Northwest Laboratories
P.O. Box 999, MS K6-96
Richland, WA 99352

1 M. J. Apted
Pacific Northwest Laboratories
P.O. Box 999, MS K6-88
Richland, WA 99352

1 D. Langford
Pacific Northwest Laboratories
P.O. Box 999, MS G2-01
Richland, WA 99352

1 M. Kreiter
Pacific Northwest Laboratories
P.O. Box 999, MS K6-35
Richland, WA 99352

1 A. E. van Luik
Pacific Northwest Laboratories
P.O. Box 999, MS K6-Z4
Richland, WA 99352

1 M. A. McGraw
Pacific Northwest Laboratories
P.O. Box 999, MS K6-96
Richland, WA 99352

1 K. T. Feldman
RE/SPEC, Inc.
4775 Indian School Road NE
Albuquerque, NM 87110

1 T. Christrian-Frear
RE/SPEC, Inc.
4775 Indian School Road NE
Albuquerque, NM 87110

1	6300	T. O. Hunter, Actg.
1	6310	T. E. Blejwas, Actg.
1	6310A	L. E. Shephard
1	6311	A. L. Stevens
1	6312	F. W. Bingham
1	6312	G. E. Barr
1	6312	H. A. Dockery
1	6312	A. R. DuCharme
1	6312	E. Dunn
1	6312	P. G. Kaplan
1	6312	F. C. Lauffer
1	6312	M. L. Wilson
1	6313	L. S. Costin
25	6313	R. W. Barnard
1	6313	M. E. Fewell
1	6313	J. H. Gauthier
1	6313	A. H. Treadway
1	6315	F. B. Nimick, Actg.
1	6315	R. J. Glass
1	6315	C. A. Rautman
1	6316	R. P. Sandoval
1	6317	S. Sinnock
2	6318	L. J. Erickson for 100/12149/SAND90-2726/NQ
1	6318	C. Crawford for Accession No. Data Base
1	6319	R. R. Richards
1	1510	J. C. Cummings
1	1511	D. K. Gartling
1	1511	R. R. Eaton
1	1511	P. L. Hopkins
1	1511	M. J. Martinez
1	1513	R. C. Dykhuizen
5	3141	S. A. Landenberger
8	3145	Document Processing for DOE/OSTI
3	3151	G. C. Claycomb
20	6341	WMT Library
1	6410	D. J. McCloskey, Actg.
1	6416	E. J. Bonano
1	6416	D. P. Gallegos
1	8523	Technical Library

The number in the lower right-hand corner is an accession number used for Office of Civilian Radioactive Waste Management purposes only. It should not be used when ordering this publication.

Org.	Bldg.	Name	Rec'd by	Org.	Bldg.	Name	Rec'd by

Sandia National Laboratories